

UNCLASSIFIED

AD NUMBER

AD911338

LIMITATION CHANGES

TO:

Approved for public release; distribution is unlimited.

FROM:

Distribution authorized to U.S. Gov't. agencies only; Proprietary Information; JUN 1973. Other requests shall be referred to Air Force Armament Lab., Eglin AFB, FL.

AUTHORITY

AFATL ltr, 1 Oct 1980

THIS PAGE IS UNCLASSIFIED

042

**STATIC STABILITY AND CONTROL EFFECTIVENESS
OF THE MK-84 HOBOS
AND THE MODULAR GUIDED GLIDE BOMB
AT TRANSONIC SPEEDS**



D. K. Smith

ARO, Inc.

THE
OFFICE

per TAB 80-26

June 1973

**TECHNICAL REPORTS
FILE COPY**

~~Distribution limited to U. S. Government agencies only;
this report contains information on test and evaluation of
military hardware; June 1973; other requests for this
document must be referred to Air Force Armament
Laboratory/DLMB, Eglin AFB, Florida 32543.~~

**PROPULSION WIND TUNNEL FACILITY
ARNOLD ENGINEERING DEVELOPMENT CENTER
AIR FORCE SYSTEMS COMMAND
ARNOLD AIR FORCE STATION, TENNESSEE**

NOTICES

When U. S. Government drawings, specifications, or other data are used for any purpose other than a definitely related Government procurement operation, the Government thereby incurs no responsibility nor any obligation whatsoever, and the fact that the Government may have formulated, furnished, or in any way supplied the said drawings, specifications, or other data, is not to be regarded by implication or otherwise, or in any manner licensing the holder or any other person or corporation, or conveying any rights or permission to manufacture, use, or sell any patented invention that may in any way be related thereto.

Qualified users may obtain copies of this report from the Defense Documentation Center.

References to named commercial products in this report are not to be considered in any sense as an endorsement of the product by the United States Air Force or the Government.

**STATIC STABILITY AND CONTROL EFFECTIVENESS
OF THE MK-84 HOBOS
AND THE MODULAR GUIDED GLIDE BOMB
AT TRANSONIC SPEEDS**

**D. K. Smith
ARO, Inc.**

Distribution limited to U. S. Government agencies only; this report contains information on test and evaluation of military hardware; June 1973; other requests for this document must be referred to Air Force Armament Laboratory/DLMB, Eglin AFB, Florida 32542.

FOREWORD

The work reported herein was done by the Arnold Engineering Development Center (AEDC) and sponsored by the Air Force Armament Laboratory (AFATL/DLMB), Air Force Systems Command (AFSC), under Program Element 63741F, Project 5975.

The test results presented were obtained by ARO, Inc. (a subsidiary of Sverdrup & Parcel and Associates, Inc.), contract operator of the AEDC, AFSC, Arnold Air Force Station, Tennessee. The test was conducted from February 15 through 22, 1973, under ARO Project No. PA303. The manuscript was submitted for publication on April 25, 1973.

This technical report has been reviewed and is approved.

L. R. KISSLING
Lt Colonel, USAF
Chief Air Force Test Director, PWT
Directorate of Test

A. L. COAPMAN
Colonel, USAF
Director of Test

ABSTRACT

Wind tunnel tests were conducted to determine the static stability and control characteristics of the MK-84 Homing Optical Bombing System (HOBOS) at high angles of attack and the Modular Guided Glide Bomb (MGGB) at moderate angles of attack. The tests were conducted in the Aerodynamic Wind Tunnel (4T) over a Mach number range from 0.50 to 1.05 and angles of attack from -2 to 35 deg with 0.25-scale models. Aerodynamic coefficients are presented to show longitudinal, directional, and lateral static stability and axial-force characteristics, as well as control effectiveness. The effect on the aerodynamic coefficients and on the calibration data for a vane-type angle-of-attack indicator produced by adding a proximity fuse on the fuselage was also investigated.

Distribution limited to U. S. Government agencies only; this report contains information on test and evaluation of military hardware; June 1973; other requests for this document must be referred to Air Force Armament Laboratory/DLMB, Eglin AFB, Florida 32542.

CONTENTS

	<u>Page</u>
ABSTRACT	iii
NOMENCLATURE	vii
I. INTRODUCTION	1
II. APPARATUS	
2.1 Test Facility	1
2.2 Test Articles	2
2.3 Instrumentation	2
III. TEST DESCRIPTION	
3.1 Test Conditions and Procedures	2
3.2 Corrections	3
3.3 Precision of Measurements	3
IV. RESULTS AND DISCUSSION	
4.1 General	4
4.2 Effect of Reynolds Number	4
4.3 Effect of Roll Angle	5
4.4 Effect of Fuselage Protuberance Changes	5
4.5 Control Deflection Effectiveness	5
4.6 Calibration Data of Vane-Type Angle-of-Attack Indicator	6
V. CONCLUSIONS	7
REFERENCES	8

APPENDIX ILLUSTRATIONS

Figure

1. Sketch of the Model Installation	11
2. Installation Photographs	12
3. Dimensional Sketch of MGGB (Configuration B9W8S1T3)	16
4. Dimensional Sketch of the MK84 HOBOS (Configuration B11T3)	17
5. Dimensional Sketch of the Wing Configuration (W8)	18
6. Dimensional Sketch of the Strongback Configuration (S1)	19
7. Dimensional Sketch of the Proximity Fuse and DME Antenna Showing Their Location on the Model	20
8. Dimensional Sketch of the Vane-Type Angle-of-Attack Indicator	21
9. Orientation of Model Forces and Moments	22
10. Orientation of Control Surface Deflections	24
11. Effect of Varying Reynolds Number on the Normal-Force and Pitching-Moment Coefficients for the MGGB Configuration without the RES (B9T3)	25
12. Effect of Varying Reynolds Number on the Rolling-Moment and Axial-Force Coefficients	27

<u>Figure</u>	<u>Page</u>
13. Effect of Varying Reynolds Number on the Side-Force and Yawing-Moment Coefficients for Configuration B9T3	29
14. Effect of Varying Reynolds Number on the Longitudinal Stability Characteristics of MGGB Configuration (B10W8S1T3)	31
15. Effect of Varying Reynolds Number on the Lift to Drag Ratio of MGGB Configuration (B10W8S1T3)	36
16. Effect of Varying Roll Angle on the Normal-Force and Pitching-Moment Coefficients for MGGB Configuration without the RES (B10T3)	41
17. Effect of Varying Roll Angle on the Rolling-Moment and Axial-Force Coefficients for MGGB Configuration without the RES (B10T3)	47
18. Effect of Varying Roll Angle on the Side-Force and Yawing-Moment Coefficient for MGGB Configuration without the RES (B10T3)	53
19. Effect of Varying Fuselage Protuberances on the Normal-Force and Pitching-Moment Coefficients for Configurations without the RES (B9T3, B10T3, and B11T3)	59
20. Effect of Varying Fuselage Protuberances on the Rolling-Moment and Axial-Force Coefficients for Configurations without the RES (B9T3, B10T3, and B11T3)	65
21. Effect of Varying Fuselage Configuration on the Side-Force and Yawing-Moment Coefficient for Configurations without the RES (B9T3, B10T3, and B11T3)	71
22. Effect of Fuselage Protuberances on the Longitudinal Stability Characteristics for MGGB Configurations (B9W8S1T3 and B10W8S1T3)	77
23. Effect of Fuselage Protuberances on the Lift-to-Drag Ratio for MGGB Configurations (B9W8S1T3 and B10W8S1T3)	82
24. Effect of Fuselage Configuration on the Lateral and Directional Stability Characteristics for MGGB Configurations (B9W8S1T3 and B10W8S1T3)	87
25. Effect of Pitch Control Deflections on the Normal-Force and Pitching-Moment Coefficients for MGGB Configuration without RES (B9T3)	92
26. Effect of Pitch Control Deflections on the Rolling-Moment and Axial-Force Coefficients for MGGB Configuration without RES (B9T3)	98
27. Effect of Pitch Control Deflection on the Side-Force and Yawing-Moment Coefficients for MGGB Configuration without RES (B9T3)	104
28. Effect of Yaw Control Deflections on the Normal-Force and Pitching-Moment Coefficients for MGGB Configuration without RES (B9T3)	110
29. Effect of Yaw Control Deflections on the Rolling-Moment and Axial-Force Coefficient for MGGB Configuration without RES (B9T3)	116
30. Effect of Yaw Control Deflections on the Side-Force and Yawing-Moment Coefficients for MGGB Configuration without RES (B9T3)	122
31. Effect of Roll Control Deflections on the Normal-Force and Pitching-Moment Coefficient for MGGB Configuration without RES (B9T3)	128

FigurePage

32. Effect of Roll Control Deflections on the Rolling-Moment and Axial-Force Coefficients for MGGB Configuration without RES (B9T3)134
33. Effect of Roll Control Deflections on the Side-Force and Yawing-Moment Coefficients for MGGB Configuration without RES (B9T3)140
34. Effect of Pitch and Roll Control Deflections on the Normal-Force and Pitching-Moment Coefficients for MGGB Configuration without RES (B9T3)146
35. Effect of Pitch and Roll Control Deflections on the Rolling-Moment and Axial-Force Coefficients for MGGB Configuration without RES (B9T3)164
36. Vane Calibration Data, α versus α_s , Comparing Low and High Reynolds Number for MGGB Configuration (B10W8S1T3)182
37. Vane Calibration Data, α versus α_s , Showing the Effect of the Proximity Fuse (Configurations B9W8S1T3 and B10W8S1T3)187
38. Comparison of Vane Calibration Data, $M_\infty = 0.75$192

NOMENCLATURE

b	Reference wing span, 2.025 ft
C_A	Axial-force coefficient, axial force/ $q_\infty S_b$
C_c	Cross-wind force coefficient, cross-wind force/ $q_\infty S$
C_D	Drag coefficient, drag/ $q_\infty S$
C_L	Lift coefficient, lift/ $q_\infty S$
$C_{l,w}$	Rolling-moment coefficient, rolling moment/ $q_\infty S_b$
C_Q	Rolling-moment coefficient, rolling moment/ $q_\infty S_b d$
$C_{m,a}$	Pitching-moment coefficient, pitching moment/ $q_\infty S_b d$ moment reference point at 19.75 in. from model nose
$C_{m,w}$	Pitching-moment coefficient, pitching moment/ $q_\infty S_c$, moment reference point at 19.896 in. from model nose
$C_{N,a}$	Normal-force coefficient, normal force/ $q_\infty S_b$
$C_{n,a}$	Yawing-moment coefficient, yawing moment/ $q_\infty S_b d$, moment reference point at 19.75 in. from model nose
$C_{n,w}$	Yawing-moment coefficient, yawing moment/ $q_\infty S_b$, moment reference point at 19.896 in. from model nose

c	Reference chord length, 0.4714 ft
d	Reference body diameter, 0.375 ft
L/D	Lift-to-drag ratio
M_∞	Free-stream Mach number
p_∞	Free-stream static pressure, psfa
q_∞	Free-stream dynamic pressure, psf
Re	Free-stream unit Reynolds number, ft^{-1}
S	Reference wing area, 0.828 sq ft
S_b	Reference body area, 0.110 sq ft
u, v, w	Velocity components along the body axes, ft/sec
V_∞	Free-stream velocity, ft/sec
$X_{x,a}$	The measured force and moment data reduced to coefficient form in the aeroballistic body-axis system for the MGGB without the RES (MK-84 HOBOS and MGGB in terminal configuration), see Fig. 9
$X_{x,w}$	The measured force and moment data reduced to coefficient form in the wind-axis system for the MGGB with the RES, see Fig. 9
α	Model angle of attack, $\tan^{-1} w/u$ (see Fig. 9), deg
α_a	Total or complex angle of attack, $\tan^{-1} (\sqrt{w^2 + v^2})/u$, deg
α_s	Angle of attack as indicated by a vane-type angle-of-attack indicator, deg
β	Model angle of sideslip, $\sin^{-1} v/V_\infty$
δ_{1-4}	Control deflection angles for the respective control surfaces 1-4 (see Fig. 10), positive when trailing edge is down, deg
δ_p, δ_P	Control deflection angle for roll control, $\delta_p = (-\delta_1 - \delta_2 + \delta_3 + \delta_4)/4$, deg
δ_q, δ_Q	Control deflection angle for pitch control, $\delta_q = (\delta_1 + \delta_2 + \delta_3 + \delta_4)/4$, deg
δ_r, δ_R	Control deflection angle for yaw control, $\delta_r = (-\delta_1 + \delta_2 - \delta_3 + \delta_4)/4$, deg
ϕ	Model roll angle, deg

CONFIGURATION NOMENCLATURE

B9	Basic fuselage faired smooth with strakes, lug adapters, cable harness conduit, umbilical, band fasteners on top, DME antenna, D/L spikes, and RES hinge fitting
B10	Same as B9 with proximity fuse
B11	Basic fuselage faired smooth with strakes, launch lugs, cable harness conduit, umbilical, band fasteners on side, and DME antenna (MK-84 HOBOS with DME antenna)
S1	Basic strongback arrangement with launch lugs and umbilical connector
T3	Basic fin and control surface arrangement
W8	Basic wing with NACA 65-410 airfoil section

CONFIGURATION TESTING

B9T3	MGGB configuration without range extension system (RES), which consists of wings and strongback
B10T3	MGGB configuration with RES but with proximity fuse
B11T3	MK-84 HOBOS with DME antenna
B9W8S1T3	MGGB configuration with RES
B10W8S1T3	MGGB configuration with RES and proximity fuse

SECTION I INTRODUCTION

Wind tunnel tests were conducted to determine the static stability, control effectiveness, and performance of the MK-84 Homing Optical Bombing System (HOBOS) at high angles of attack and the Modular Guided Glide Bomb (MGGB) at moderate angles of attack. The MK-84 HOBOS, also called MK-84 EO Guided Bomb, is a lock-on-before-launch air-dropped munition; the MGGB is a high-speed air-launched glide weapon system that has evolved from the MK-84 HOBOS configuration.

The Modular Guided Glide Bomb is an MK-84 HOBOS with the addition of the range extension system (RES), which is a combination of wings and strongback. The swing wings of the MGGB are deployed after aircraft release to provide the desired lifting surfaces for range extension. Near the end of the MGGB trajectory, the RES is jettisoned. Control surfaces on the tail fins are used to provide aerodynamic control for the MK-84 HOBOS and the MGGB.

The tests were conducted in the Aerodynamic Wind Tunnel (4T), Propulsion Wind Tunnel Facility (PWT) over a Mach number range from 0.5 to 1.05 and angles of attack from -2 to 35 deg. The effect of control surface deflections and roll angles at high angles of attack on static stability and control effectiveness of the MK-84 HOBOS and the MGGB terminal configuration were determined.

Also, tests were conducted on the MGGB to determine the effect produced on the static stability and on the calibration of a vane-type angle-of-attack sensor located on the RES package by adding an externally mounted infrared (IR) proximity fuse on the fuselage. Similar tests have been previously conducted in Tunnels 4T and 16T, and the results are documented in Refs. 1 and 2.

SECTION II APPARATUS

2.1 TEST FACILITY

Tunnel 4T is a closed-loop, continuous flow, variable density tunnel in which the Mach number can be varied from 0.1 to 1.3. At all Mach numbers, the stagnation pressure can be varied from 300 to 3700 psfa. The test section is 4 ft square and 12.5 ft long with perforated, variable porosity (0.5- to 10-percent open) walls. It is completely enclosed in a plenum chamber from which the air can be evacuated, allowing part of the tunnel airflow to be removed through the perforated walls of the test section. The model support system consisted of a pitch sector, boom, and 7-deg bent sting which provided for this particular model a pitch capability from -2 to 35 deg with respect to the tunnel centerline.

2.2 TEST ARTICLES

A sketch showing the model installation is shown in Fig. 1 (Appendix). The test articles were 0.25-scale models of the MGGB and MK-84 HOBOS (Fig. 2). Dimensions of the MGGB model configuration B9W8S1T3 are shown in Fig. 3. The complete MGGB configuration consists of four basic components which include a fuselage, a strongback, a wing, and four tail fins with control surfaces. The basic fuselage configuration is identified in Fig. 4 which is a standard MK-84 HOBOS.

The various fuselage protuberances are identified in Figs. 2, 3, and 4. The tail fin and control surface configuration (T3) is shown in Fig. 4. The control surfaces were set at nominal values of 0, ± 5 , ± 10 , ± 15 , and ± 20 deg relative to the tail fins. The wing, shown in Fig. 5, was set at a sweep angle of 35 deg and at an incidence angle of 6 deg relative to the fuselage centerline plane. The incidence angle is measured in a plane normal to the wing leading edge. Shown in Fig. 6 is the strongback configuration which is mounted on the fuselage and supports the wings. A dimensional sketch of the proximity fuse and the DME antenna is shown in Fig. 7.

Included in the MGGB model configuration and shown in a dimensional sketch in Fig. 8 is a vane-type angle-of-attack indicator and located on the model as shown in Fig. 3. The angle-of-attack vane had an 18-deg included angle wedge-shaped section. The vane was mounted on a gimbaled shaft which allowed the vane to remain aligned with the local airflow around the model.

2.3 INSTRUMENTATION

A six-component, moment-type, internal strain-gage balance was used to obtain the aerodynamic forces and moments acting on the model. Model base pressure measurements were made with differential pressure transducers. The MGGB angle-of-attack indicator used a potentiometer to measure the angle of rotation of the vane shaft with respect to the MGGB fuselage centerline. The model attitude was measured with the pitch sector and roll indicators. Electrical signals from the balance, pressure transducers, vane potentiometer, and standard tunnel instrumentation were processed by the PWT data acquisition system and digital computer for on-line data reduction.

SECTION III TEST DESCRIPTION

3.1 TEST CONDITIONS AND PROCEDURES

Steady-state force and moment data and vane-angle calibration data were obtained in tunnel 4T at Mach numbers from 0.5 to 1.05. During most of the test, the total pressure was held at approximately 1000 psfa. For the above Mach numbers and total pressure the dynamic pressure was 150 to 400 psf and the Reynolds number per foot was from

1.5 to 2.3×10^6 . Data were also obtained at a high Reynolds number, 5.0 to 6.0×10^6 per foot, for certain configurations. The free-stream total temperature varied from 60 to 90°F. Tunnel conditions were held constant at each Mach number while the pitch angle or roll angle was varied, and data recorded at each selected attitude. The model pitch attitude was varied from -2 to 35 deg for configurations without the RES. The pitch and sideslip angle was varied from -2 to 10 deg for configurations with the RES. For configurations without the RES, data were also obtained at roll angles of 22.5, 45, and 180 deg. All configurations were tested with transition fixed on the wings and/or the strakes and tail fins. Boundary-layer transition was fixed with a 0.1-in.-wide band of No. 180 grit (0.0035-in. diameter) located 0.3 in. aft of the wing leading edge, and located 0.6 in. aft of the leading edge on the strakes and tail fins.

3.2 CORRECTIONS

The model angle of attack was corrected for tunnel flow angularity. The maximum correction applied to the data was 0.25 deg and is a function of Mach number and Reynolds number. Balance and sting deflections caused by aerodynamic loads on the model were also accounted for in the data reduction to determine model angle of attack. Model tare corrections were also made to calculate the net aerodynamic forces on the model.

3.3 PRECISION OF MEASUREMENTS

The precision of the data which can be attributed to the errors of the balance measurements and in setting tunnel conditions was determined using a method which assumes a normal error distribution and a 95-percent confidence level. Precision of the data in reduced coefficient form is presented below for both the low and high Reynolds numbers and selected Mach numbers.

	Low Reynolds Number			High Reynolds Number	
	$M_\infty = 0.50$	$M_\infty = 0.75$	$M_\infty = 0.95$	$M_\infty = 0.50$	$M_\infty = 0.95$
$\Delta C_{N,a}$	±0.194	±0.107	±0.079	±0.099	±0.038
$\Delta C_{Y,a}$	±0.063	±0.035	±0.027	±0.020	±0.010
$\Delta C_{A,a}$	±0.021	±0.012	±0.008	±0.011	±0.004
$\Delta C_{m,a}$	±0.178	±0.098	±0.075	±0.062	±0.030
$\Delta C_{n,a}$	±0.088	±0.048	±0.036	±0.041	±0.016
$\Delta C_{\ell,a}$	±0.016	±0.008	±0.006	±0.008	±0.003
ΔC_L	±0.027	±0.015	±0.011	±0.015	±0.005
ΔC_c	±0.009	±0.005	±0.004	±0.004	±0.002
ΔC_D	±0.004	±0.003	±0.002	±0.003	±0.0008
ΔC_m	±0.018	±0.010	±0.008	±0.006	±0.003
ΔC_n	±0.002	±0.001	±0.0008	±0.0006	±0.0003
ΔC_ℓ	±0.0005	±0.0003	±0.0002	±0.0004	±0.0001
q_∞	150	270	350	500	940
Δq_∞	±2.50	±2.34	±1.75	±8.35	±4.69
ΔM_∞	±0.0031	±0.0051	±0.0089	±0.002	±0.005

The errors quoted for Mach number relate to the variation of Mach number in the portion of the test section occupied by the model. The error in setting Mach numbers is within ± 0.005 . The error in the angle of attack, sideslip angle, and roll angle is within ± 0.1 deg.

SECTION IV RESULTS AND DISCUSSION

4.1 GENERAL

The measured force and moment data were reduced to coefficient form in the aeroballistic body axis system for the MGGB without the RES (MK-84 HOBOS and MGGB in terminal configuration). The moment reference point for those configurations without the RES was 19.75 in. aft from the model nose. The measured force and moment data for the MGGB with the RES were reduced to coefficient form in the wind-axis system. The moment reference point for those configurations was 19.896 in. from the model nose. The force and moment orientation for both coordinate systems is shown in Fig. 9. The deflections of the control surfaces for pitch, yaw, and roll control are illustrated in Fig. 10. The control surfaces pivot very close to the leading edge, or in other words, the trailing edge moves either up or down as shown in the figure. The test data presented in this report are machine plotted and faired with straight lines. The Reynolds number per foot is given for all test data presented. Also, the control surface deflection angles given for the test data are the actual measured deflection angles.

4.2 EFFECT OF REYNOLDS NUMBER

The effect of varying the Reynolds number on the aerodynamic coefficients for the MGGB configurations B9T3 (without RES) and B10W8S1T3 (with RES) is shown in Figs. 11 through 15. For configuration B9T3, the effect of varying the Reynolds number on the aerodynamic coefficients was small. However, as shown in Figs. 12 and 13, the C_A was reduced and the $C_{Y,a}$ reduced and/or changed sign as the Reynolds number was increased at Mach number 0.65 and $\delta_q = 0.3$. For configuration B10W8S1T3, increasing the Reynolds number produced little, if any, change in C_L at Mach numbers 0.50 through 0.75 (Fig. 14). However, at Mach numbers 0.85 and 0.95 increasing the Reynolds number decreased the slope of the C_L versus angle-of-attack curve. The drag coefficient either remained constant or decreased for a given C_L as the Reynolds number was increased (Fig. 14). The stability characteristic of the configuration showed very little change with increasing Reynolds number. The lift-to-drag ratio (see Fig. 15) increased as the Reynolds number was increased only at Mach numbers 0.50, 0.60, and 0.75. At the higher Mach numbers the lift-to-drag ratio was not influenced by changes in Reynolds number.

Data were also obtained, although not presented, for configuration B9T3 with and without transition grit at a Reynolds number per foot of 5.5×10^6 and at Mach numbers 0.65 and 0.95. An examination of the data showed that the grit produced no differences at the selected Reynolds number.

4.3 EFFECT OF ROLL ANGLE

Data plots showing the effect of roll angle on the aerodynamic coefficients for MGGB configuration B10T3 (without RES but with proximity fuse) are shown in Figs. 16 through 18. The normal-force coefficient showed a large increase for roll angles of 22.5 and 45 deg as would be expected at the high angles of attack (Fig. 16). The longitudinal stability and the axial-force coefficient showed some changes attributable to roll angle at the high angles of attack (Figs. 16 and 17). In general, the configuration was neutrally stable or unstable at the high angles of attack when rolled 22.5 deg. Moreover, the rolling-moment, side-force, and yawing-moment coefficients showed very large changes caused by roll angle (Figs. 17 and 18). The effects of varying roll angle just discussed were typical for all configurations tested without the RES (B9T3 and B11T3).

4.4 EFFECT OF FUSELAGE PROTUBERANCE CHANGES

The effect on the aerodynamic coefficients produced by changes in the fuselage protuberances B9, B10, and B11 on configurations without the RES (MK-84 HOBOS and MGGB terminal configurations) are presented in Figs. 19 through 21. The addition of the IR proximity fuse to the body, a comparison of the data for configurations B9T3 and B10T3, had little influence on the normal-force and pitching-moment coefficients (Fig. 19); however, it had a significant influence on the rolling-moment and side-force coefficients at the high angles of attack (Figs. 20 and 21). The addition of the proximity fuse also increased the axial-force coefficient at the lower Mach numbers, $M_\infty < 0.95$, and had a small influence on the yawing-moment coefficient (Figs. 20 and 21). A comparison of the data for configuration B11T3 (MK-84 HOBOS with DME antenna) with those data for the other configurations showed no changes in $C_{N,a}$ but did show a small change in $C_{m,a}$ for Mach numbers greater than 0.75 (Fig. 19). However, when comparing the data of configuration B11T3 with those for the other configurations, a large change was seen in $C_{Y,a}$ and a small change in C_A , C_Q , and $C_{n,a}$ (Figs. 20 and 21).

The effect on the aerodynamic coefficients produced by affixing the proximity fuse to the MGGB configuration with the RES (configurations B9W8S1T3 and B10W8S1T3) is presented in Figs. 22 through 24. The addition of the proximity fuse to the fuselage had no apparent effect on the lift or drag coefficients and only a small effect on the pitching-moment coefficient (Fig. 22), but did decrease the lift-to-drag ratio at the lower Mach numbers, $M_\infty \leq 0.75$ (Fig. 23). The addition of the proximity fuse had no effect on the lateral or directional stability coefficients (Fig. 24).

4.5 CONTROL DEFLECTION EFFECTIVENESS

Aerodynamic coefficients for several control deflections in pitch (δ_q) are shown in Figs. 25 through 27 for the MGGB configuration with RES (B9T3). The control surfaces were effective in producing trim conditions over a wide range of angle of attack (Fig. 25). The trim angle of attack for $\delta_Q = -10$ deg at Mach number 0.5 was 20 deg and the trim angle of attack decreased with Mach number. The axial-force coefficient increased

substantially with an increase in control deflection angles as would be expected (Fig. 26). The effect of pitch control deflection on C_q ; $C_{Y,a}$ and $C_{n,a}$ was small; thus, there was very little cross coupling, and this occurred only at the high angles of attack (Figs. 26 and 27).

The effect of control deflections in yaw (δ_R) for configuration B9T3 is shown in Figs. 28 through 30. Shown in Fig. 28, the longitudinal static stability decreases as the yaw control deflection angle is increased. The control surfaces were effective in producing adequate side-force and yawing-moment control at all angles of attack (Fig. 30).

The effect of roll control deflections is shown in Figs. 31 through 33 for configuration B9T3. The control surfaces were effective in producing adequate roll control at the lower angles of attack, $\alpha_a \leq 20$ deg, but were marginal in roll control at the higher angles of attack (Fig. 32). At least 15 deg of roll control deflection is required at the higher angles of attack to trim the vehicle at the lower Mach numbers. The roll control did improve somewhat with increasing Mach number at the higher angles of attack.

The effect of superimposed pitch and roll control which is the case for a pitching maneuver is shown for configuration B9T3 in Figs. 34 and 35 for several combinations of pitch and roll control. The effect of superimposed pitch and roll control on the normal-force coefficients was small. For $\delta_q = \delta_p = -10$ deg (Fig. 34), the pitch control effectiveness decreased significantly at the lower angles of attack and the trim angle of attack was decreased. The effect of superimposed pitch and roll control on the rolling-moment coefficient was large for all combinations of δ_q and δ_p (Fig. 35). The roll control effectiveness was significantly reduced at the lower angles of attack, $\alpha_a < 20$ deg, whenever pitch control was superimposed with roll control. At the higher angles of attack the roll-control effectiveness increased when pitch and roll control were superimposed for the lower Mach numbers $M_\infty = 0.75$, and was either the same or decreased somewhat at the higher Mach numbers. Also, at the high angles of attack a δ_p of 5 deg was not sufficient to trim the vehicle in roll.

4.6 CALIBRATION DATA OF VANE-TYPE ANGLE-OF-ATTACK INDICATOR

The effect of varying Reynolds number on the data from the angle-of-attack sensor is presented for MGGB configuration (B9W8S1T3) in Fig. 36. The Reynolds number variation had virtually no effect on the calibration data.

The effect of adding the proximity fuse onto the fuselage on the angle-of-attack calibration data is presented in Fig. 37. In general, the difference in the angle-of-attack data, α_s , between configurations with and without the proximity fuse (configurations B10W8S1T3 and B9W8S1T3, respectively) was very small, with the maximum difference being 0.7 deg and occurring at the negative angles of attack.

A comparison of the angle-of-attack calibration data from Refs. 1 and 2 and the present test is shown in Fig. 38. As can be seen in the figure, the data from Ref. 2

(full-scale tests in PWT 16T) and the present test agreed very well, whereas the data from Ref. 1 had the same slope as the other data but had a 3-deg offset when the model angle of attack equaled zero. This discrepancy in the data in Ref. 1 cannot be explained. For the angle data compared, the model configurations had only minor differences. The data from the present test and Ref. 2 agreed well with data taken previously in 4T on essentially identical configurations (unpublished) and with flight test data.

SECTION V CONCLUSIONS

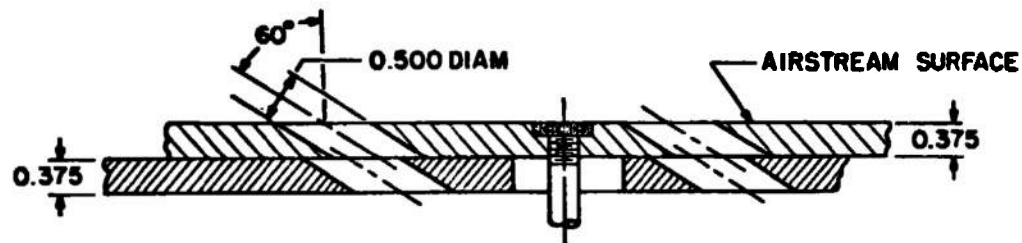
The following conclusions were made from the results of the investigation:

1. Varying the Reynolds number had a moderate effect on the aerodynamic coefficients of configurations with the range extension system but had little effect on the aerodynamic coefficients of configurations without the range extension system.
2. Varying the roll angle had a large effect on the aerodynamic coefficients of configurations without the range extension system and the configuration was neutrally stable or unstable at the high angles of attack when rolled 22.5 deg.
3. The addition of the proximity fuse to the fuselage had a significant effect on the lateral and directional stability characteristics and the axial-force coefficient of configurations without the range extension system but had little effect on the longitudinal stability characteristics.
4. The addition of the proximity fuse to the fuselage had little effect on the aerodynamic coefficients of configurations with the range extension system.
5. For configurations without the range extension system, the pitch, yaw, and roll controls were generally effective at all angles of attack with the roll control being just marginal at the high angles of attack; at least a δ_p of -15 deg required for $\alpha \geq 28$ deg at the lower Mach numbers, $M_\infty \leq 0.65$.
6. For configurations without the range extension system, the effect of superimposed pitch and roll control was to decrease the pitch effectiveness and significantly decrease the roll control at the low angles of attack for all Mach numbers.
7. The Reynolds number had no apparent effect on the calibration data of a vane-type angle-of-attack indicator on the model. Also, the addition of the proximity fuse onto the fuselage had only a very small effect on the calibration data of the angle-of-attack indicator on the model.

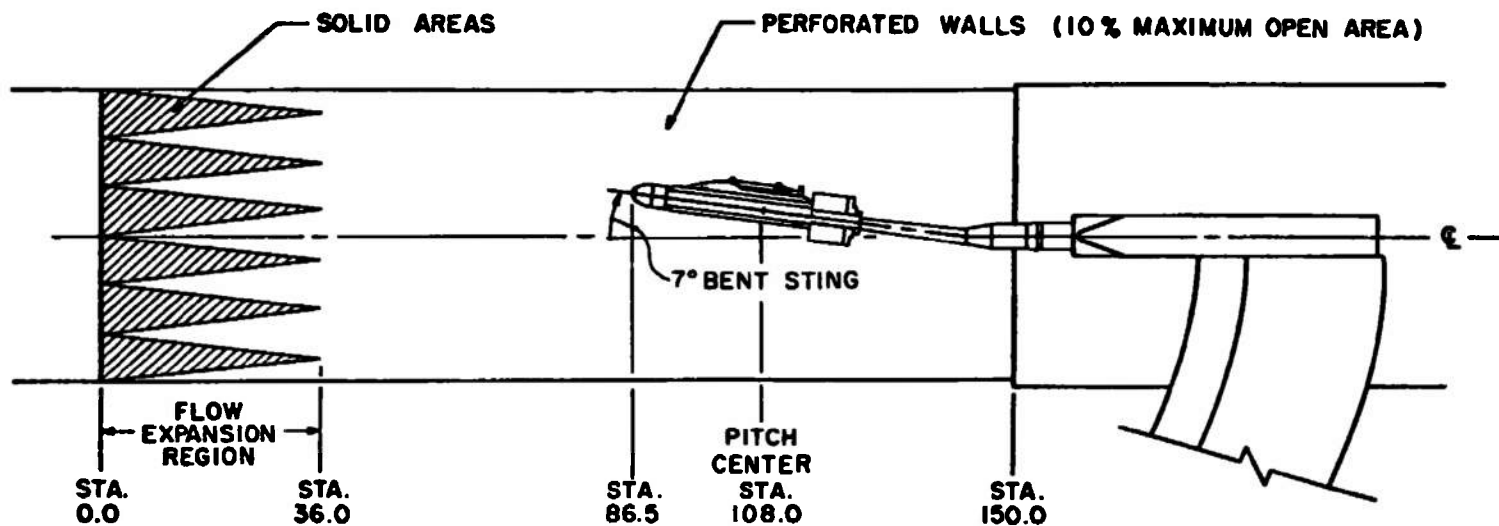
REFERENCES

1. Gomillion, G. R. "Results of a 0.25-Scale Modular Guided Glide Bomb at Transonic Mach Numbers (U)." AEDC-TR-71-168 (AFATL-TR-71-103) (AD517266L), September 1971. (Confidential Report)
2. MacLanahan, D. A., Jr. "Calibration of Angle-of-Attack and Dynamic Pressure Sensors on the Modular Guided Glide Bomb at Transonic Mach Numbers." AEDC-TR-72-124 (AFATL-TR-72-171) (AD902886L), September 1972.
3. Test Facilities Handbook (Ninth Edition). "Propulsion Wind Tunnel Facility, Vol. 4." Arnold Engineering Development Center, July 1971.

APPENDIX ILLUSTRATIONS

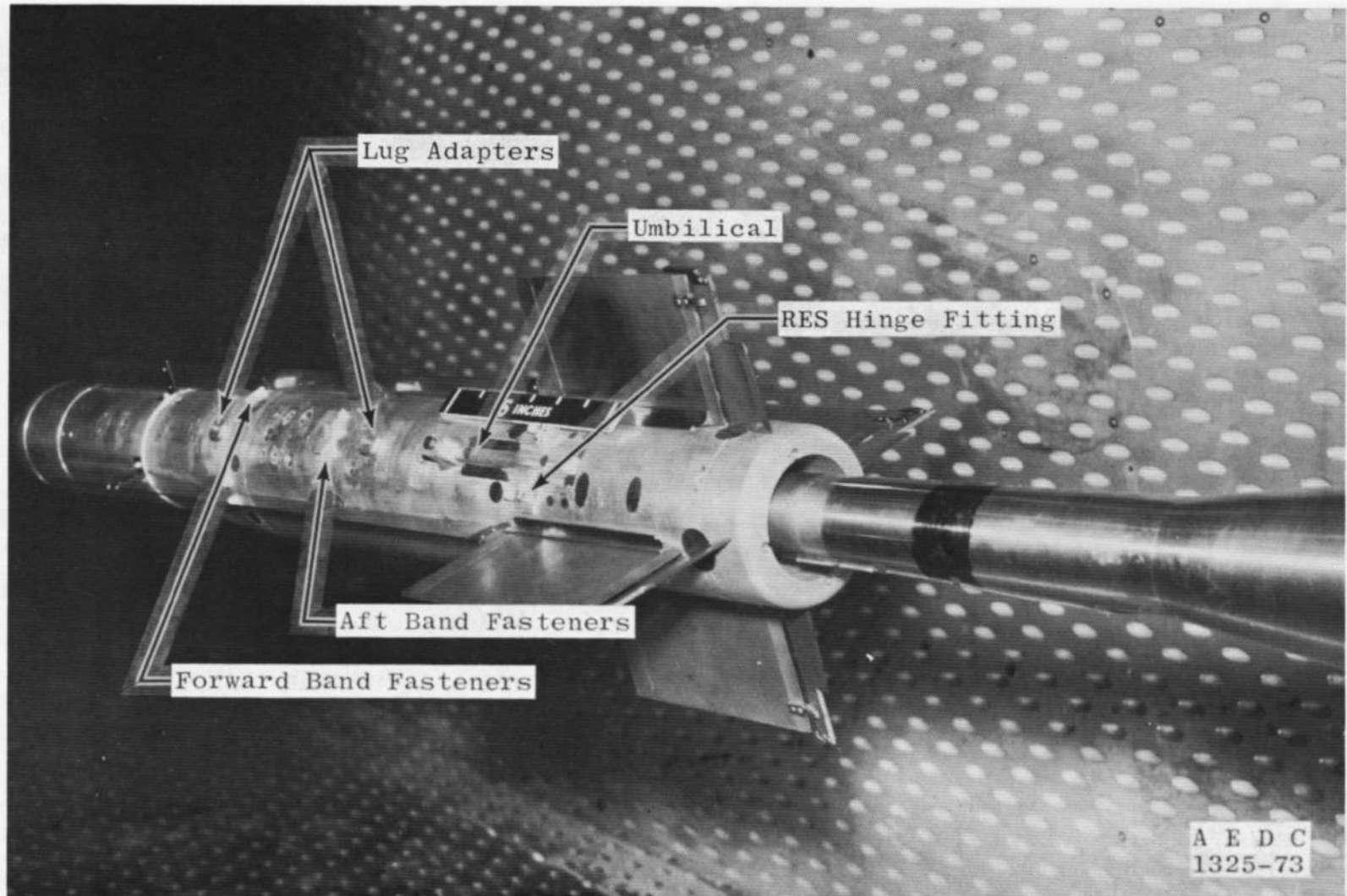


TYPICAL PERFORATED WALL CROSS SECTION

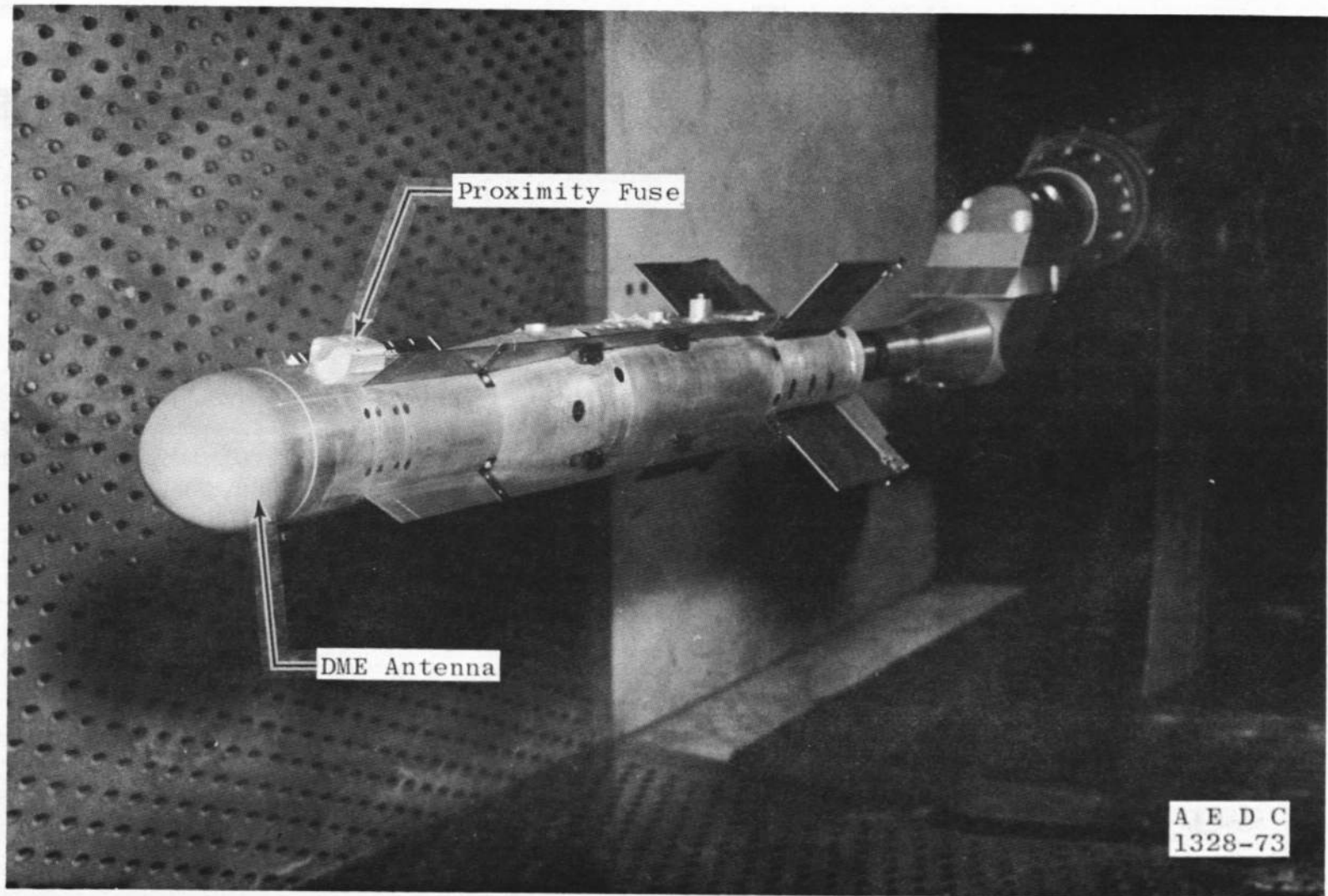


TUNNEL STATIONS AND DIMENSIONS IN INCHES

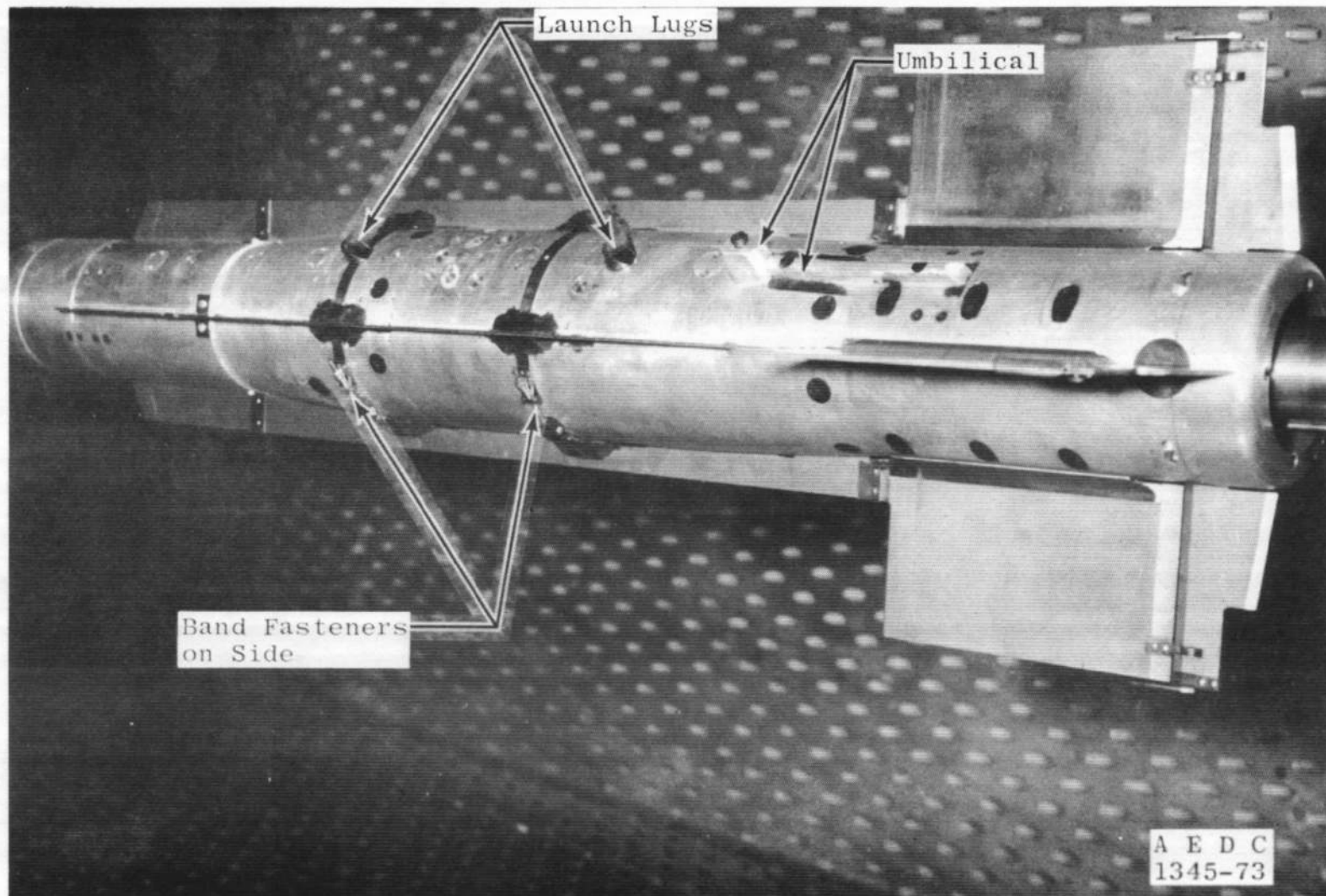
Fig. 1 Sketch of the Model Installation



a. MGGB Configuration without RES (B9T3)
Fig. 2 Installation Photographs



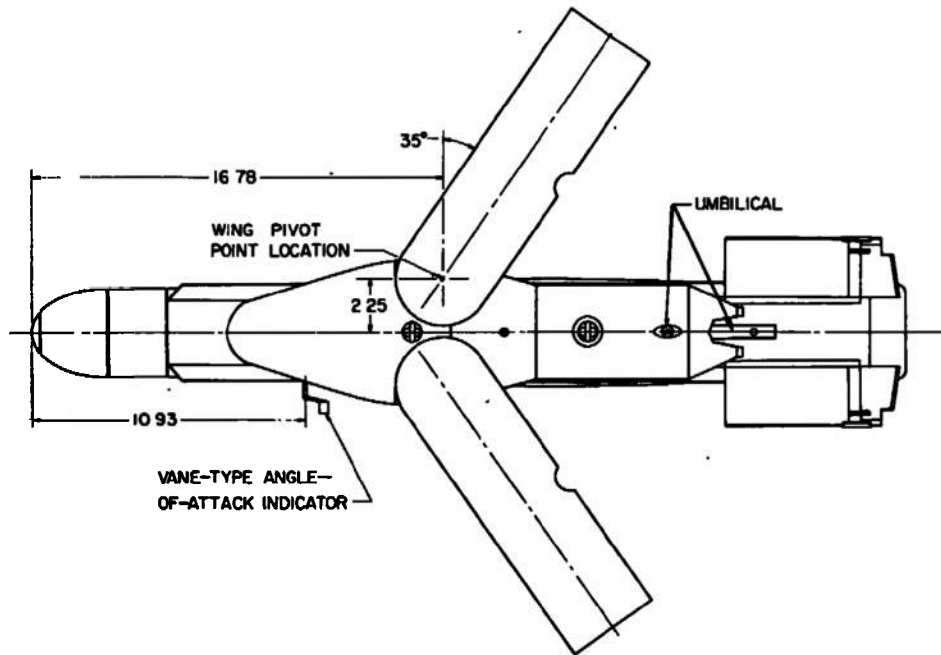
b. MGGB Configuration without the RES but with Proximity Fuse (B10T3)
Fig. 2 Continued



c. MK-84 HOBOS Configuration (B11T3)
Fig. 2 Continued



d. MGGB Configuration (B9W8S1T3)
Fig. 2 Concluded



ALL DIMENSIONS IN INCHES

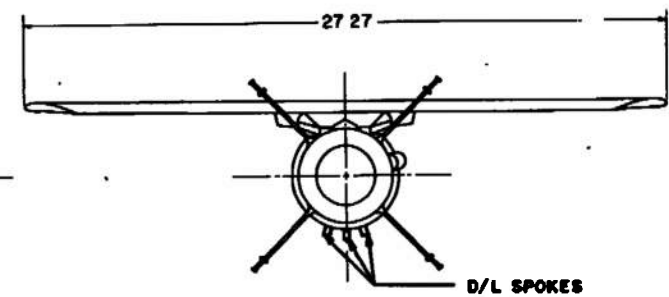
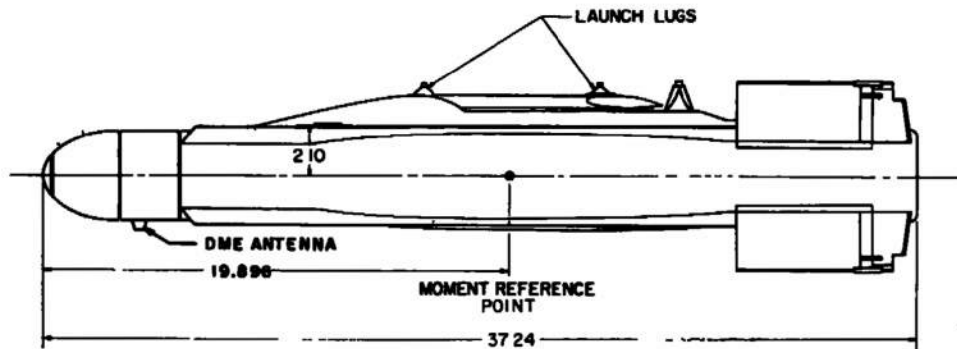


Fig. 3 Dimensional Sketch of MGGB (Configuration B9W8S1T3)

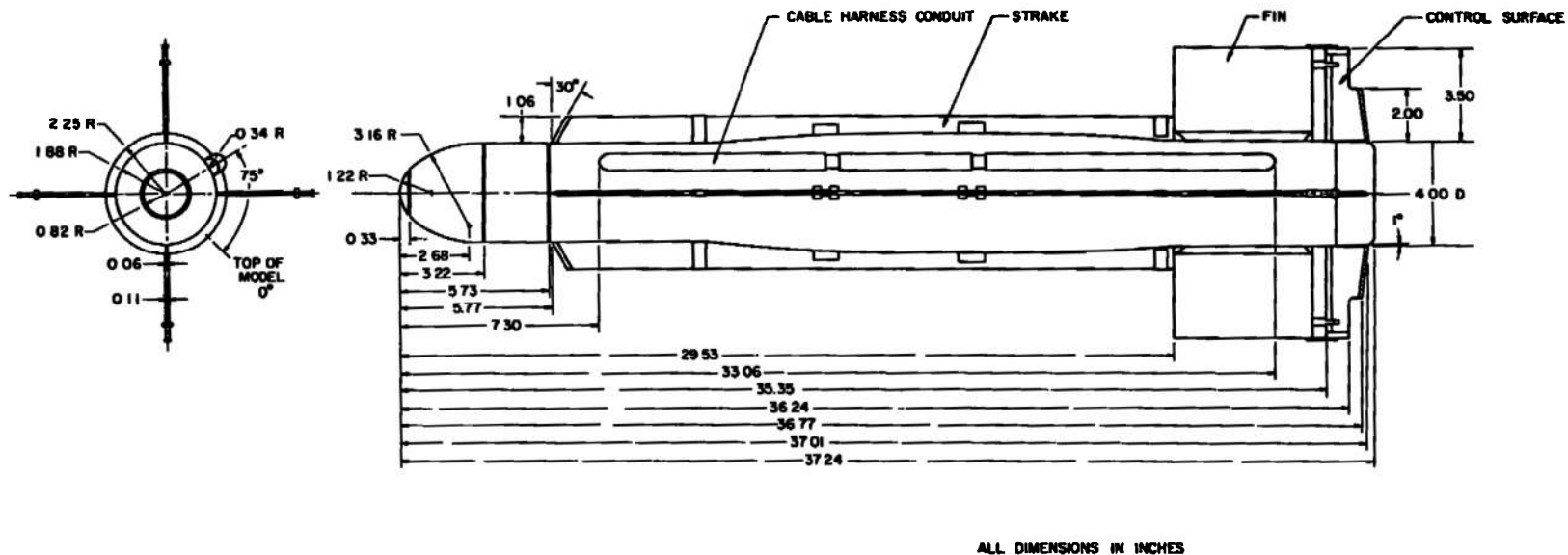
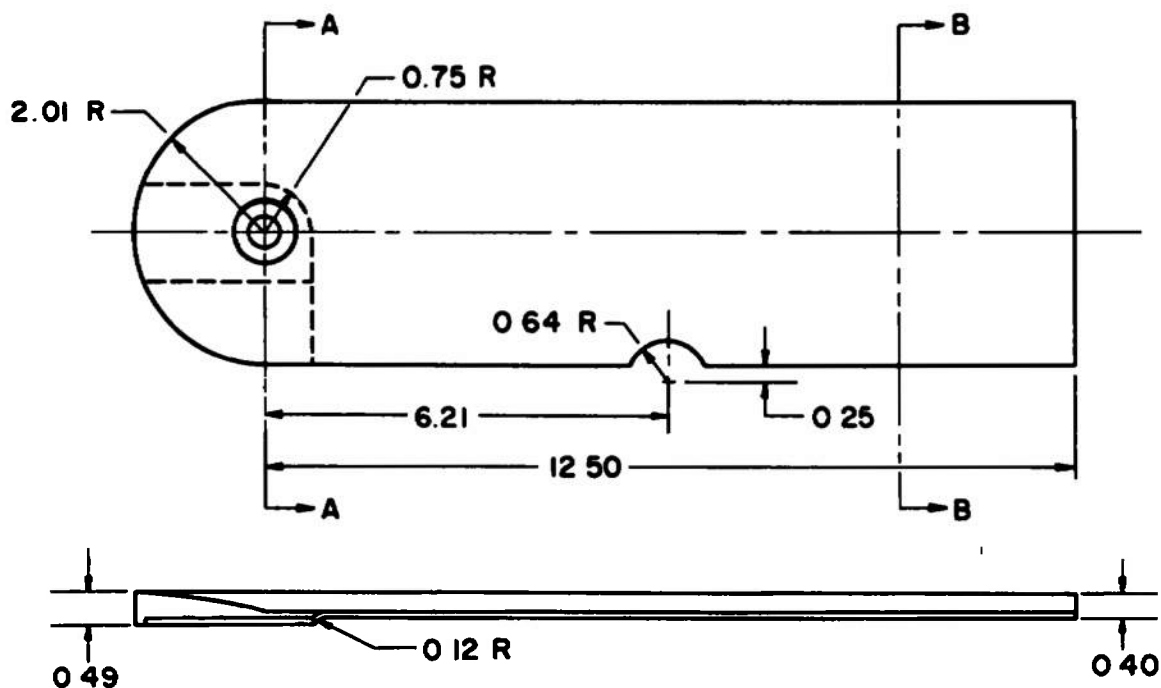
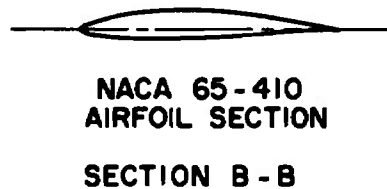
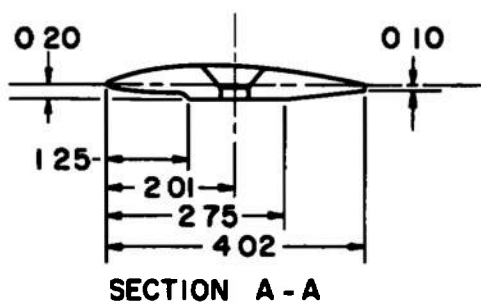


Fig. 4 Dimensional Sketch of the MK-84 HOBOS (Configuration B11T3)



W 8



ALL DIMENSIONS IN INCHES

Fig. 5 Dimensional Sketch of the Wing Configuration (W8)

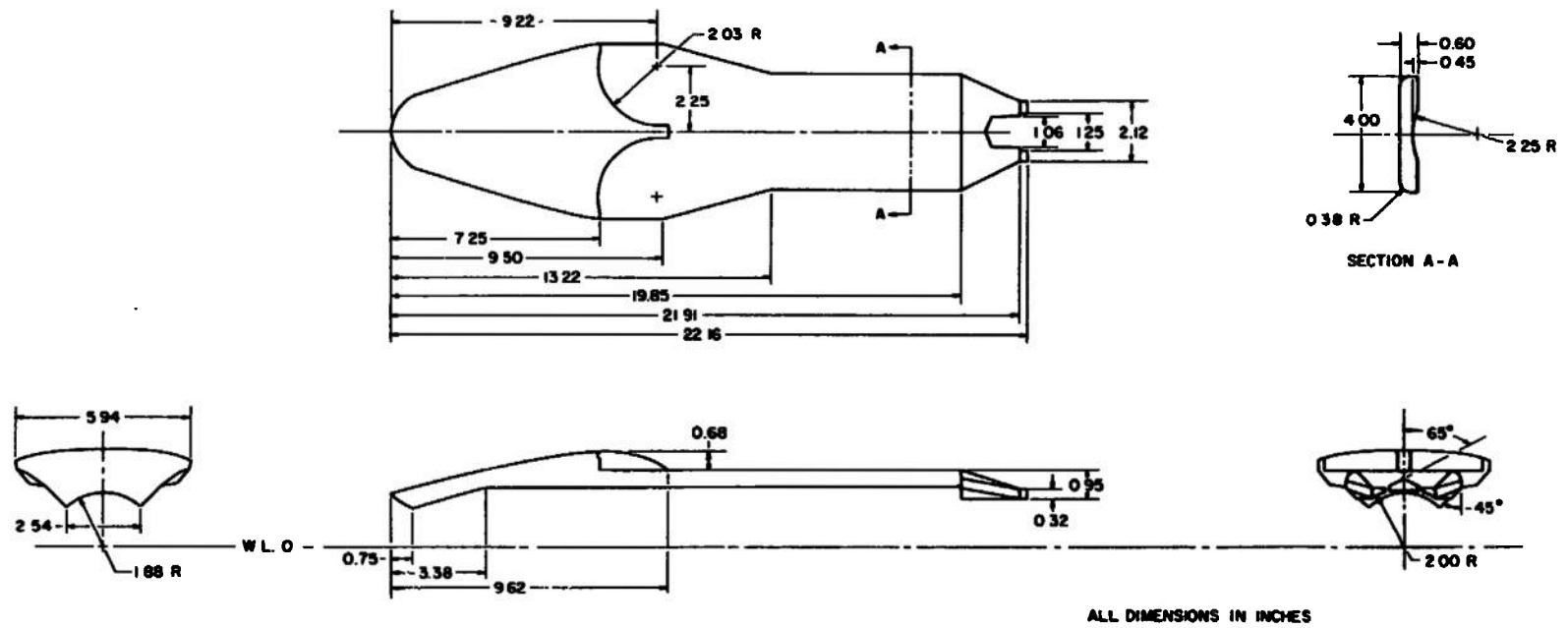


Fig. 6 Dimensional Sketch of the Strongback Configuration (S1)

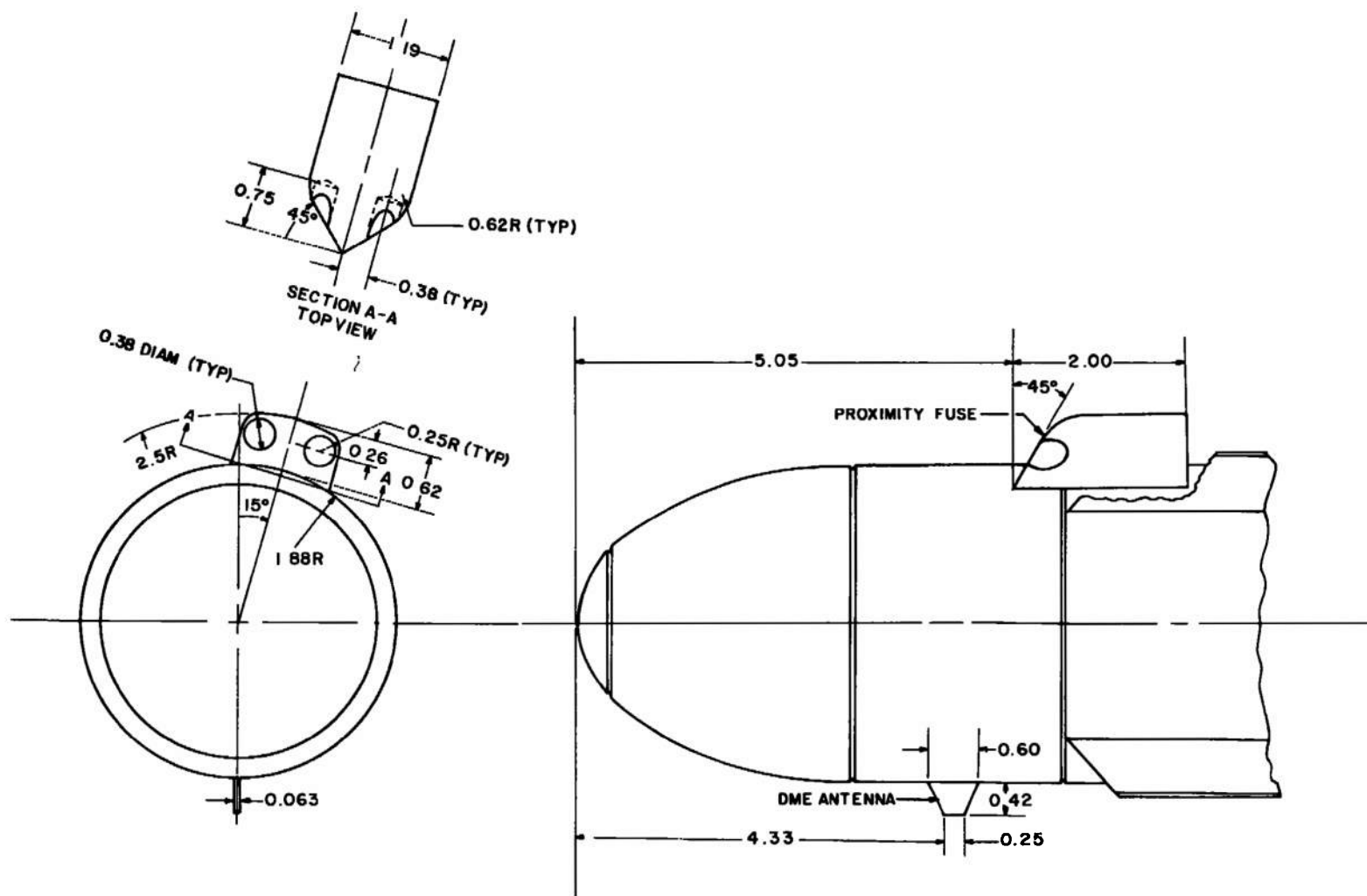


Fig. 7 Dimensional Sketch of the Proximity Fuse and DME Antenna Showing Their Location on the Model

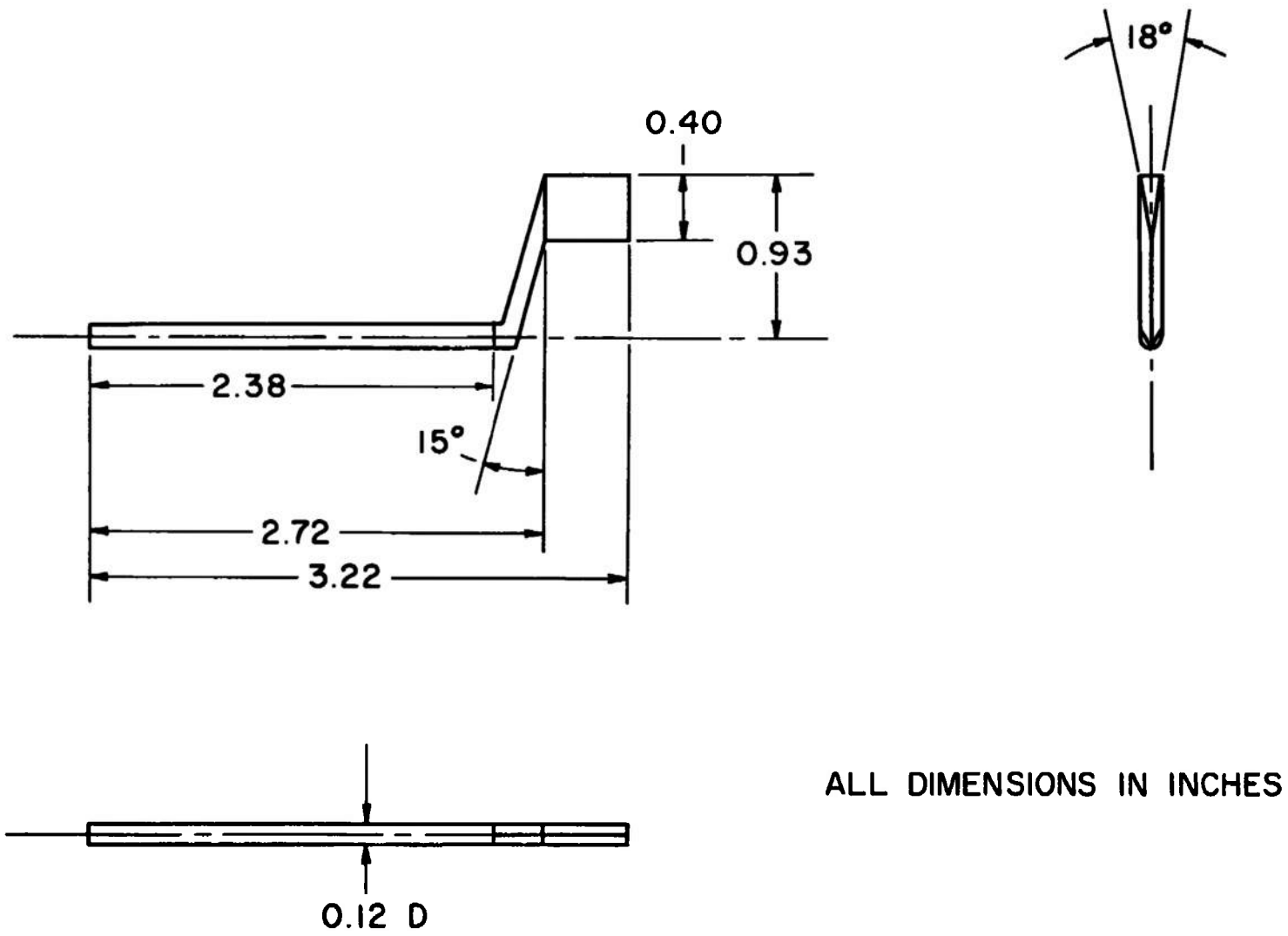


Fig. 8 Dimensional Sketch of the Vane-Type Angle-of-Attack Indicator

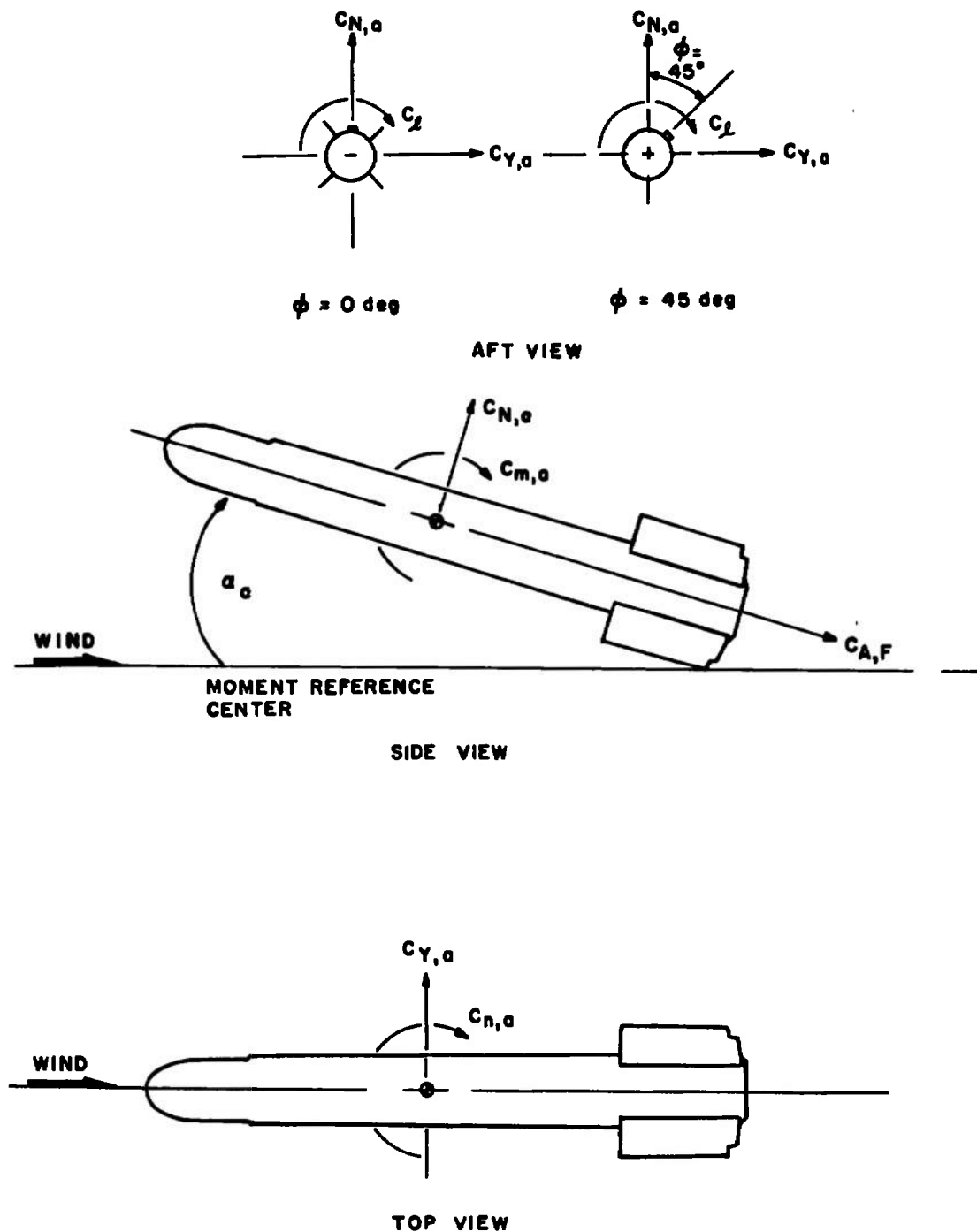


Fig. 9 Orientation of Model Forces and Moments

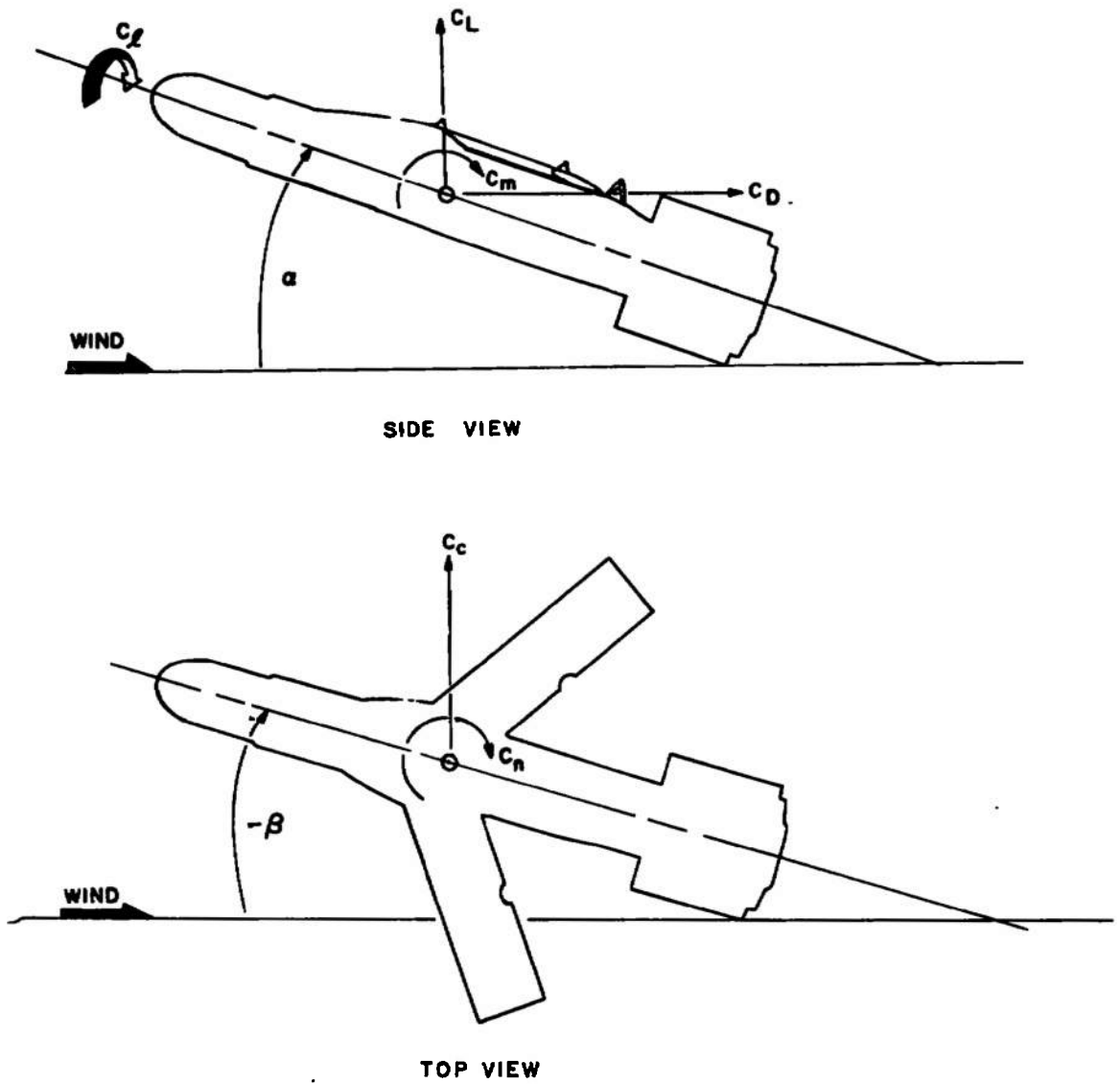


Fig. 9 Concluded

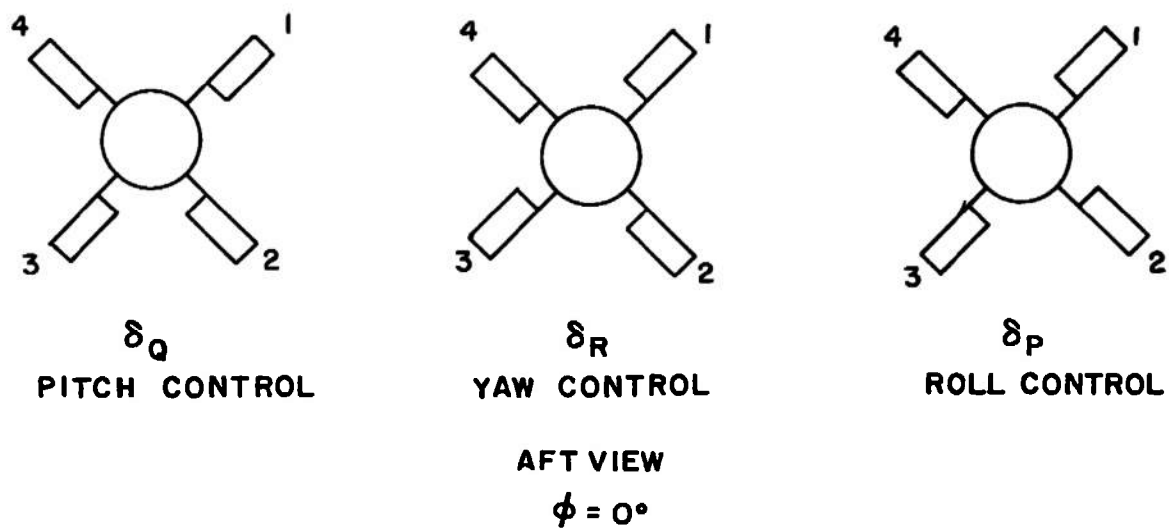


Fig. 10 Orientation of Control Surface Deflections

EFFECT OF REYNOLDS NUMBER NORMAL FORCE AND PITCHING MOMENT COEFFICIENTS							
SYMBOL	CONFIG	MACH NO	•	b_0	b_n	b_p	$R_E \times 10^{-5}$
□	B9T3	0.65	0	0.3	0.5	0.3	5.4
○	B9T3	0.65	0	0.3	0.5	0.3	1.8
△	B9T3	0.65	0	-20.5	0.2	-0.1	5.4
◇	B9T3	0.65	0	-20.5	0.2	-0.1	1.8

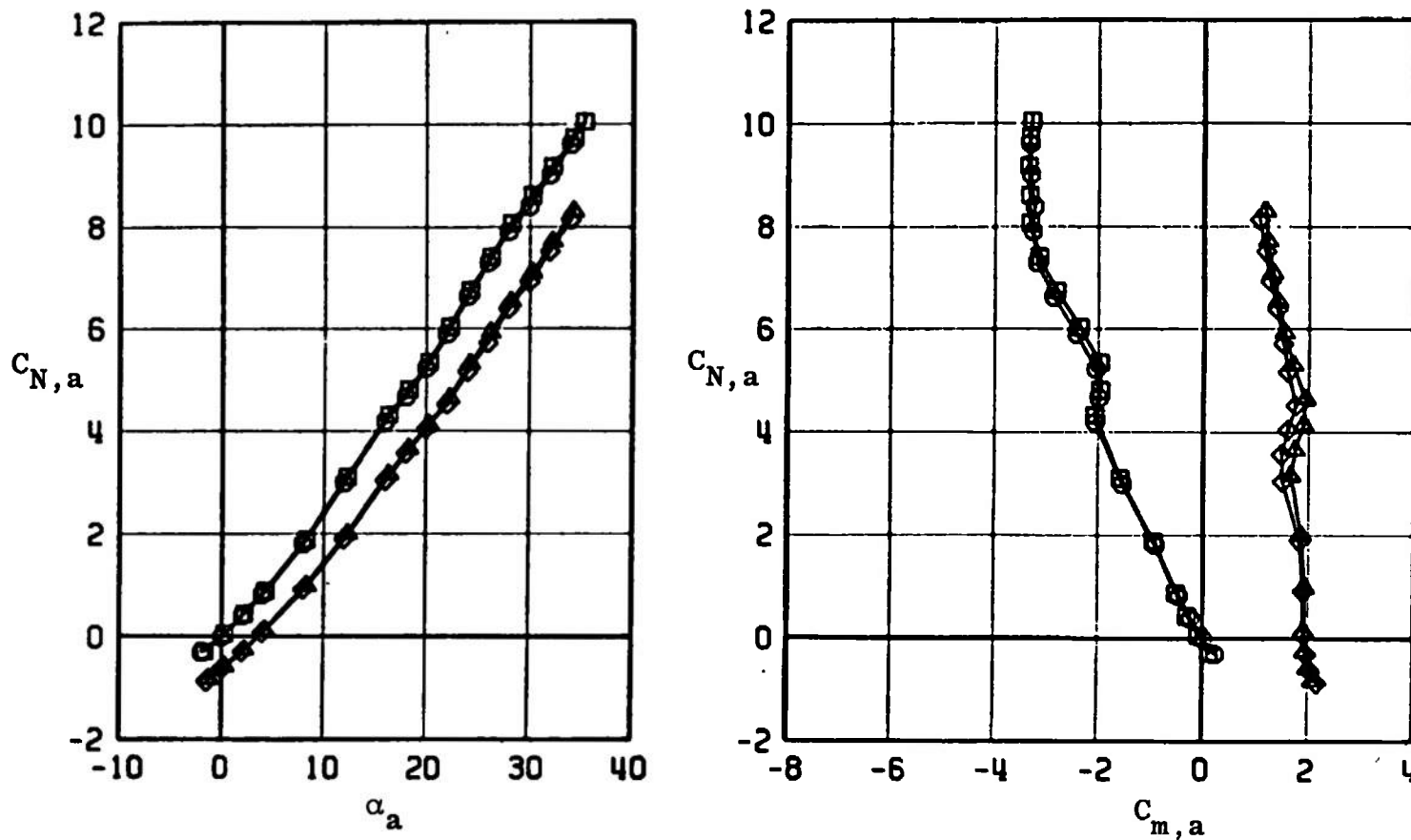


Fig. 11 Effect of Varying Reynolds Number on the Normal-Force and Pitching-Moment Coefficients for the MGBB Configuration without the RES (B9T3)

EFFECT OF REYNOLDS NUMBER NORMAL FORCE AND PITCHING MOMENT COEFFICIENTS							
SYMBOL	CONFIG	MACH NO	ϕ	δ_D	δ_H	δ_T	$R_E \times 10^{-6}$
\square	B9T3	0.95	0	0.3	0.5	0.3	5.6
\circ	B9T3	0.95	0	0.3	0.5	0.3	2.2
\triangle	B9T3	0.95	0	-20.5	0.2	-0.1	5.6
\diamond	B9T3	0.95	0	-20.5	0.2	-0.1	2.2

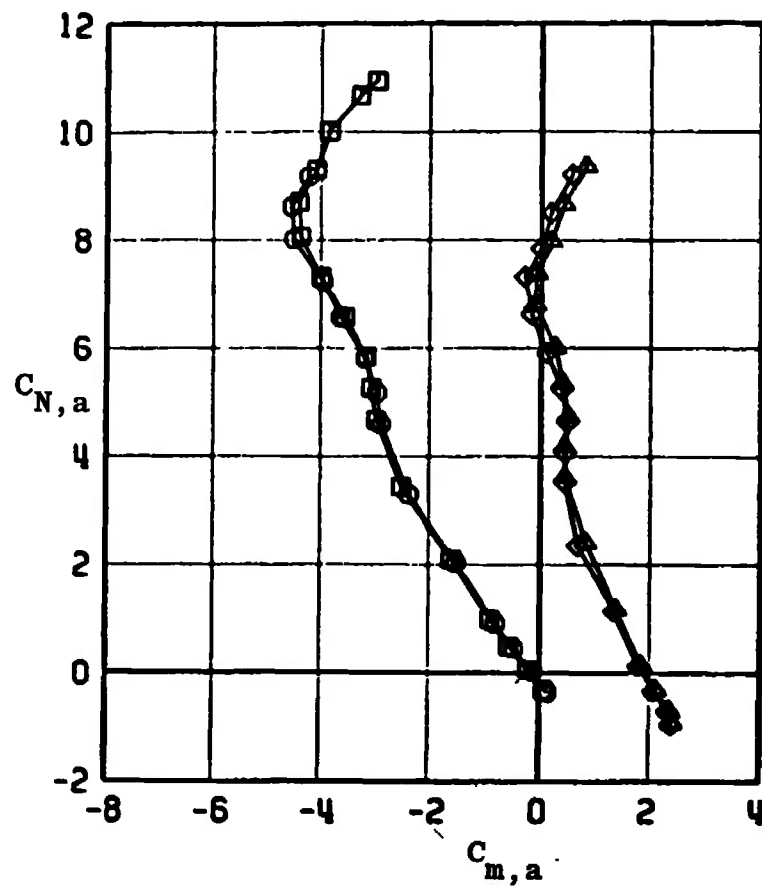
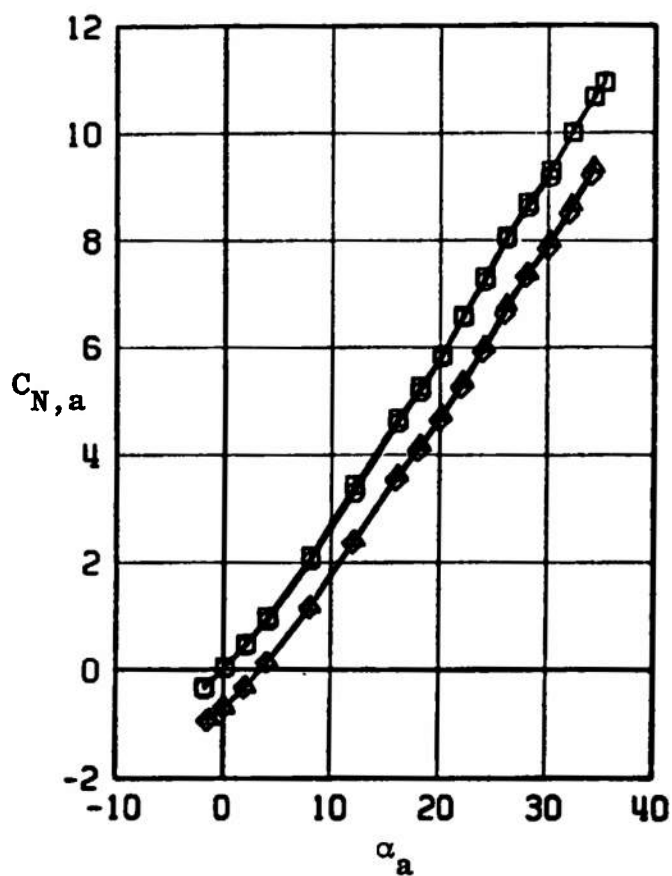


Fig. 11 Concluded

EFFECT OF REYNOLDS NUMBER ROLLING MOMENT AND AXIAL FORCE COEFFICIENTS							
SYMBOL	CONFIG	MACH NO	ϕ	δ_0	δ_R	δ_P	$R_E \times 10^{-6}$
□	B9T3	0.65	0	0.3	0.5	0.3	5.4
○	B9T3	0.65	0	0.3	0.5	0.3	1.8
△	B9T3	0.65	0	-20.5	0.2	-0.1	5.4
◇	B9T3	0.65	0	-20.5	0.2	-0.1	1.8

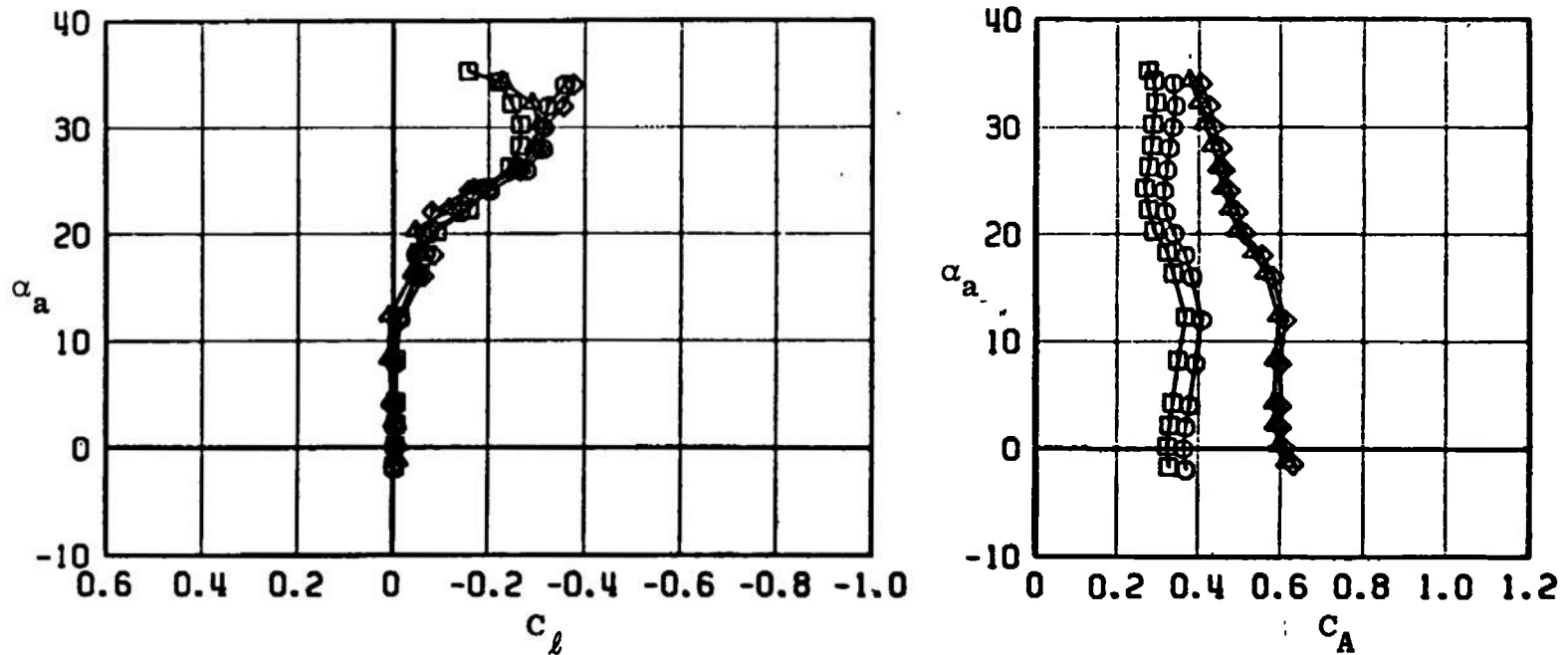


Fig. 12 Effect of Varying Reynolds Number on the Rolling-Moment and Axial-Force Coefficients

EFFECT OF REYNOLDS NUMBER

ROLLING MOMENT AND AXIAL FORCE COEFFICIENTS

SYMBOL	CONFIG	MACH NO	ϕ	δ_0	δ_H	δ_P	$R_E \times 10^{-6}$
□	B9T3	0.95	0	0.3	0.5	0.3	5.6
○	B9T3	0.95	0	0.3	0.5	0.3	2.2
△	B9T3	0.95	0	-20.5	0.2	-0.1	5.6
◇	B9T3	0.95	0	-20.5	0.2	-0.1	2.2

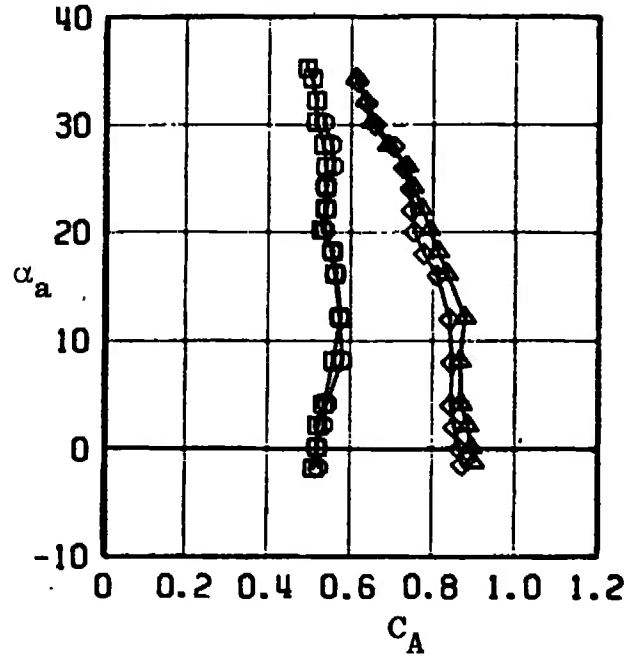
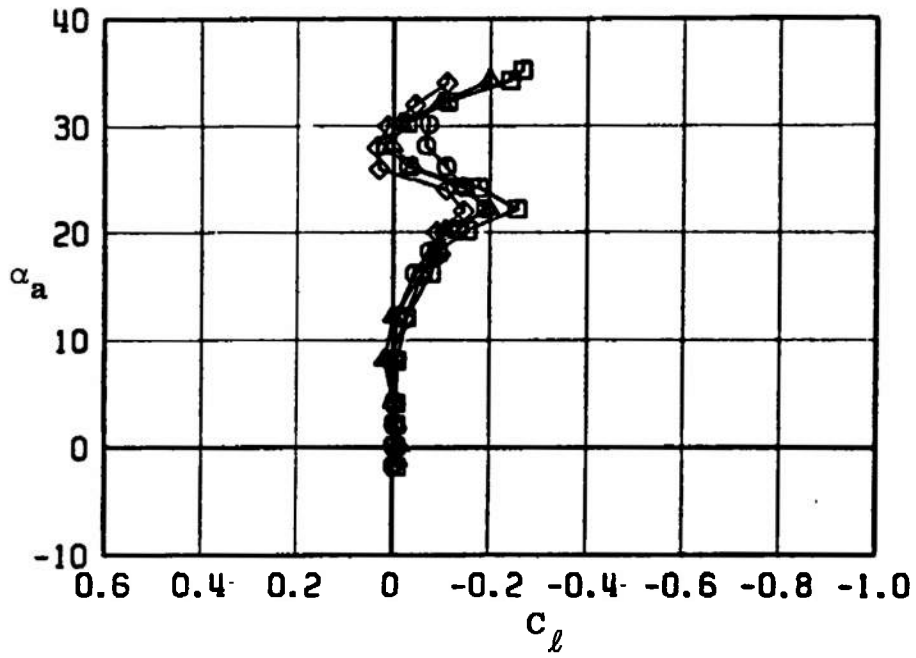


Fig. 12 Concluded

EFFECT OF REYNOLDS NUMBER
SIDE FORCE AND YAWING MOMENT COEFFICIENTS :

SYMBOL	CONFIG	MACH NO	ϕ	δ_a	δ_n	δ_p	$R_E \times 10^{-6}$
□	B9T3	0.65	0	0.3	0.5	0.3	5.4
○	B9T3	0.65	0	0.3	0.5	0.3	1.8
△	B9T3	0.65	0	-20.5	0.2	-0.1	5.4
◇	B9T3	0.65	0	-20.5	0.2	-0.1	1.8

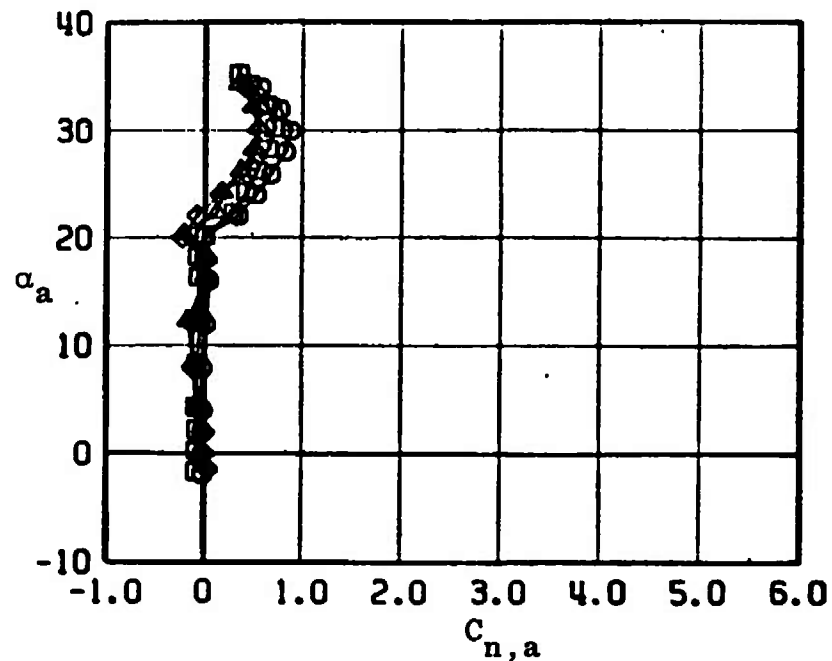
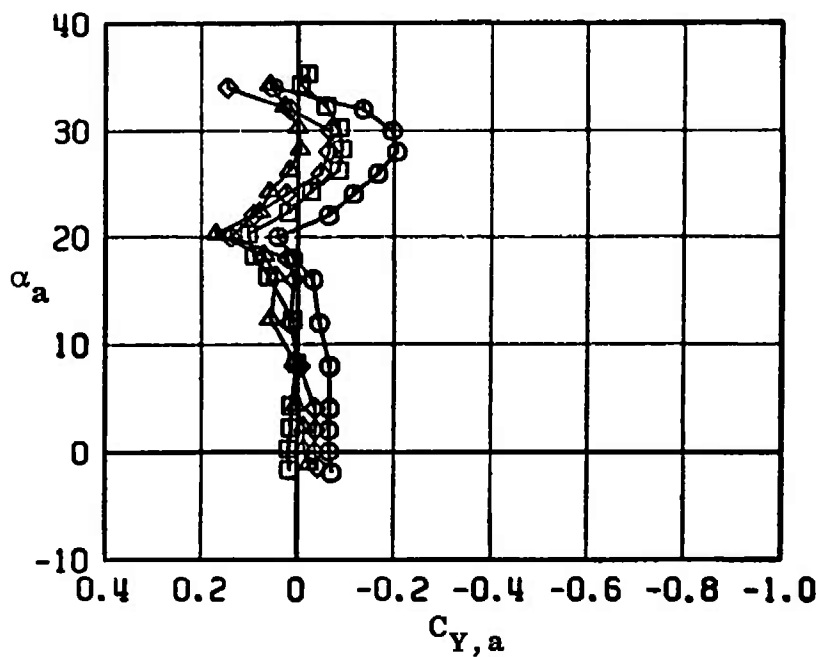


Fig. 13 Effect of Varying Reynolds Number on the Side-Force and Yawing-Moment Coefficients for Configuration B9T3

EFFECT OF REYNOLDS NUMBER
SIDE FORCE AND YAWING MOMENT COEFFICIENTS

SYMBOL	CONFIG	MACH NO	\bullet	b_0	b_n	b_p	$R_E \times 10^{-6}$
\square	B9T3	0.95	0	0.3	0.5	0.3	5.6
\circ	B9T3	0.95	0	0.3	0.5	0.3	2.2
\triangle	B9T3	0.95	0	-20.5	0.2	-0.1	5.6
\diamond	B9T3	0.95	0	-20.5	0.2	-0.1	2.2

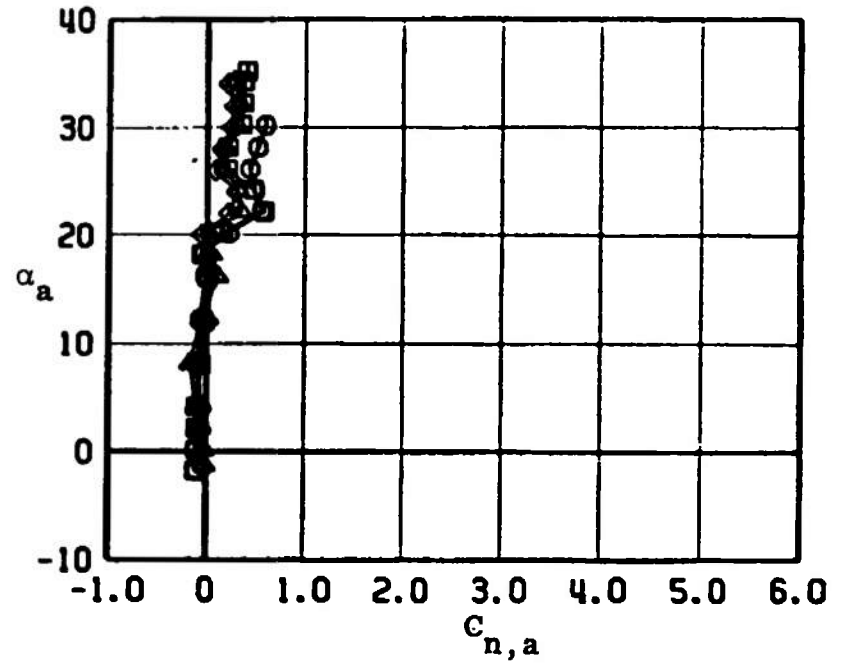
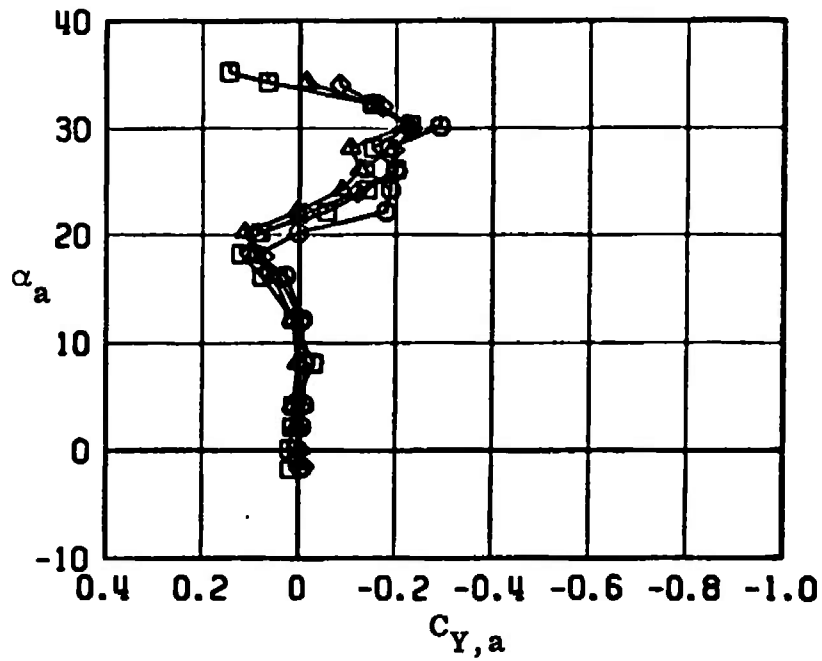


Fig. 13 Concluded

EFFECT OF REYNOLDS NUMBER							
MGG B LONGITUDINAL STABILITY CHARACTERISTICS							
SYMBOL	CONFIG	MACH NO	ϕ	δ_D	δ_H	δ_P	$R_E \times 10^{-6}$
□	B10W8S1T3	0.50	0	0.4	-0.3	0.5	4.8
○	B10W8S1T3	0.50	0	0.4	-0.3	0.5	1.5

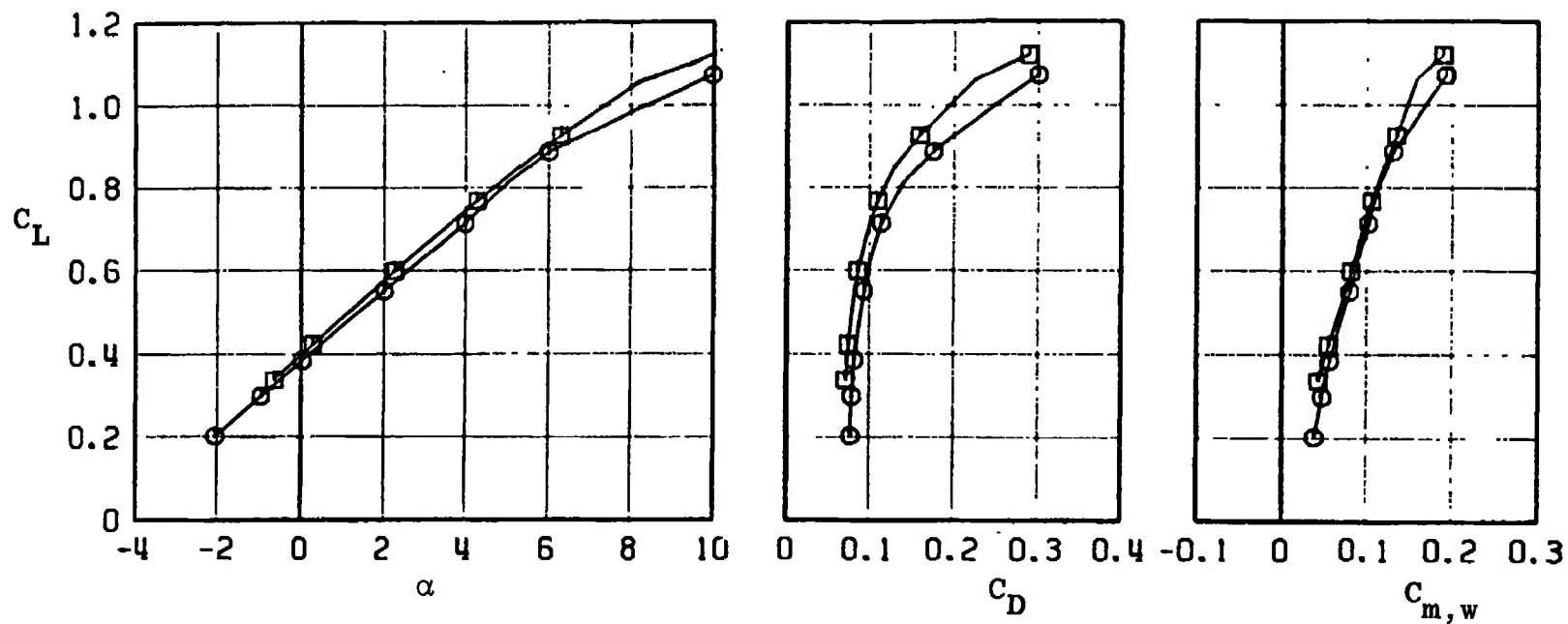


Fig. 14 Effect of Varying Reynolds Number on the Longitudinal Stability Characteristics of MGG B Configuration (B10W8S1T3)

EFFECT OF REYNOLDS NUMBER
 MGB LONGITUDINAL STABILITY CHARACTERISTICS

SYMBOL	CONFIG	MACH NO	ϕ	ξ_0	ξ_R	ξ_P	$R_E \times 10^{-6}$
\square	B10W8S1T3	0.60	0	0.4	-0.3	0.5	5.2
\circ	B10W8S1T3	0.60	0	0.4	-0.3	0.5	1.7

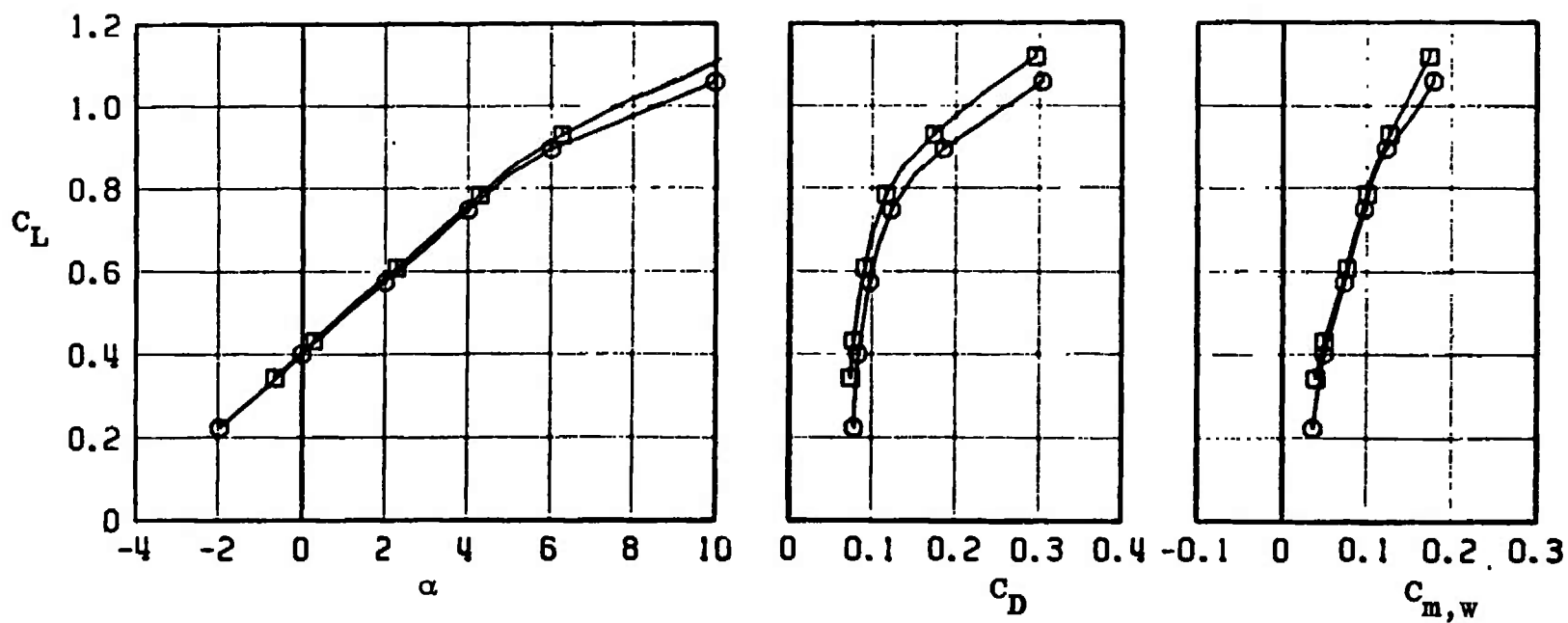


Fig. 14 Continued

EFFECT OF REYNOLDS NUMBER
MGGB LONGITUDINAL STABILITY CHARACTERISTICS

SYMBOL	CONFIG	MACH NO	ϵ	ϵ_D	ϵ_H	ϵ_P	$R_E \times 10^{-6}$
\square	B10W8S1T3	0.75	0	0.4	-0.3	0.5	5.8
\circ	B10W8S1T3	0.75	0	0.4	-0.3	0.5	2.0

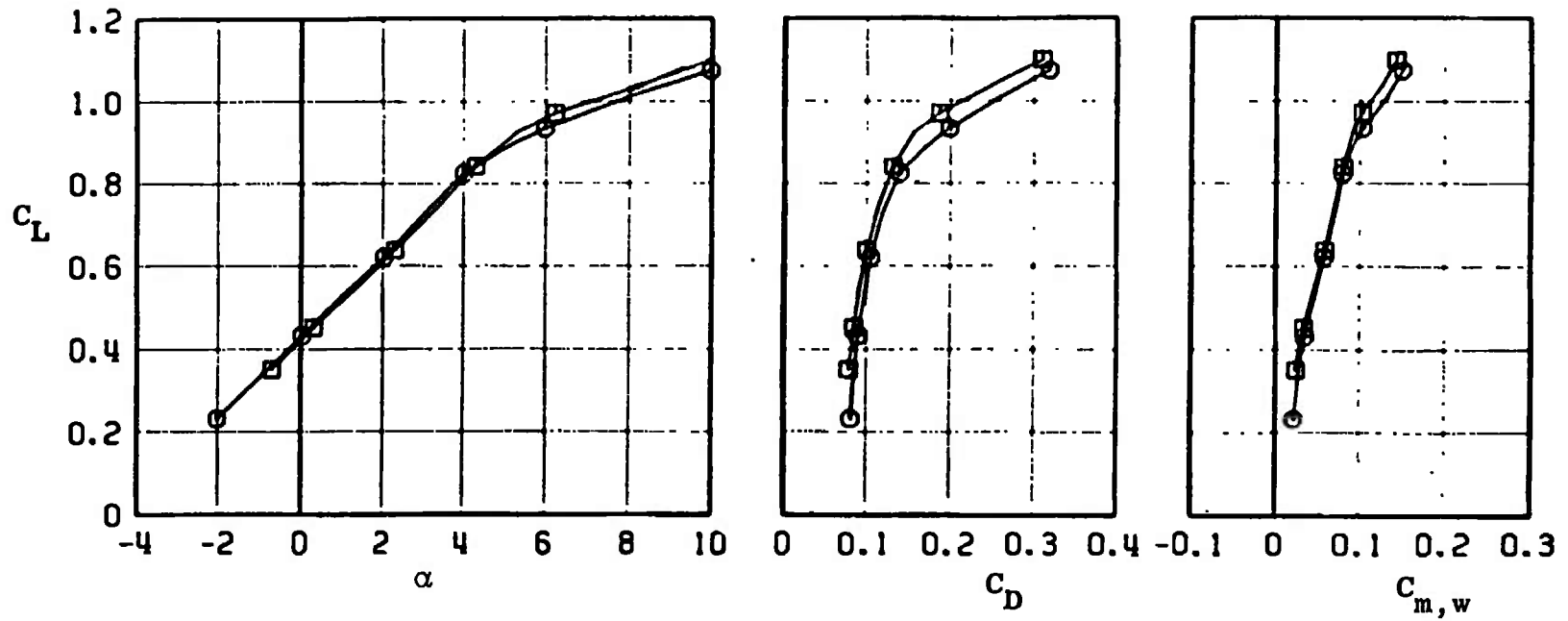


Fig. 14 Continued

EFFECT OF REYNOLDS NUMBER

MGGB LONGITUDINAL STABILITY CHARACTERISTICS

SYMBOL	CONFIG	MACH NO	ϕ	δ_0	δ_n	δ_p	$R_E \times 10^{-6}$
\square	B10W8S1T3	0.85	0	0.4	-0.3	0.5	6.0
\circ	B10W8S1T3	0.85	0	0.4	-0.3	0.5	2.1

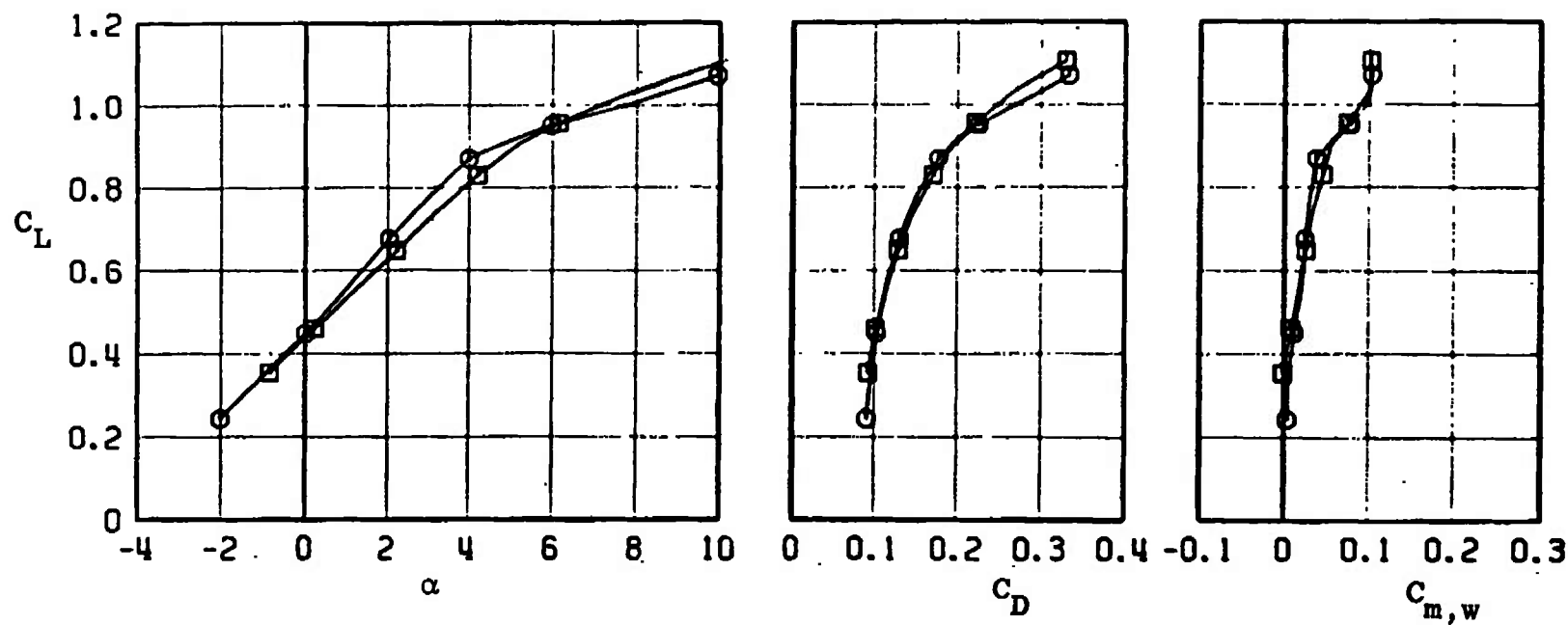


Fig. 14 Continued

EFFECT OF REYNOLDS NUMBER							
MGBB LONGITUDINAL STABILITY CHARACTERISTICS							
SYMBOL	CONFIG	MACH NO	ϕ	b_0	b_R	b_p	$R_E \times 10^{-6}$
\square	B10W8S1T3	0.95	0	0.4	-0.3	0.5	5.6
\circ	B10W8S1T3	0.95	0	0.4	-0.3	0.5	2.2

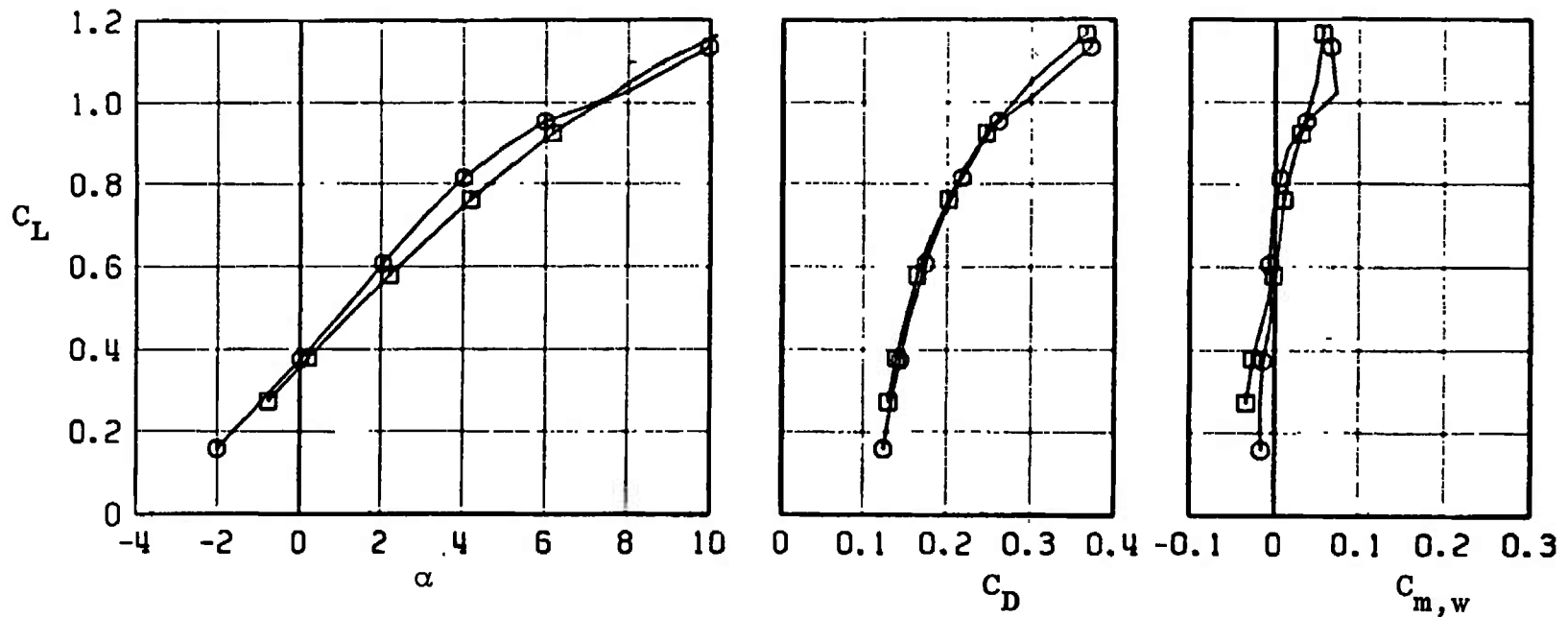


Fig. 14 Concluded

EFFECT OF REYNOLDS NUMBER

MGGB L/D CHARACTERISTICS

SYMBOL	CONFIG	MACH NO	θ	δ_0	δ_R	δ_P	$R_E \times 10^{-6}$
\square	B10W8S1T3	0.50	0	0.4	-0.3	0.5	4.8
\circ	B10W8S1T3	0.50	0	0.4	-0.3	0.5	1.5

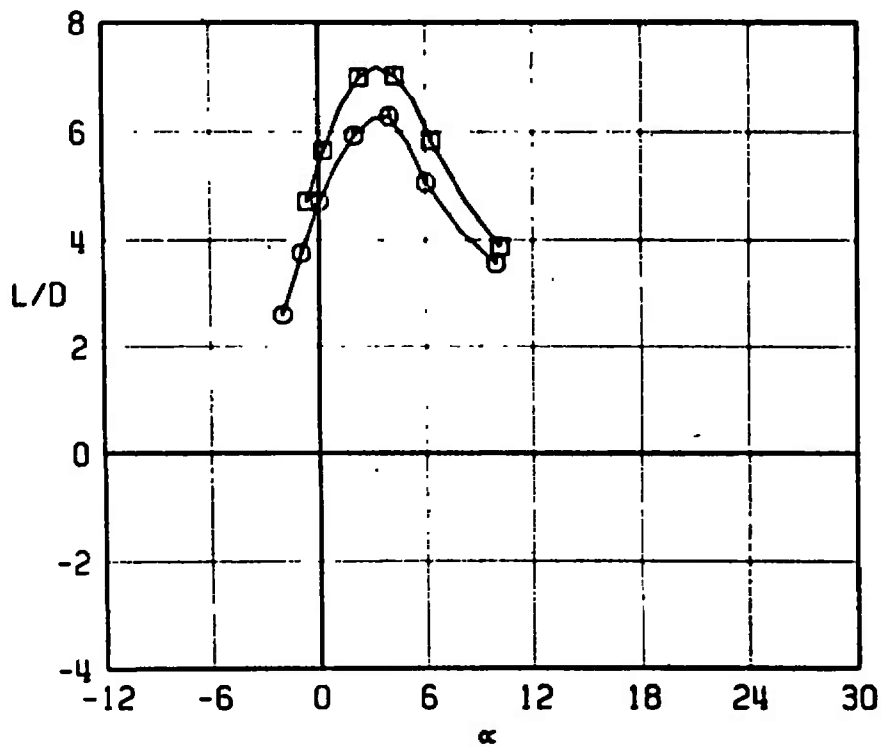


Fig. 15 Effect of Varying Reynolds Number on the Lift to Drag Ratio of MGGB Configuration (B10W8S1T3)

EFFECT OF REYNOLDS NUMBER

MGG8 L/D CHARACTERISTICS

SYMBOL	CONFIG	MACH NO	ϵ	ϵ_0	ϵ_n	ϵ_p	$R_L \times 10^{-6}$
\square	B10W8S1T3	0.60	0	0.4	-0.3	0.5	5.2
\circ	B10W8S1T3	0.60	0	0.4	-0.3	0.5	1.7

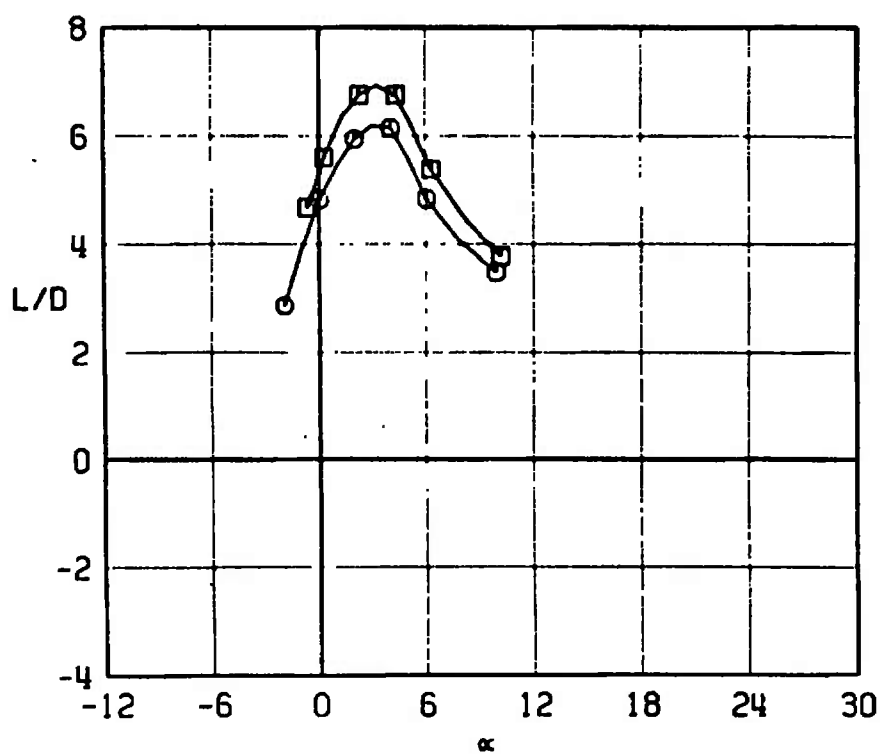


Fig. 15 Continued

EFFECT OF REYNOLDS NUMBER

MGGB L/D CHARACTERISTICS

SYMBOL	CONFIG	MACH NO	●	ϵ_0	ϵ_H	ϵ_P	$R_E \times 10^{-6}$
□	B10W8S1T3	0.75	0	0.4	-0.3	0.5	5.8
○	B10W8S1T3	0.75	0	0.4	-0.3	0.5	2.0

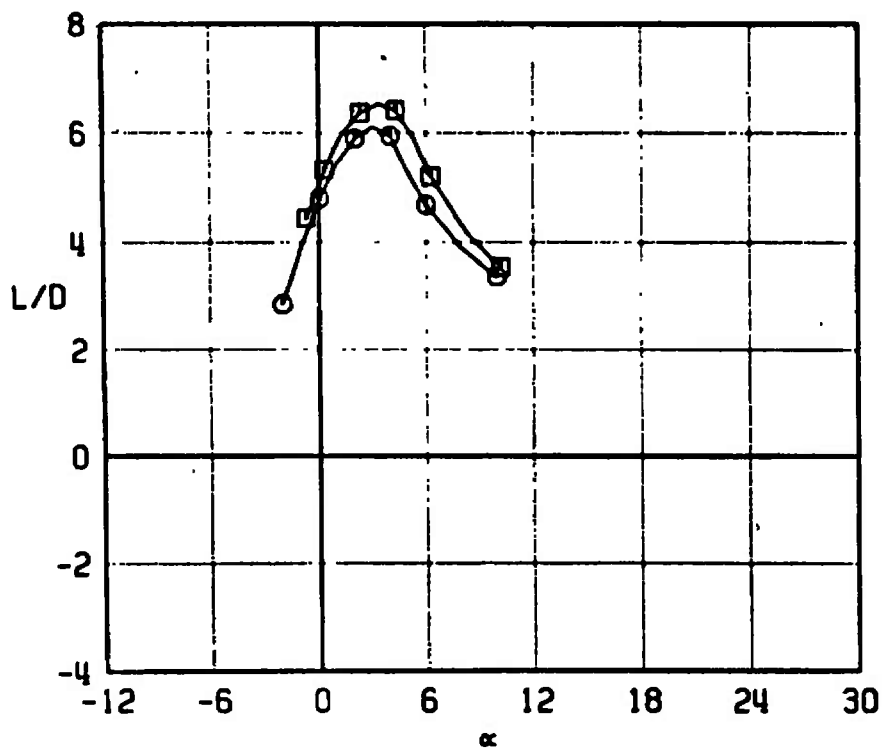


Fig. 15 Continued

EFFECT OF REYNOLDS NUMBER

MGGB L/D CHARACTERISTICS

SYMBOL	CONFIG	MACH NO	ϕ	δ_0	δ_R	δ_P	$R_E \times 10^{-6}$
\square	B10W8S1T3	0.85	0	0.4	-0.3	0.5	6.0
\circ	B10W8S1T3	0.85	0	0.4	-0.3	0.5	2.1

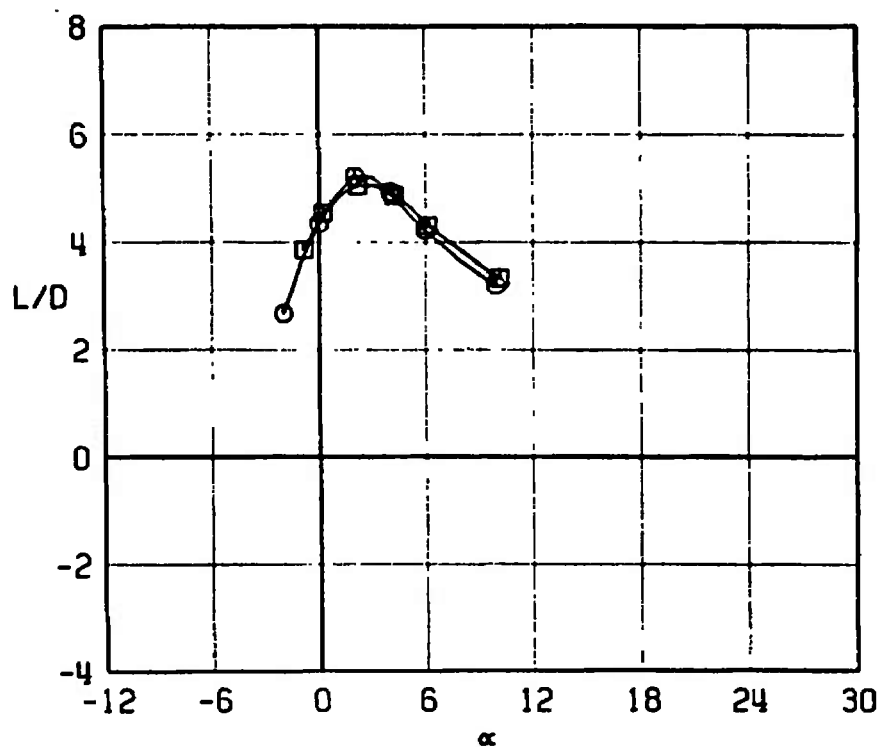


Fig. 15 Continued

EFFECT OF REYNOLDS NUMBER

MGGB L/D CHARACTERISTICS

SYMBOL	CONFIG	MACH NO	ϕ	δ_D	δ_H	δ_P	$R_E \times 10^{-6}$
\square	B10W8S1T3	0.95	0	0.4	-0.3	0.5	5.6
\odot	B10W8S1T3	0.95	0	0.4	-0.3	0.5	2.2

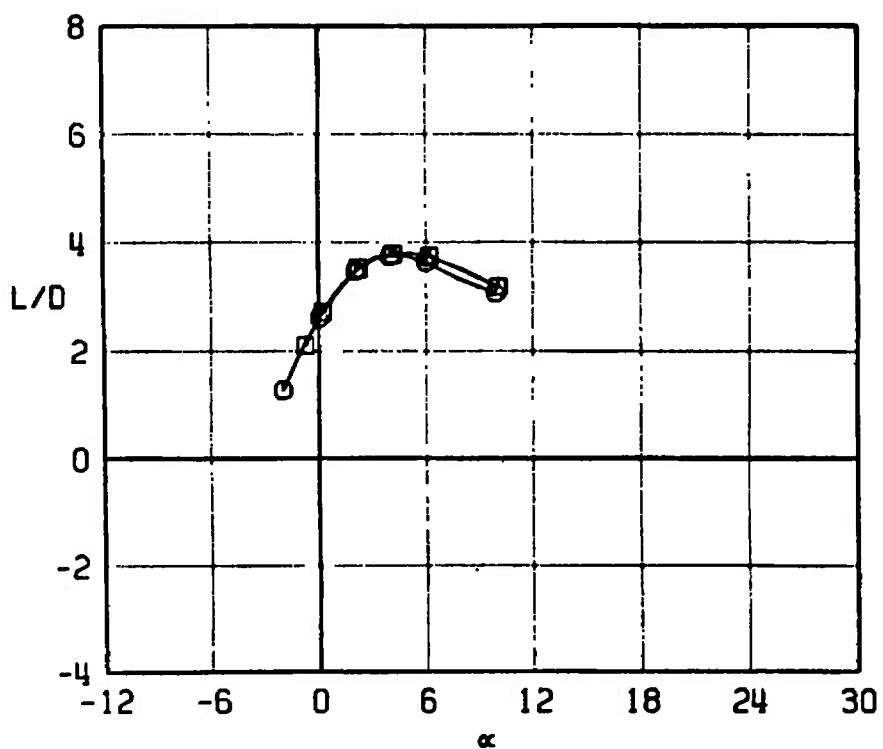


Fig. 15 Concluded

EFFECT OF ROLL ANGLE							
NORMAL FORCE AND PITCHING MOMENT COEFFICIENTS							
SYMBOL	CONFIG	MACH NO	ϕ	ϵ_a	ϵ_n	ϵ_p	$R_L \times 10^{-6}$
\square	B10T3	0.50	0.0	0.4	-0.3	0.5	4.8
\circ	B10T3	0.50	22.5	0.4	-0.3	0.5	4.8
\triangle	B10T3	0.50	45.0	0.4	-0.3	0.5	4.8
\diamond	B10T3	0.50	180.0	0.4	-0.3	0.5	4.8

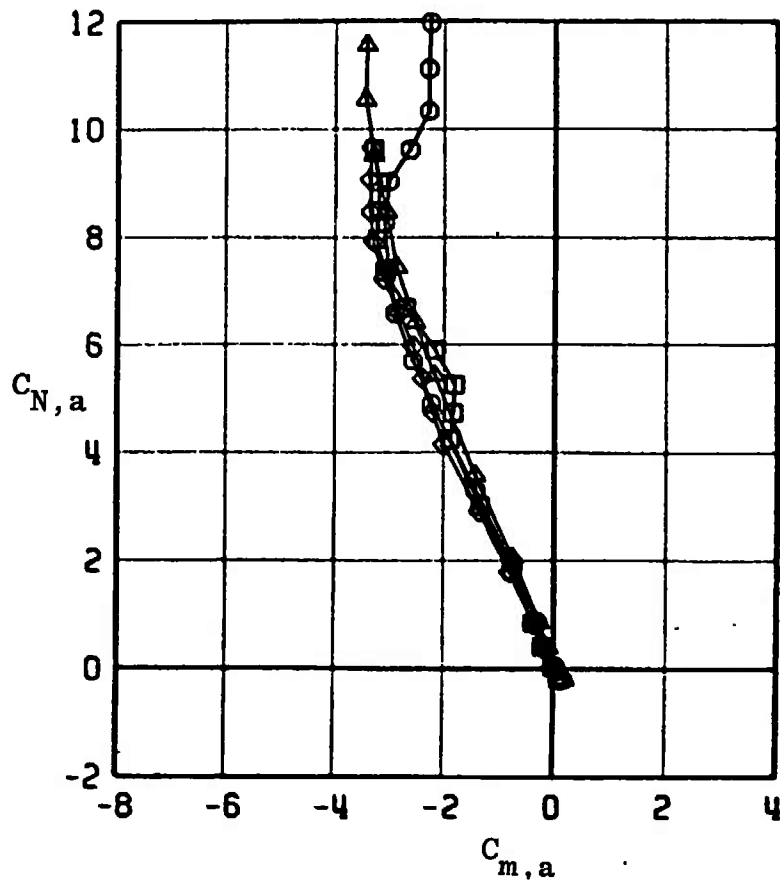
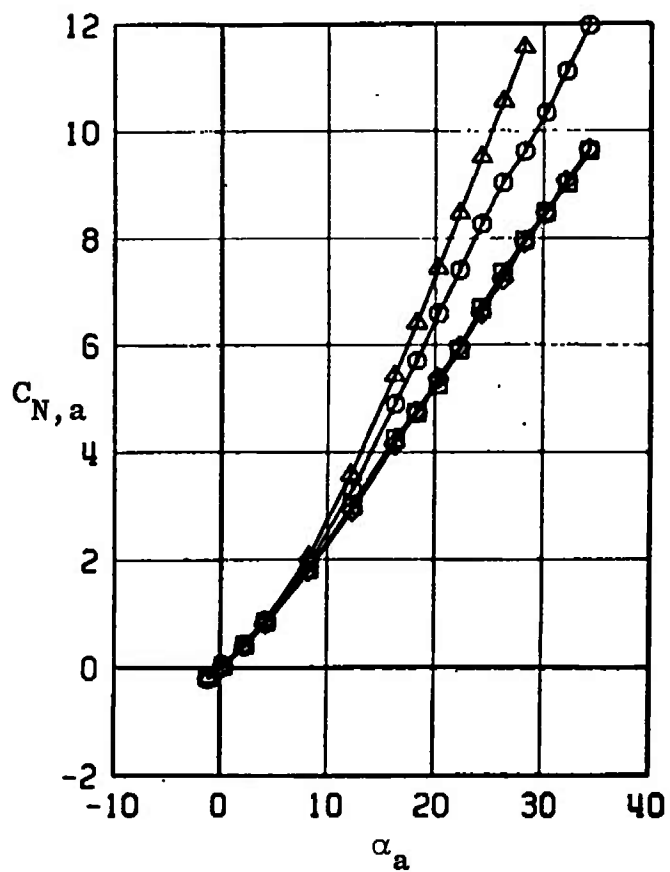


Fig. 16 Effect of Varying Roll Angle on the Normal-Force and Pitching-Moment Coefficients for MGB Configuration without the RES (B10T3)

EFFECT OF ROLL ANGLE							
NORMAL FORCE AND PITCHING MOMENT COEFFICIENTS							
SYMBOL	CONFIG	MACH NO	ϕ	δ_D	δ_R	δ_P	$R_F \times 10^{-6}$
\square	B10T3	0.65	0.0	0.4	-0.3	0.5	5.4
\circ	B10T3	0.65	22.5	0.4	-0.3	0.5	5.4
\triangle	B10T3	0.65	45.0	0.4	-0.3	0.5	3.9
\diamond	B10T3	0.65	180.0	0.4	-0.3	0.5	5.4

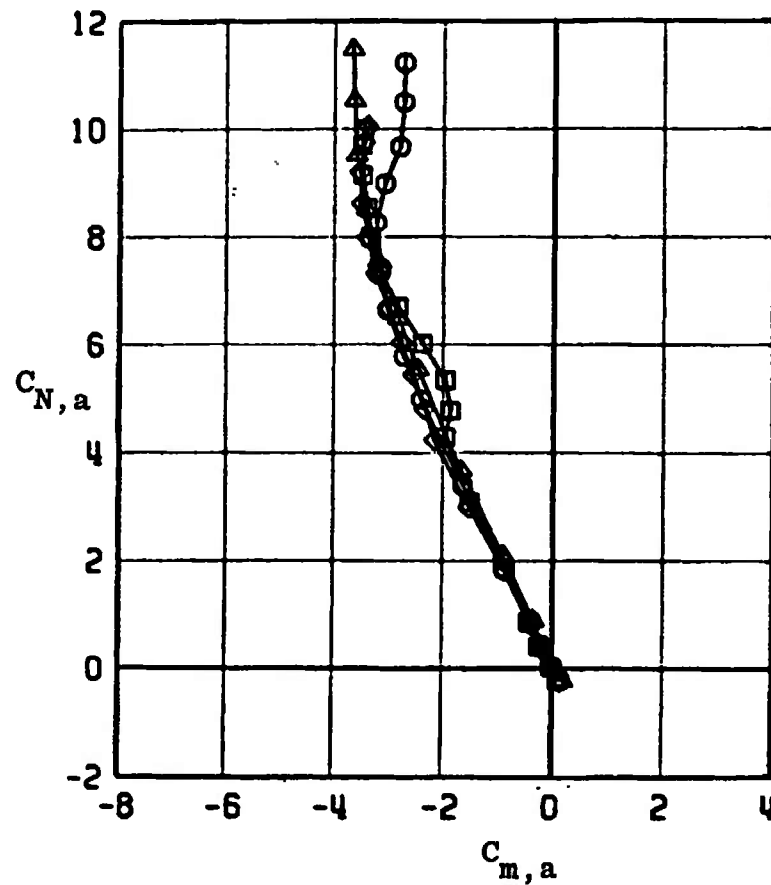
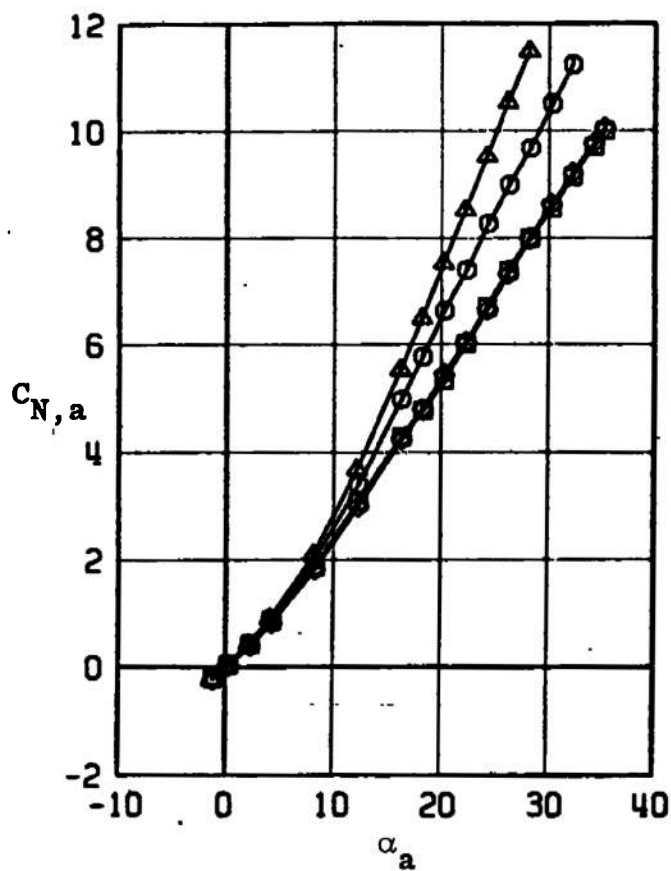


Fig. 16 Continued

EFFECT OF ROLL ANGLE

NORMAL FORCE AND PITCHING MOMENT COEFFICIENTS

SYMBOL	CONFIG	MACH NO	ϕ	ϵ_D	ϵ_H	ϵ_P	$R_E \times 10^{-5}$
\square	BIOT3	0.75	0.0	0.4	-0.3	0.5	5.8
\circ	BIOT3	0.75	22.5	0.4	-0.3	0.5	5.8
\triangle	BIOT3	0.75	45.0	0.4	-0.3	0.5	3.6
\diamond	BIOT3	0.75	180.0	0.4	-0.3	0.5	5.8

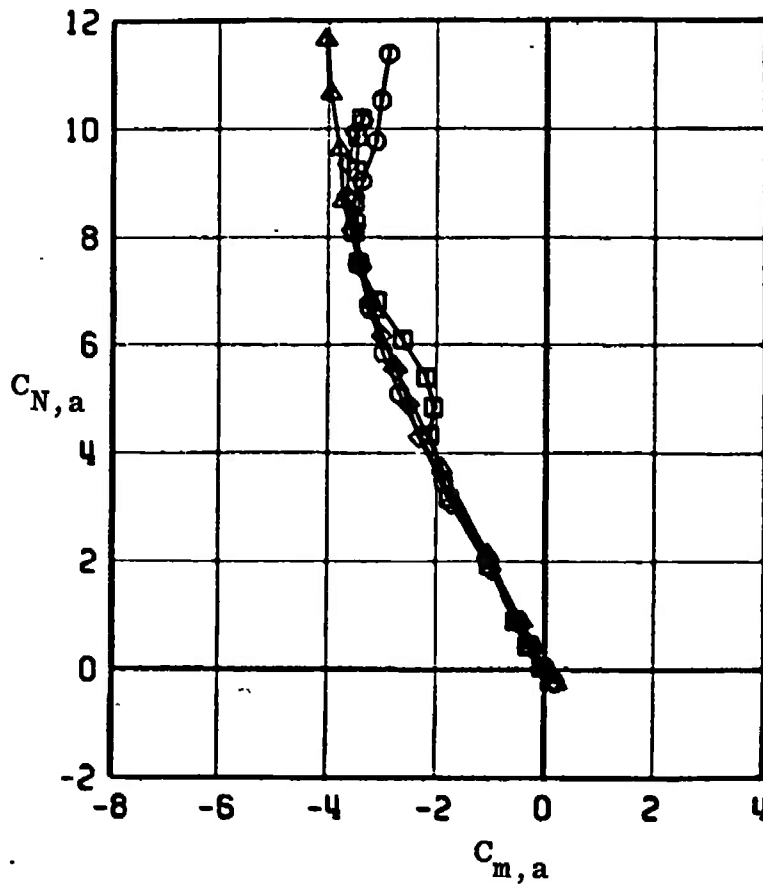
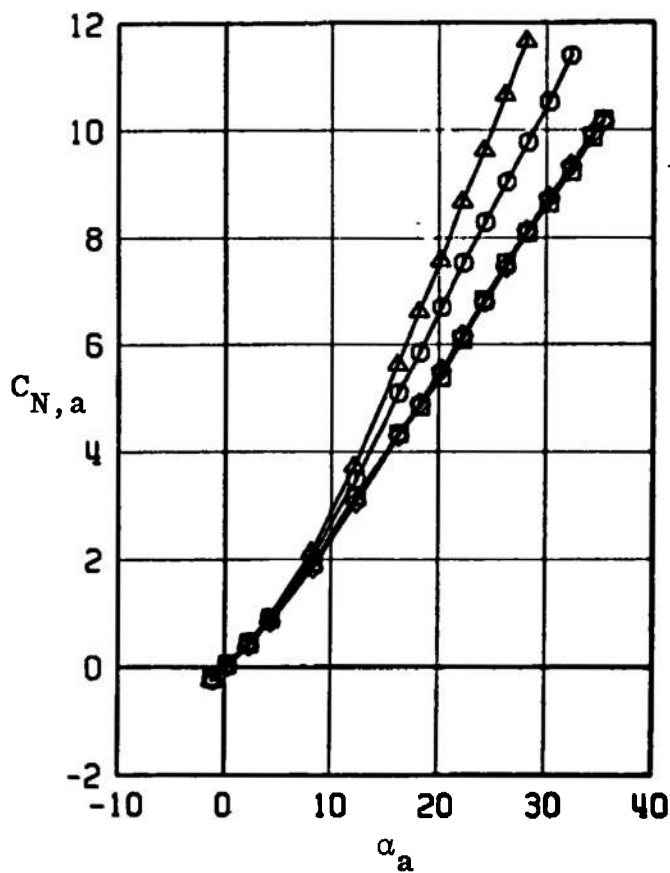


Fig. 16 Continued

EFFECT OF ROLL ANGLE							
NORMAL FORCE AND PITCHING MOMENT COEFFICIENTS							
SYMBOL	CONFIG	MACH NO	ϕ	δ_D	δ_R	δ_P	$R_E \times 10^{-6}$
\square	B10T3	0.85	0.0	0.4	-0.3	0.5	6.0
\circ	B10T3	0.85	22.5	0.4	-0.3	0.5	6.0
\triangle	B10T3	0.85	45.0	0.4	-0.3	0.5	3.3
\diamond	B10T3	0.85	180.0	0.4	-0.3	0.5	6.0

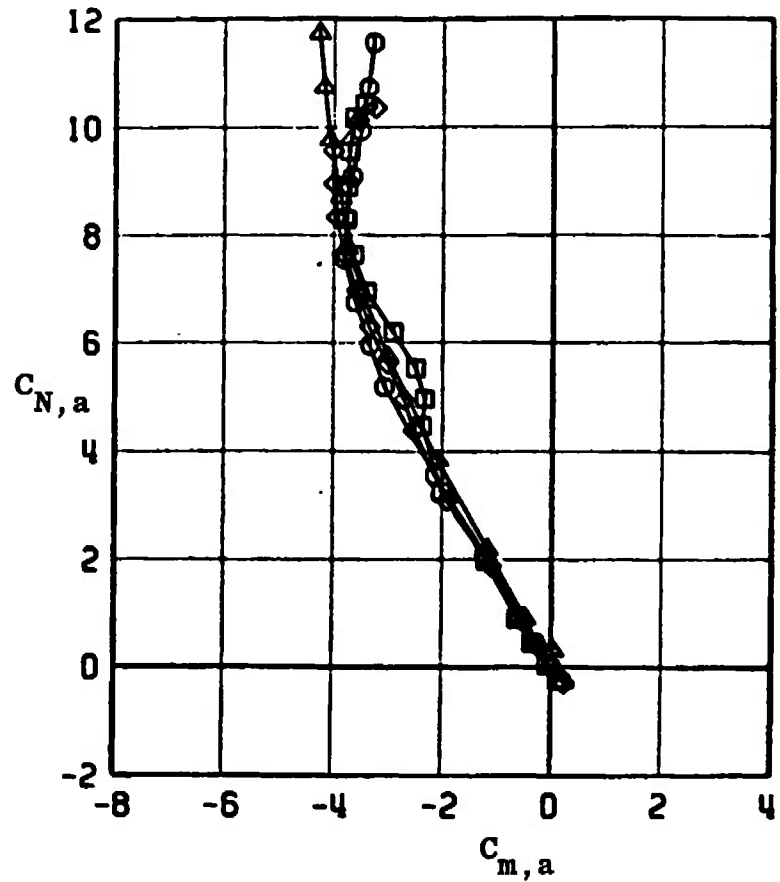
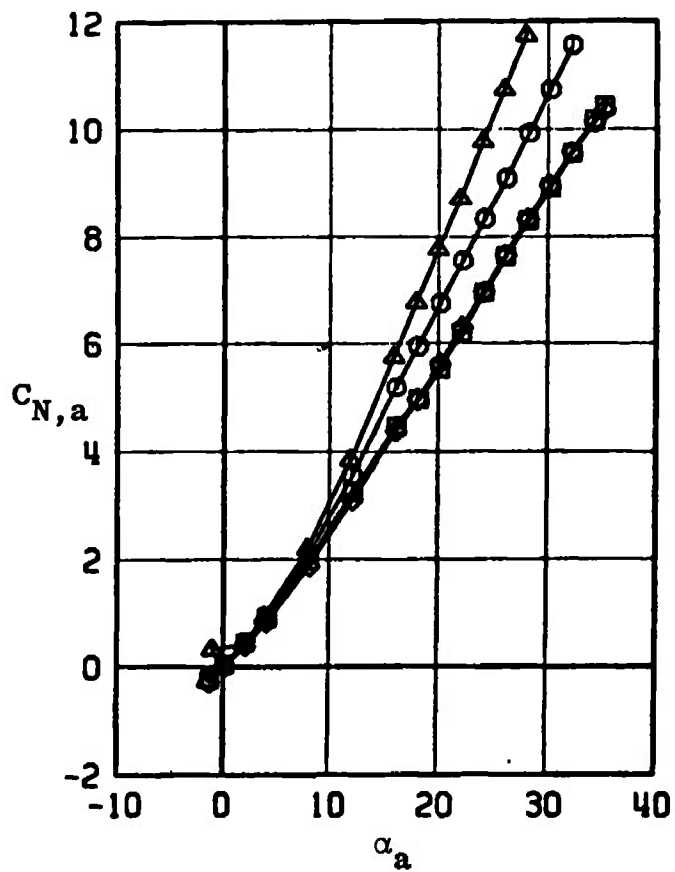


Fig. 16 Continued

EFFECT OF ROLL ANGLE NORMAL FORCE AND PITCHING MOMENT COEFFICIENTS							
SYMBOL	CONFIG	MACH NO	ϕ	ϵ_0	ϵ_η	ϵ_γ	$R_E \times 10^{-5}$
\square	B10T3	0.95	0.0	0.4	-0.3	0.5	5.6
\circ	B10T3	0.95	22.5	0.4	-0.3	0.5	5.6
\triangle	B10T3	0.95	45.0	0.4	-0.3	0.5	3.0
\diamond	B10T3	0.95	180.0	0.4	-0.3	0.5	5.6

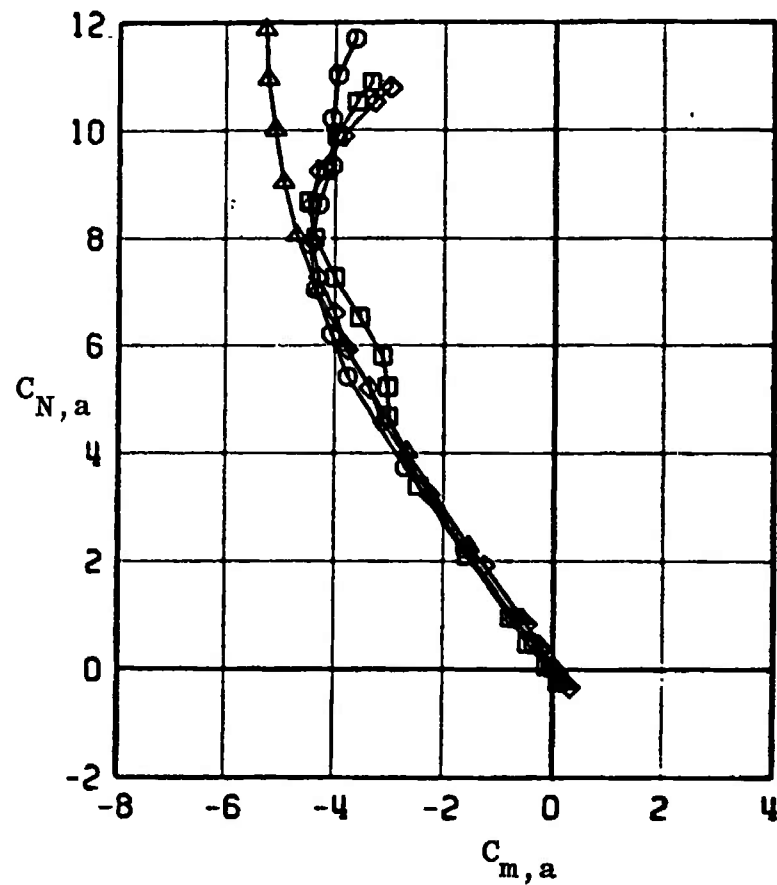
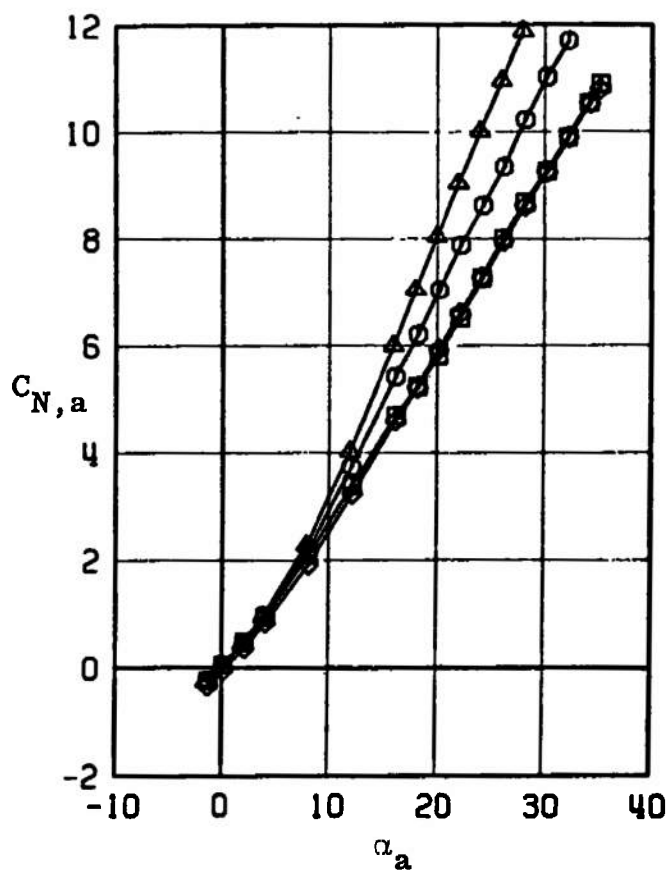


Fig. 16 Continued

EFFECT OF ROLL ANGLE							
NORMAL FORCE AND PITCHING MOMENT COEFFICIENTS							
SYMBOL	CONFIG	MACH NO	ϕ	δ_0	δ_H	δ_P	$R_E \times 10^{-5}$
\square	B10T3	1.05	0.0	0.4	-0.3	0.5	5.8
\circ	B10T3	1.05	22.5	0.4	-0.3	0.5	5.8
\triangle	B10T3	1.05	45.0	0.4	-0.3	0.5	2.9
\diamond	B10T3	1.05	180.0	0.4	-0.3	0.5	5.8

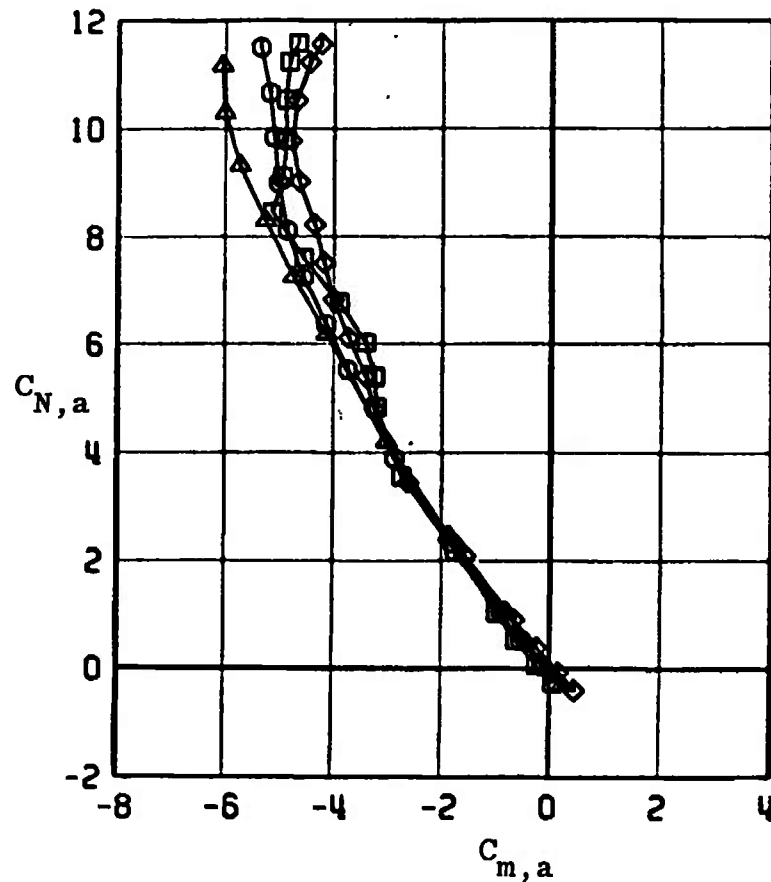
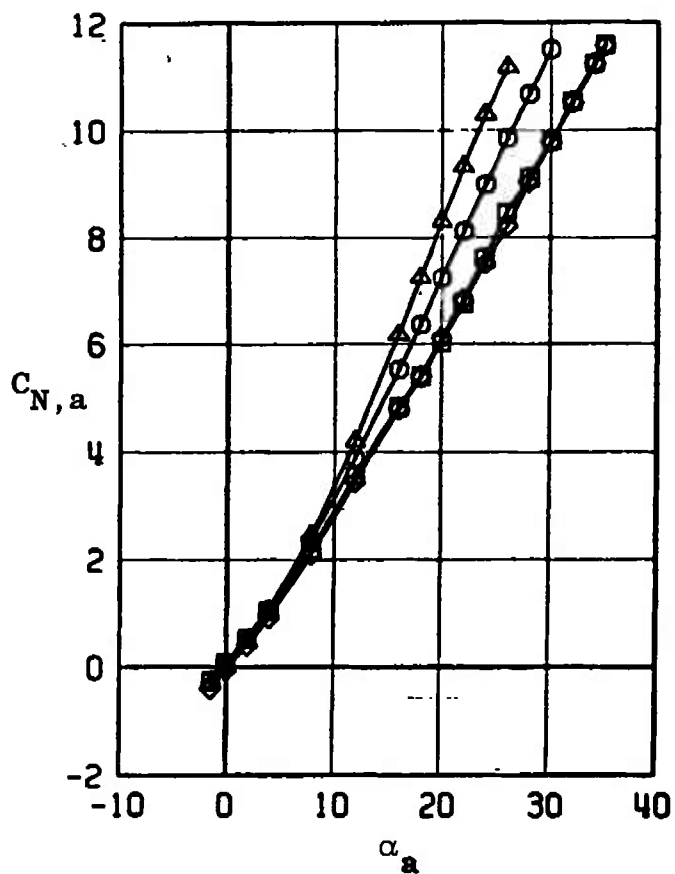


Fig. 16 Concluded

EFFECT OF ROLL ANGLE ROLLING MOMENT AND AXIAL FORCE COEFFICIENTS							
SYMBOL	CONFIG	MACH NO	ϕ	ϵ_a	ϵ_n	ϵ_p	$R_L \times 10^{-6}$
□	B10T3	0.50	0.0	0.4	-0.3	0.5	4.8
○	B10T3	0.50	22.5	0.4	-0.3	0.5	4.8
△	B10T3	0.50	45.0	0.4	-0.3	0.5	4.8
◇	B10T3	0.50	180.0	0.4	-0.3	0.5	4.8

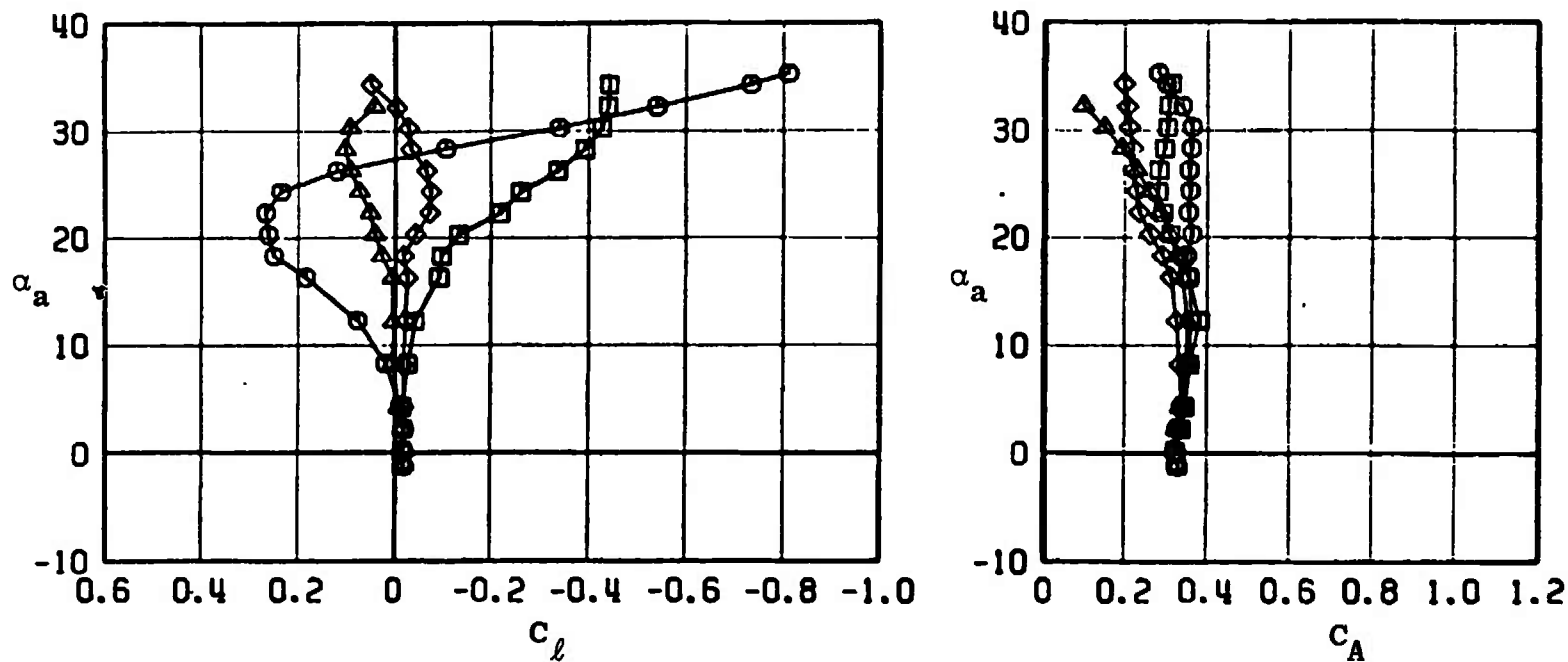


Fig. 17 Effect of Varying Roll Angle on the Rolling-Moment and Axial-Force Coefficients for MGB Configuration without the RES (B10T3)

EFFECT OF ROLL ANGLE							
ROLLING MOMENT AND AXIAL FORCE COEFFICIENTS							
SYMBOL	CONFIG	MACH NO	ϕ	ϕ_0	ϕ_R	ϕ_T	$R_F \times 10^{-6}$
\square	B10T3	0.65	0.0	0.4	-0.3	0.5	5.4
\circ	B10T3	0.65	22.5	0.4	-0.3	0.5	5.4
\triangle	B10T3	0.65	45.0	0.4	-0.3	0.5	3.9
\diamond	B10T3	0.65	180.0	0.4	-0.3	0.5	5.4

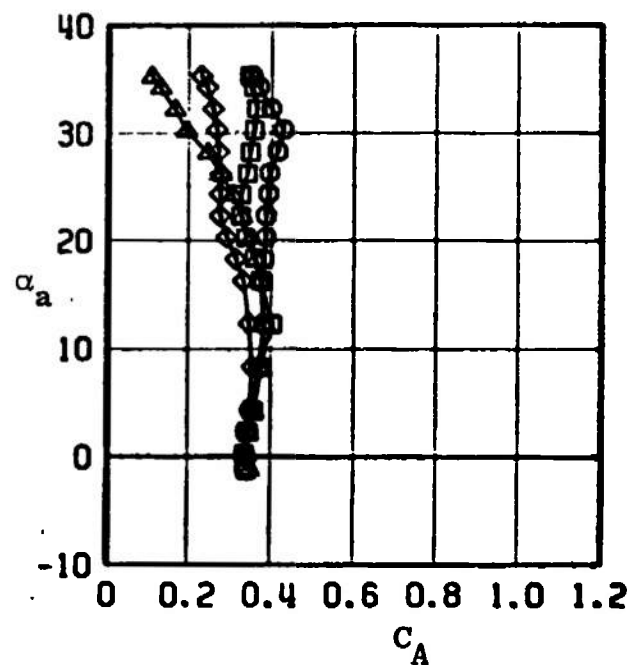
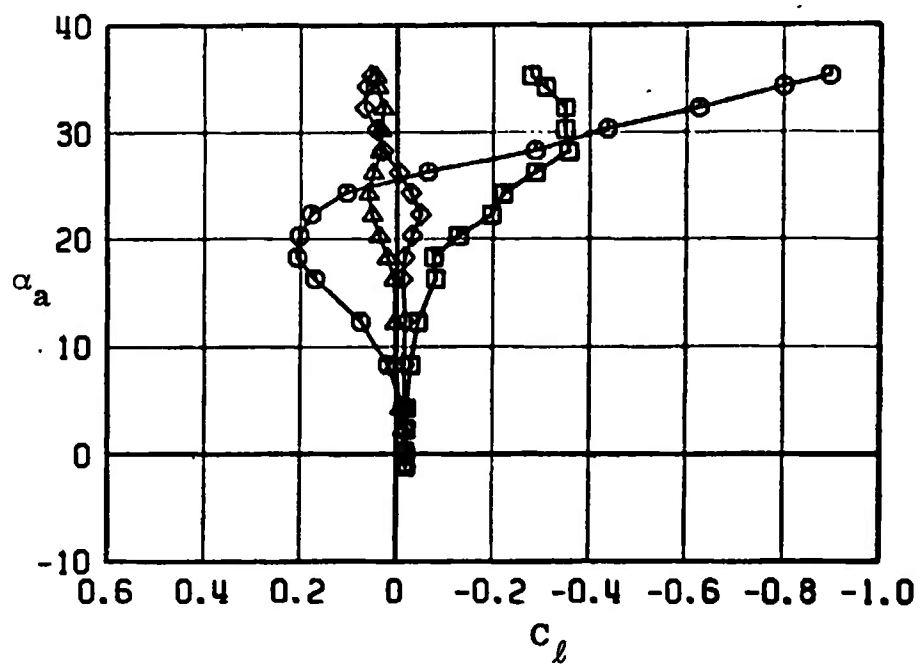


Fig. 17 Continued

EFFECT OF ROLL ANGLE
ROLLING MOMENT AND AXIAL FORCE COEFFICIENTS

SYMBOL	CONFIG	MACH NO	ϕ	ξ_D	ξ_H	ξ_P	$R_L \times 10^{-6}$
\square	B10T3	0.75	0.0	0.4	-0.3	0.5	5.8
\circ	B10T3	0.75	22.5	0.4	-0.3	0.5	5.8
\triangle	B10T3	0.75	45.0	0.4	-0.3	0.5	3.6
\diamond	B10T3	0.75	180.0	0.4	-0.3	0.5	5.8

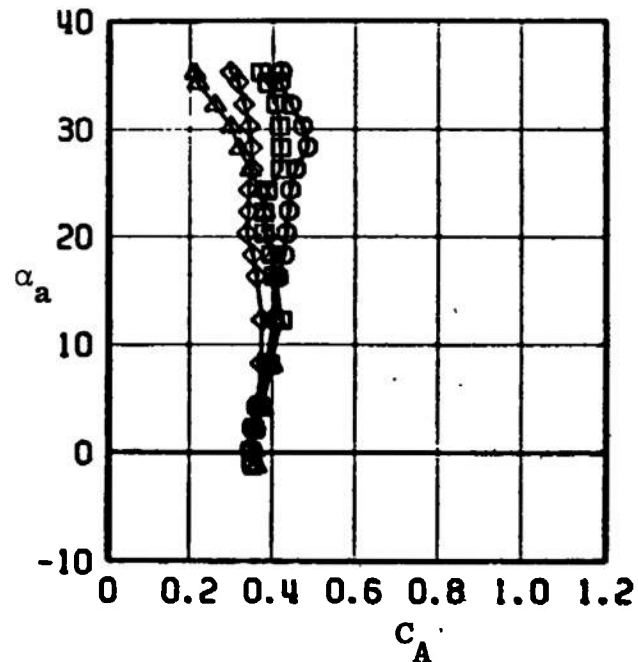
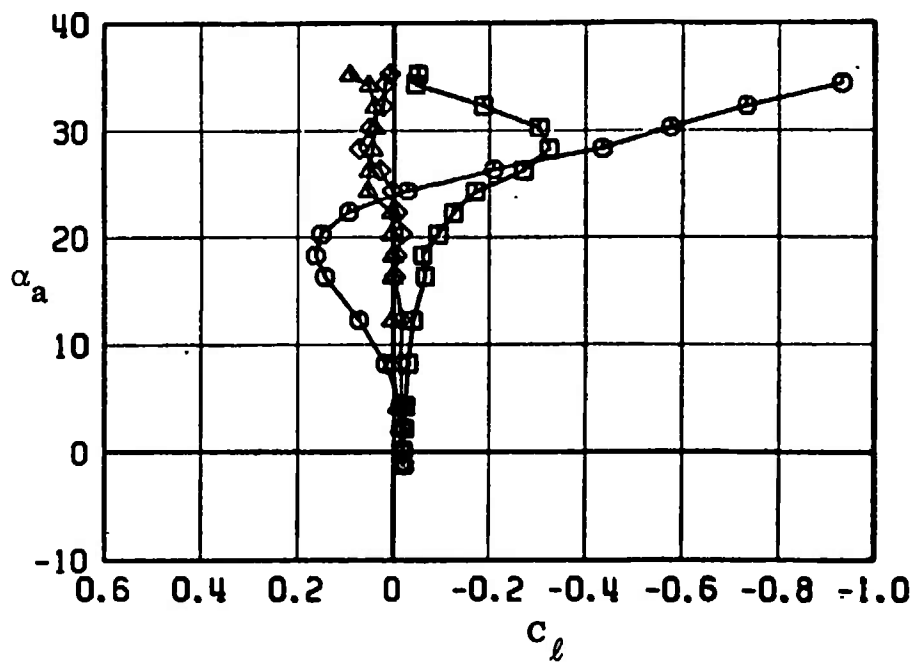


Fig. 17 Continued

EFFECT OF ROLL ANGLE
ROLLING MOMENT AND AXIAL FORCE COEFFICIENTS

SYMBOL	CONFIG	MACH NO	ϕ	ϵ_D	ϵ_H	ϵ_P	$R_F \times 10^{-6}$
\square	810T3	0.85	0.0	0.4	-0.3	0.5	6.0
\circ	810T3	0.85	22.5	0.4	-0.3	0.5	6.0
\triangle	810T3	0.85	45.0	0.4	-0.3	0.5	3.3
\diamond	810T3	0.85	180.0	0.4	-0.3	0.5	6.0

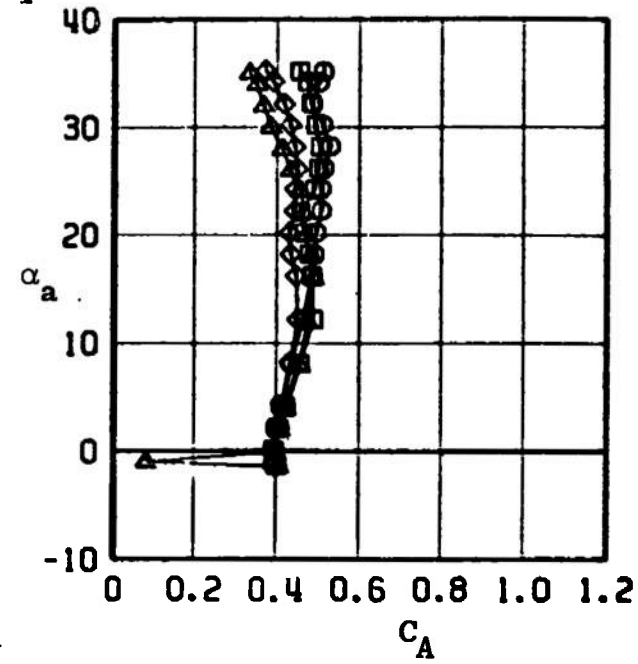
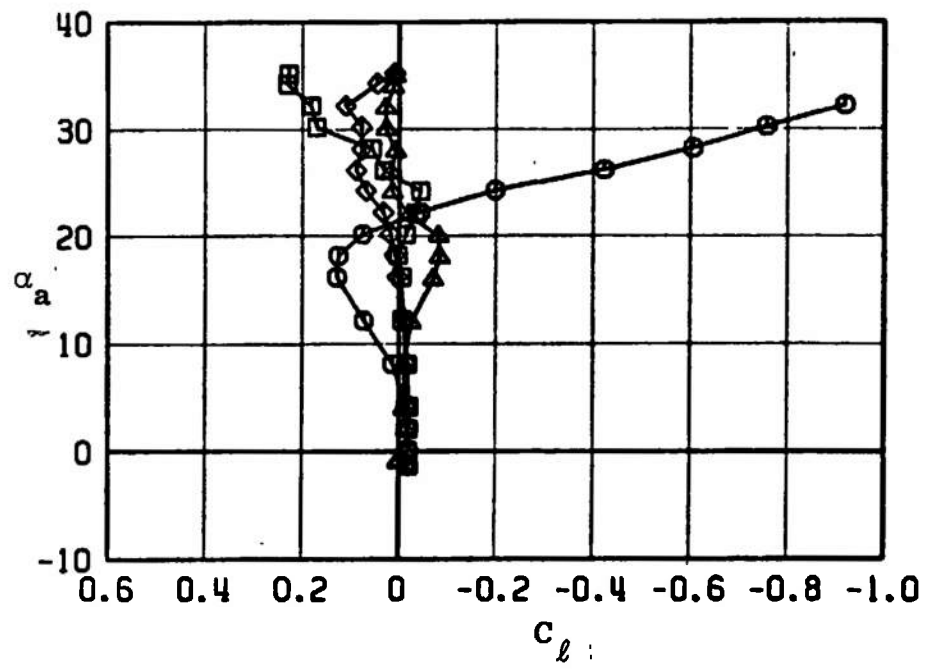


Fig. 17 Continued

EFFECT OF ROLL ANGLE
ROLLING MOMENT AND AXIAL FORCE COEFFICIENTS

SYMBOL	CONFIG	MACH NO	ϕ	ϵ_D	ϵ_H	ϵ_P	$R_L \times 10^{-6}$
\square	B10T3	0.95	0.0	0.4	-0.3	0.5	5.6
\circ	B10T3	0.95	22.5	0.4	-0.3	0.5	5.6
\triangle	B10T3	0.95	45.0	0.4	-0.3	0.5	3.0
\diamond	B10T3	0.95	180.0	0.4	-0.3	0.5	5.6

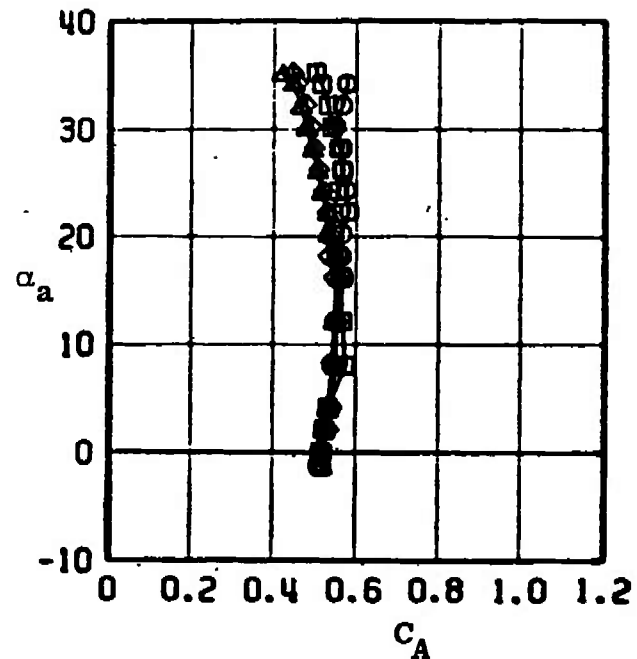
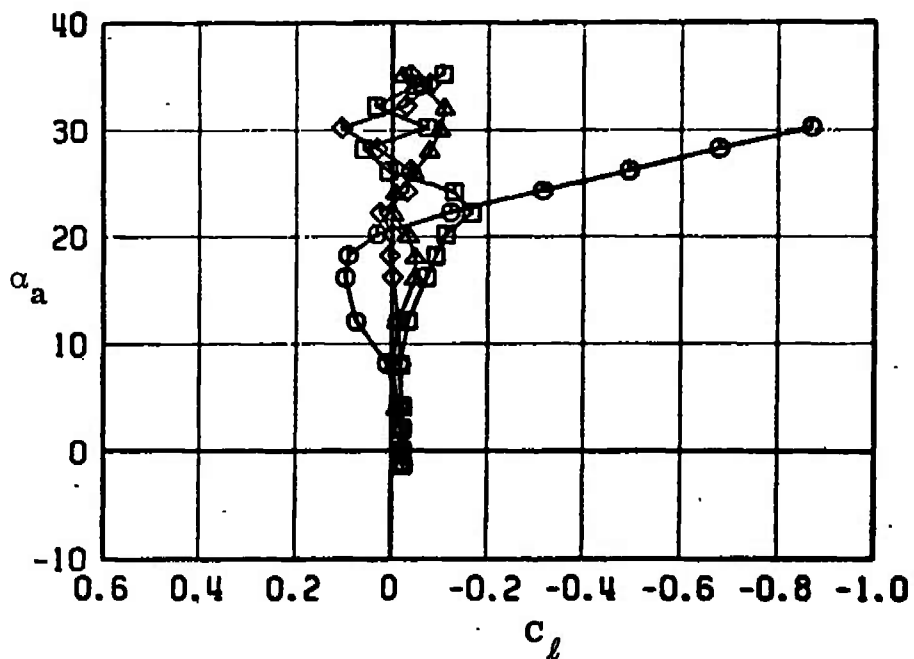


Fig. 17 Continued

EFFECT OF ROLL ANGLE							
ROLLING MOMENT AND AXIAL FORCE COEFFICIENTS							
SYMBOL	CONFIG	MACH NO	ϕ	δ_D	δ_H	δ_P	$R_E \times 10^{-6}$
\square	B10T3	1.05	0.0	0.4	-0.3	0.5	5.8
\circ	B10T3	1.05	22.5	0.4	-0.3	0.5	5.8
\triangle	B10T3	1.05	45.0	0.4	-0.3	0.5	2.9
\diamond	B10T3	1.05	180.0	0.4	-0.3	0.5	5.8

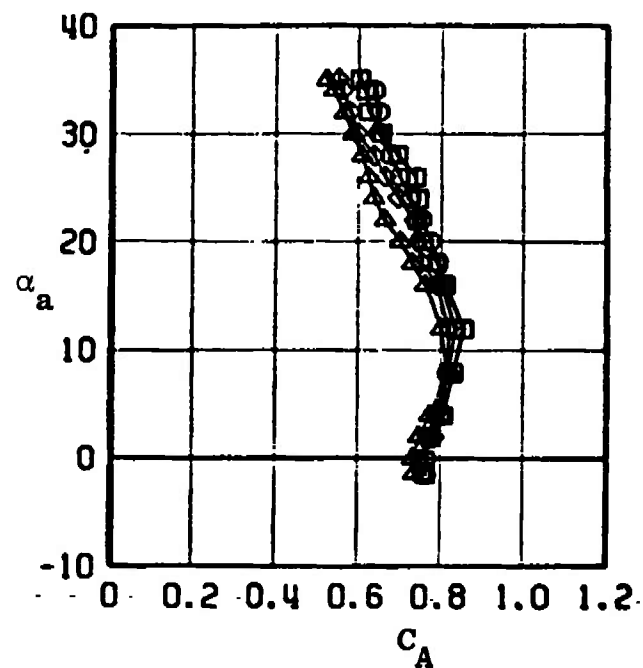
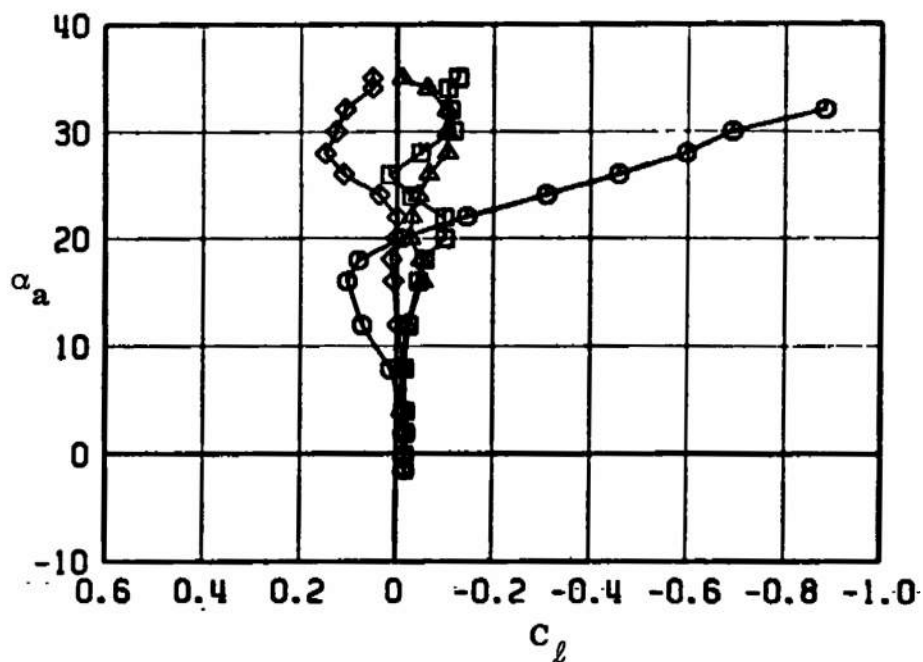


Fig. 17 Concluded

EFFECT OF ROLL ANGLE

SIDE FORCE AND YAWING MOMENT COEFFICIENTS

SYMBOL	CONFIG	MACH NO	ϕ	$C_{Y,0}$	$C_{Y,\phi}$	$C_{Y,\phi}$	$R_E \times 10^{-5}$
□	B10T3	0.50	0.0	0.4	-0.3	0.5	4.8
○	B10T3	0.50	22.5	0.4	-0.3	0.5	4.8
△	B10T3	0.50	45.0	0.4	-0.3	0.5	4.8
◇	B10T3	0.50	180.0	0.4	-0.3	0.5	4.8

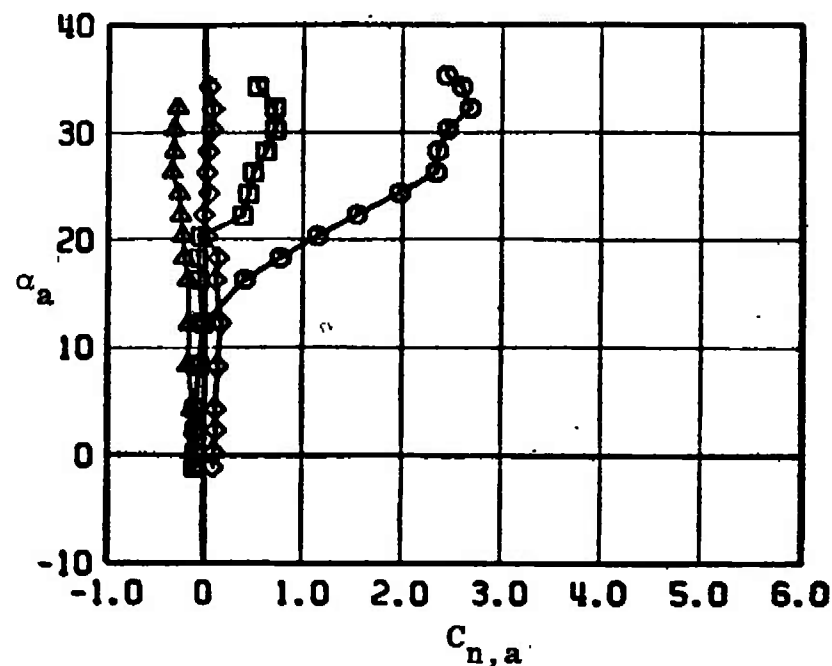
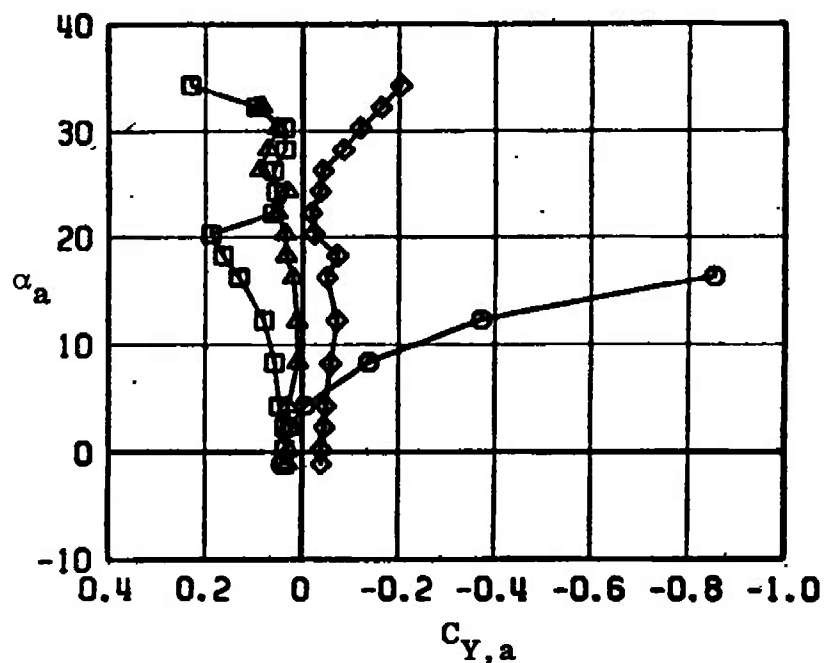


Fig. 18 Effect of Varying Roll Angle on the Side-Force and Yawing-Moment Coefficient for MGGB Configuration without the RES (B10T3)

EFFECT OF ROLL ANGLE							
SIDE FORCE AND YAWING MOMENT COEFFICIENTS							
SYMBOL	CONFIG	MACH NO	•	ϵ_0	ϵ_n	ϵ_p	$R_F \times 10^{-6}$
□	B10T3	0.65	0.0	0.4	-0.3	0.5	5.4
○	B10T3	0.65	22.5	0.4	-0.3	0.5	5.4
△	B10T3	0.65	45.0	0.4	-0.3	0.5	3.9
◇	B10T3	0.65	180.0	0.4	-0.3	0.5	5.4

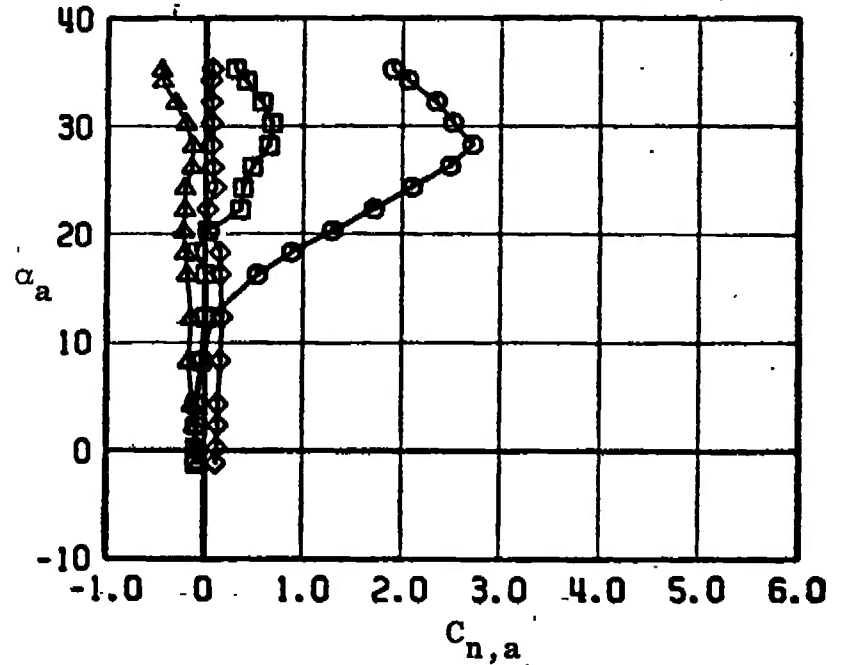
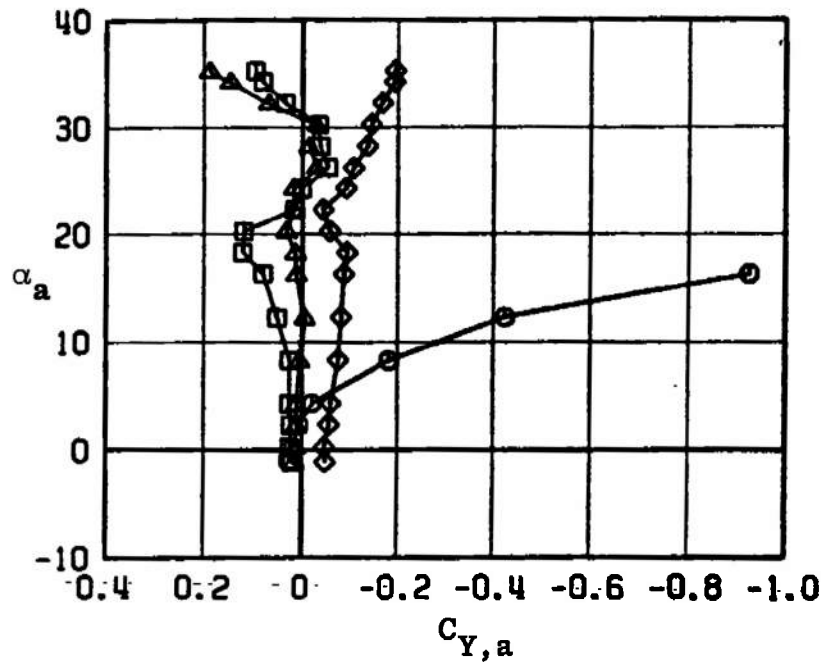


Fig. 18 Continued

EFFECT OF ROLL ANGLE
SIDE FORCE AND YAWING MOMENT COEFFICIENTS .

SYMBOL	CONFIG	MACH NO	ϕ	δ_0	δ_H	δ_V	$R_E \times 10^{-6}$
□	B10T3	0.75	0.0	0.4	-0.3	0.5	5.8
○	B10T3	0.75	22.5	0.4	-0.3	0.5	5.8
△	B10T3	0.75	45.0	0.4	-0.3	0.5	3.6
◇	B10T3	0.75	180.0	0.4	-0.3	0.5	5.8

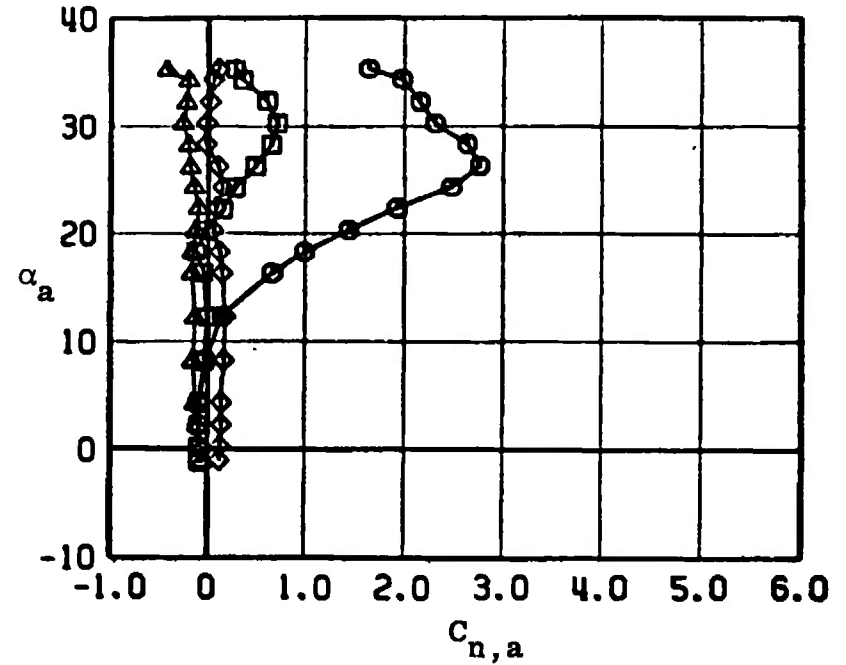
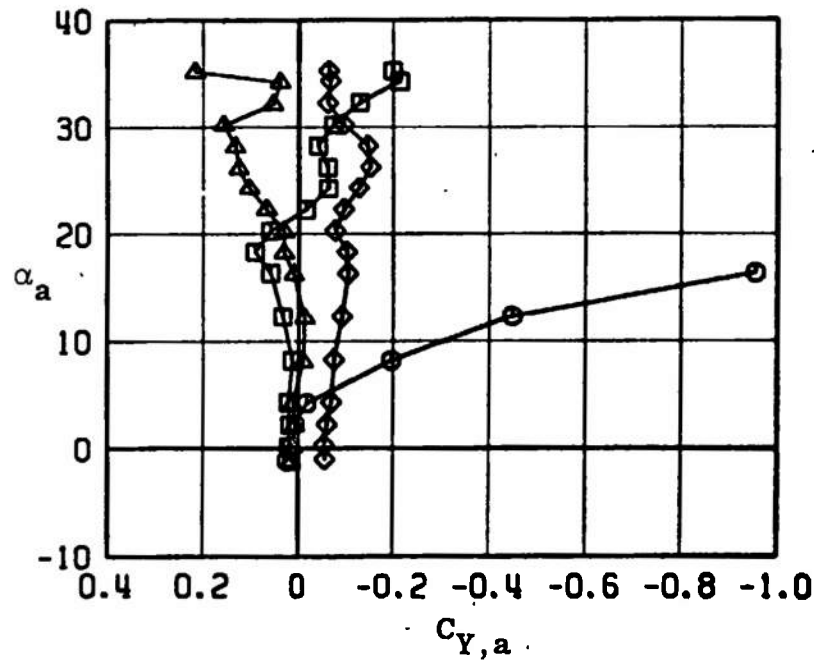


Fig. 18 Continued

EFFECT OF ROLL ANGLE
SIDE FORCE AND YAWING MOMENT COEFFICIENTS

SYMBOL	CONFIG	MACH NO	ϕ	$C_{D,0}$	$C_{D,\alpha}$	$C_{Y,0}$	$R_E \times 10^{-6}$
□	B10T3	0.85	0.0	0.4	-0.3	0.5	6.0
○	B10T3	0.85	22.5	0.4	-0.3	0.5	6.0
△	B10T3	0.85	45.0	0.4	-0.3	0.5	3.3
◇	B10T3	0.85	180.0	0.4	-0.3	0.5	6.0

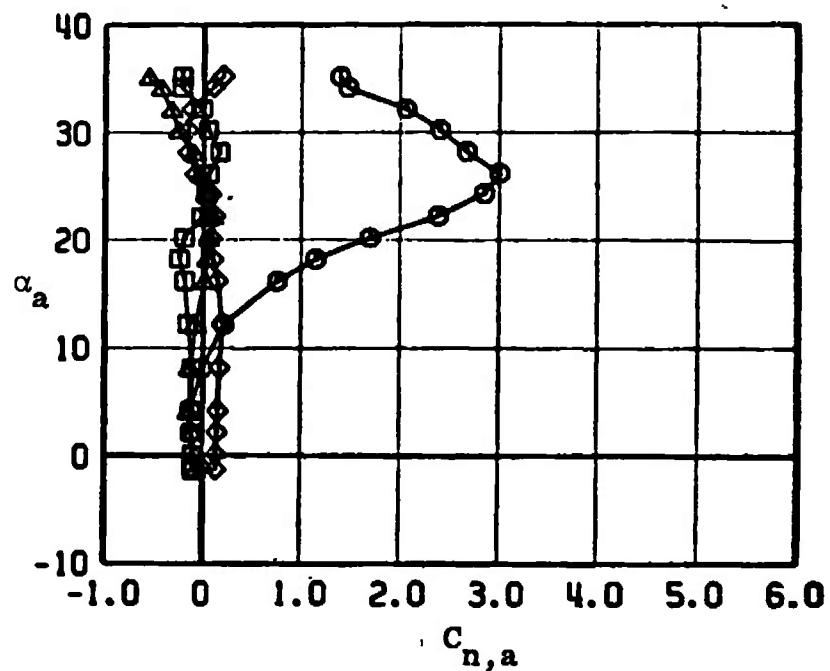
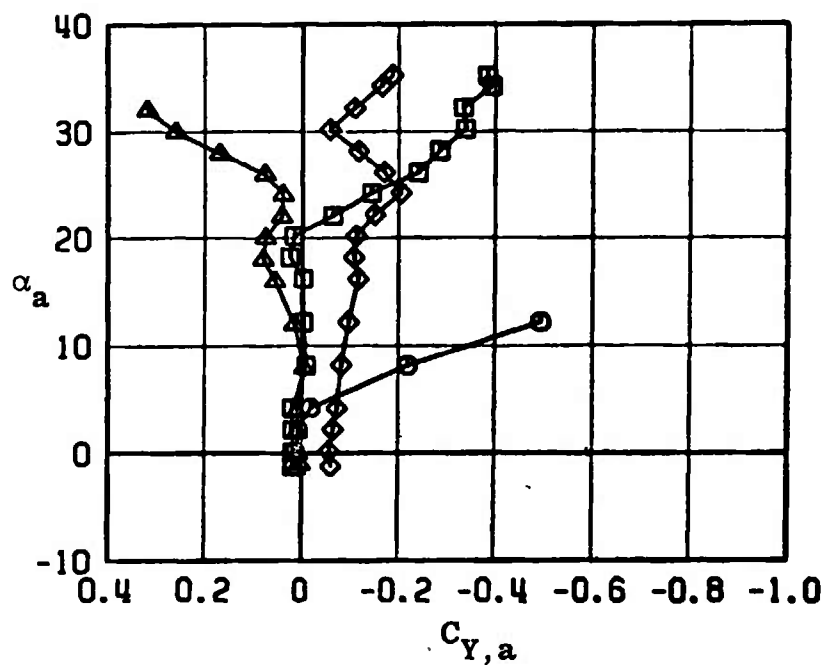


Fig. 18 Continued

EFFECT OF ROLL ANGLE							
SIDE FORCE AND YAWING MOMENT COEFFICIENTS							
SYMBOL	CONFIG	MACH NO	ϕ	δ_D	δ_H	δ_P	$R_E \times 10^{-6}$
□	B10T3	0.95	0.0	0.4	-0.3	0.5	5.6
○	B10T3	0.95	22.5	0.4	-0.3	0.5	5.6
△	B10T3	0.95	45.0	0.4	-0.3	0.5	3.0
◇	B10T3	0.95	180.0	0.4	-0.3	0.5	5.6

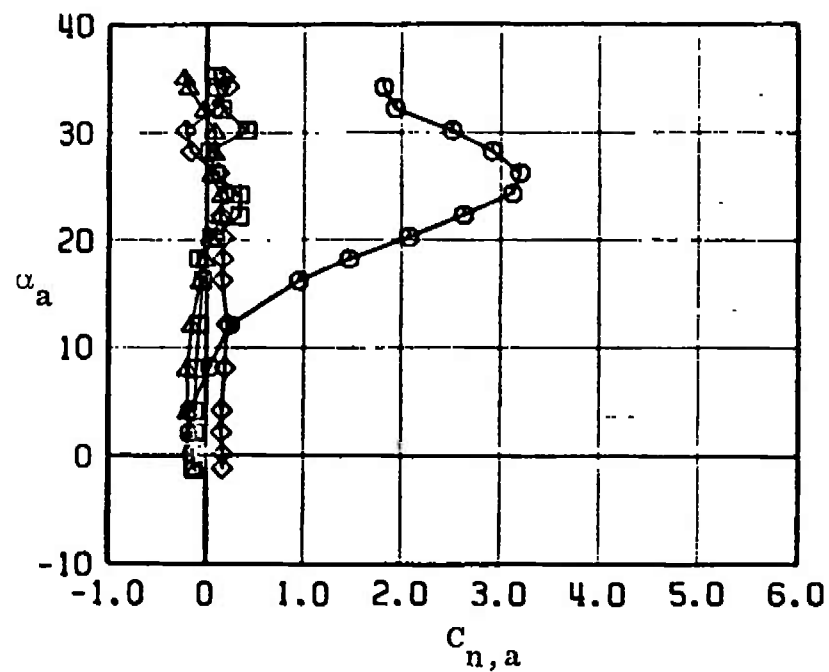
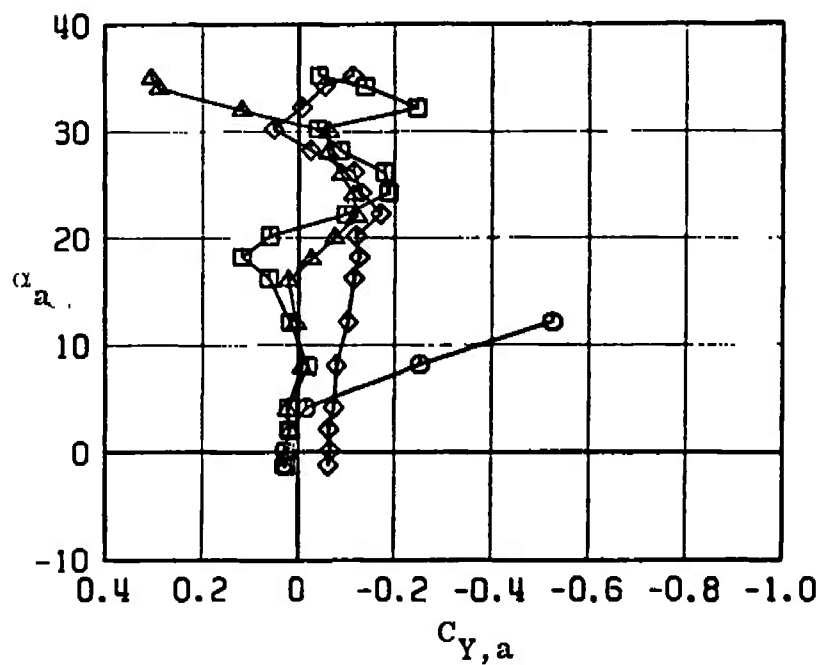


Fig. 18 Continued

EFFECT OF ROLL ANGLE
SIDE FORCE AND YAWING MOMENT COEFFICIENTS

SYMBOL	CONFIG	MACH NO	ϕ	b_0	b_R	b_P	$P_E \times 10^{-6}$
□	B10T3	1.05	0.0	0.4	-0.3	0.5	5.8
○	B10T3	1.05	22.5	0.4	-0.3	0.5	5.8
△	B10T3	1.05	45.0	0.4	-0.3	0.5	2.9
◇	B10T3	1.05	180.0	0.4	-0.3	0.5	5.8

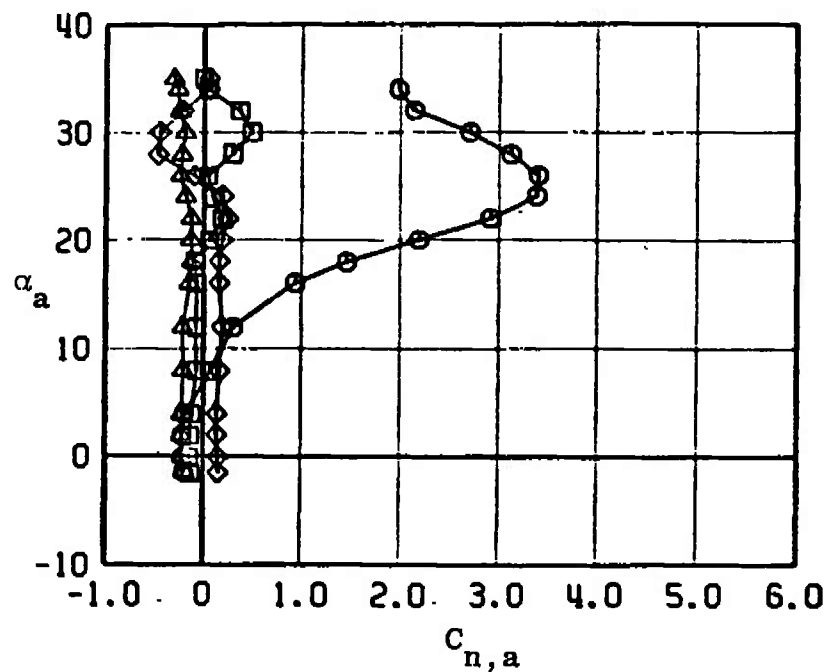
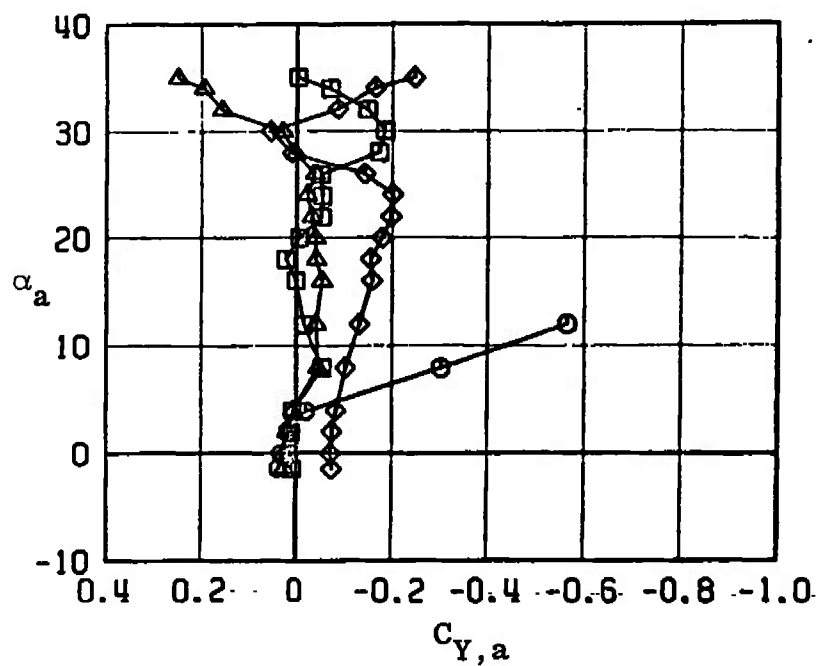


Fig. 18 Concluded

CONFIGURATION COMPARISON							
NORMAL FORCE AND PITCHING MOMENT COEFFICIENTS							
SYMBOL	CONFIG	MACH NO	ϕ	δ_D	δ_R	δ_P	$R_E \times 10^{-6}$
\square	B9T3	0.50	0	0.3	0.5	0.3	4.8
\circ	B10T3	0.50	0	0.4	-0.3	0.5	4.8
Δ	B11T3	0.50	0	0.4	-0.3	0.5	4.8

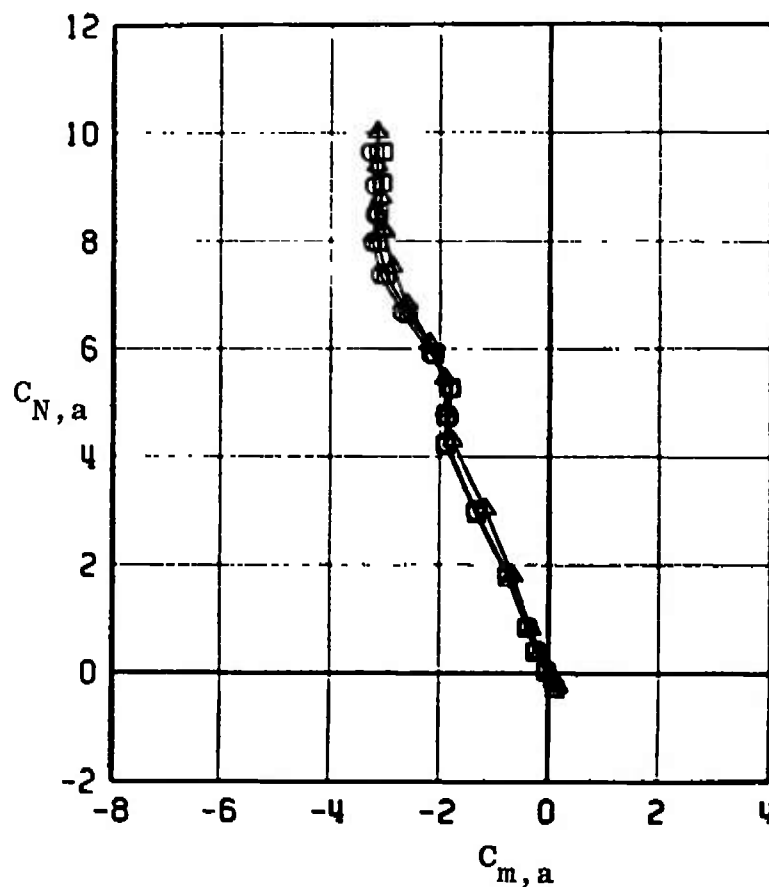
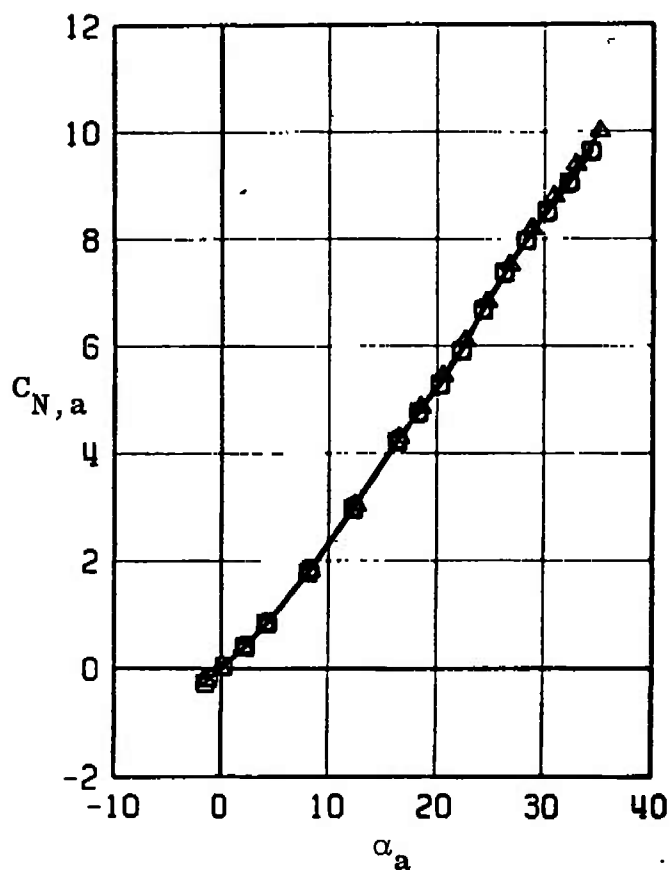


Fig. 19 Effect of Varying Fuselage Protuberances on the Normal-Force and Pitching-Moment Coefficients for Configurations without the RES (B9T3, B10T3, and B11T3)

CONFIGURATION COMPARISON							
NORMAL FORCE AND PITCHING MOMENT COEFFICIENTS							
SYMBOL	CONFIG	MACH NO	ϕ	δ_0	δ_H	δ_P	$R_E \times 10^{-6}$
\square	B9T3	0.65	0	0.3	0.5	0.3	5.4
\circ	B10T3	0.65	0	0.4	-0.3	0.5	5.4
Δ	B11T3	0.65	0	0.4	-0.3	0.5	5.4

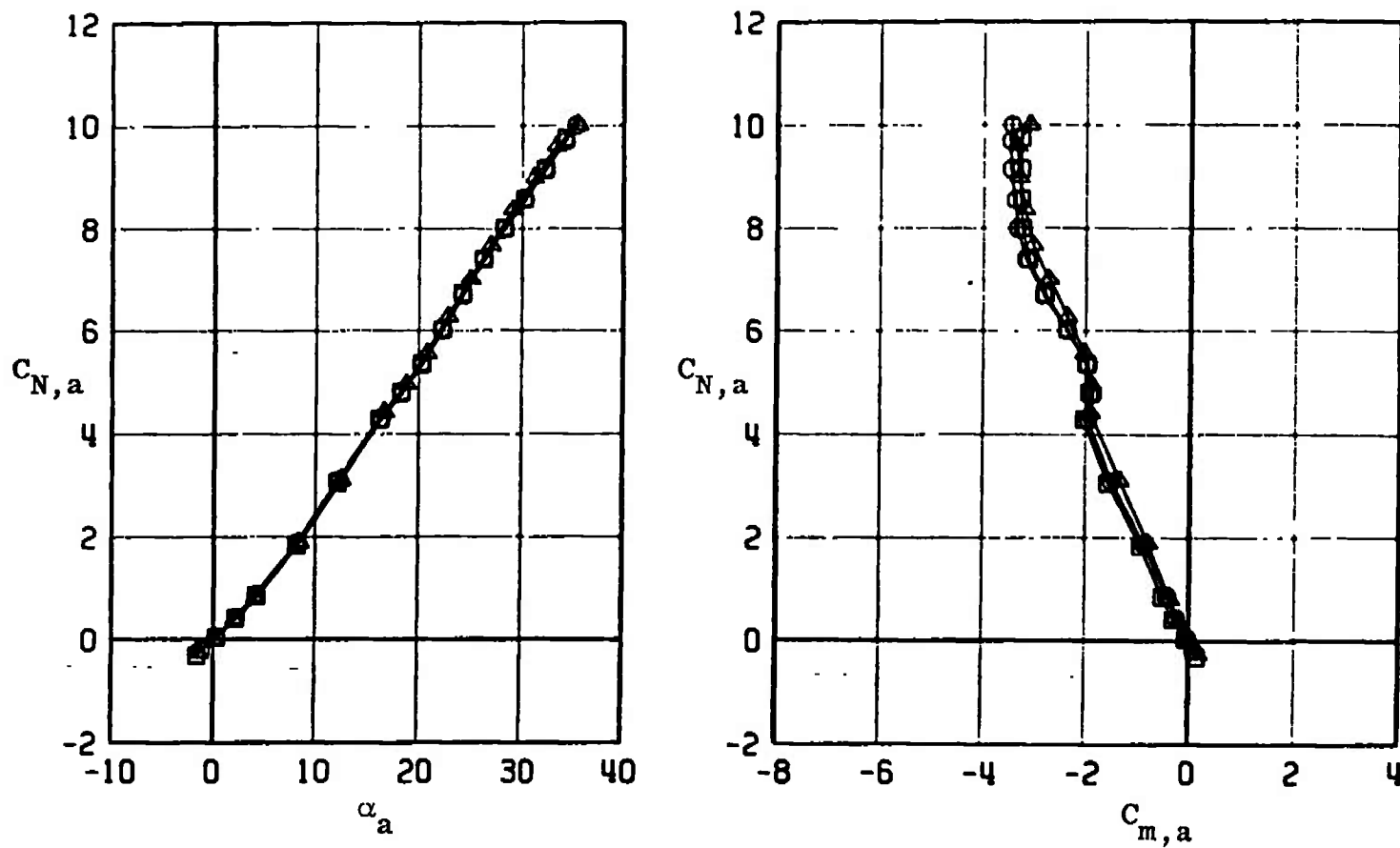


Fig. 19 Continued

CONFIGURATION COMPARISON							
NORMAL FORCE AND PITCHING MOMENT COEFFICIENTS							
SYMBOL	CONFIG	MACH NO	ϕ	δ_D	δ_R	δ_P	$R_E \times 10^{-6}$
\square	B9T3	0.75	0	0.3	0.5	0.3	5.8
\circ	B10T3	0.75	0	0.4	-0.3	0.5	5.8
Δ	B11T3	0.75	0	0.4	-0.3	0.5	5.8

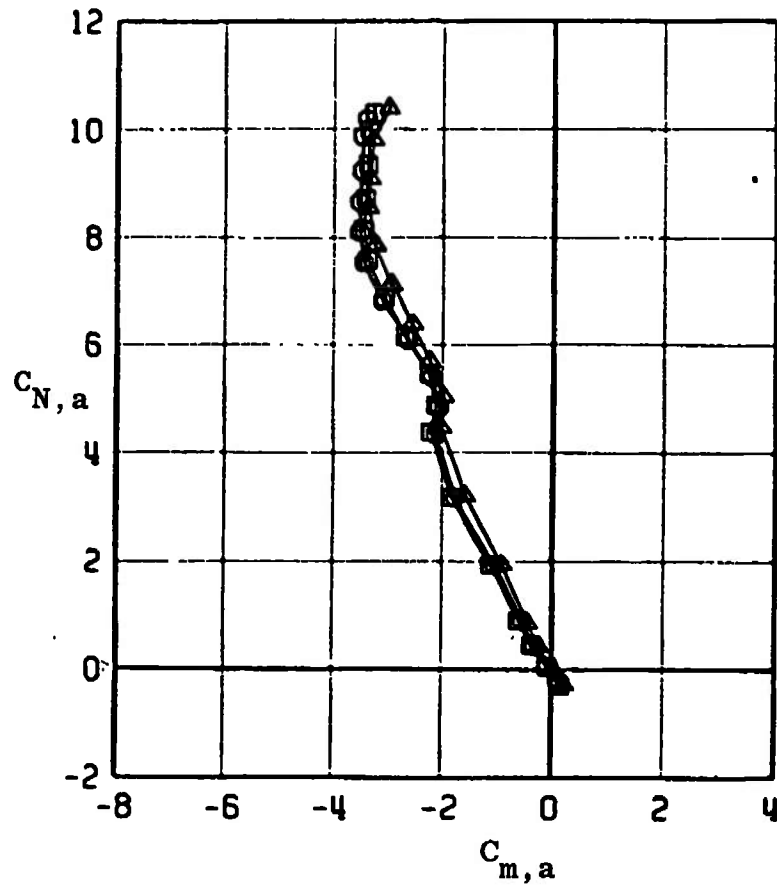
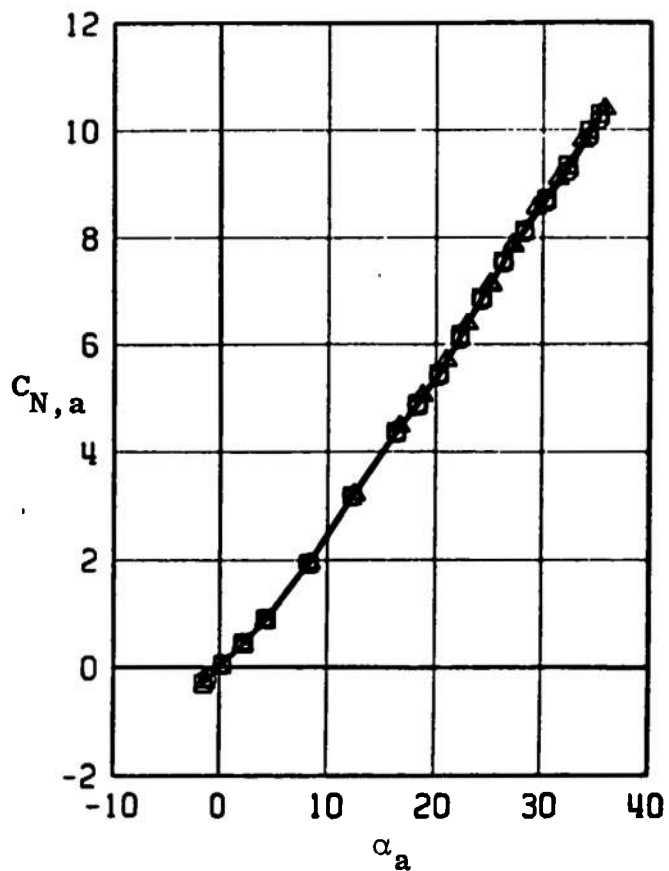


Fig. 19 Continued

CONFIGURATION COMPARISON							
NORMAL FORCE AND PITCHING MOMENT COEFFICIENTS							
SYMBOL	CONFIG	MACH NO	ϕ	ϵ_D	ϵ_H	ϵ_P	$R_E \times 10^{-6}$
□	B9T3	0.85	0	0.3	0.5	0.3	6.0
○	B10T3	0.85	0	0.4	-0.3	0.5	6.0
△	B11T3	0.85	0	0.4	-0.3	0.5	6.0

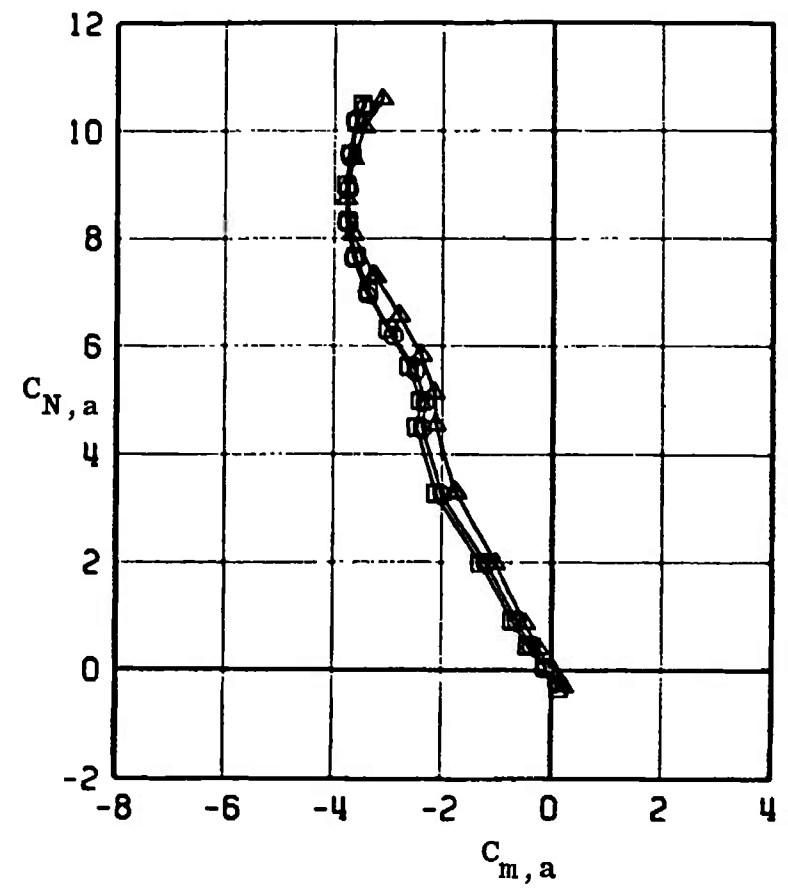
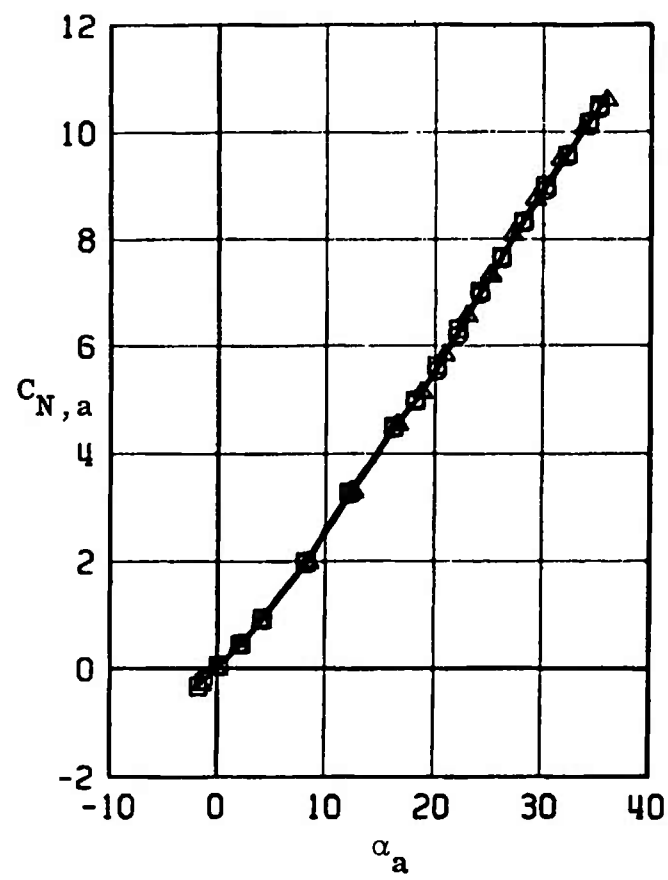


Fig. 19 Continued

CONFIGURATION COMPARISON

NORMAL FORCE AND PITCHING MOMENT COEFFICIENTS

SYMBOL	CONFIG	MACH NO	ϕ	δ_D	δ_H	δ_P	$R_E \times 10^{-6}$
\square	89T3	0.95	0	0.3	0.5	0.3	5.6
\circ	810T3	0.95	0	0.4	-0.3	0.5	5.6
\triangle	811T3	0.95	0	0.4	-0.3	0.5	5.6

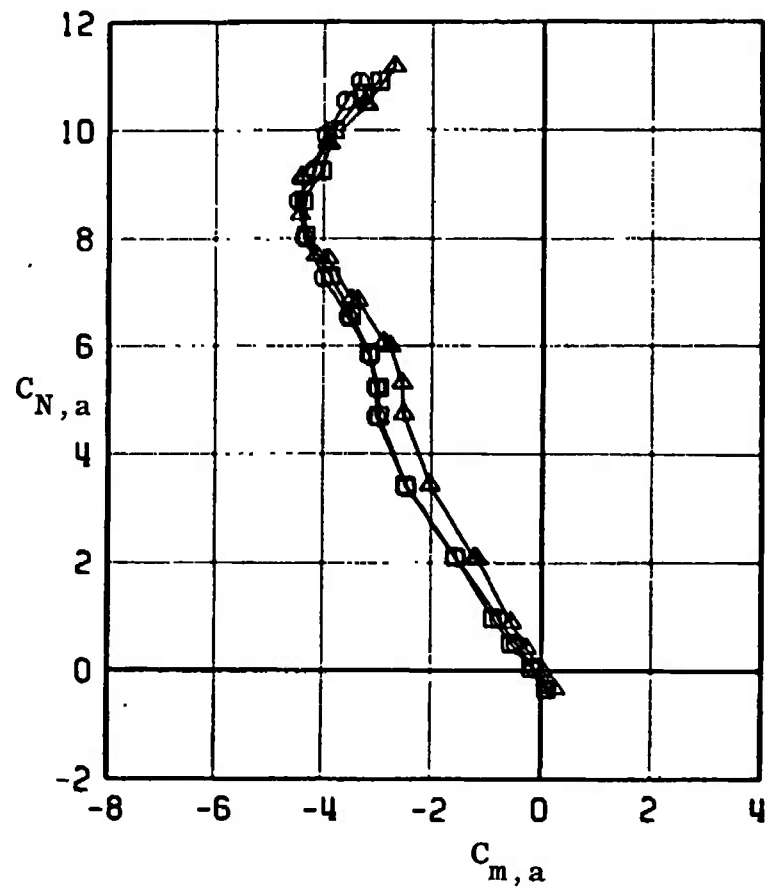
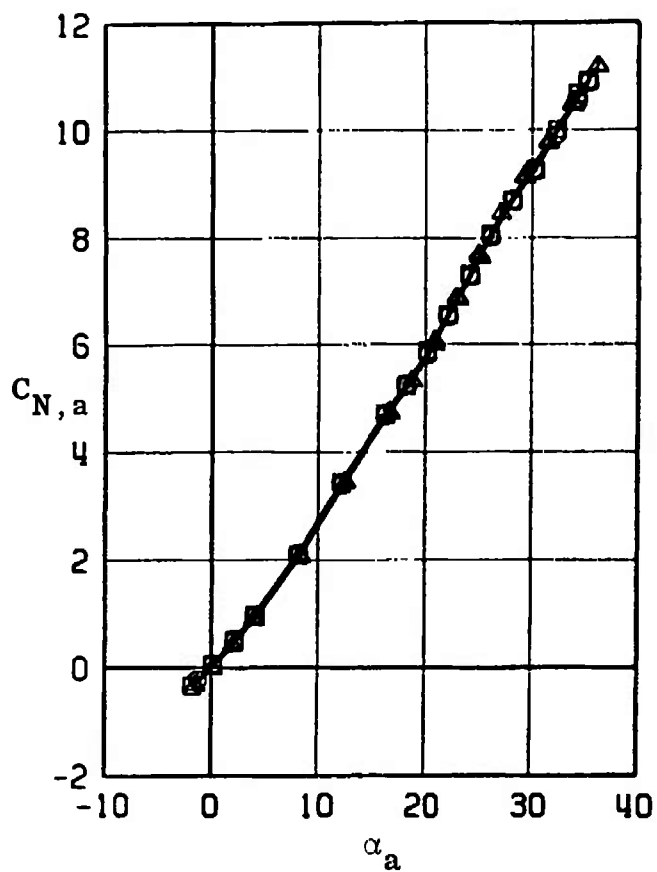


Fig. 19 Continued

CONFIGURATION COMPARISON							
NORMAL FORCE AND PITCHING MOMENT COEFFICIENTS							
SYMBOL	CONFIG	MACH NO	ϕ	ϵ_0	ϵ_R	ϵ_P	$R_E \times 10^{-6}$
□	B9T3	1.05	0	0.3	0.5	0.3	5.8
○	B10T3	1.05	0	0.4	-0.3	0.5	5.8
△	B11T3	1.05	0	0.4	-0.3	0.5	5.8

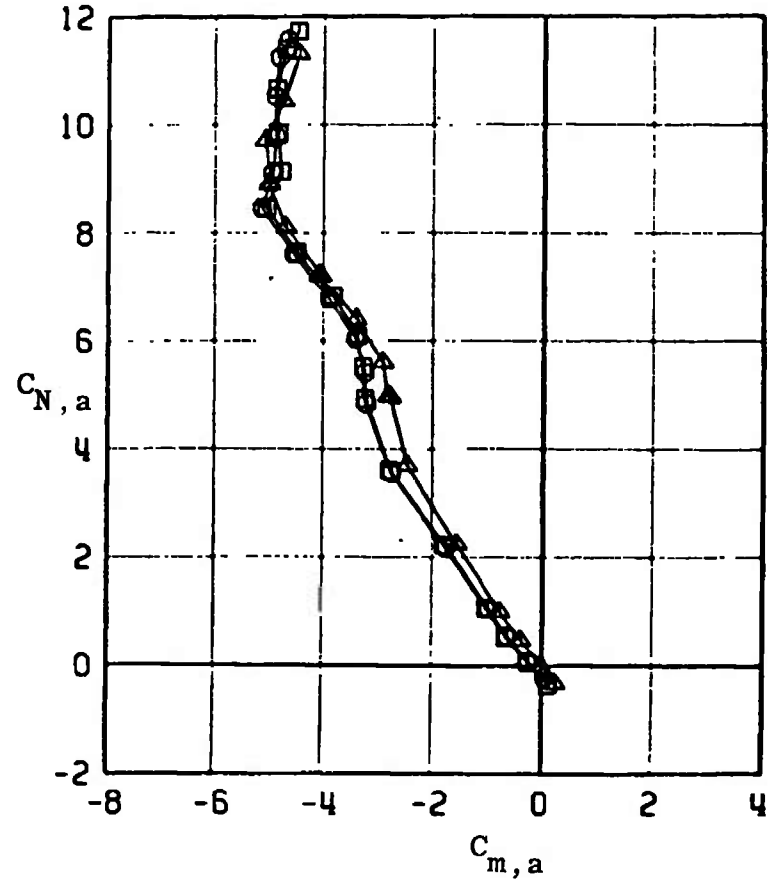
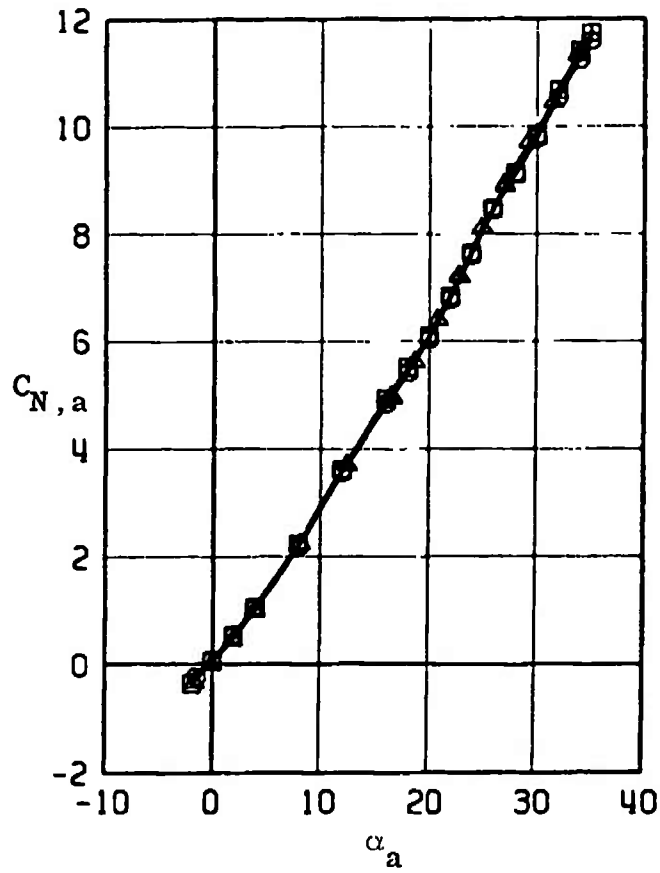


Fig. 19 Concluded

CONFIGURATION COMPARISON							
ROLLING MOMENT AND AXIAL FORCE COEFFICIENTS							
SYMBOL	CONFIG	MACH NO	ϕ	δ_0	δ_R	δ_P	$R_L \times 10^{-5}$
□	B9T3	0.50	0	0.3	0.5	0.3	4.8
○	B10T3	0.50	0	0.4	-0.3	0.5	4.8
△	B11T3	0.50	0	0.4	-0.3	0.5	4.8

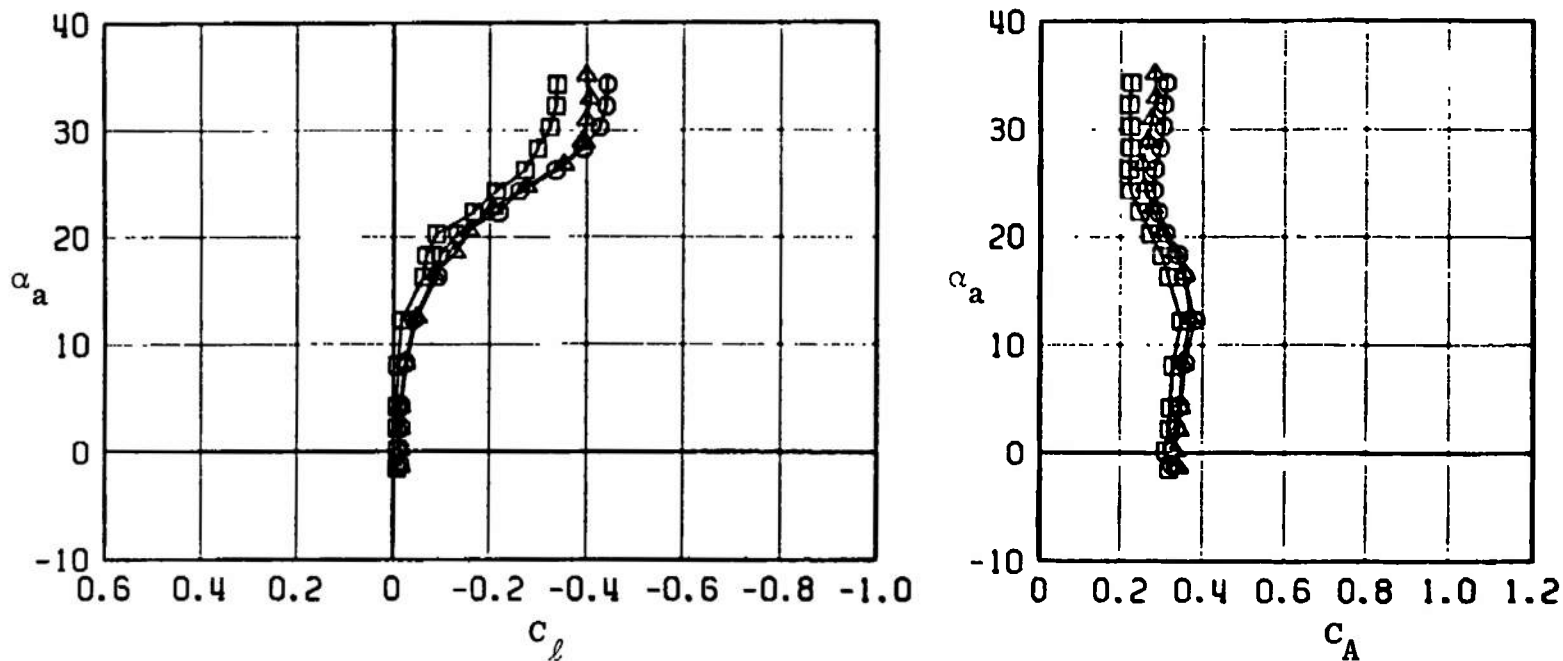


Fig. 20 Effect of Varying Fuselage Protuberances on the Rolling-Moment and Axial-Force Coefficients for Configurations without the RES (B9T3, B10T3, and B11T3)

CONFIGURATION COMPARISON ROLLING MOMENT AND AXIAL FORCE COEFFICIENTS							
SYMBOL	CONFIG	MACH NO	ϕ	b_0	b_R	b_P	$R_E \times 10^{-6}$
□	89T3	0.65	0	0.3	0.5	0.3	5.4
○	810T3	0.65	0	0.4	-0.3	0.5	5.4
△	811T3	0.65	0	0.4	-0.3	0.5	5.4

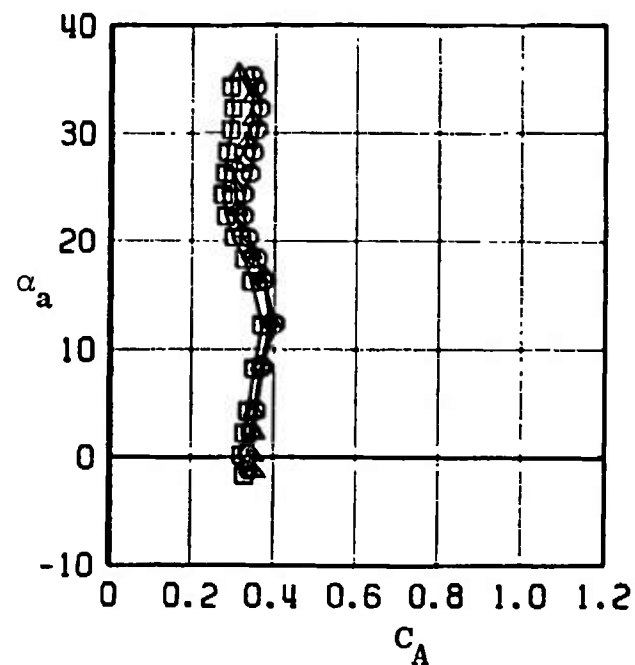
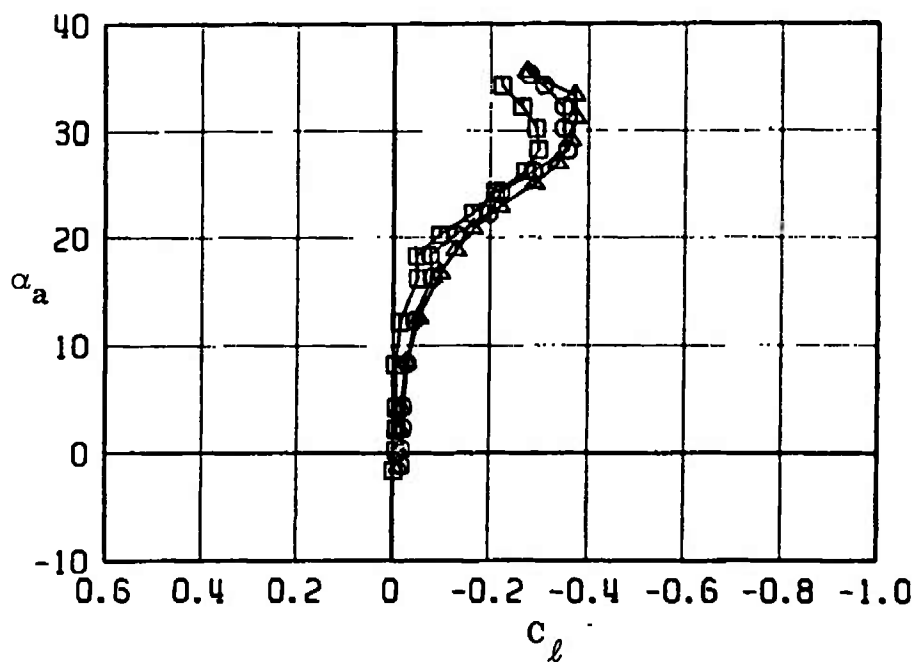


Fig. 20 Continued

CONFIGURATION COMPARISON							
ROLLING MOMENT AND AXIAL FORCE COEFFICIENTS							
SYMBOL	CONFIG	MACH NO	ϕ	δ_D	δ_H	δ_P	$R_L \times 10^{-6}$
\square	B9T3	0.75	0	0.3	0.5	0.3	5.8
\circ	B10T3	0.75	0	0.4	-0.3	0.5	5.8
\triangle	B11T3	0.75	0	0.4	-0.3	0.5	5.8

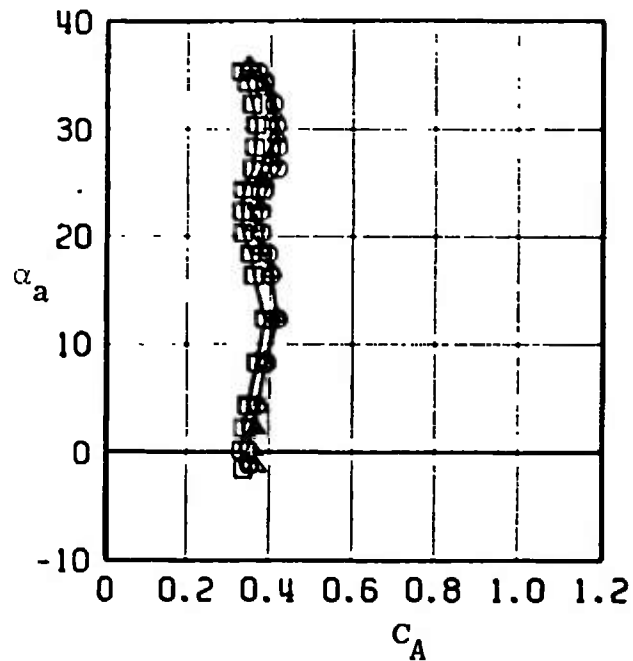
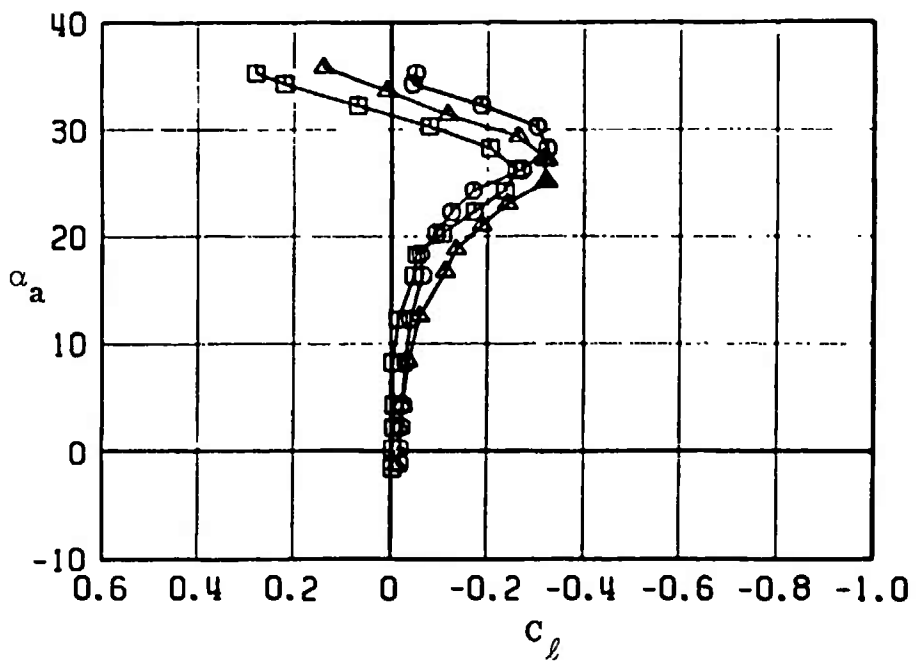
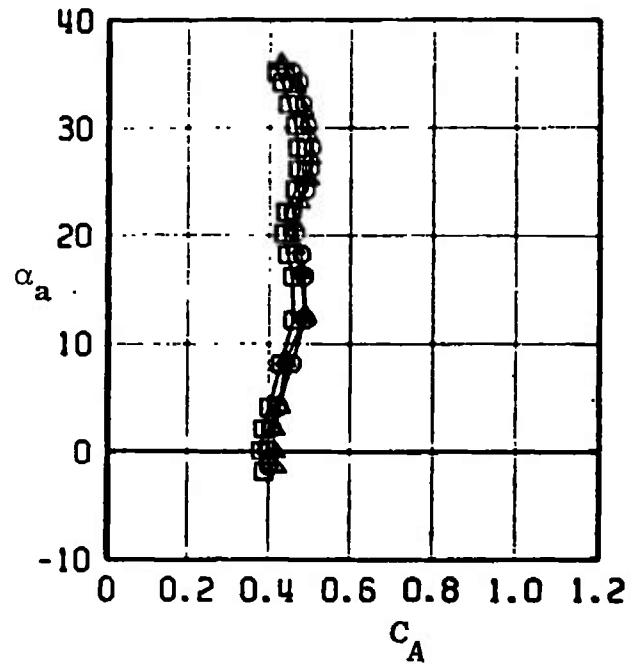
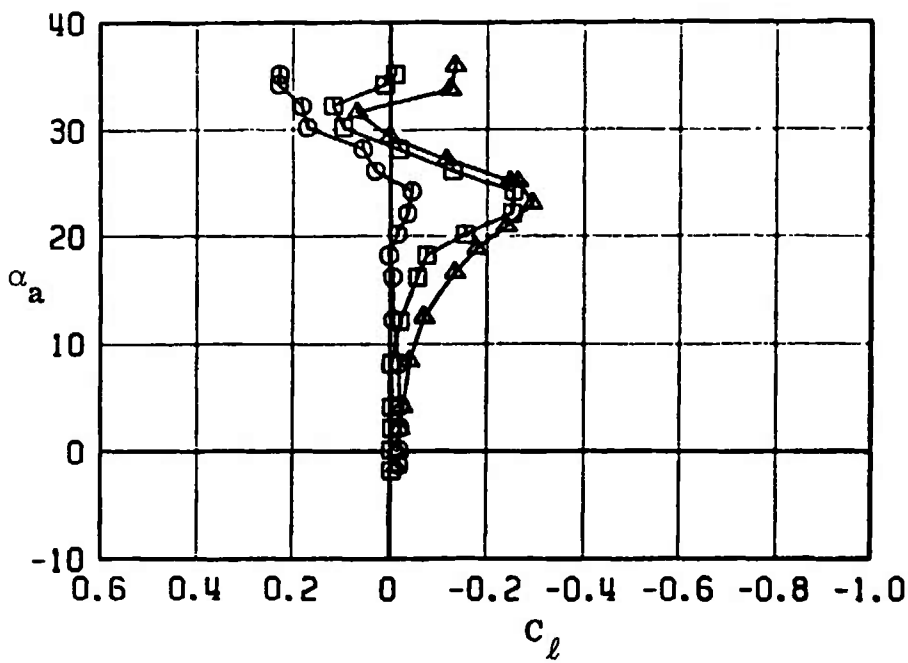


Fig. 20 Continued

CONFIGURATION COMPARISON							
ROLLING MOMENT AND AXIAL FORCE COEFFICIENTS							
SYMBOL	CONFIG	MACH NO	ϕ	ϵ_D	ϵ_H	ϵ_P	$R_E \times 10^{-6}$
□	B9T3	0.85	0	0.3	0.5	0.3	6.0
○	B10T3	0.85	0	0.4	-0.3	0.5	6.0
△	B11T3	0.85	0	0.4	-0.3	0.5	6.0



.Fig. 20 Continued

CONFIGURATION COMPARISON
ROLLING MOMENT AND AXIAL FORCE COEFFICIENTS

SYMBOL	CONFIG	MACH NO	ϕ	δ_D	δ_R	δ_P	$R_L \times 10^{-6}$
□	B9T3	0.95	0	0.3	0.5	0.3	5.6
○	B10T3	0.95	0	0.4	-0.3	0.5	5.6
△	B11T3	0.95	0	0.4	-0.3	0.5	5.6

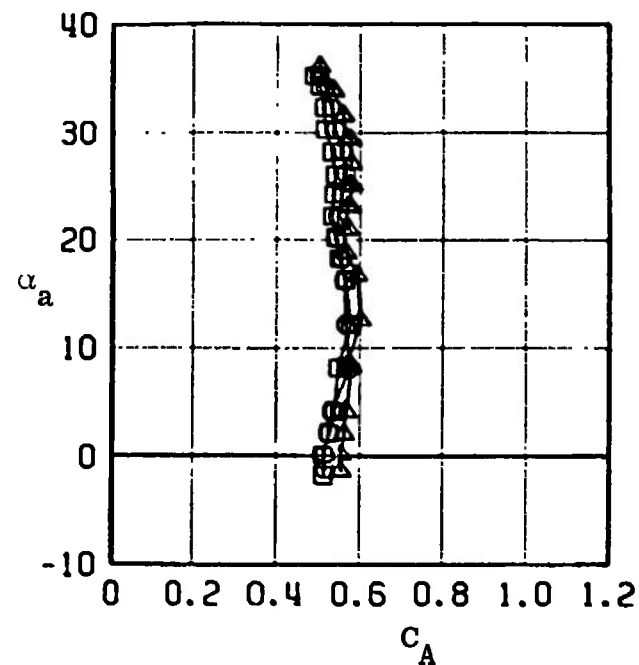
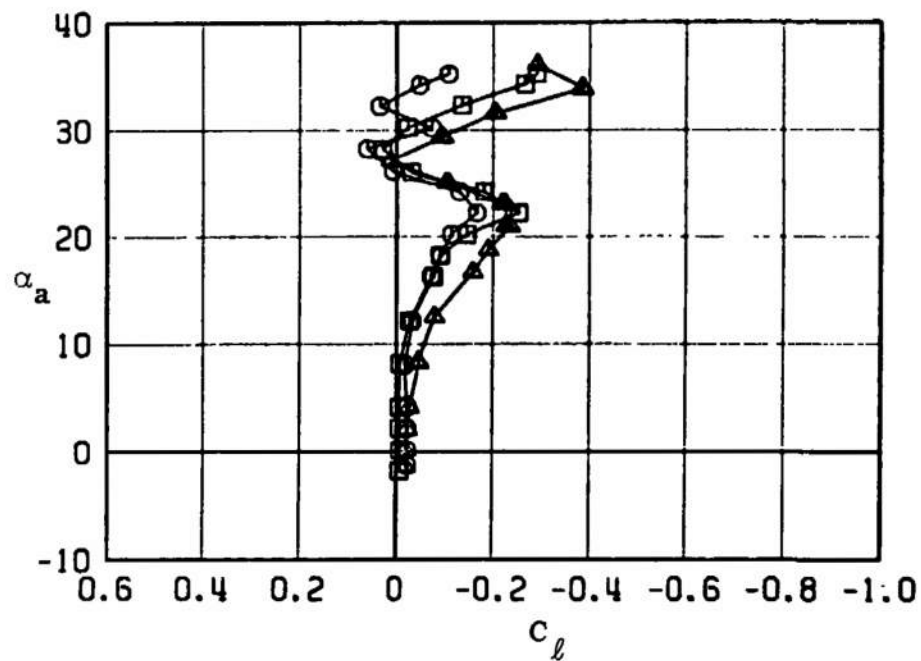


Fig. 20 Continued

CONFIGURATION COMPARISON
ROLLING MOMENT AND AXIAL FORCE COEFFICIENTS

SYMBOL	CONFIG	MACH NO	ϕ	δ_D	δ_H	δ_P	$R_E \times 10^{-6}$
\square	B9T3	1.05	0	0.3	0.5	0.3	5.8
\circ	B10T3	1.05	0	0.4	-0.3	0.5	5.8
\triangle	B11T3	1.05	0	0.4	-0.3	0.5	5.8

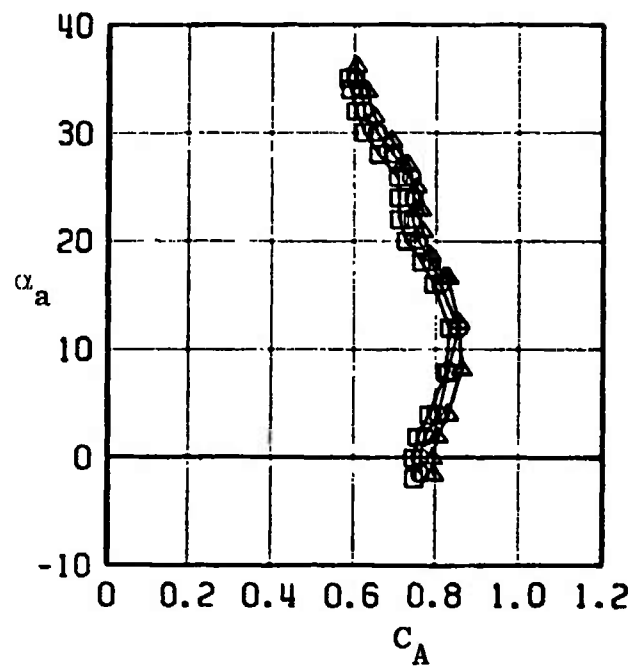
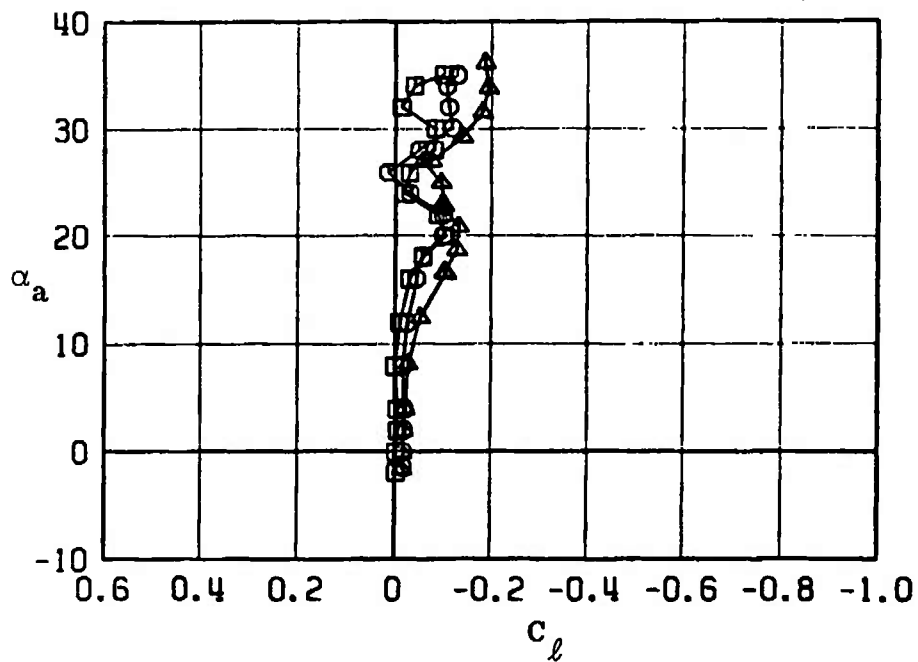


Fig. 20 Concluded

CONFIGURATION COMPARISON SIDE FORCE AND YAWING MOMENT COEFFICIENTS							
SYMBOL	CONFIG	MACH NO	ϕ	b_ϕ	b_η	δ_p	$R_\xi \times 10^{-6}$
□	B9T3	0.50	0	0.3	0.5	0.3	4.8
○	B10T3	0.50	0	0.4	-0.3	0.5	4.8
△	B11T3	0.50	0	0.4	-0.3	0.5	4.8

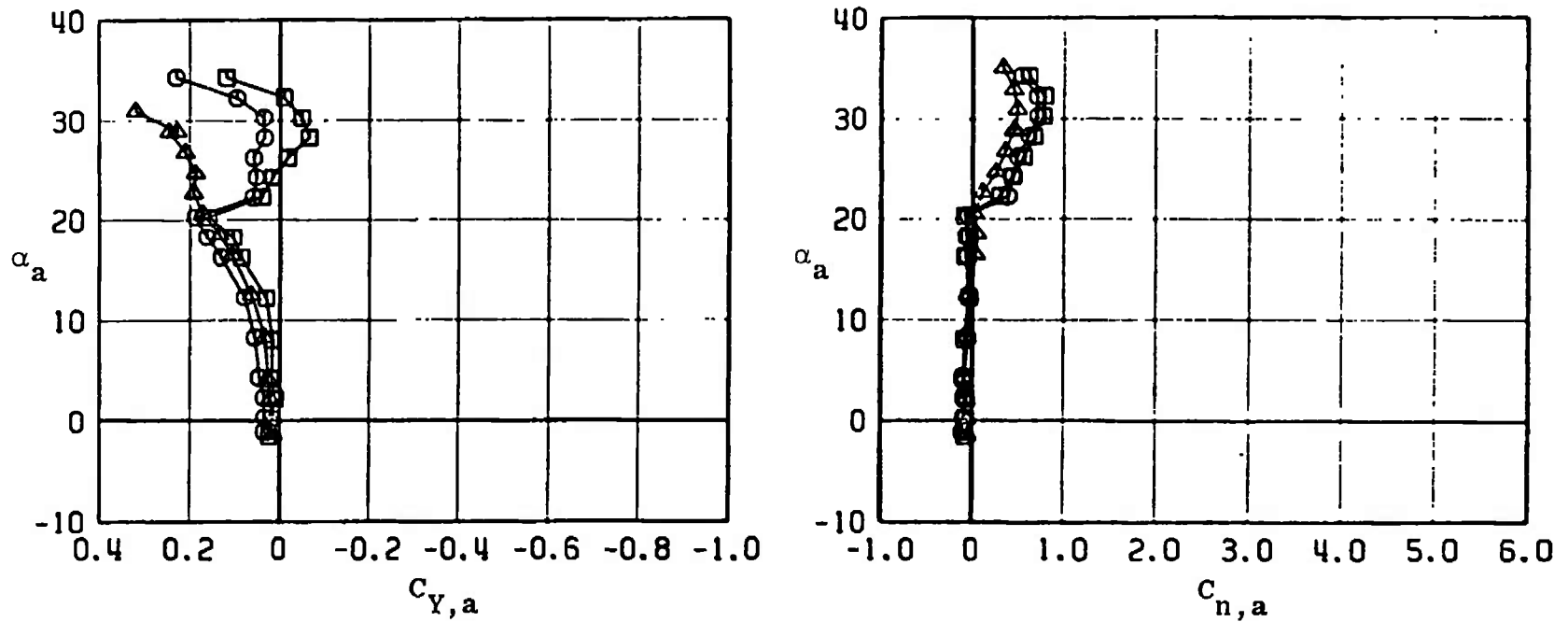


Fig. 21 Effect of Varying Fuselage Configuration on the Side-Force and Yawing-Moment Coefficient for Configurations without the RES (B9T3, B10T3, and B11T3)

CONFIGURATION COMPARISON							
SIDE FORCE AND YAWING MOMENT COEFFICIENTS							
SYMBOL	CONFIG	MACH NO	ϕ	δ_a	δ_n	δ_p	$R_E \times 10^{-6}$
\square	B9T3	0.65	0	0.3	0.5	0.3	5.4
\circ	B10T3	0.65	0	0.4	-0.3	0.5	5.4
\triangle	B11T3	0.65	0	0.4	-0.3	0.5	5.4

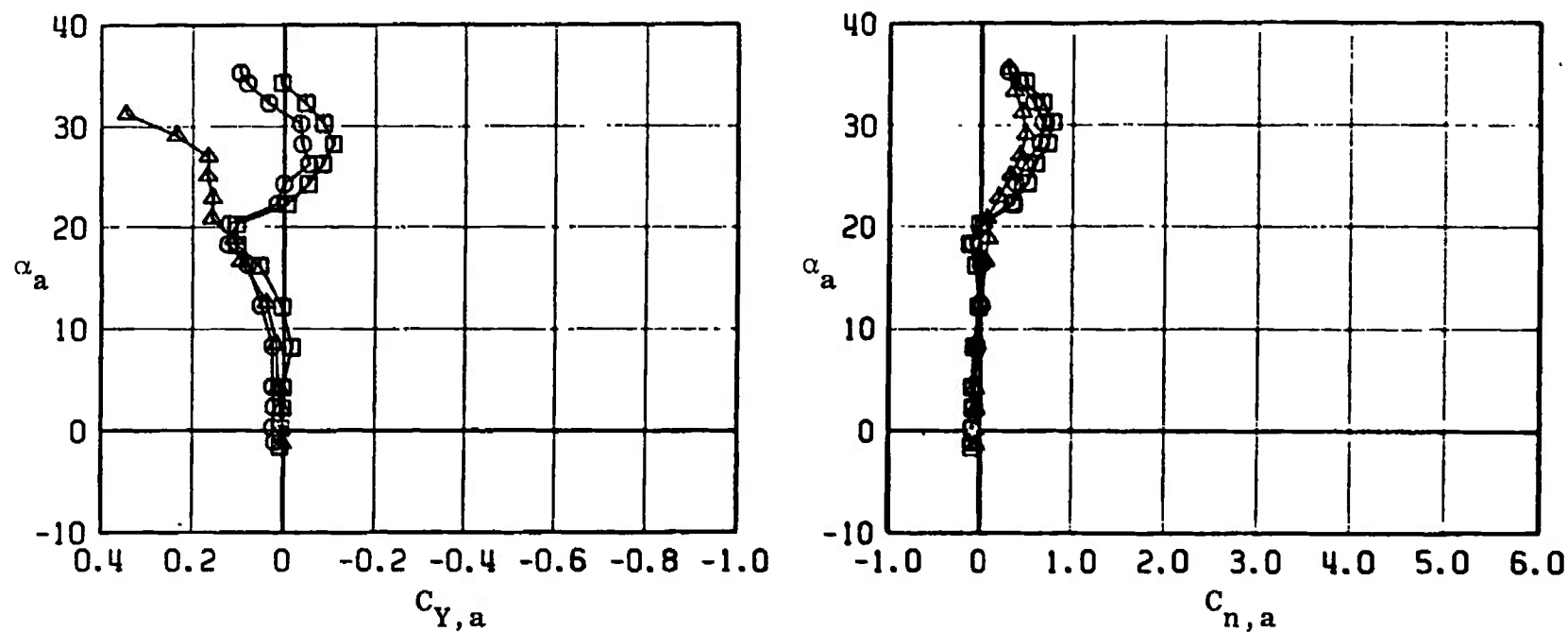


Fig. 21 Continued

CONFIGURATION COMPARISON

SIDE FORCE AND YAWING MOMENT COEFFICIENTS :

SYMBOL	CONFIG	MACH NO	ϕ	δ_D	δ_R	δ_P	$R_E \times 10^{-6}$
□	B9T3	0.75	0	0.3	0.5	0.3	5.8
○	B10T3	0.75	0	0.4	-0.3	0.5	5.8
△	B11T3	0.75	0	0.4	-0.3	0.5	5.8

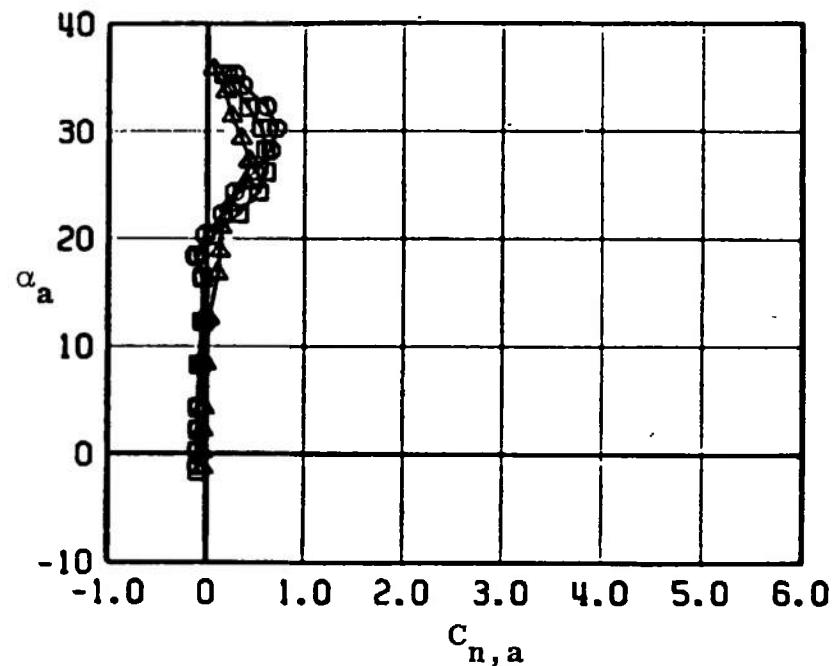
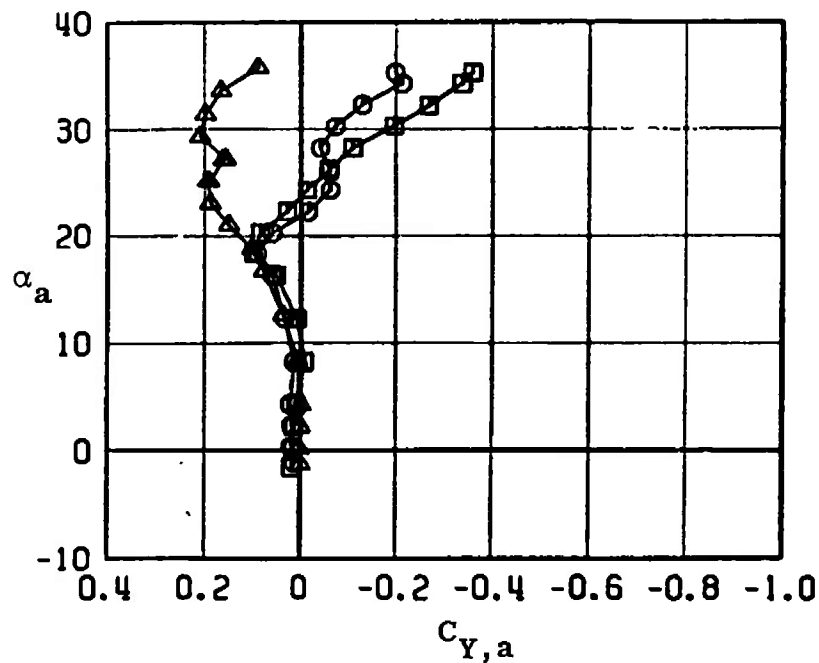


Fig. 21 Continued

CONFIGURATION COMPARISON							
SIDE FORCE AND YAWING MOMENT COEFFICIENTS							
SYMBOL	CONFIG	MACH NO	ϕ	δ_a	δ_n	δ_p	$R_E \times 10^{-6}$
\square	B9T3	0.85	0	0.3	0.5	0.3	6.0
\circ	B10T3	0.85	0	0.4	-0.3	0.5	6.0
\triangle	B11T3	0.85	0	0.4	-0.3	0.5	6.0

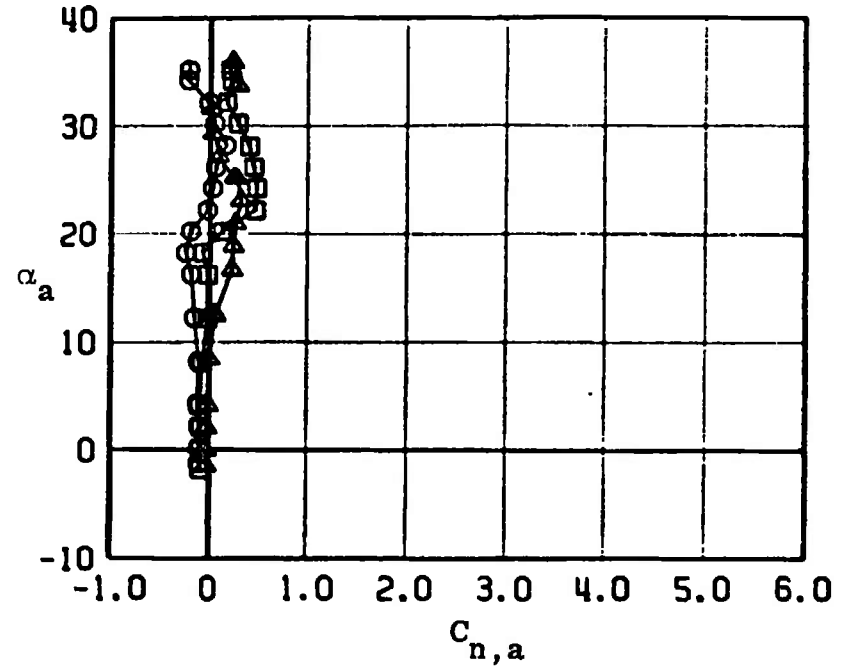
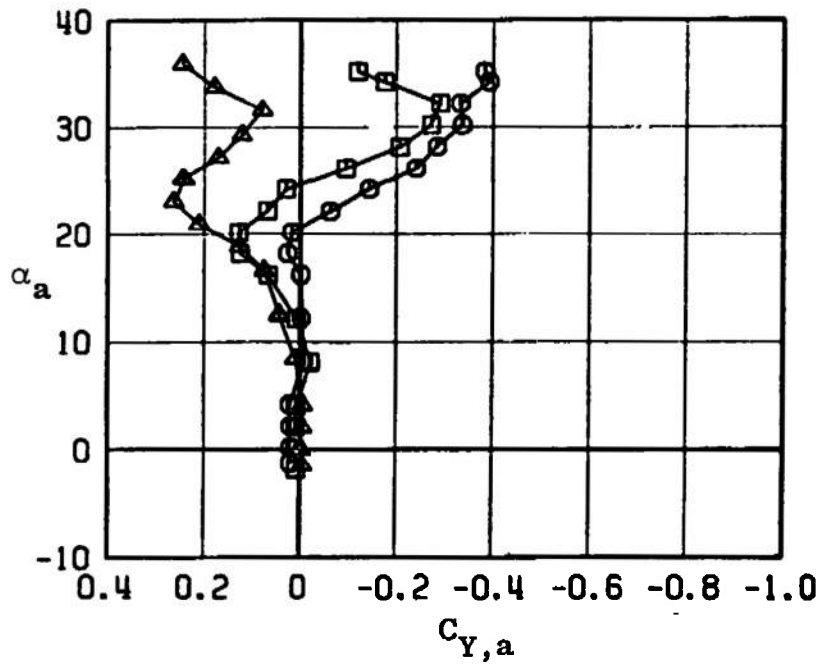


Fig. 21 Continued

CONFIGURATION COMPARISON

SIDE FORCE AND YAWING MOMENT COEFFICIENTS

SYMBOL	CONFIG	MACH NO	ϕ	ϵ_D	ϵ_H	ϵ_P	$R_E \times 10^{-6}$
□	B9T3	0.95	0	0.3	0.5	0.3	5.6
○	B10T3	0.95	0	0.4	-0.3	0.5	5.6
△	B11T3	0.95	0	0.4	-0.3	0.5	5.6

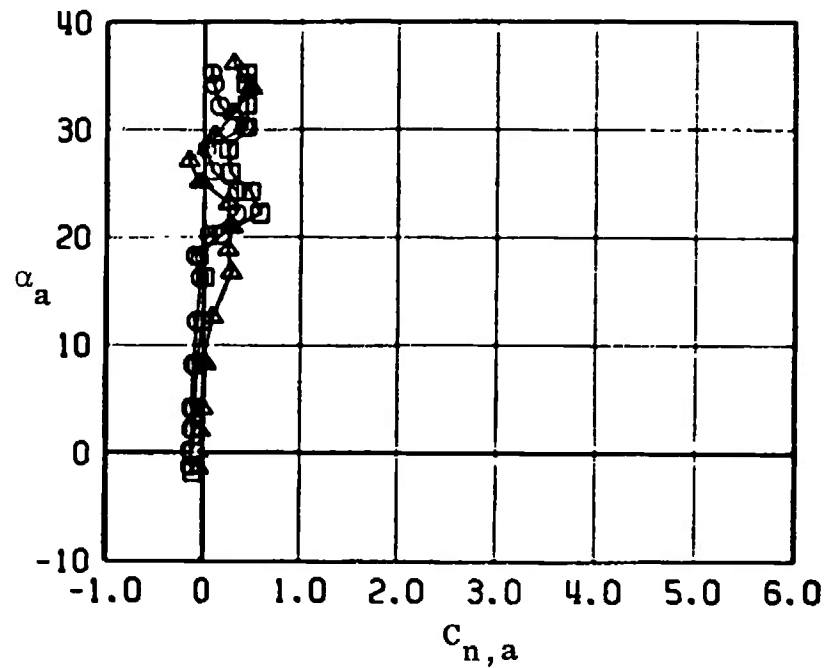
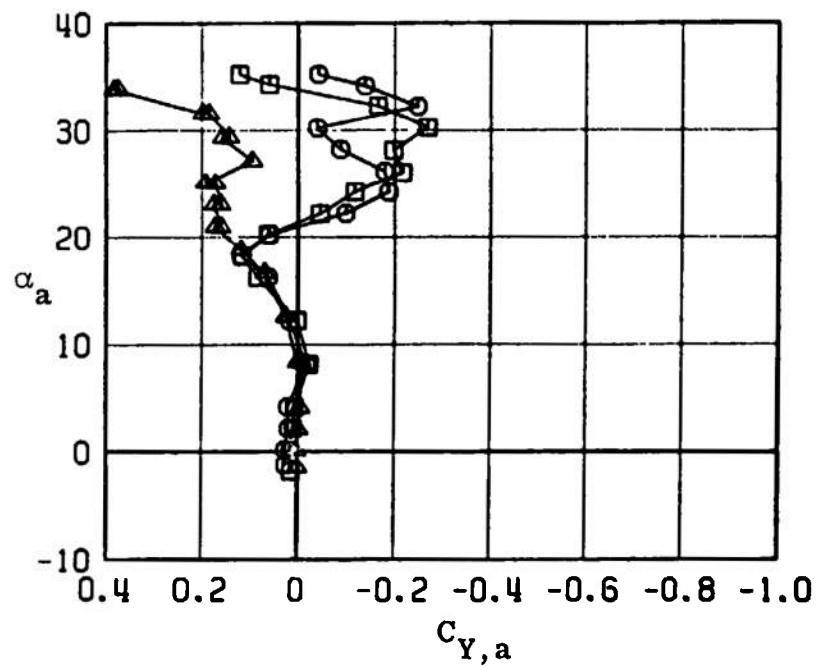


Fig. 21 Continued

CONFIGURATION COMPARISON							
SIDE FORCE AND YAWING MOMENT COEFFICIENTS							
SYMBOL	CONFIG	MACH NO	ϕ	δ_0	δ_n	δ_r	$R_E \times 10^{-6}$
\square	B9T3	1.05	0	0.3	0.5	0.3	5.8
\circ	B10T3	1.05	0	0.4	-0.3	0.5	5.8
\triangle	B11T3	1.05	0	0.4	-0.3	0.5	5.8

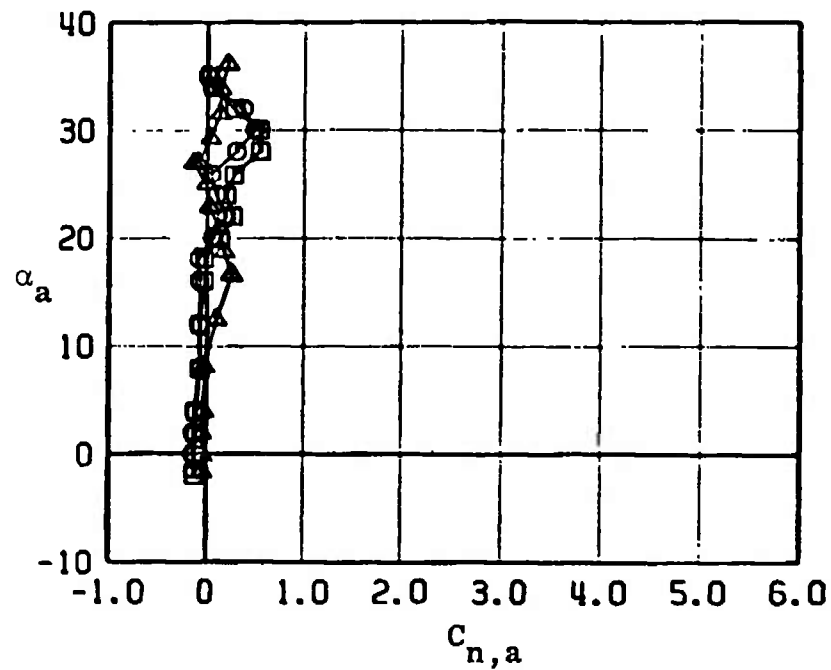
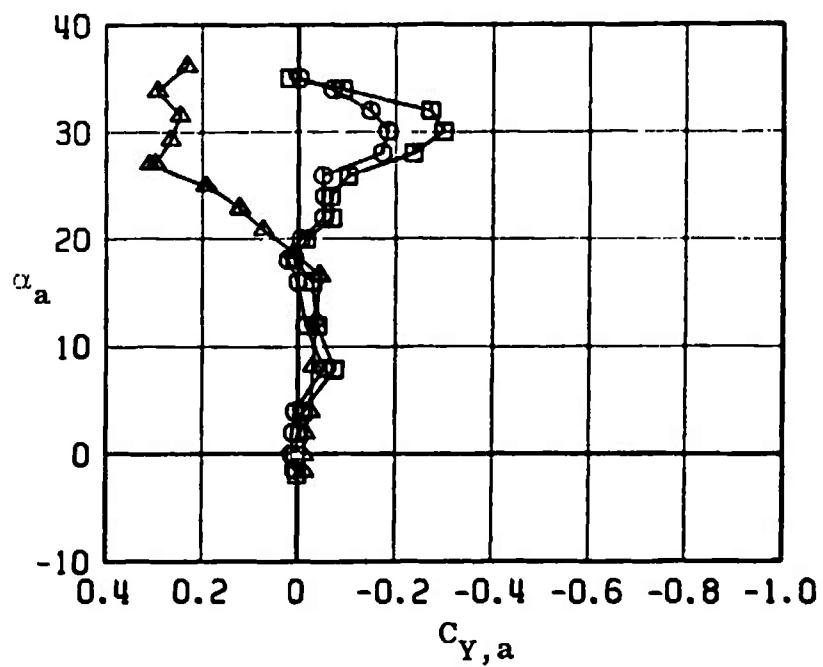


Fig. 21 Concluded

CONFIGURATION COMPARISON							
MGGB LONGITUDINAL STABILITY CHARACTERISTICS							
SYMBOL	CONFIG	MACH NO	ϕ	δ_D	δ_R	δ_P	$R_E \times 10^{-6}$
\square	B10W8S1T3	0.50	0	0.4	-0.3	0.3	1.5
\circ	B9W8S1T3	0.50	0	0.4	-0.3	0.3	1.5

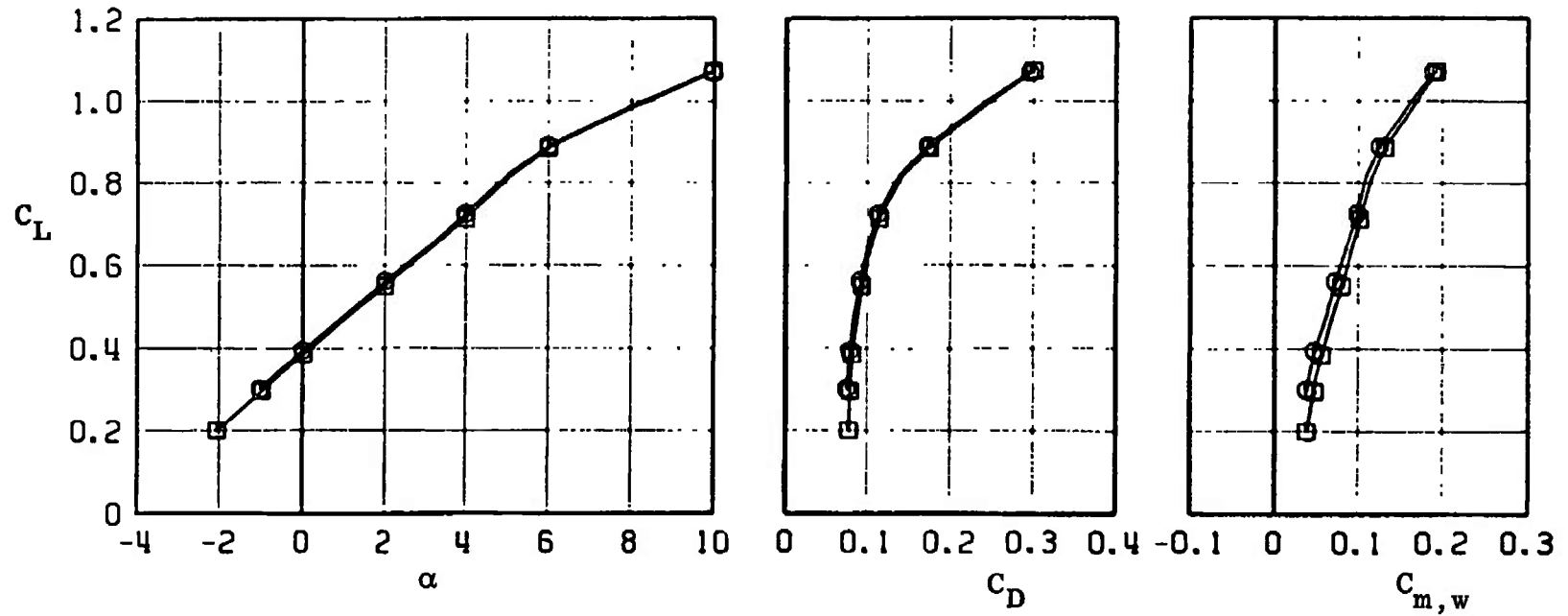


Fig. 22 Effect of Fuselage Protuberances on the Longitudinal Stability Characteristics for MGGB Configurations (B9W8S1T3 and B10W8S1T3)

CONFIGURATION COMPARISON							
MGG B LONGITUDINAL STABILITY CHARACTERISTICS							
SYMBOL	CONFIG	MACH NO	ϕ	δ_0	δ_R	δ_P	$R_F \times 10^{-6}$
□	B10W8S1T3	0.60	0	0.4	-0.3	0.3	1.7
○	B9W8S1T3	0.60	0	0.4	-0.3	0.3	1-7

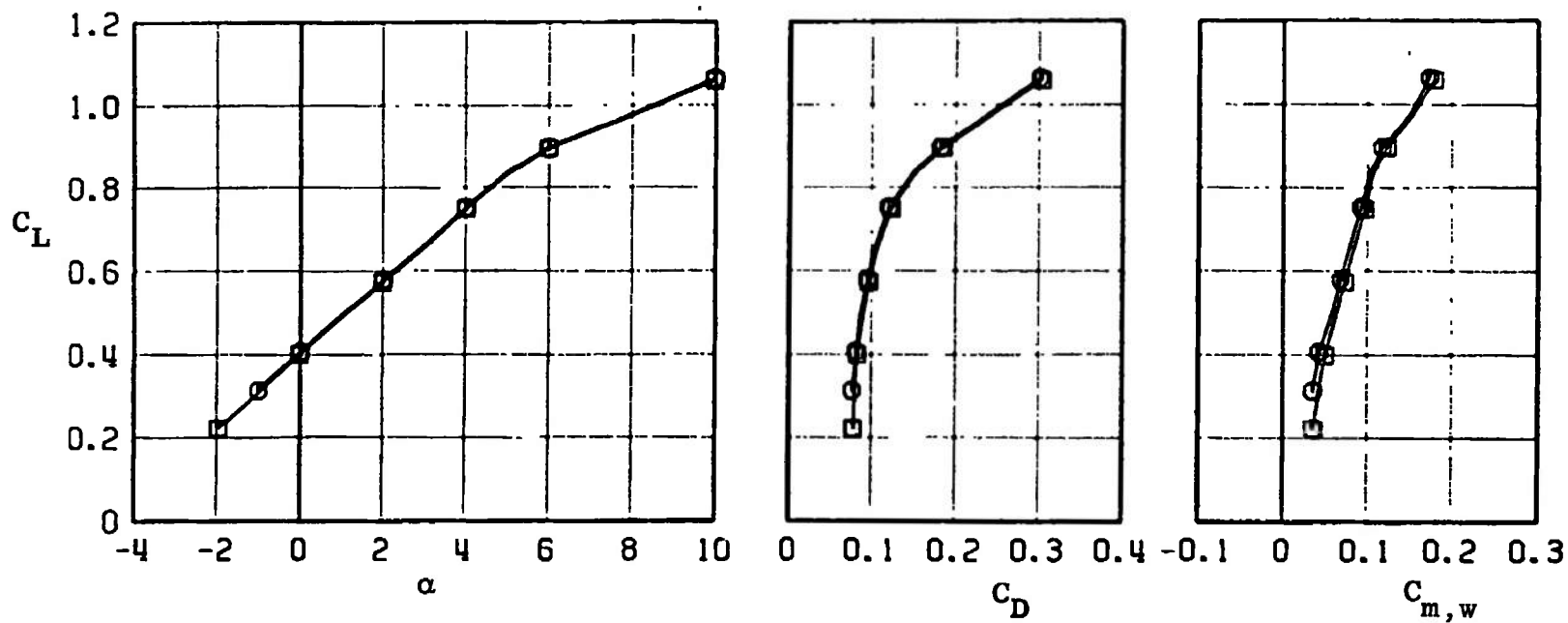


Fig. 22 Continued

CONFIGURATION COMPARISON						
MGGB LONGITUDINAL STABILITY CHARACTERISTICS						
SYMBOL	CONFIG	MACH NO	ϵ	δ_D	δ_R	δ_P
\square	B10W8S1T3	0.75	0	0.4	-0.3	0.3
\circ	B9W8S1T3	0.75	0	0.4	-0.3	0.3
						$R_E \times 10^{-6}$
						2.0
						2.0

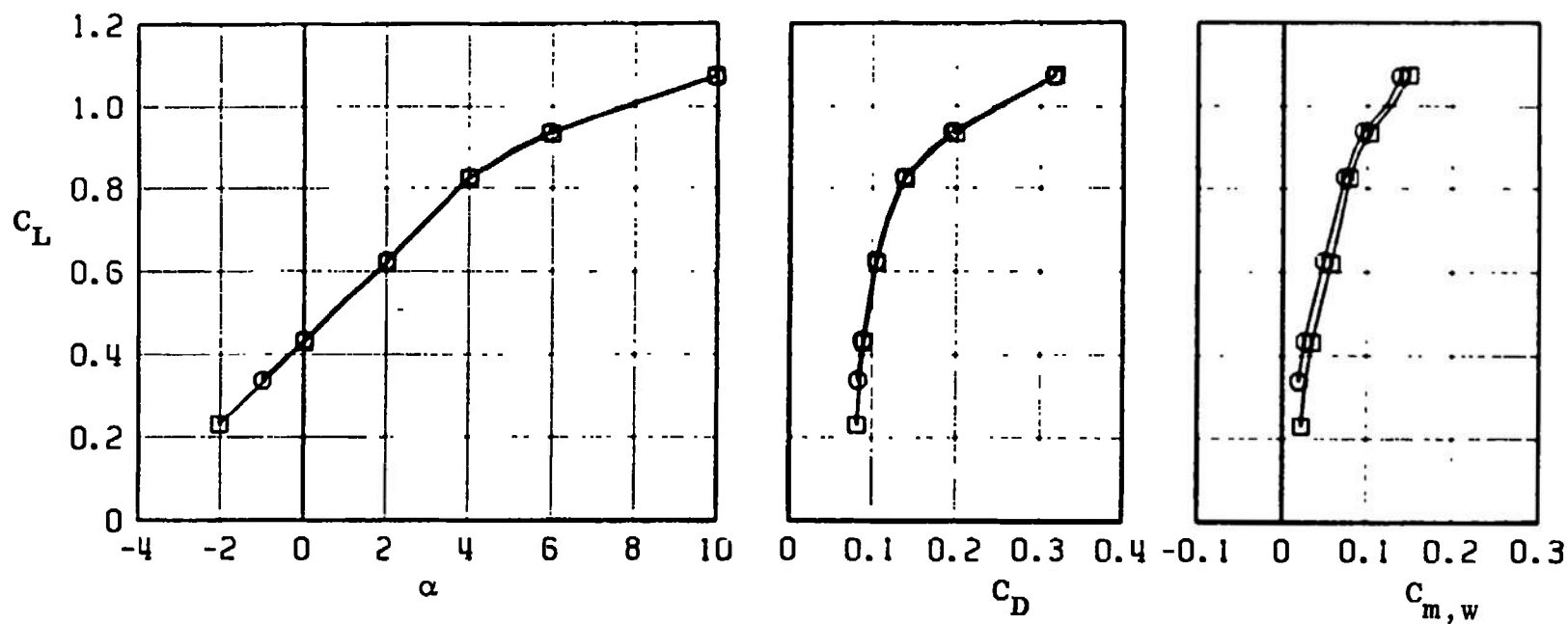


Fig. 22 Continued

CONFIGURATION COMPARISON
MGB LONGITUDINAL STABILITY CHARACTERISTICS

SYMBOL	CONFIG	MACH NO	ϕ	δ_a	δ_n	δ_p	$R_E \times 10^{-6}$
\square	B10W8S1T3	0.85	0	0.4	-0.3	0.3	2.1
\circ	B9W8S1T3	0.85	0	0.4	-0.3	0.3	2.1

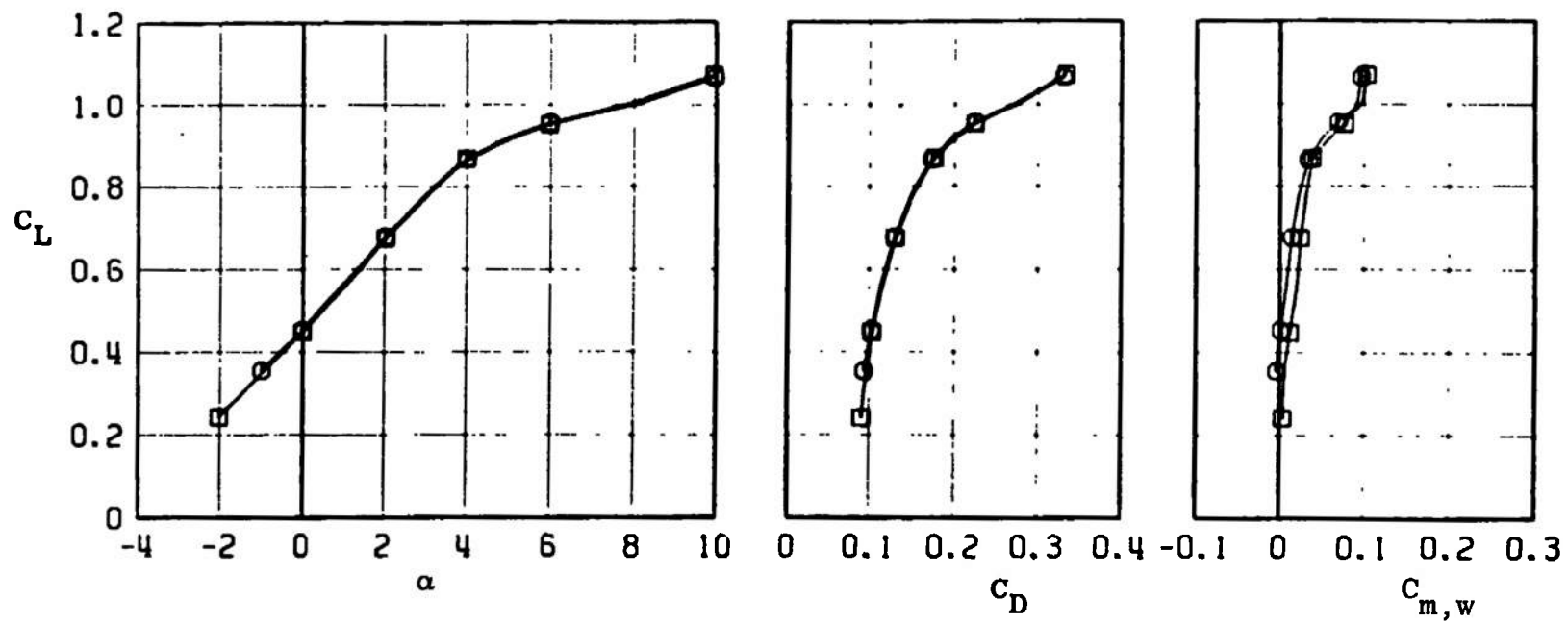


Fig. 22 Continued

CONFIGURATION COMPARISON

MGB LONGITUDINAL STABILITY CHARACTERISTICS

SYMBOL	CONFIG	MACH NO	ϕ	ϵ_a	ϵ_R	ϵ_P	$R_E \times 10^{-6}$
\square	B10W8S1T3	0.95	0	0.4	-0.3	0.3	2.2
\circ	B9W8S1T3	0.95	0	0.4	-0.3	0.3	2.2

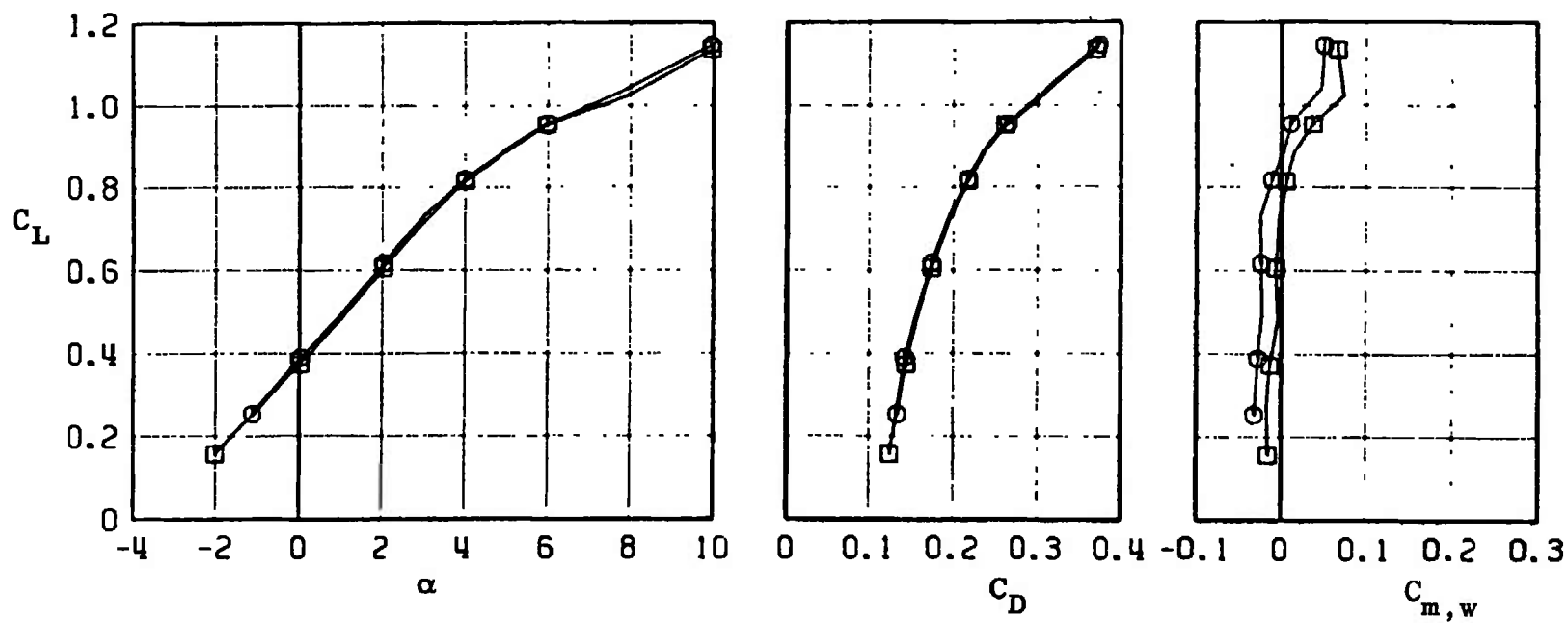


Fig. 22 Concluded

CONFIGURATION COMPARISON

MGGB L/D CHARACTERISTICS

SYMBOL	CONFIG	MACH NO	ϕ	δ_0	δ_H	δ_P	$R_E \times 10^{-6}$
\square	B10W8S1T3	0.50	0	0.4	-0.3	0.3	1.5
\circ	B9W8S1T3	0.50	0	0.4	-0.3	0.3	1.5

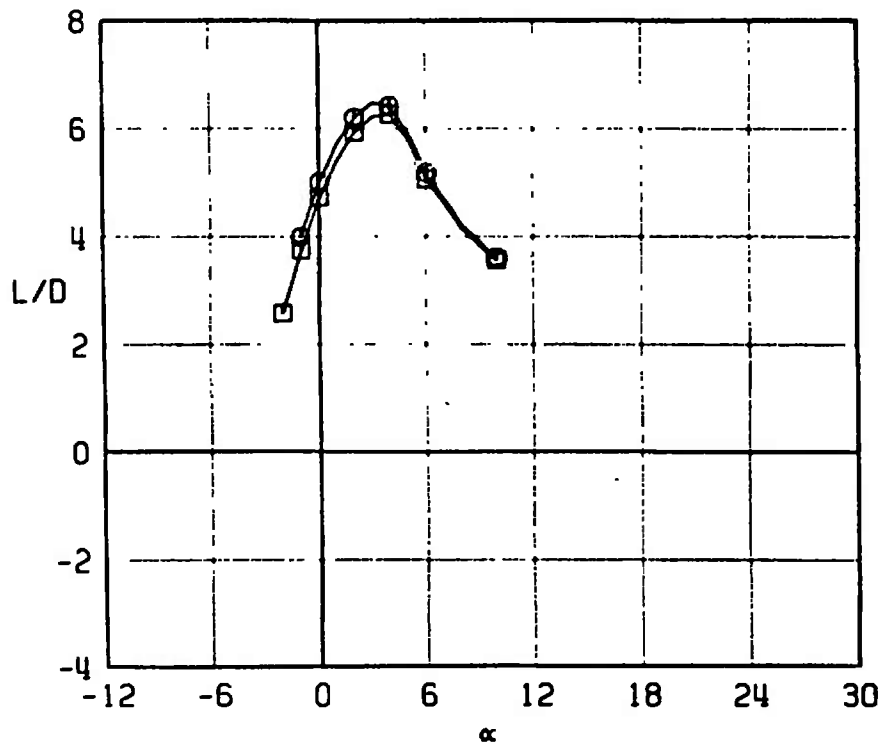


Fig. 23 Effect of Fuselage Protuberances on the Lift-to-Drag Ratio for MGGB Configurations (B9W8S1T3 and B10W8S1T3)

CONFIGURATION COMPARISON

MGCB L/D CHARACTERISTICS

SYMBOL	CONFIG	MACH NO	ϕ	δ_0	δ_H	δ_P	$R_E \times 10^{-6}$
\square	B10W8S1T3	0.60	0	0.4	-0.3	0.3	1.7
\circ	B9W8S1T3	0.60	0	0.4	-0.3	0.3	1.7

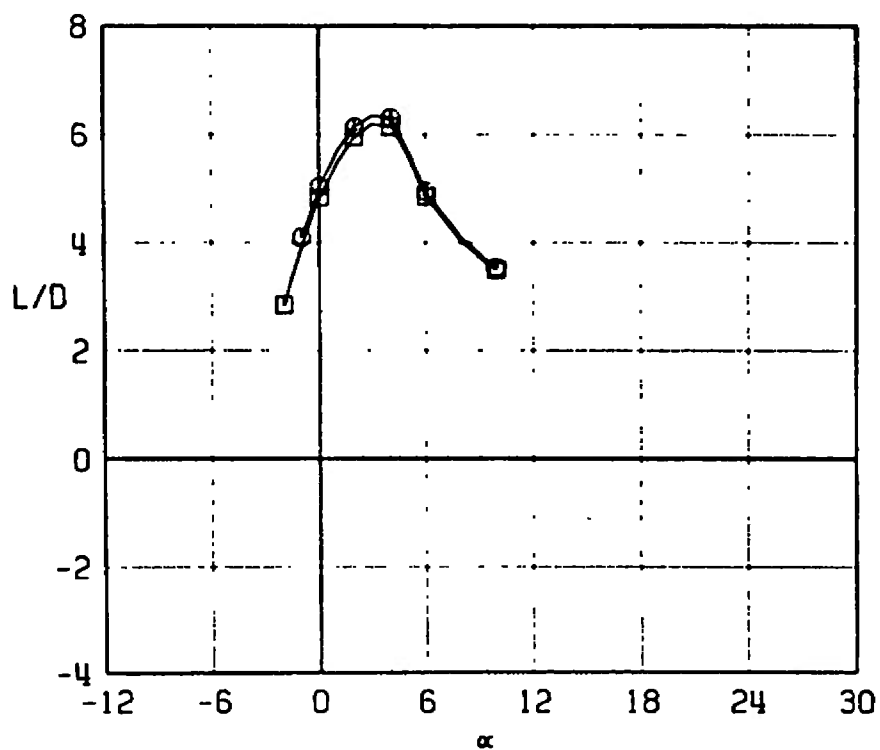


Fig. 23 Continued

CONFIGURATION COMPARISON
MCCB L/D CHARACTERISTICS

SYMBOL	CONFIG	MACH NO	ϕ	δ_D	δ_H	δ_P	$R_L \times 10^{-6}$
\square	B10W8S1T3	0.75	0	0.4	-0.3	0.3	2.0
\circ	B9W8S1T3	0.75	0	0.4	-0.3	0.3	2.0

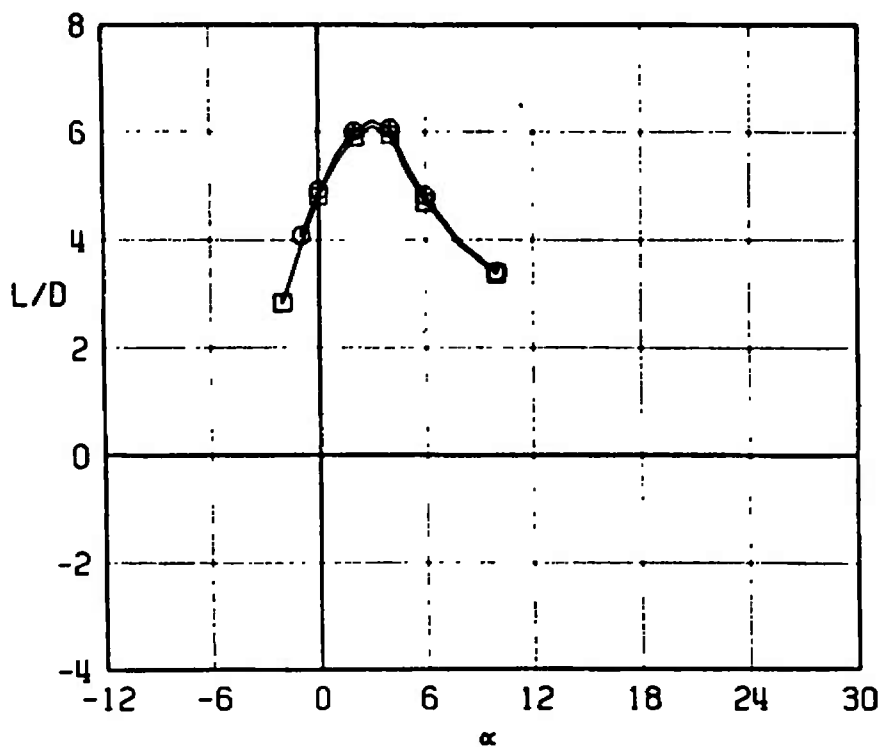


Fig. 23 Continued

CONFIGURATION COMPARISON
MGG B L/D CHARACTERISTICS

SYMBOL	CONFIG	MACH NO	ϕ	δ_0	δ_n	δ_p	$R_L \times 10^{-6}$
□	B10W8S1T3	0.85	0	0.4	-0.3	0.3	2.1
○	B9W8S1T3	0.85	0	0.4	-0.3	0.3	2.1

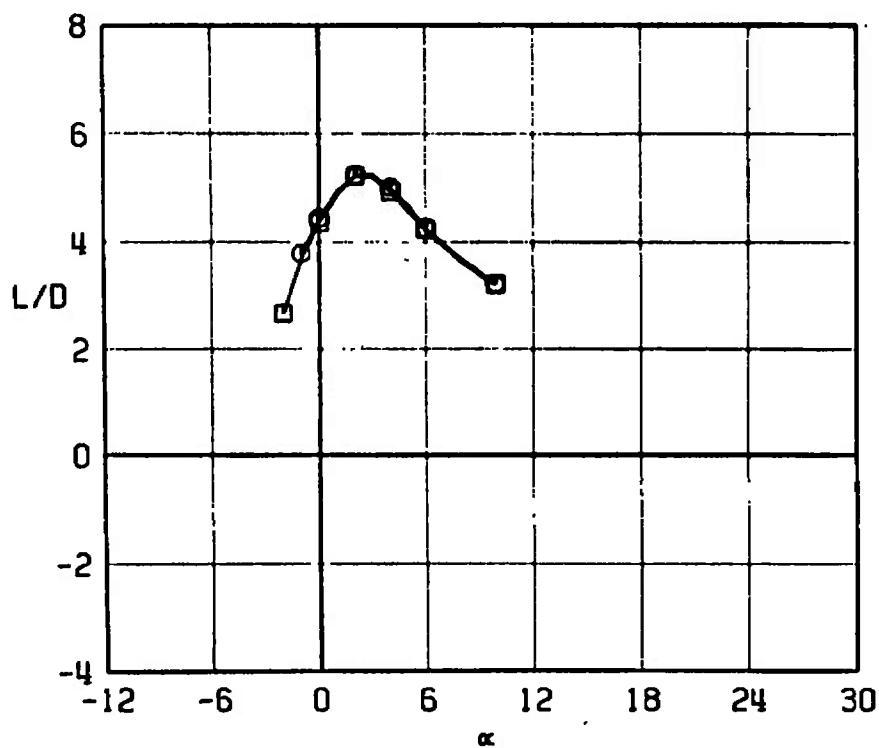


Fig. 23 Continued

CONFIGURATION COMPARISON

MCCB L/D CHARACTERISTICS

SYMBOL	CONFIG	MACH NO	ϕ	δ_D	δ_H	δ_P	$R_E \times 10^{-6}$
\square	B10W8S1T3	0.95	0	0.4	-0.3	0.3	2.2
\circ	B9W8S1T3	0.95	0	0.4	-0.3	0.3	2.2

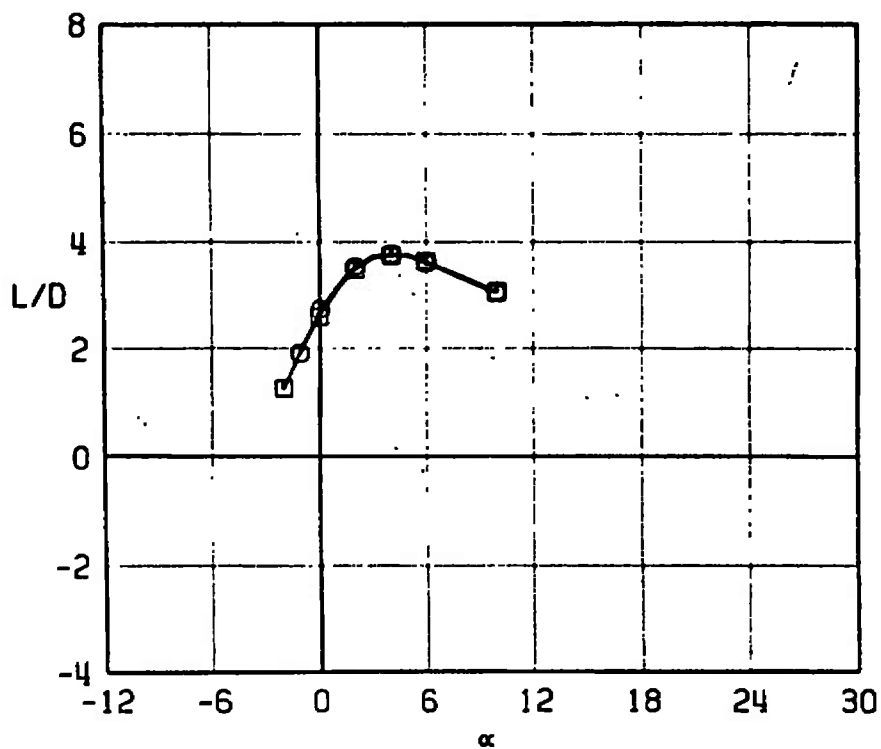


Fig. 23 Concluded

CONFIGURATION COMPARISON

MGGB LATERAL-DIRECTIONAL STABILITY CHARACTERISTICS

SYMBOL	CONFIG	MACH NO	ϕ	b_0	b_R	b_P	$R_E \times 10^{-5}$
\square	B10W8S1T3	0.50	90	0.4	-0.3	0.3	1.5
\circ	B9W8S1T3	0.50	90	0.4	-0.3	0.3	1.5

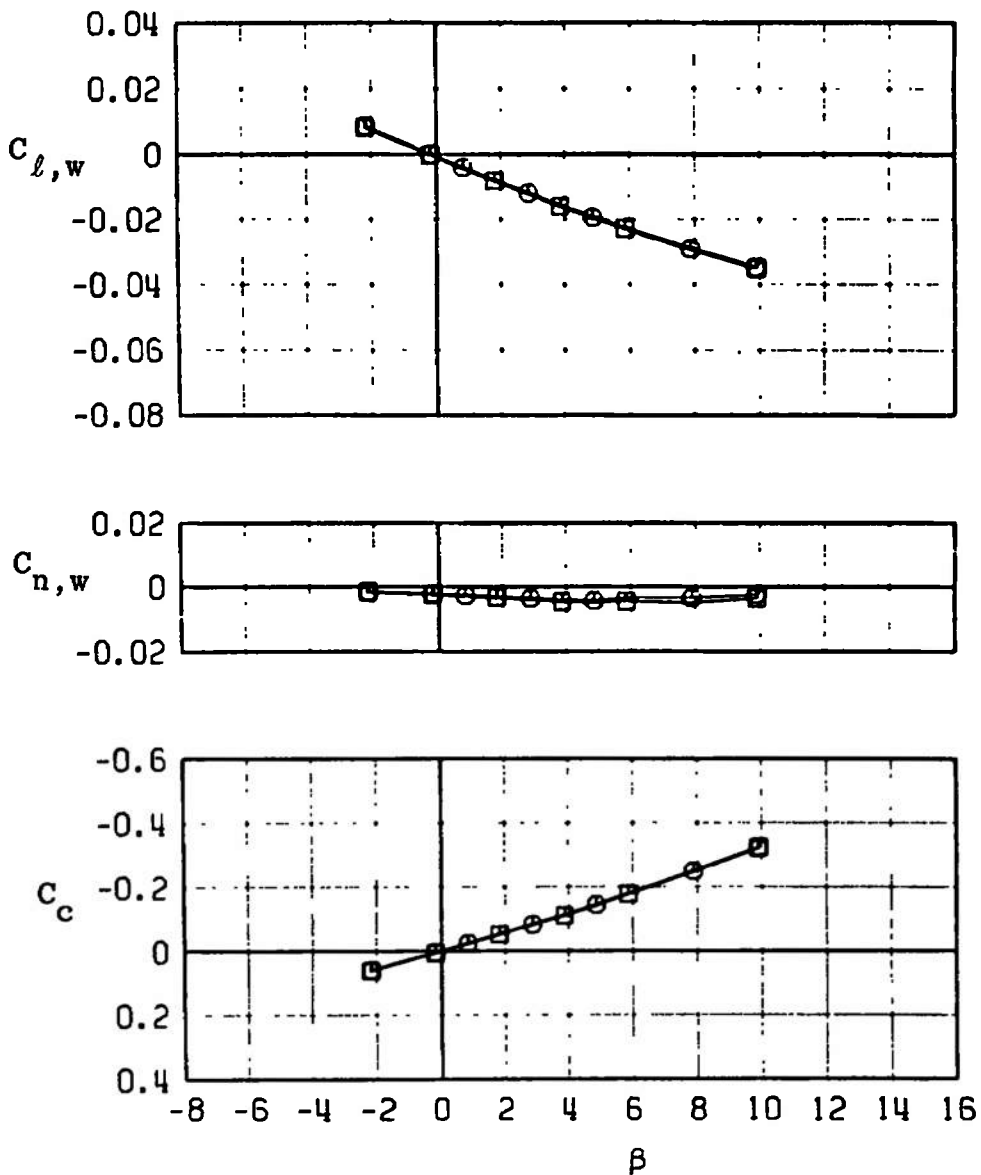


Fig. 24 Effect of Fuselage Configuration on the Lateral and Directional Stability Characteristics for MGGB Configurations (B9W8S1T3 and B10W8S1T3)

CONFIGURATION COMPARISON

MCCB LATERAL-DIRECTIONAL STABILITY CHARACTERISTICS

SYMBOL	CONFIG	MACH NO	ϕ	b_0	b_R	b_P	$R_L \times 10^{-6}$
□	B10W8S1T3	0.60	90	0.4	-0.3	0.3	1.7
○	B9W8S1T3	0.60	90	0.4	-0.3	0.3	1.7

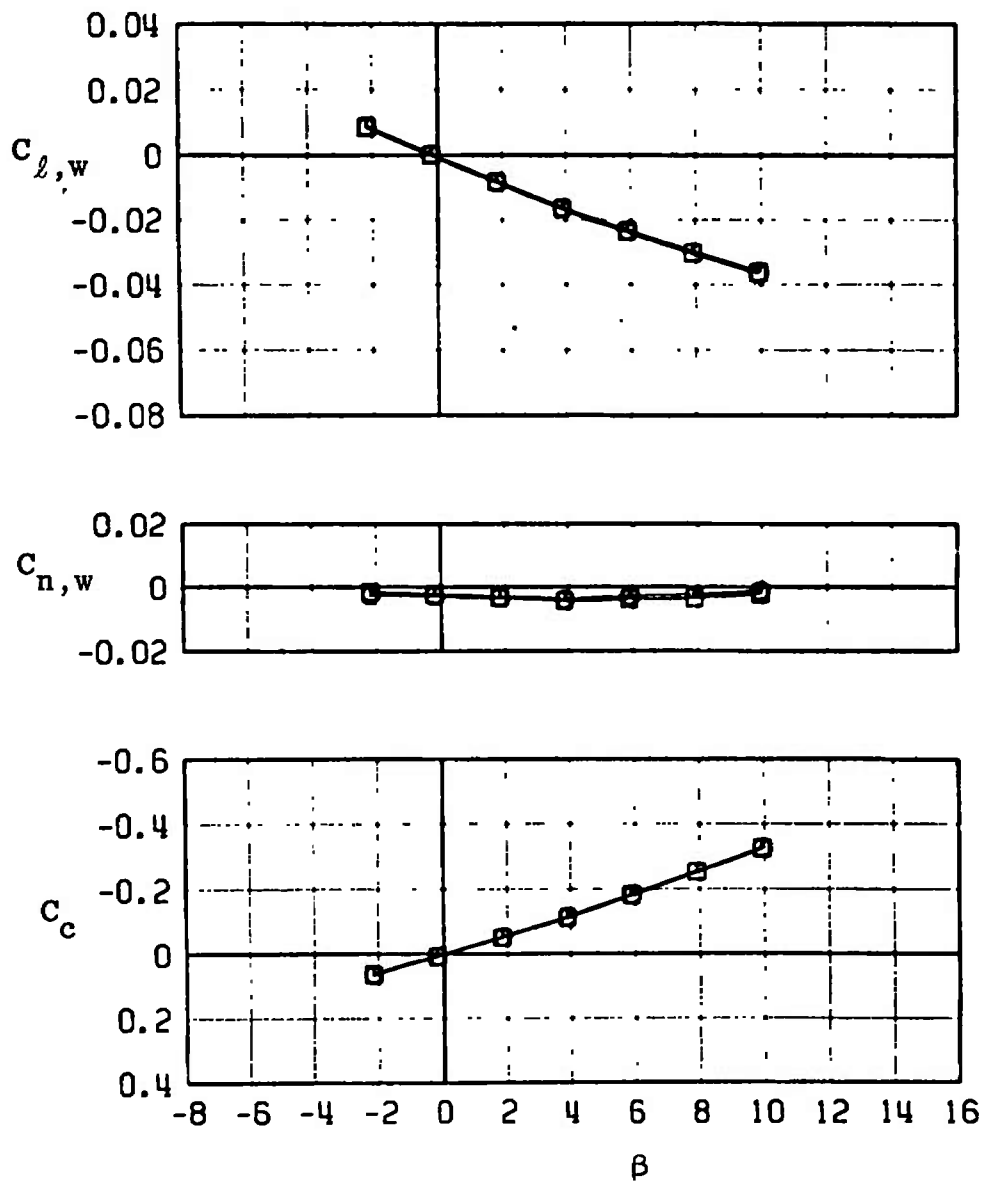


Fig. 24 Continued

CONFIGURATION COMPARISON

MGB LATERAL-DIRECTIONAL STABILITY CHARACTERISTICS

SYMBOL	CONFIG	MACH NO	ϕ	δ_0	δ_R	δ_P	$R_L \times 10^{-6}$
\square	B10W8S1T3	0.75	90	0.4	-0.3	0.3	2.0
\circ	B9W8S1T3	0.75	90	0.4	-0.3	0.3	2.0

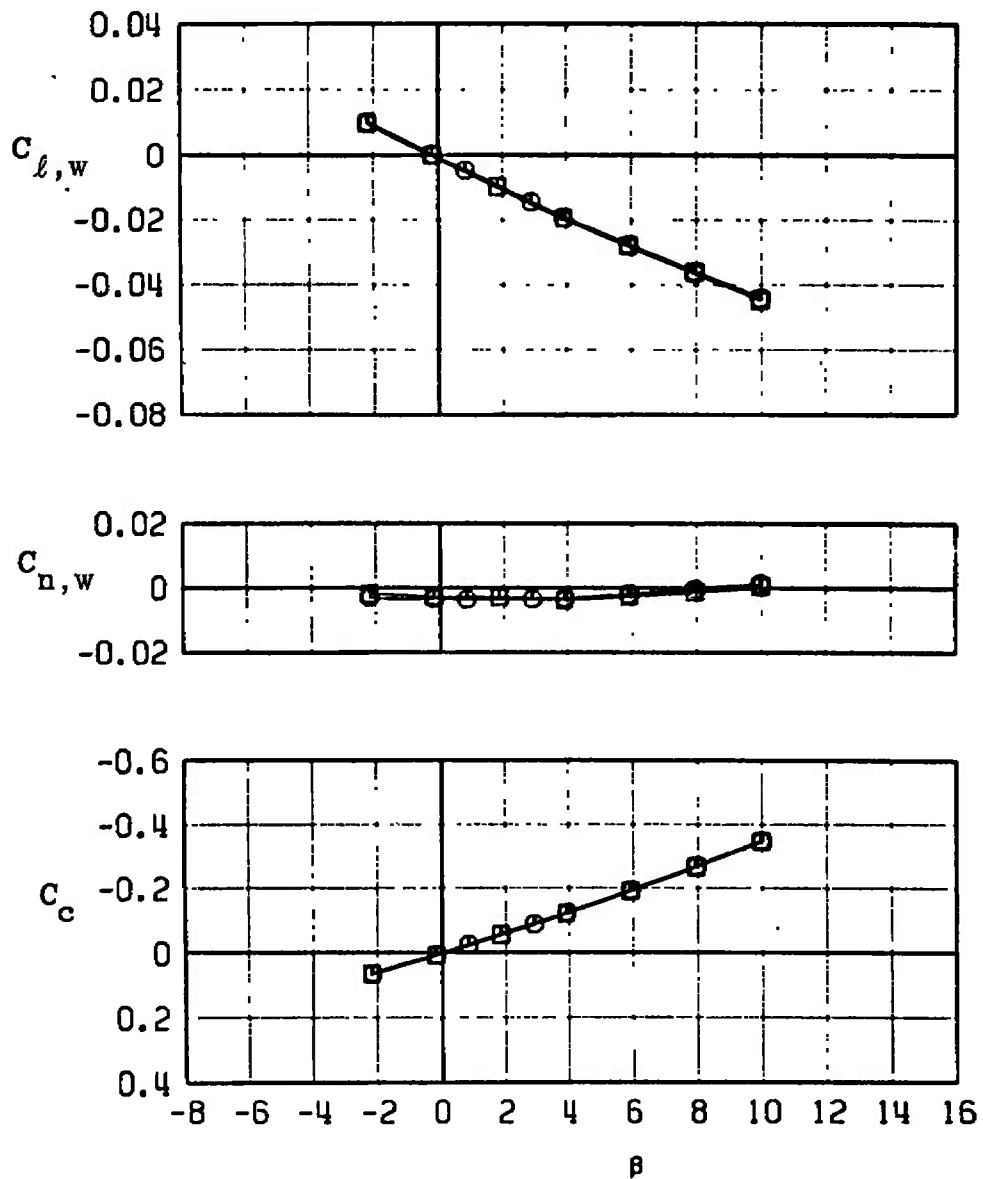


Fig. 24 Continued

CONFIGURATION COMPARISON

MGGB LATERAL-DIRECTIONAL STABILITY CHARACTERISTICS

SYMBOL	CONFIG	MACH NO	ϕ	ξ_0	ξ_R	ξ_P	$R_E \times 10^{-6}$
\square	B10W8S1T3	0.85	90	0.4	-0.3	0.3	2.1
\circ	B9W8S1T3	0.85	90	0.4	-0.3	0.3	2.1

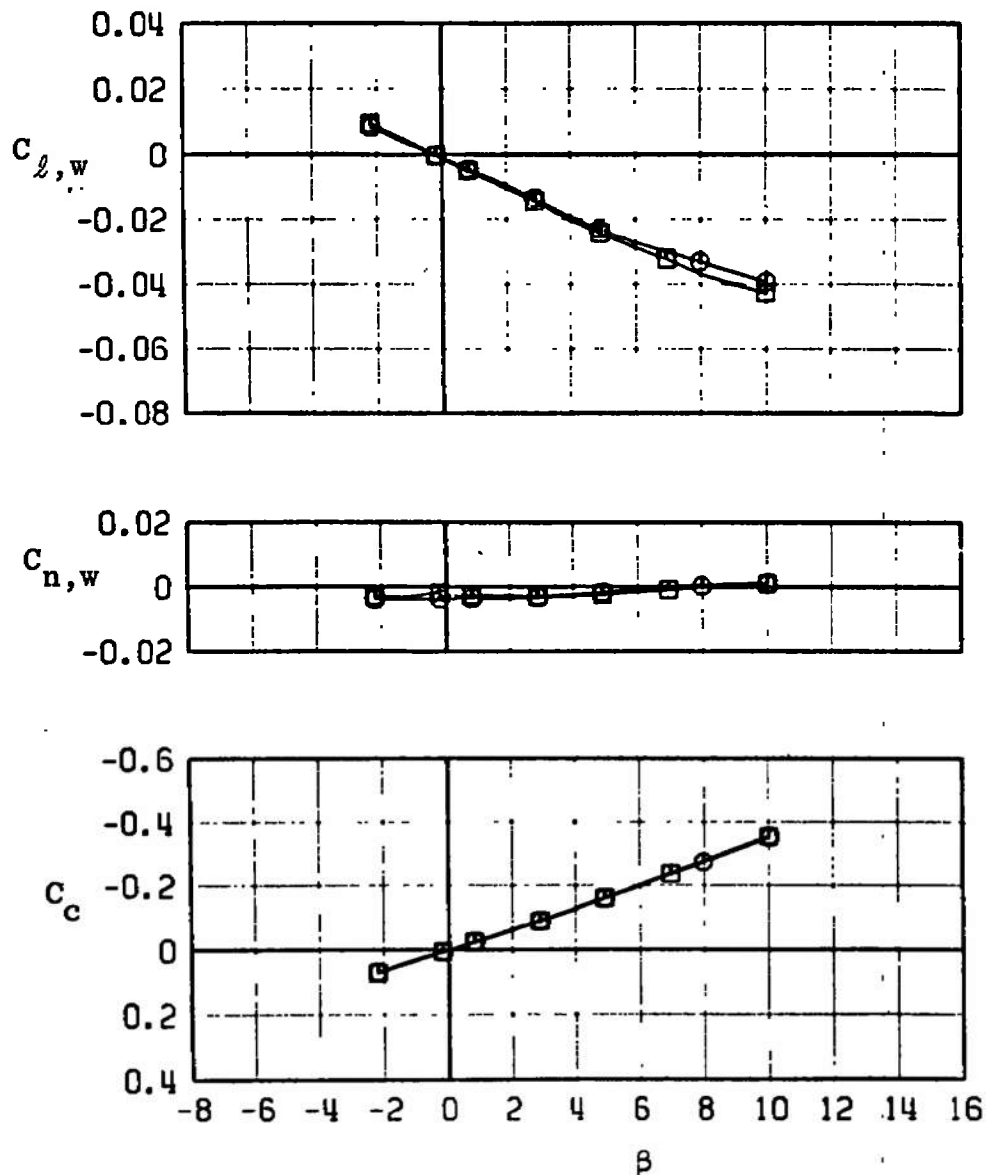


Fig. 24 Continued

CONFIGURATION COMPARISON

MGBB LATERAL-DIRECTIONAL STABILITY CHARACTERISTICS

SYMBOL	CONFIG	MACH NO	ϕ	b_0	b_R	b_P	$R_L \times 10^{-6}$
\square	B10W8S1T3	0.95	90	0.4	-0.3	0.3	2.2
\circ	B9W8S1T3	0.95	90	0.4	-0.3	0.3	2.2

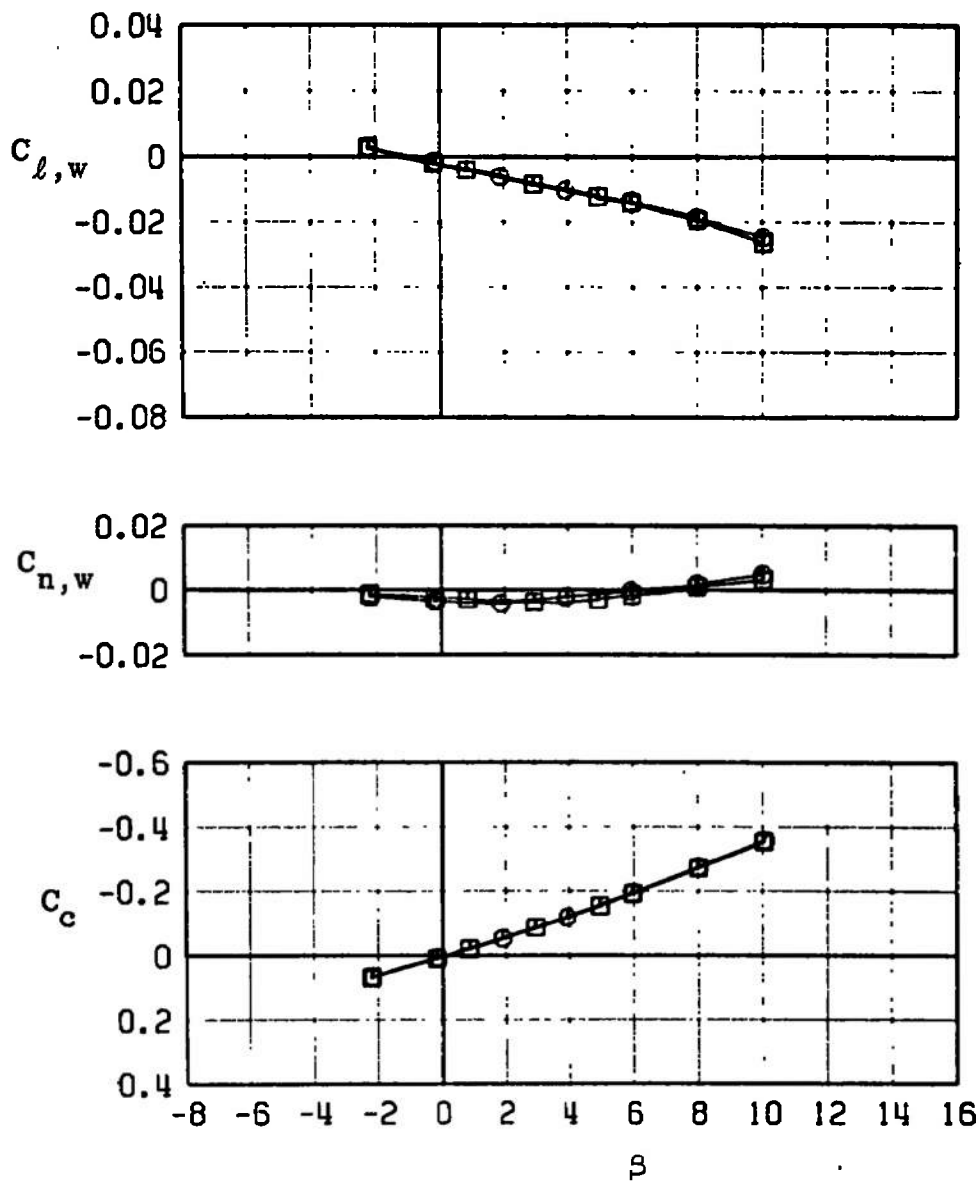


Fig. 24 Concluded

PITCH CONTROL EFFECTIVENESS
NORMAL FORCE AND PITCHING MOMENT COEFFICIENTS

SYMBOL	CONFIG	MACH NO	ϕ	b_0	b_R	b_P	$R_E \times 10^{-6}$
□	B9T3	0.50	0	0.3	0.5	0.3	1.5
○	B9T3	0.50	0	-10.1	0.1	0.3	1.5
△	B9T3	0.50	0	-14.9	0.1	-0.1	1.5
◇	B9T3	0.50	0	-20.5	0.2	-0.1	1.5

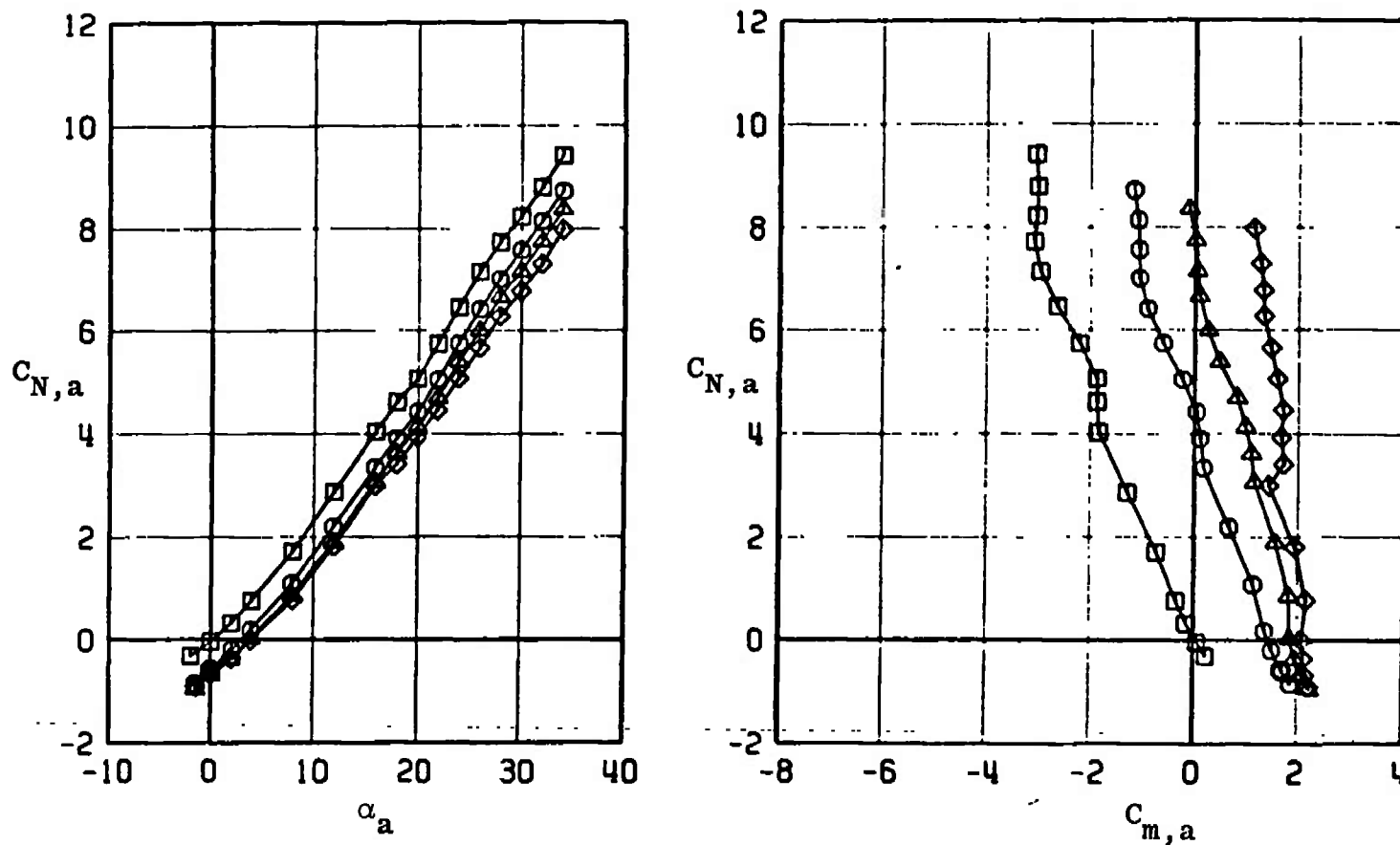


Fig. 25 Effect of Pitch Control Deflections on the Normal-Force and Pitching-Moment Coefficients for MGGB Configuration without RES (B9T3)

PITCH CONTROL EFFECTIVENESS

NORMAL FORCE AND PITCHING MOMENT COEFFICIENTS

SYMBOL	CONFIG	MACH NO	ϕ	δ_0	δ_R	δ_P	$R_E \times 10^{-6}$
□	B9T3	0.65	0	0.3	0.5	0.3	1.8
○	B9T3	0.65	0	-10.1	0.1	0.3	1.8
△	B9T3	0.65	0	-14.9	0.1	-0.1	1.8
◇	B9T3	0.65	0	-20.5	0.2	-0.1	1.8

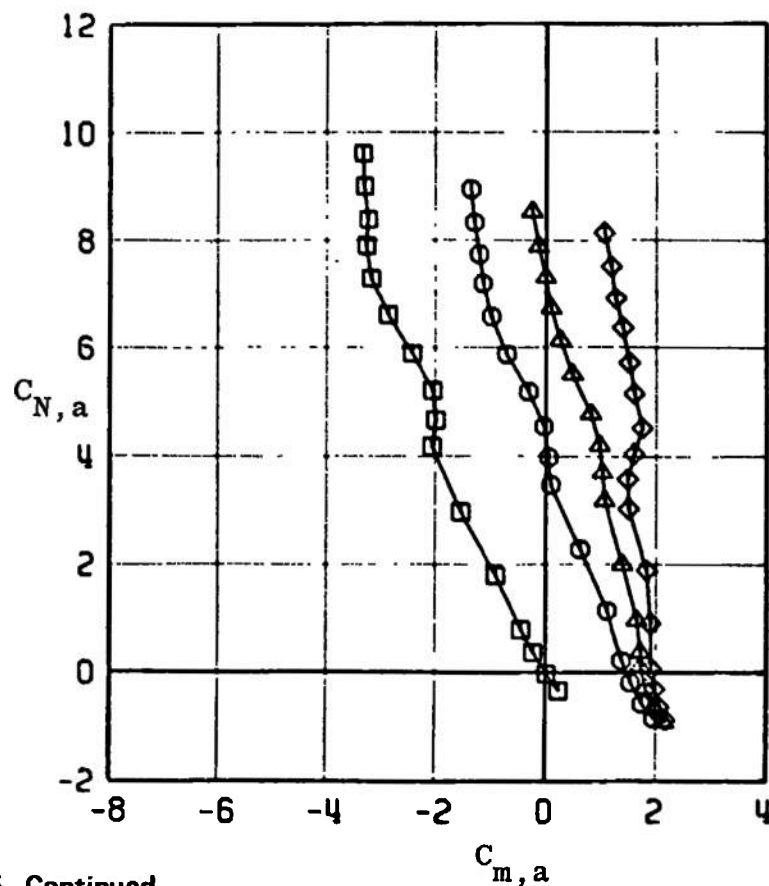
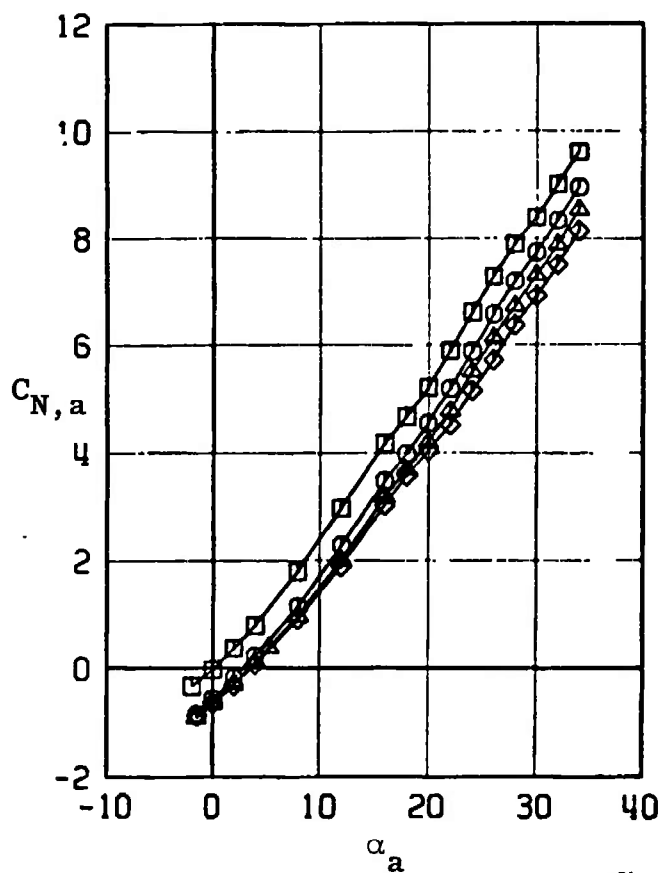


Fig. 25 Continued

PITCH CONTROL EFFECTIVENESS							
NORMAL FORCE AND PITCHING MOMENT COEFFICIENTS							
SYMBOL	CONFIG	MACH NO	ϕ	δ_0	δ_R	δ_P	$R_F \times 10^{-6}$
□	B9T3	0.75	0	0.3	0.5	0.3	2.0
○	B9T3	0.75	0	-10.1	0.1	0.3	2.0
△	B9T3	0.75	0	-14.9	0.1	-0.1	2.0
◇	B9T3	0.75	0	-20.5	0.2	-0.1	2.0

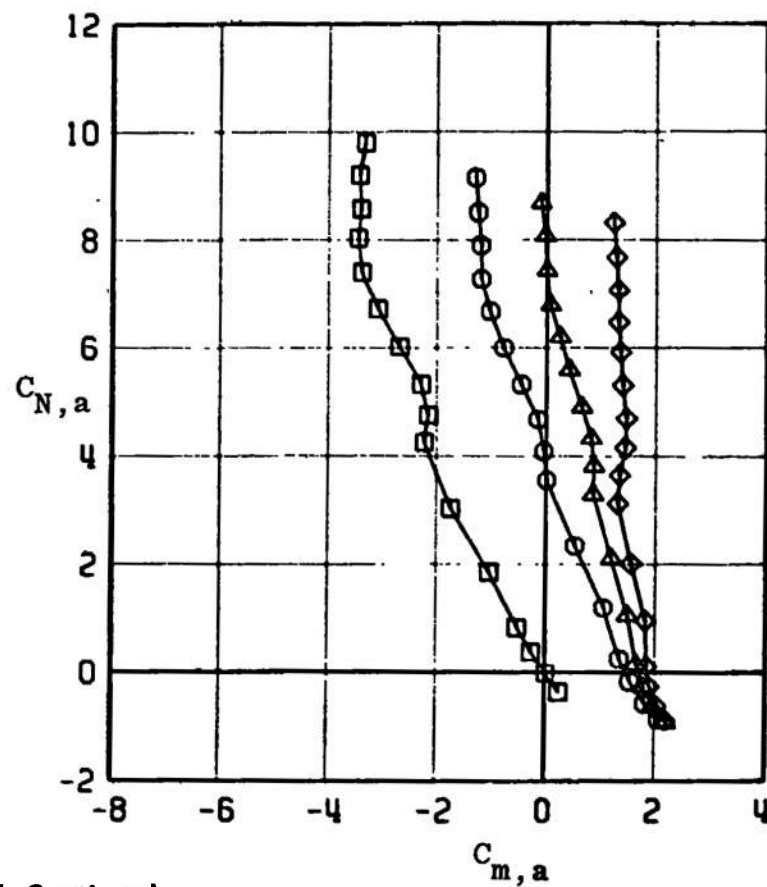
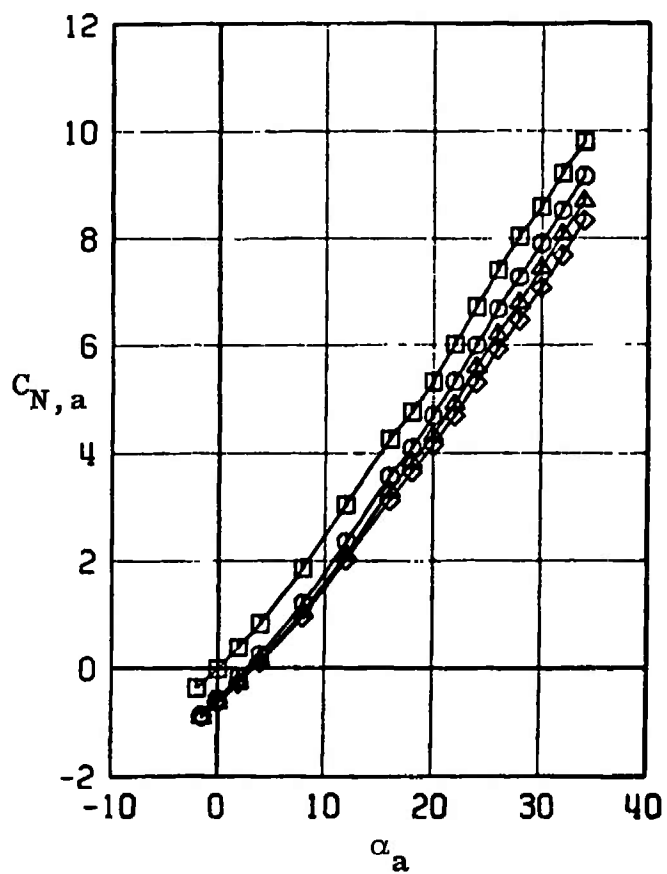


Fig. 25 Continued

PITCH CONTROL EFFECTIVENESS

NORMAL FORCE AND PITCHING MOMENT COEFFICIENTS

SYMBOL	CONFIG	MACH NO	ϕ	δ_0	δ_R	δ_P	$R_E \times 10^{-6}$
\square	B9T3	0.85	0	0.3	0.5	0.3	2.1
\circ	B9T3	0.85	0	-10.1	0.1	0.3	2.1
\triangle	B9T3	0.85	0	-14.9	0.1	-0.1	2.1
\diamond	B9T3	0.85	0	-20.5	0.2	-0.1	2.1

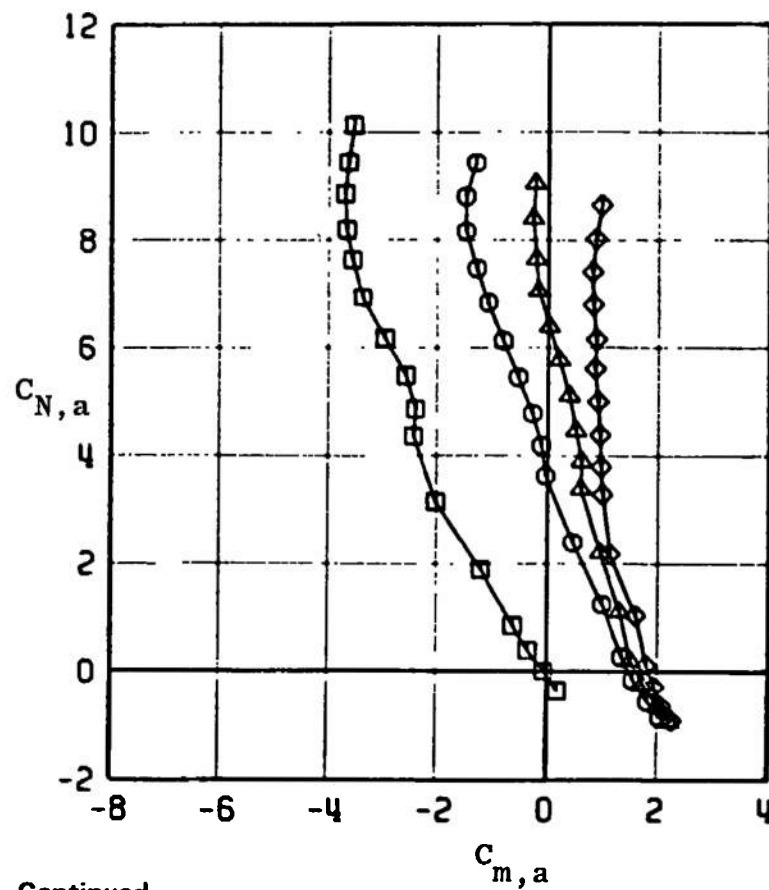
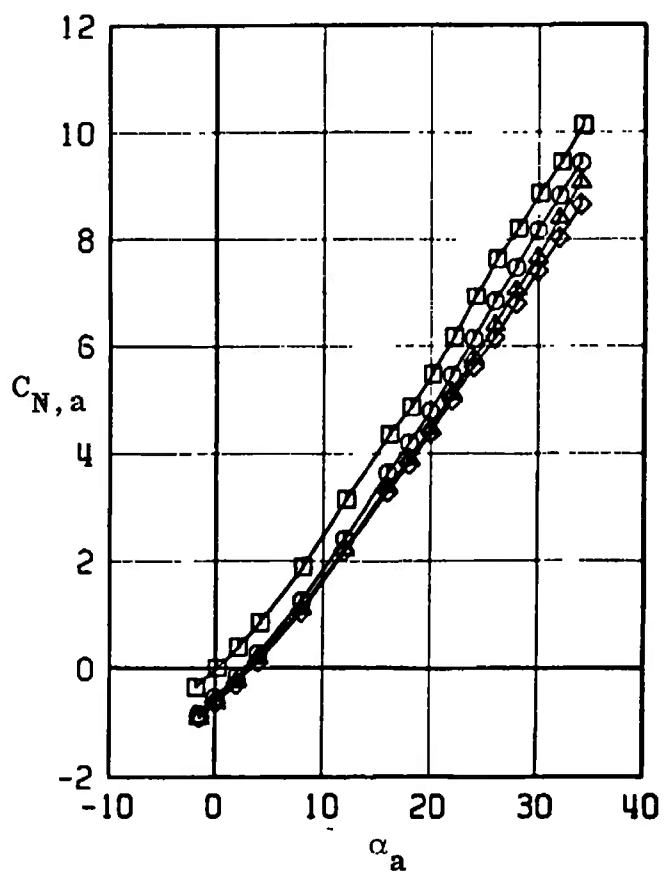


Fig. 25 Continued

PITCH CONTROL EFFECTIVENESS							
NORMAL FORCE AND PITCHING MOMENT COEFFICIENTS							
SYMBOL	CONFIG	MACH NO	ϕ	b_D	b_R	b_P	$R_E \times 10^{-6}$
□	B9T3	0.95	0	0.3	0.5	0.3	2.1
○	B9T3	0.95	0	-10.1	0.1	0.3	2.1
△	B9T3	0.95	0	-14.9	0.1	-0.1	2.1
◇	B9T3	0.95	0	-20.5	0.2	-0.1	2.1

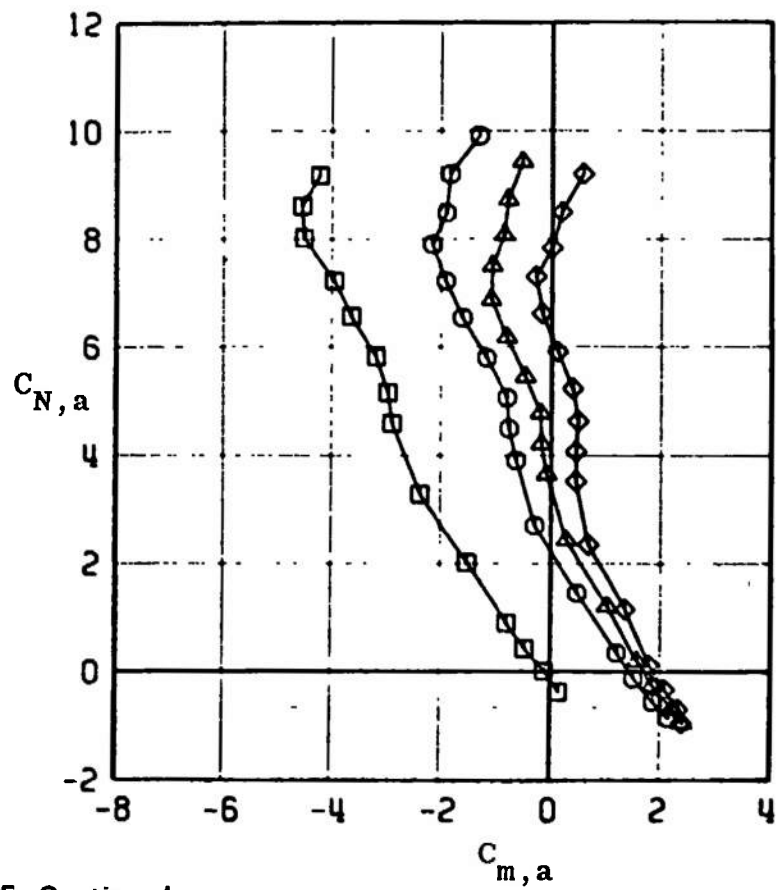
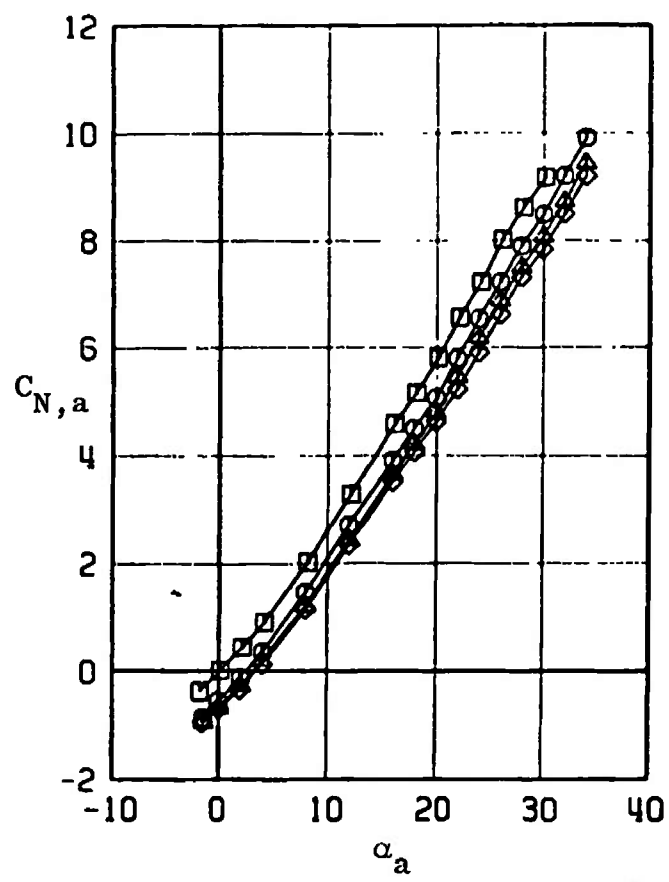


Fig. 25 Continued

PITCH CONTROL EFFECTIVENESS

NORMAL FORCE AND PITCHING MOMENT COEFFICIENTS

SYMBOL	CONFIG	MACH NO	ϕ	δ_0	δ_R	δ_P	$R_E \times 10^{-6}$
□	B9T3	1.05	0	0.3	0.5	0.3	2.3
○	B9T3	1.05	0	-10.1	0.1	0.3	2.3
△	B9T3	1.05	0	-14.9	0.1	-0.1	2.3
◇	B9T3	1.05	0	-20.5	0.2	-0.1	2.3

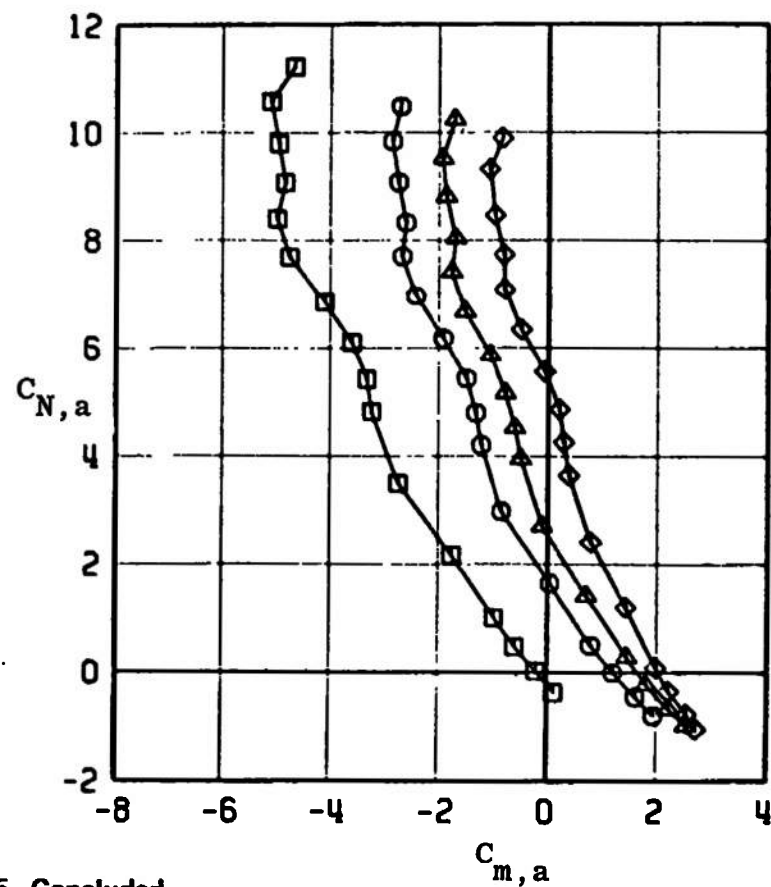
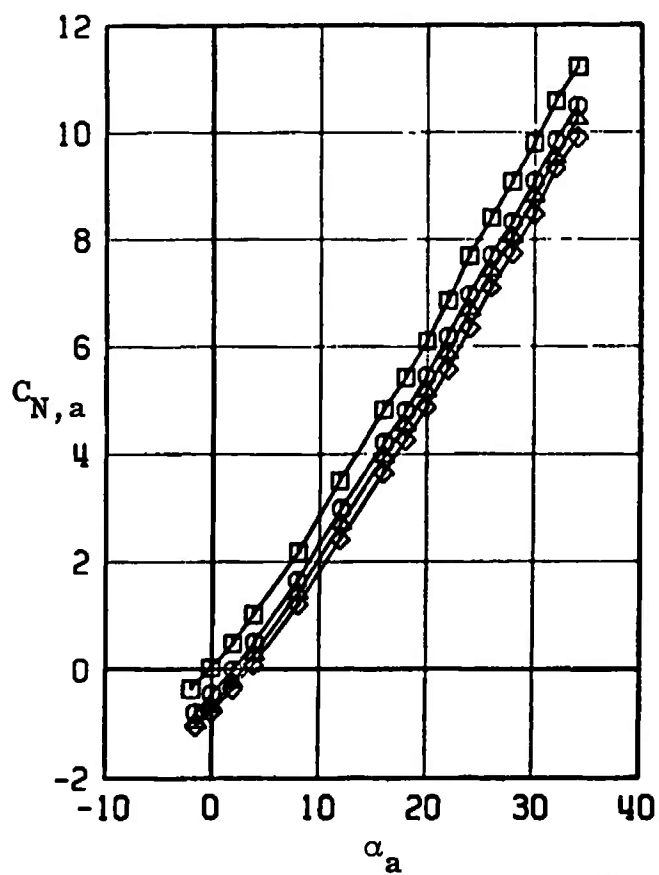


Fig. 25 Concluded

PITCH CONTROL EFFECTIVENESS							
ROLLING MOMENT AND AXIAL FORCE COEFFICIENTS							
SYMBOL	CONFIG	MACH NO	ϕ	δ_0	δ_H	δ_P	$R_F \times 10^{-6}$
□	B9T3	0.50	0	0.3	0.5	0.3	1.5
○	B9T3	0.50	0	-10.1	0.1	0.3	1.5
△	B9T3	0.50	0	-14.9	0.1	-0.1	1.5
◇	B9T3	0.50	0	-20.5	0.2	-0.1	1.5

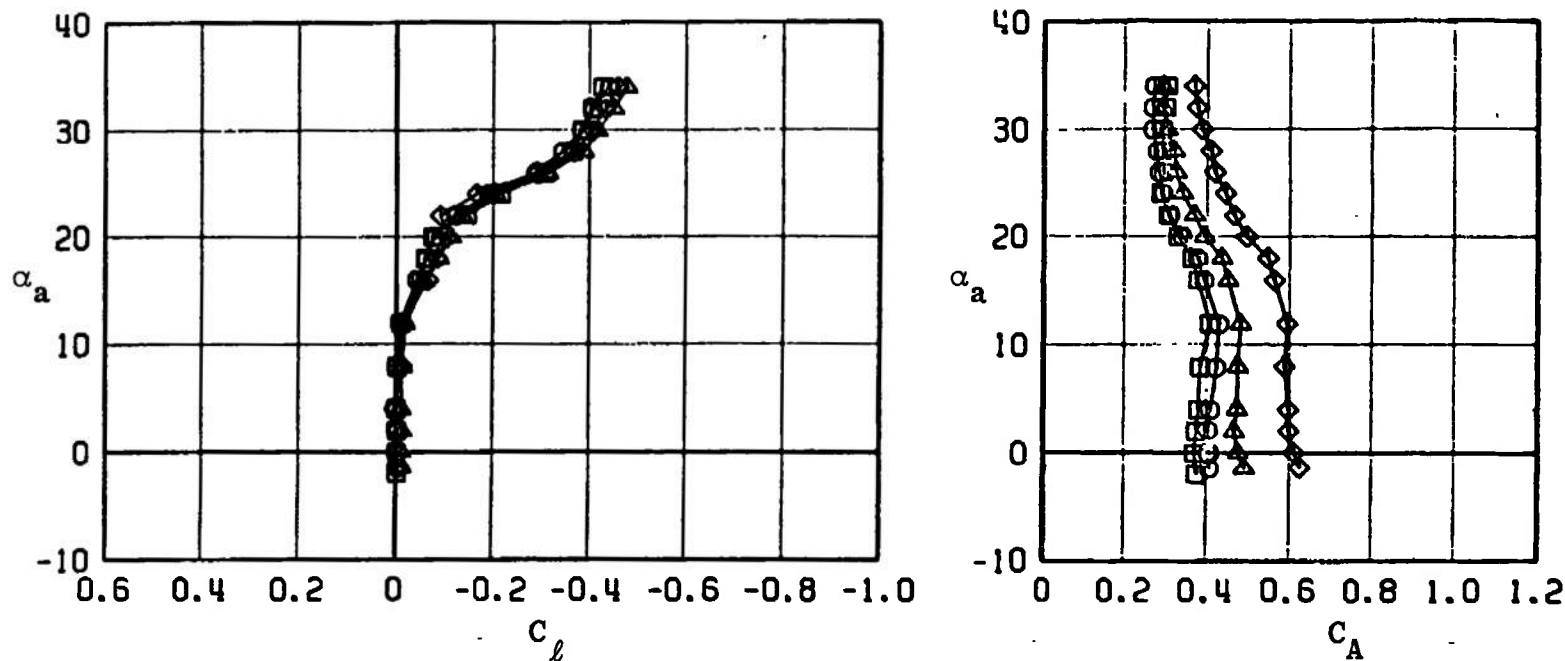


Fig. 26 Effect of Pitch Control Deflections on the Rolling-Moment and Axial-Force Coefficients for MGB Configuration without RES (B9T3)

PITCH CONTROL EFFECTIVENESS							
ROLLING MOMENT AND AXIAL FORCE COEFFICIENTS							
SYMBOL	CONFIG	MACH NO	ϕ	b_0	b_H	b_P	$R_L \times 10^{-6}$
□	B9T3	0.65	0	0.3	0.5	0.3	1.8
○	B9T3	0.65	0	-10.1	0.1	0.3	1.8
△	B9T3	0.65	0	-14.9	0.1	-0.1	1.8
◇	B9T3	0.65	0	-20.5	0.2	-0.1	1.8

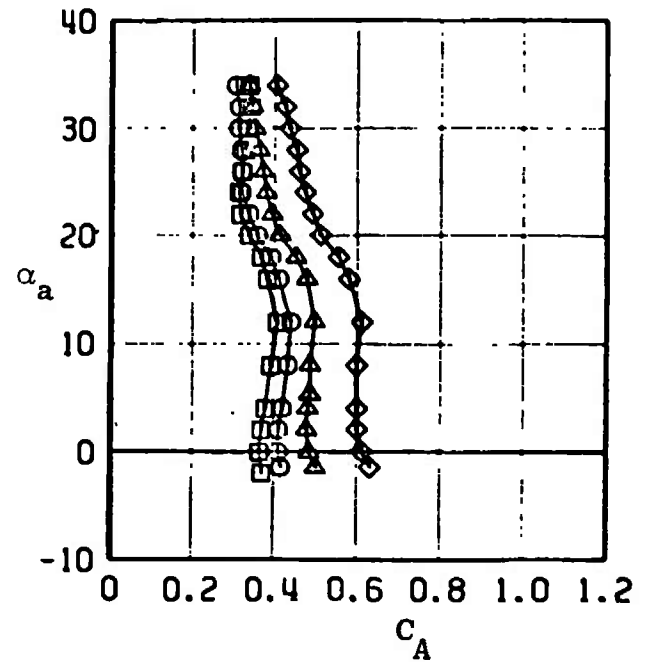
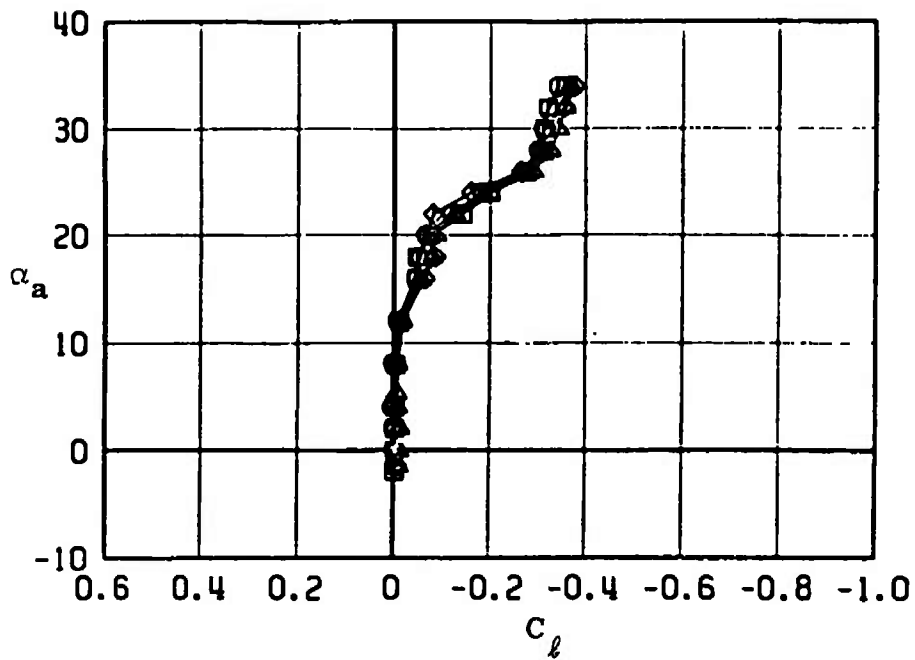


Fig. 26 Continued

PITCH CONTROL EFFECTIVENESS ROLLING MOMENT AND AXIAL FORCE COEFFICIENTS							
SYMBOL	CONFIG	MACH NO	ϕ	b_0	b_R	b_P	$R_E \times 10^{-6}$
□	B9T3	0.75	0	0.3	0.5	0.3	2.0
○	B9T3	0.75	0	-10.1	0.1	0.3	2.0
△	B9T3	0.75	0	-14.9	0.1	-0.1	2.0
◇	B9T3	0.75	0	-20.5	0.2	-0.1	2.0

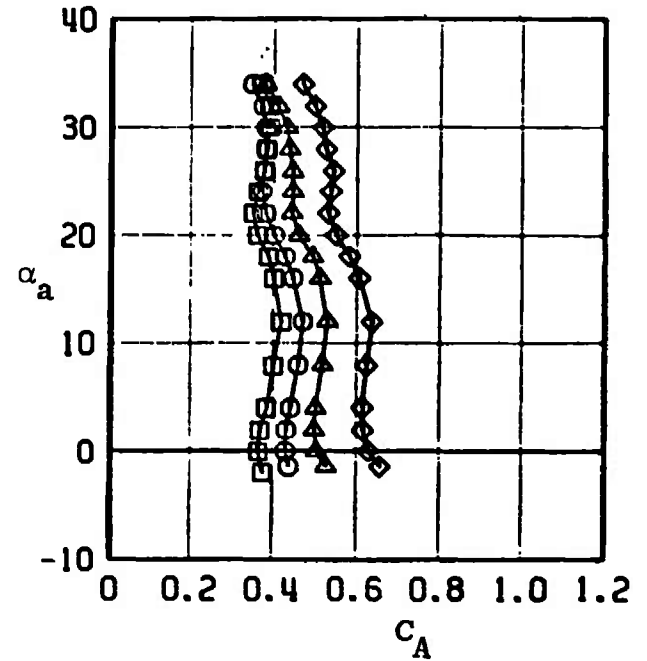
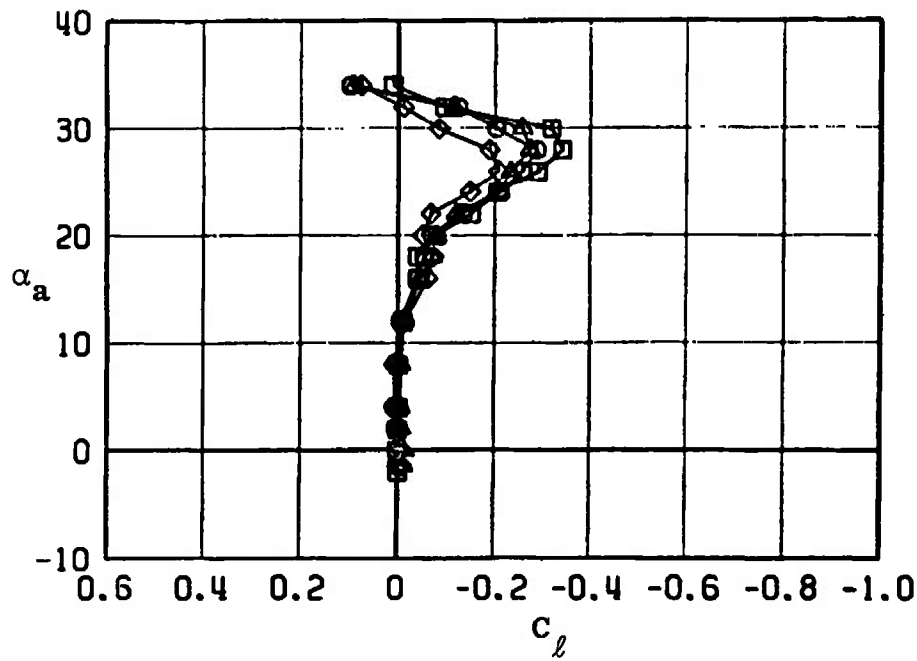


Fig. 26 Continued

PITCH CONTROL EFFECTIVENESS

ROLLING MOMENT AND AXIAL FORCE COEFFICIENTS

SYMBOL	CONFIG	MACH NO	ϕ	b_0	b_R	b_P	$R_L \times 10^{-6}$
□	B9T3	0.85	0	0.3	0.5	0.3	2.1
○	B9T3	0.85	0	-10.1	0.1	0.3	2.1
△	B9T3	0.85	0	-14.9	0.1	-0.1	2.1
◇	B9T3	0.85	0	-20.5	0.2	-0.1	2.1

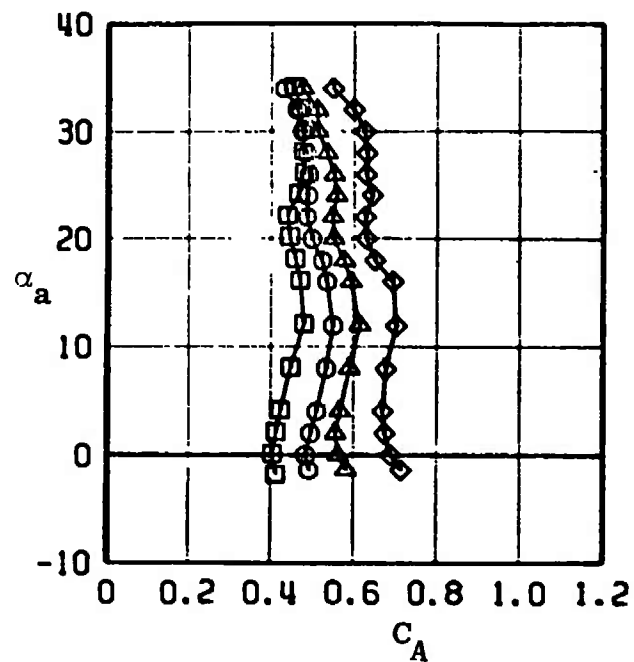
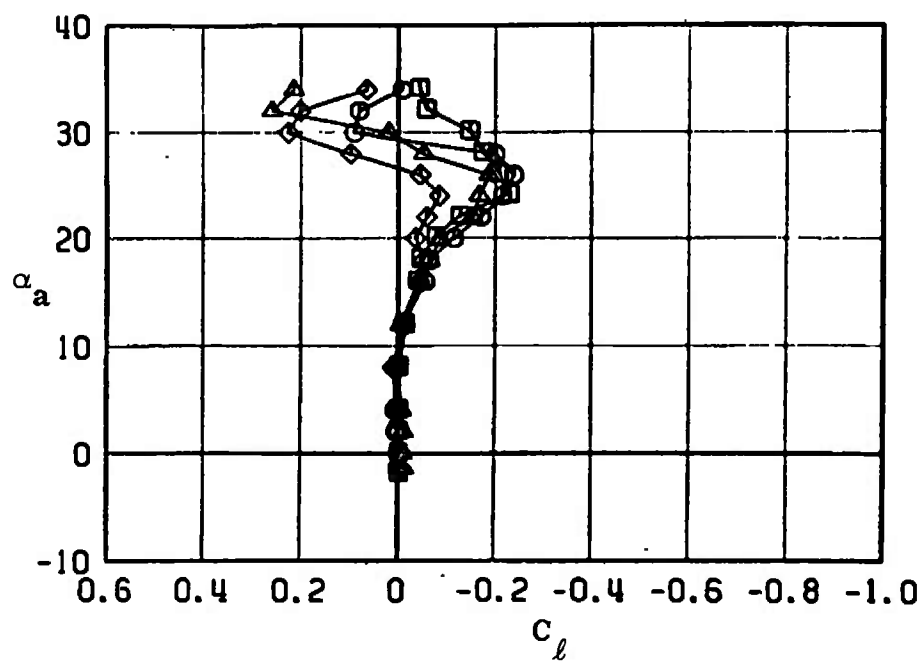


Fig. 26 Continued

PITCH CONTROL EFFECTIVENESS
ROLLING MOMENT AND AXIAL FORCE COEFFICIENTS

SYMBOL	CONFIG	MACH NO	ϕ	δ_0	δ_R	δ_P	$R_E \times 10^{-6}$
□	B9T3	0.95	0	0.3	0.5	0.3	2.1
○	B9T3	0.95	0	-10.1	0.1	0.3	2.1
△	B9T3	0.95	0	-14.9	0.1	-0.1	2.1
◇	B9T3	0.95	0	-20.5	0.2	-0.1	2.1

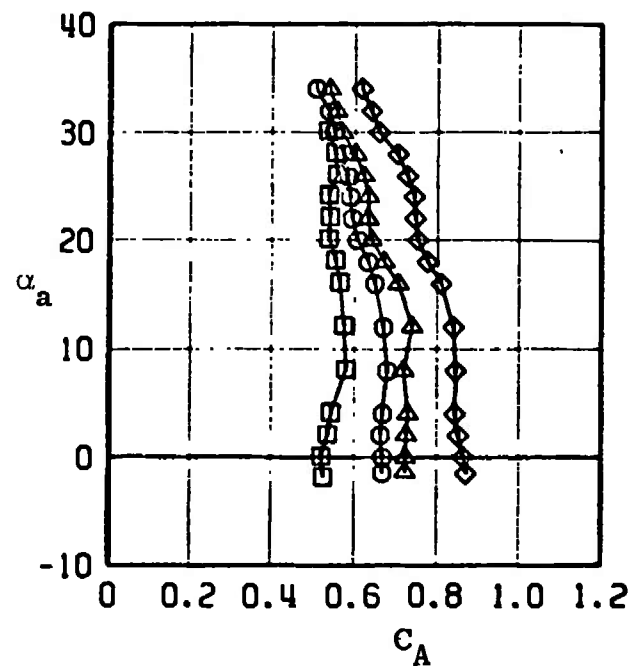
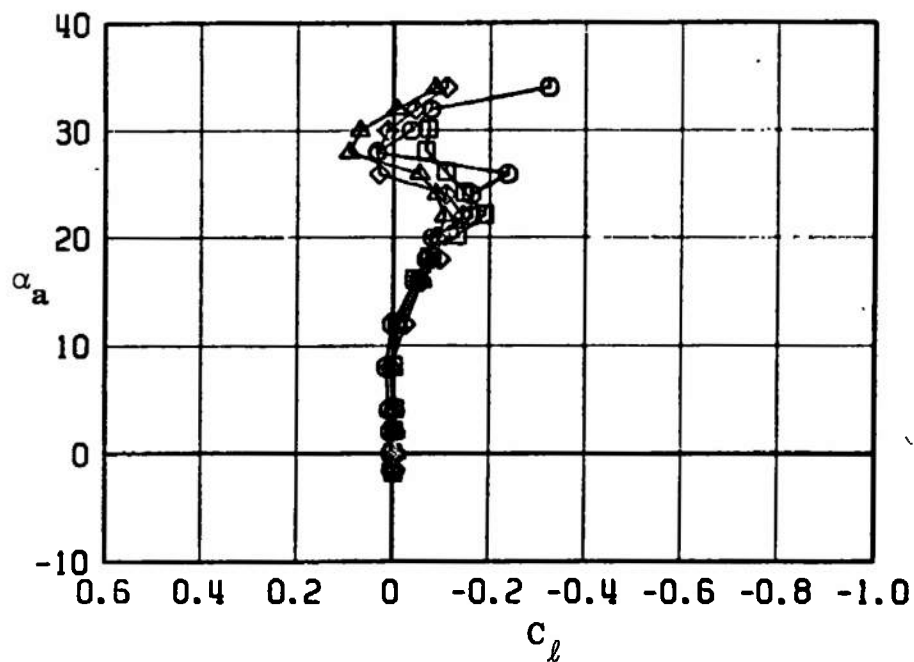


Fig. 26 Continued

PITCH CONTROL EFFECTIVENESS							
ROLLING MOMENT AND AXIAL FORCE COEFFICIENTS							
SYMBOL	CONFIG	MACH NO	ϕ	b_0	b_R	b_P	$R_E \times 10^{-6}$
□	B9T3	1.05	0	0.3	0.5	0.3	2.3
○	B9T3	1.05	0	-10.1	0.1	0.3	2.3
△	B9T3	1.05	0	-14.9	0.1	-0.1	2.3
◇	B9T3	1.05	0	-20.5	0.2	-0.1	2.3

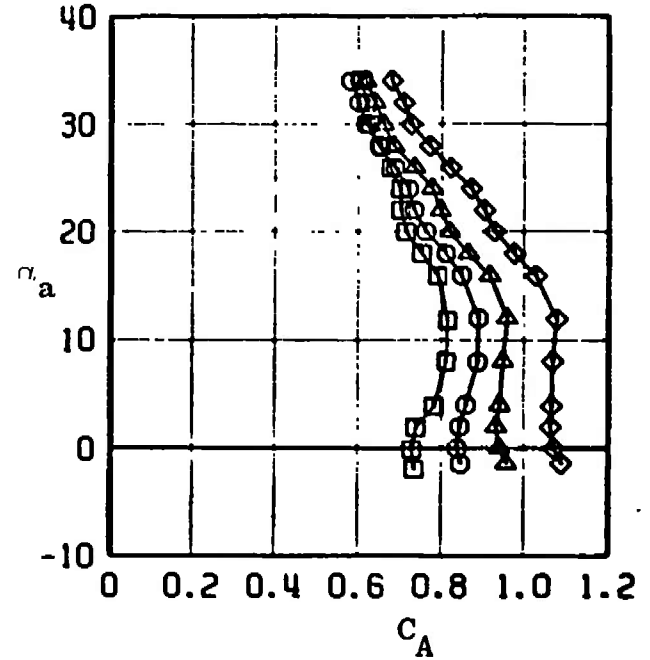
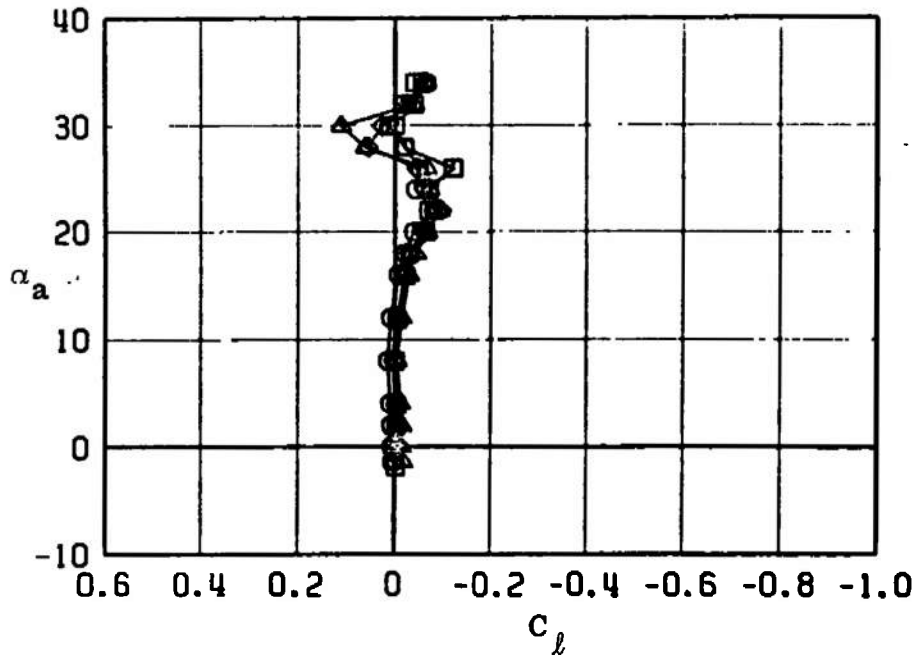


Fig. 26 Concluded

PITCH CONTROL EFFECTIVENESS							
SIDE FORCE AND YAWING MOMENT COEFFICIENTS							
SYMBOL	CONFIG	MACH NO	ϕ	δ_a	δ_n	δ_p	$R_E \times 10^{-6}$
□	B9T3	0.50	0	0.3	0.5	0.3	1.5
○	B9T3	0.50	0	-10.1	0.1	0.3	1.5
△	B9T3	0.50	0	-14.9	0.1	-0.1	1.5
◇	B9T3	0.50	0	-20.5	0.2	-0.1	1.5

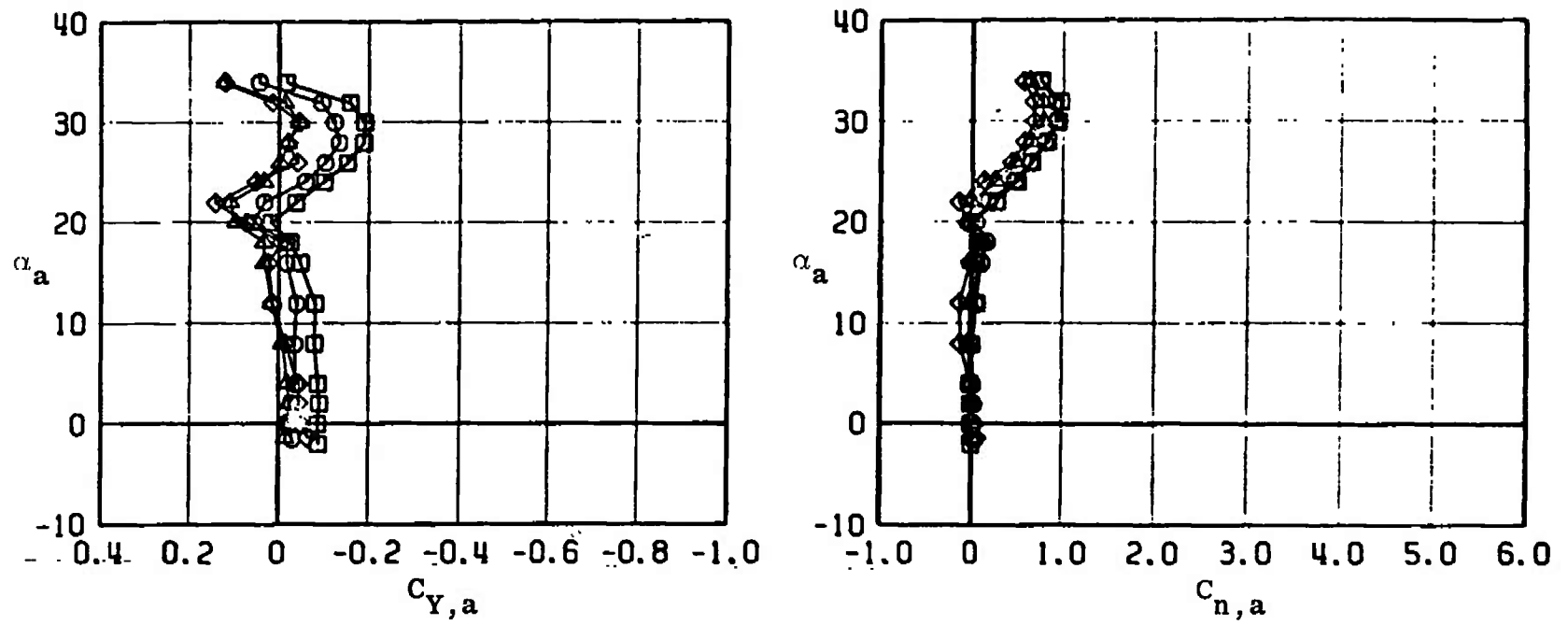


Fig. 27 Effect of Pitch Control Deflection on the Side-Force and Yawing-Moment Coefficients for MGGB Configuration without RES (B9T3)

PITCH CONTROL EFFECTIVENESS							
SIDE FORCE AND YAWING MOMENT COEFFICIENTS							
SYMBOL	CONFIG	MACH NO	ϕ	δ_0	δ_n	δ_p	$R_E \times 10^{-6}$
□	B9T3	0.65	0	0.3	0.5	0.3	1.8
○	B9T3	0.65	0	-10.1	0.1	0.3	1.8
△	B9T3	0.65	0	-14.9	0.1	-0.1	1.8
◇	B9T3	0.65	0	-20.5	0.2	-0.1	1.8

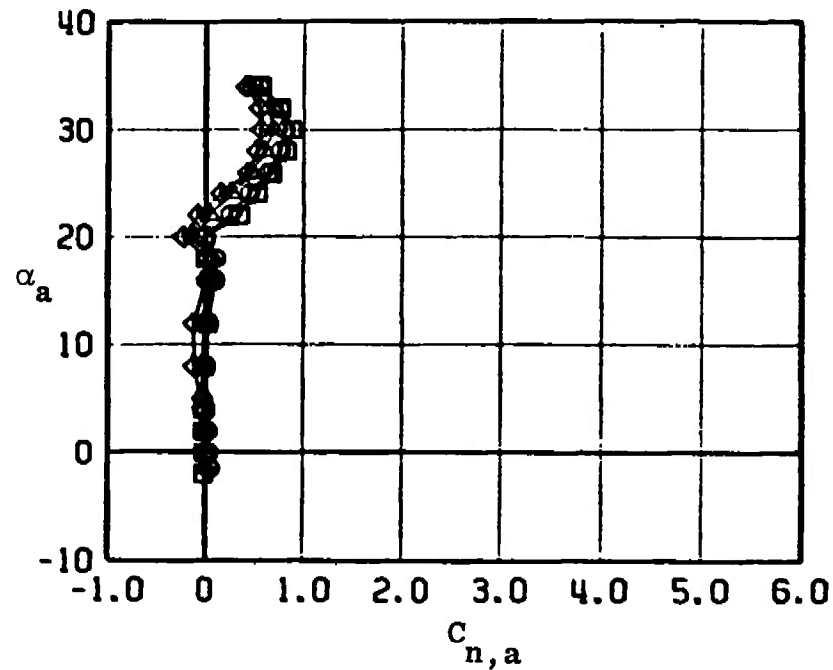
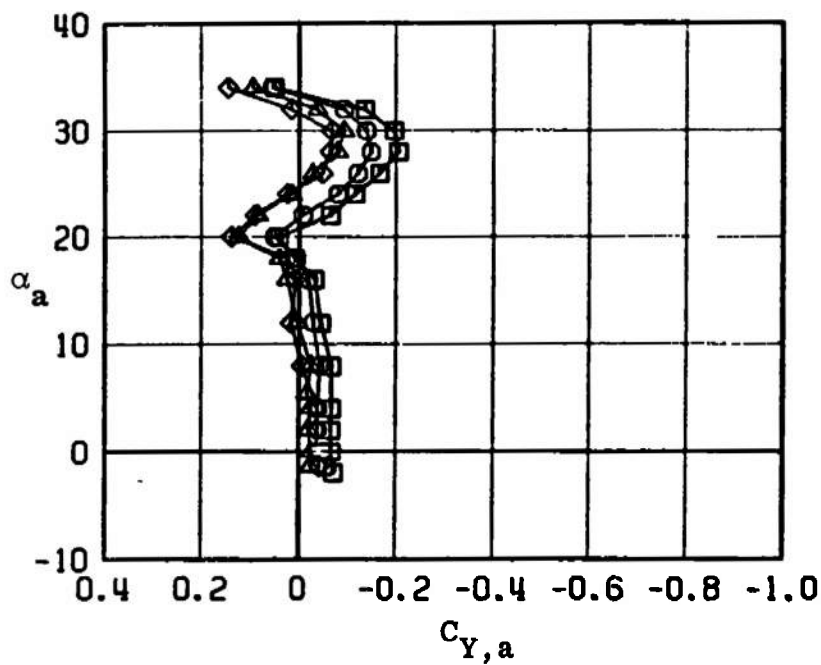


Fig. 27 Continued

PITCH CONTROL EFFECTIVENESS

SIDE FORCE AND YAWING MOMENT COEFFICIENTS

SYMBOL	CONFIG	MACH NO	ϕ	δ_D	δ_H	δ_P	$R_E \times 10^{-6}$
\square	B9T3	0.75	0	0.3	0.5	0.3	2.0
\circ	B9T3	0.75	0	-10.1	0.1	0.3	2.0
\triangle	B9T3	0.75	0	-14.9	0.1	-0.1	2.0
\diamond	B9T3	0.75	0	-20.5	0.2	-0.1	2.0

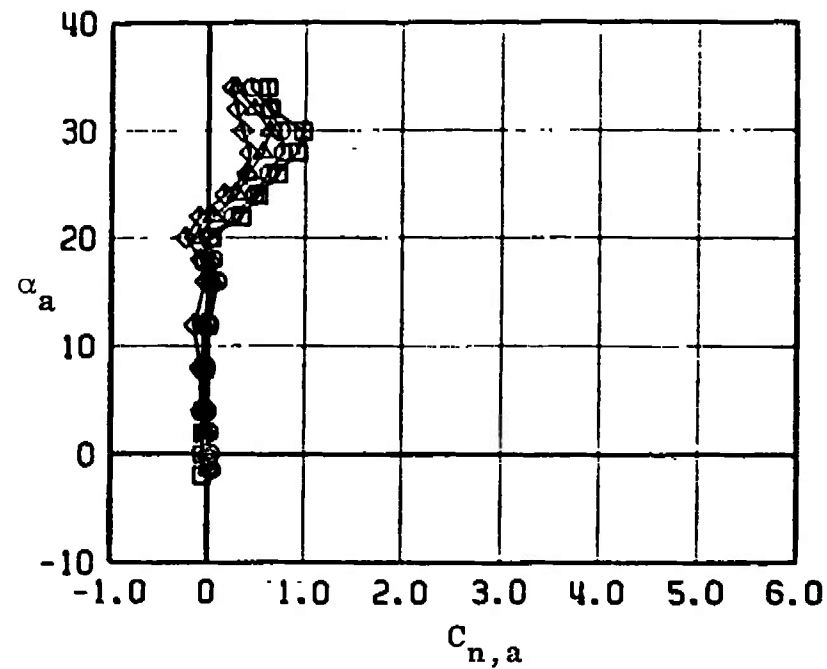
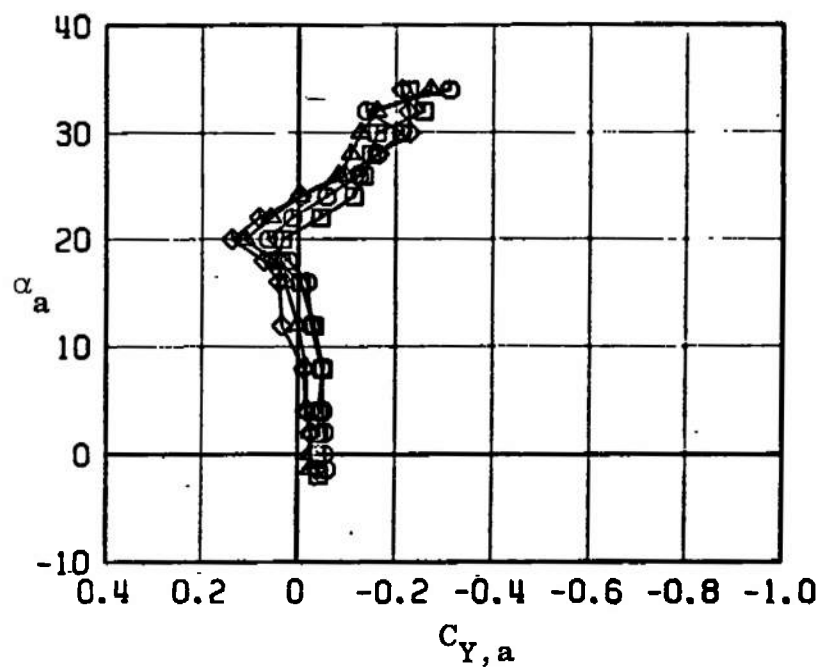


Fig. 27 Continued

PITCH CONTROL EFFECTIVENESS SIDE FORCE AND YAWING MOMENT COEFFICIENTS							
SYMBOL	CONFIG	MACH NO	ϕ	δ_a	δ_n	δ_p	$R_E \times 10^{-6}$
□	B9T3	0.85	0	0.3	0.5	0.3	2.1
○	B9T3	0.85	0	-10.1	0.1	0.3	2.1
△	B9T3	0.85	0	-14.9	0.1	-0.1	2.1
◇	B9T3	0.85	0	-20.5	0.2	-0.1	2.1

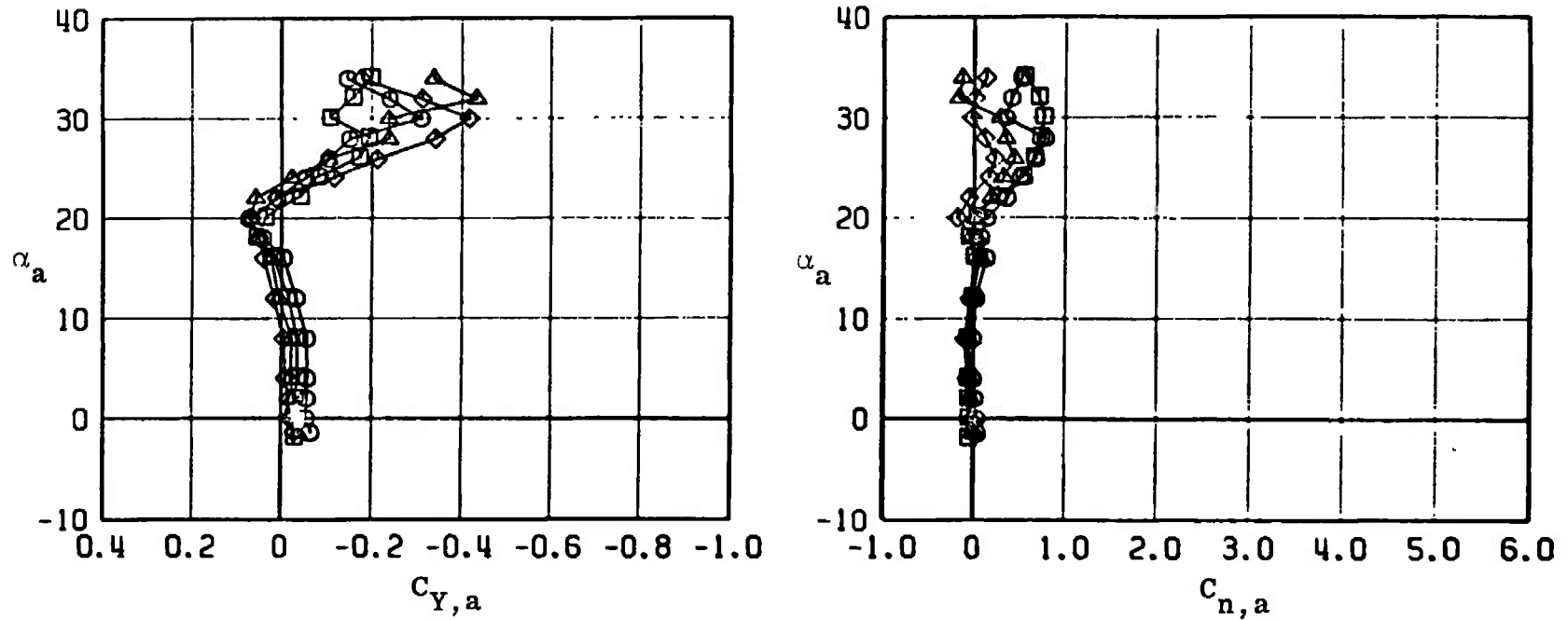


Fig. 27 Continued

PITCH CONTROL EFFECTIVENESS SIDE FORCE AND YAWING MOMENT COEFFICIENTS							
SYMBOL	CONFIG	MACH NO	ϕ	δ_0	δ_n	δ_p	$R_F \times 10^{-6}$
□	B9T3	0.95	0	0.3	0.5	0.3	2.1
○	B9T3	0.95	0	-10.1	0.1	0.3	2.1
△	B9T3	0.95	0	-14.9	0.1	-0.1	2.1
◇	B9T3	0.95	0	-20.5	0.2	-0.1	2.1

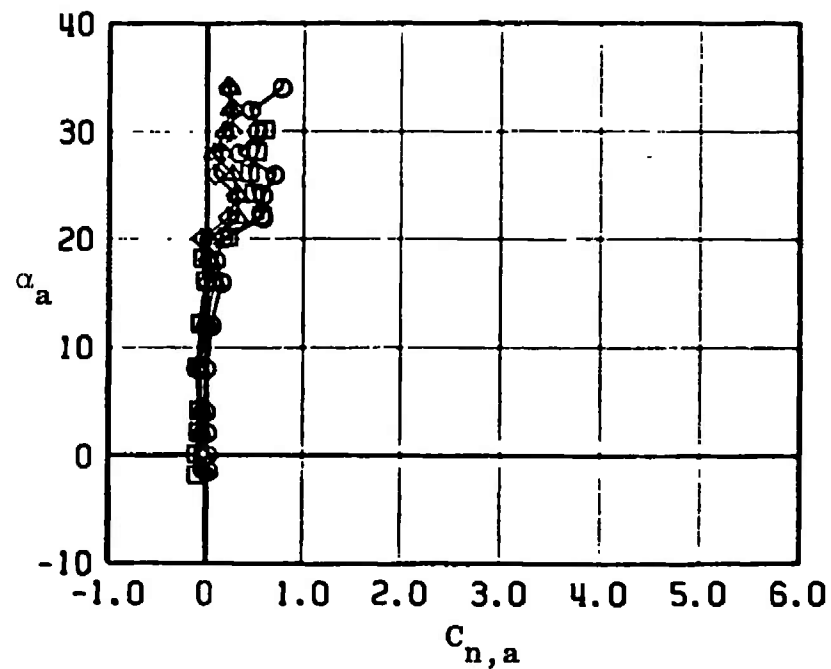
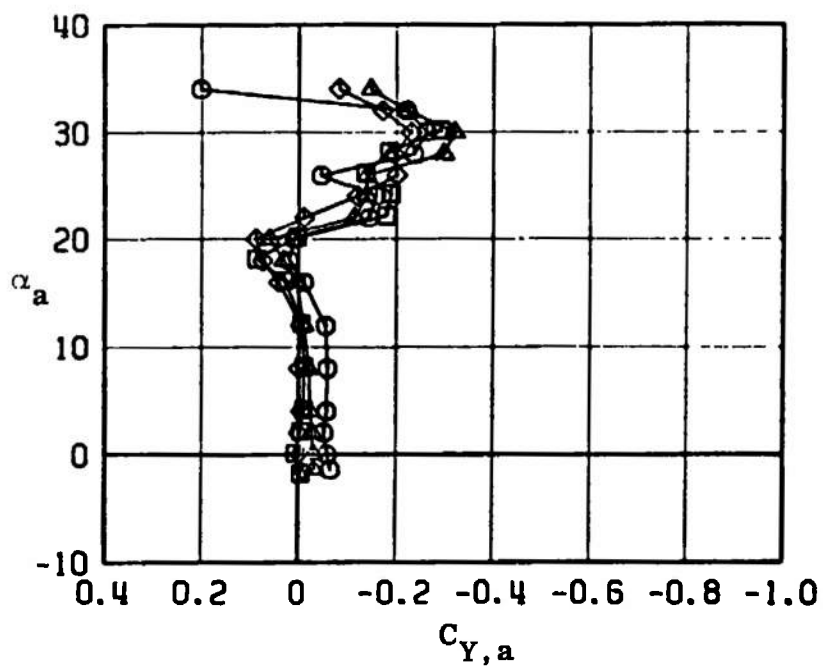


Fig. 27 Continued

PITCH CONTROL EFFECTIVENESS SIDE FORCE AND YAWING MOMENT COEFFICIENTS							
SYMBOL	CONFIG	MACH NO	ϕ	b_q	b_r	b_p	$R_E \times 10^{-6}$
□	B9T3	1.05	0	0.3	0.5	0.3	2.3
○	B9T3	1.05	0	-10.1	0.1	0.3	2.3
△	B9T3	1.05	0	-14.9	0.1	-0.1	2.3
◇	B9T3	1.05	0	-20.5	0.2	-0.1	2.3

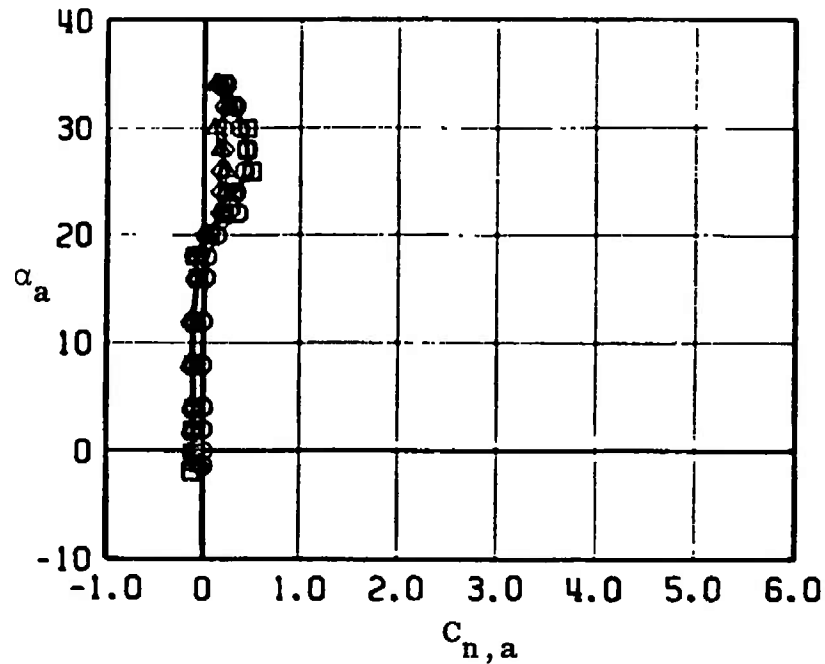
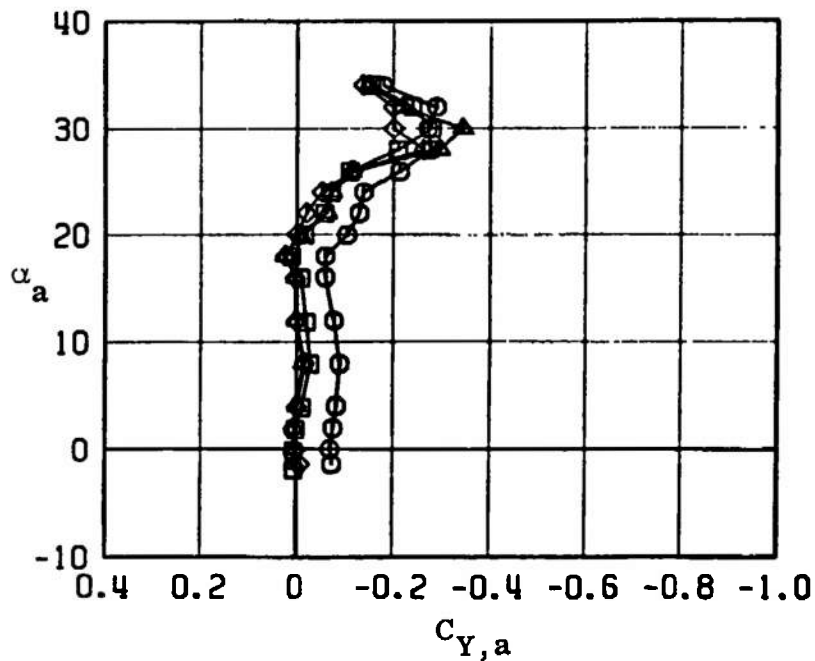


Fig. 27 Concluded

YAW CONTROL EFFECTIVENESS							
NORMAL FORCE AND PITCHING MOMENT COEFFICIENTS							
SYMBOL	CONFIG	MACH NO	ϕ	δ_0	δ_R	δ_P	$R_E \times 10^{-6}$
\square	B9T3	0.50	0	0.3	0.5	0.3	1.5
\circ	B9T3	0.50	0	0	-4.9	0.2	1.5
\triangle	B9T3	0.50	0	0.2	-10.0	0.1	1.5
\diamond	B9T3	0.50	0	0.1	-14.9	0	1.5
∇	B9T3	0.50	0	-0.6	-19.7	-0.1	1.5

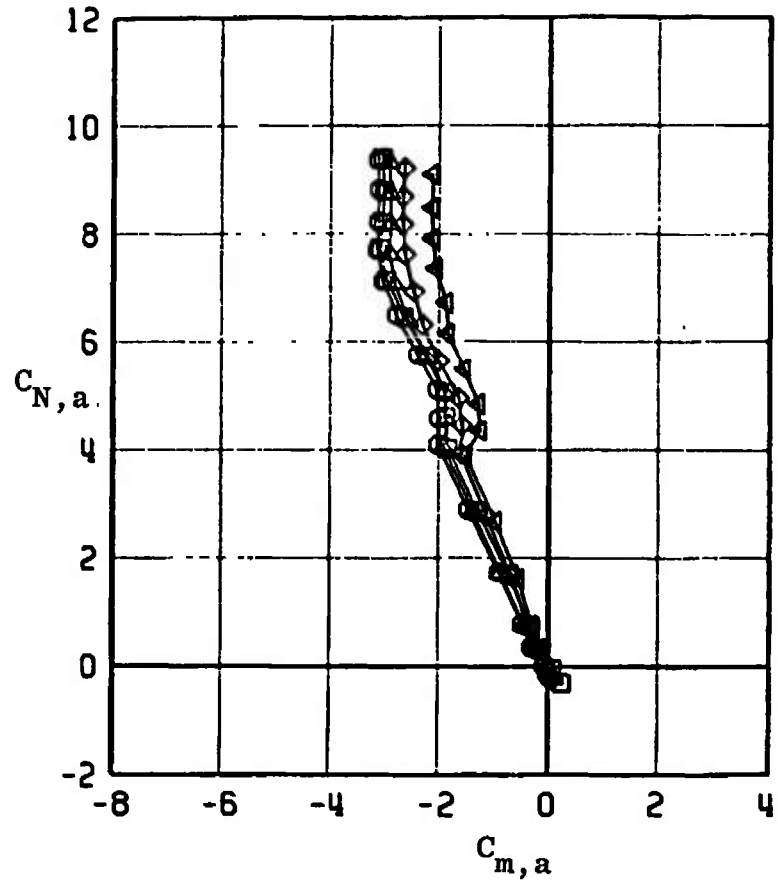
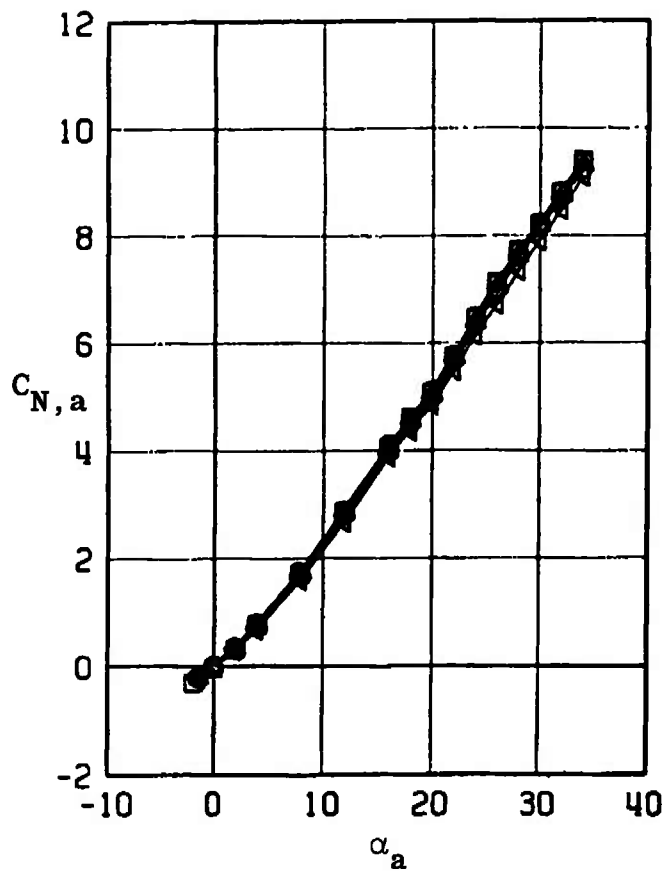


Fig. 28 Effect of Yaw Control Deflections on the Normal-Force and Pitching-Moment Coefficients for MGGB Configuration without RES (B9T3)

YAW CONTROL EFFECTIVENESS							
NORMAL FORCE AND PITCHING MOMENT COEFFICIENTS							
SYMBOL	CONFIG	MACH NO	δ	δ_0	δ_n	δ_p	$R_z \times 10^{-6}$
□	B9T3	0.65	0	0.3	0.5	0.3	1.8
○	B9T3	0.65	0	0	-4.9	0.2	1.8
△	B9T3	0.65	0	0.2	-10.0	0.1	1.8
◇	B9T3	0.65	0	0.1	-14.9	0	1.8
◁	B9T3	0.65	0	-0.6	-19.7	-0.1	1.8

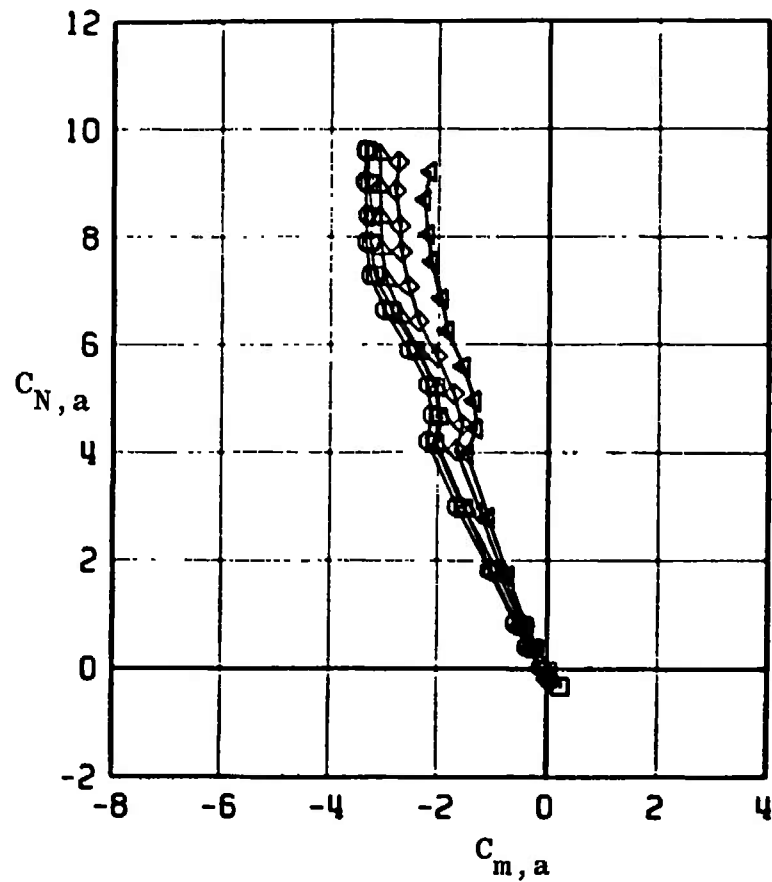
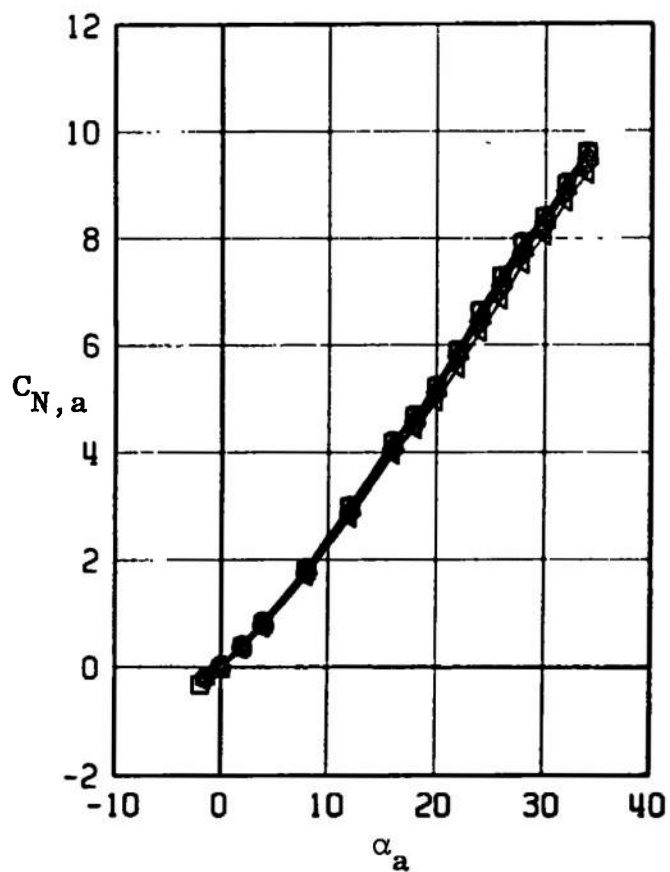


Fig. 28 Continued

YAW CONTROL EFFECTIVENESS							
NORMAL FORCE AND PITCHING MOMENT COEFFICIENTS							
SYMBOL	CONFIG	MACH NO	ϕ	ξ_0	ξ_R	ξ_P	$R_F \times 10^{-6}$
\square	B9T3	0.75	0	0.3	0.5	0.3	2.0
\circ	B9T3	0.75	0	0	-4.9	0.2	2.0
\triangle	B9T3	0.75	0	0.2	-10.0	0.1	2.0
\diamond	B9T3	0.75	0	0.1	-14.9	0	2.0
\blacktriangleleft	B9T3	0.75	0	-0.6	-19.7	-0.1	2.0

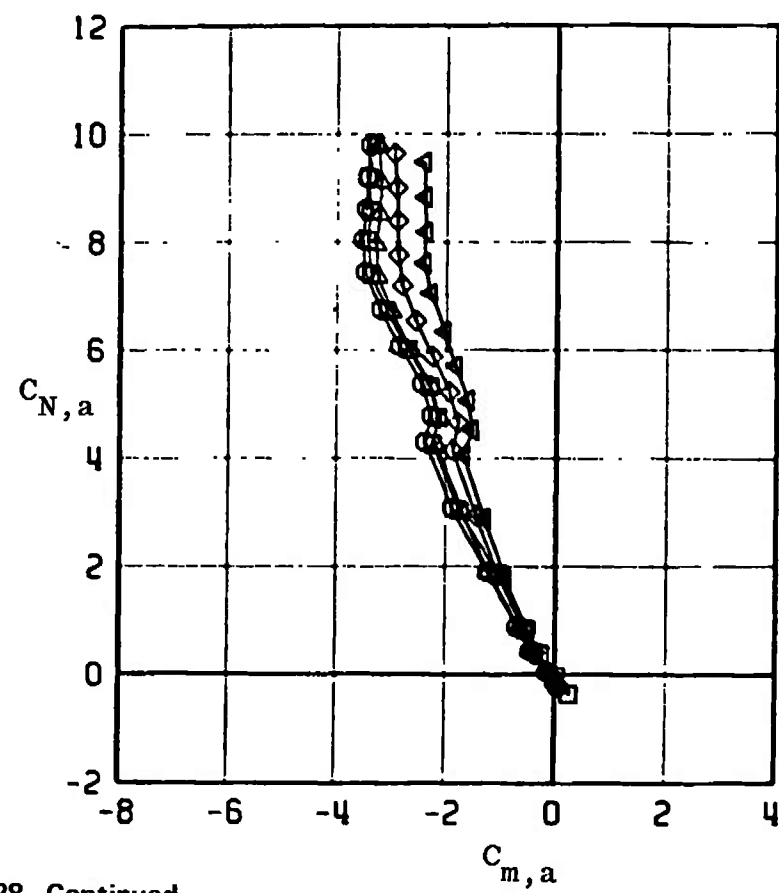
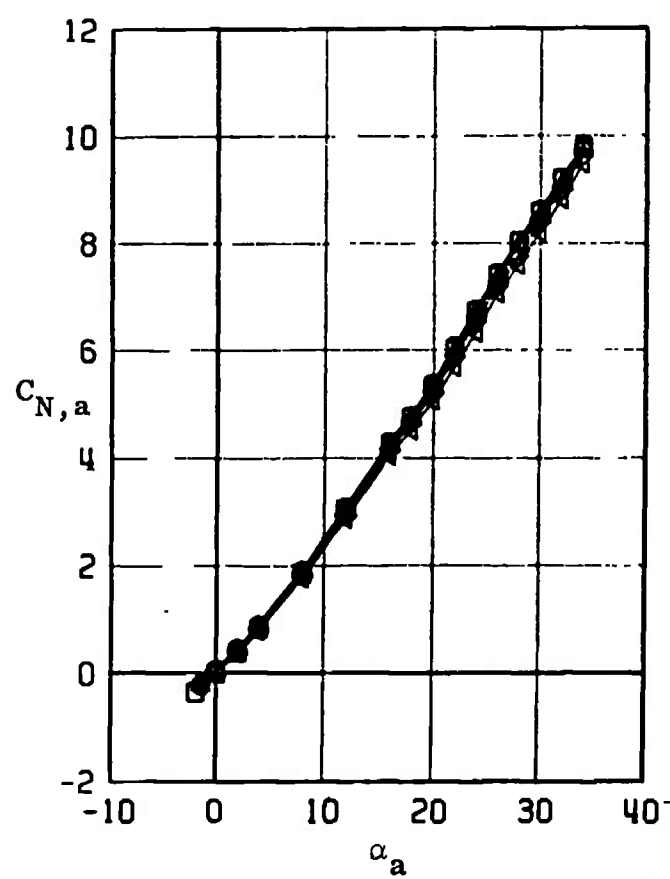


Fig. 28 Continued

YAW CONTROL EFFECTIVENESS

NORMAL FORCE AND PITCHING MOMENT COEFFICIENTS

SYMBOL	CONFIG	MACH NO	ϕ	δ_D	δ_R	δ_P	$R_E \times 10^{-6}$
\square	B9T3	0.85	0	0.3	0.5	0.2	2.1
\circ	B9T3	0.85	0	0	-4.9	0.2	2.1
\triangle	B9T3	0.85	0	0.2	-10.0	0.1	2.1
\diamond	B9T3	0.85	0	0.1	-14.9	0	2.1
\blacktriangleleft	B9T3	0.85	0	-0.6	-19.7	-0.1	2.1

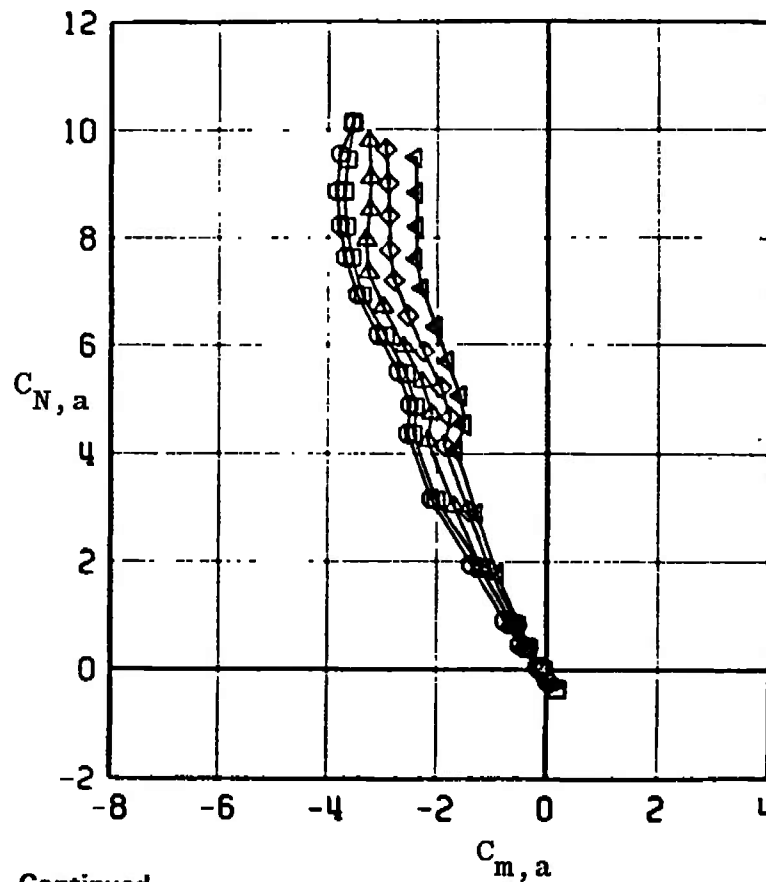
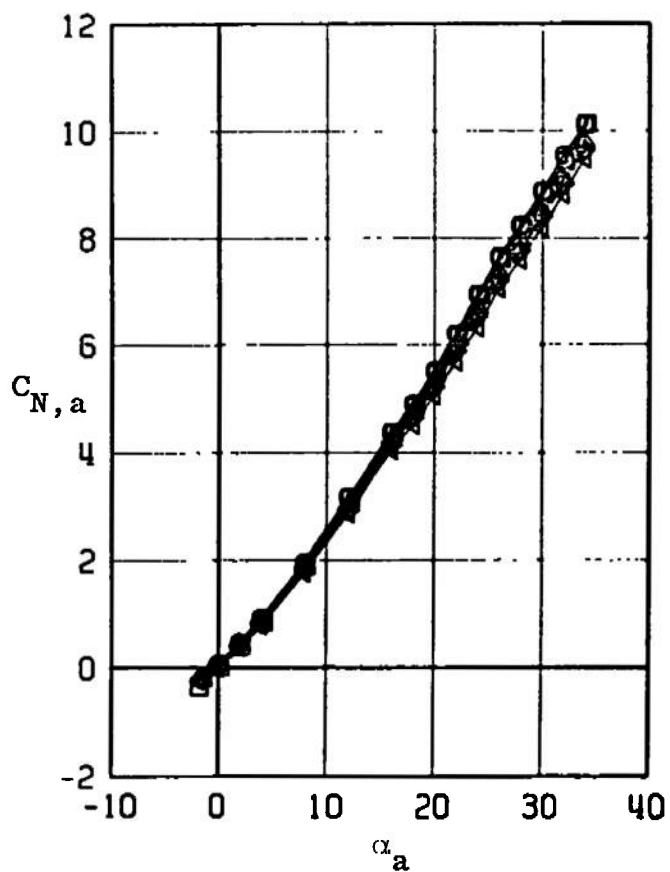


Fig. 28 Continued

YAW CONTROL EFFECTIVENESS							
NORMAL FORCE AND PITCHING MOMENT COEFFICIENTS							
SYMBOL	CONFIG	MACH NO	ϕ	δ_D	δ_R	δ_P	$R_E \times 10^{-5}$
□	B9T3	0.95	0	0.3	0.5	0.3	2.2
○	B9T3	0.95	0	0	-4.9	0.2	2.2
△	B9T3	0.95	0	0.2	-10.0	0.1	2.2
◇	B9T3	0.95	0	0.1	-14.9	0	2.2
◁	B9T3	0.95	0	-0.6	-19.7	-0.1	2.2

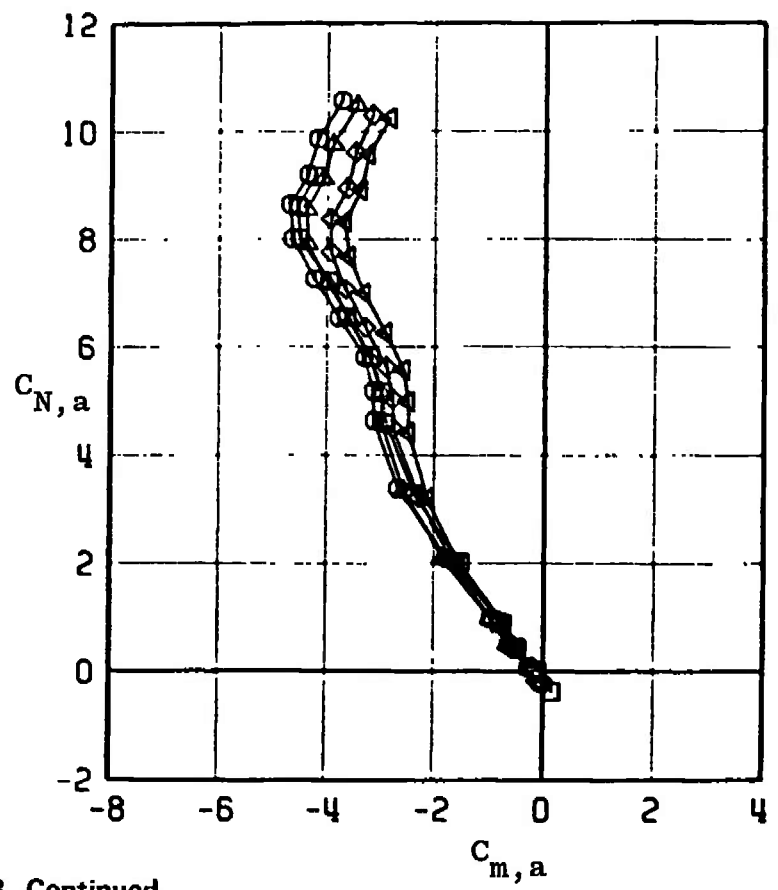
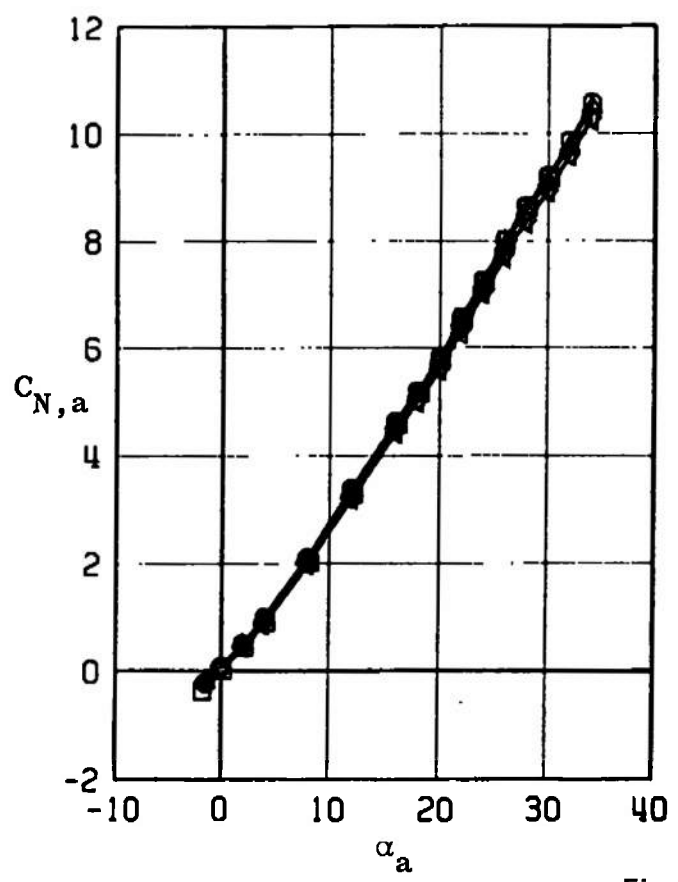


Fig. 28 Continued

YAW CONTROL EFFECTIVENESS

NORMAL FORCE AND PITCHING MOMENT COEFFICIENTS

SYMBOL	CONFIG	MACH NO	ϕ	δ_D	δ_R	δ_P	$R_E \times 10^{-6}$
□	B9T3	1.05	0	0.3	0.5	0.3	2.3
○	B9T3	1.05	0	0	-4.9	0.2	2.3
△	B9T3	1.05	0	0.2	-10.0	0.1	2.3
◇	B9T3	1.05	0	0.1	-14.9	0	2.3
◁	B9T3	1.05	0	-0.6	-19.7	-0.1	2.3

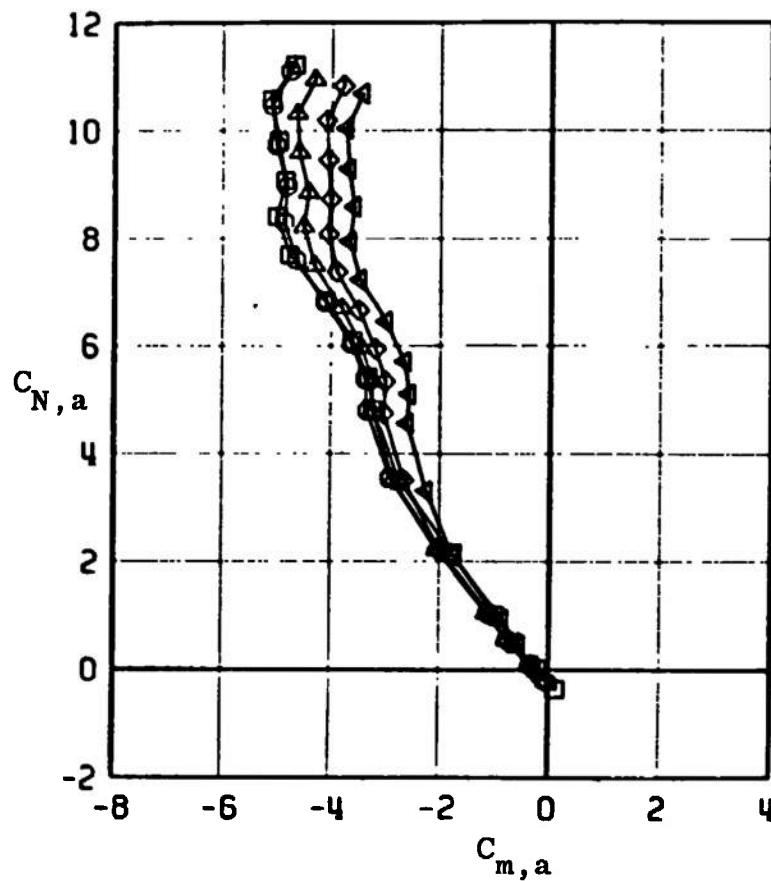
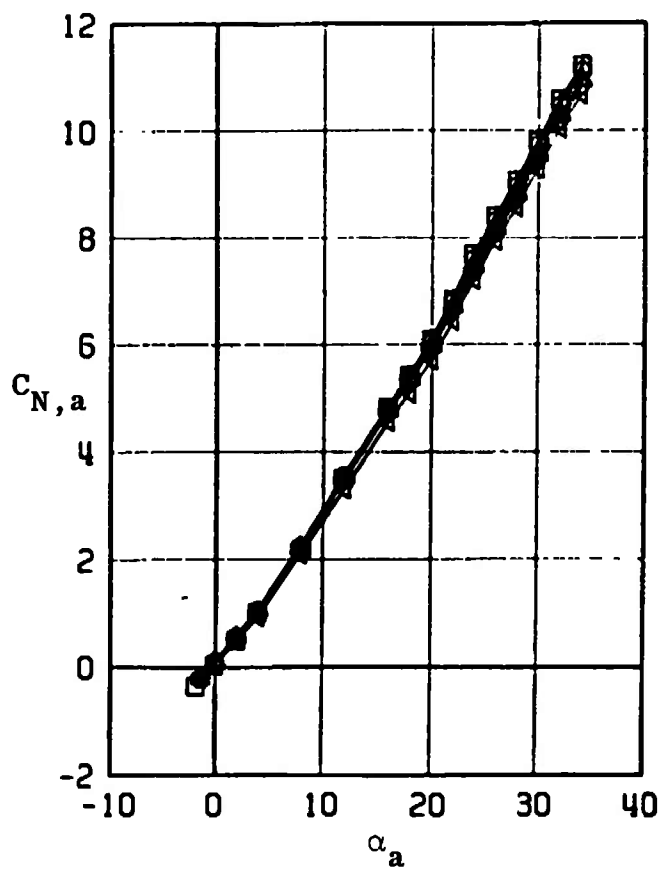


Fig. 28 Concluded

YAW CONTROL EFFECTIVENESS							
ROLLING MOMENT AND AXIAL FORCE COEFFICIENTS							
SYMBOL	CONFIG	MACH NO	ϕ	δ_D	δ_R	δ_P	$R_{\xi} \times 10^{-6}$
□	B9T3	0.50	0	0.3	0.5	0.3	1.5
○	B9T3	0.50	0	0	-4.9	0.2	1.5
△	B9T3	0.50	0	0.2	-10.0	0.1	1.5
◇	B9T3	0.50	0	0.1	-14.9	0	1.5
◁	B9T3	0.50	0	-0.6	-19.7	-0.1	1.5

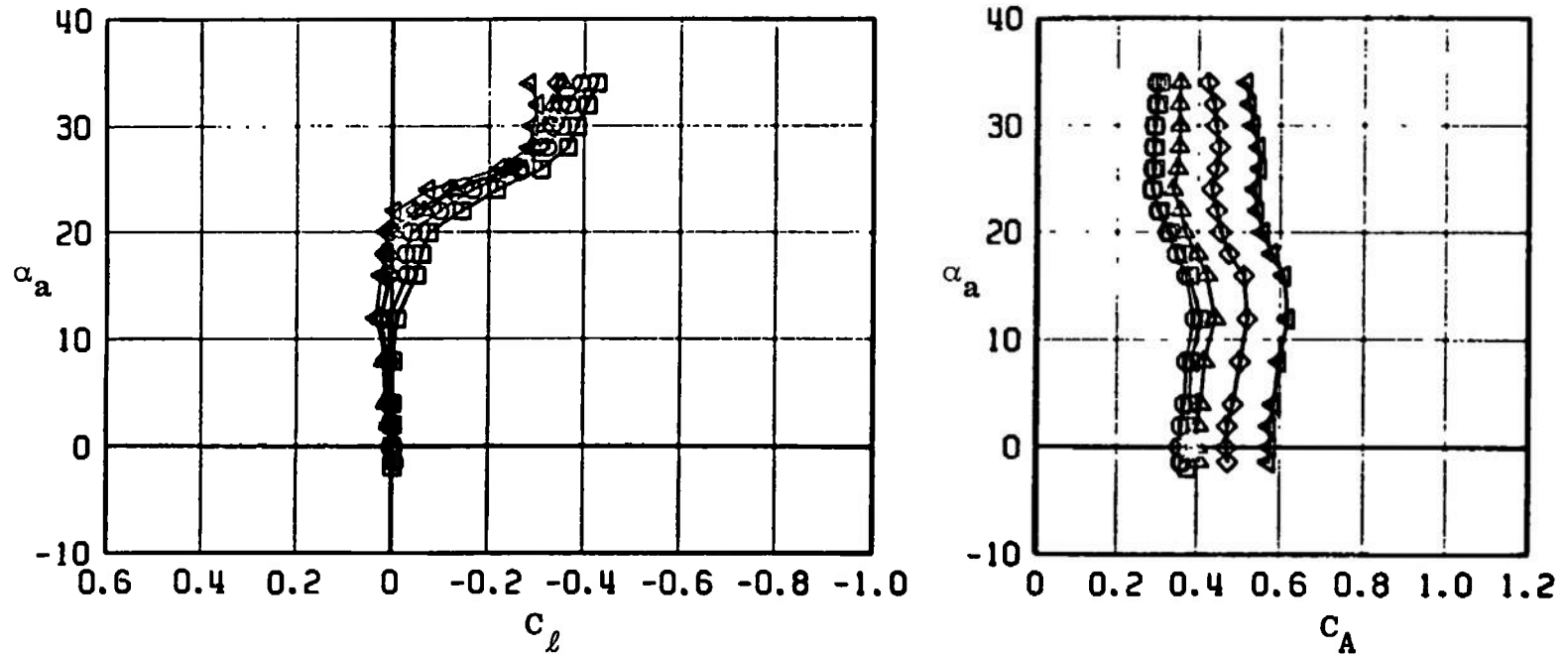


Fig. 29 Effect of Yaw Control Deflections on the Rolling-Moment and Axial-Force Coefficient for MGB Configuration without RES (B9T3)

YAW CONTROL EFFECTIVENESS							
ROLLING MOMENT AND AXIAL FORCE COEFFICIENTS							
SYMBOL	CONFIG	MACH NO	ϕ	δ_R	δ_H	δ_P	$R_L \times 10^{-6}$
□	B9T3	0.65	0	0.3	0.5	0.3	1.8
○	B9T3	0.65	0	0	-4.9	0.2	1.8
△	B9T3	0.65	0	0.2	-10.0	0.1	1.8
◇	B9T3	0.65	0	0.1	-14.9	0	1.8
◀	B9T3	0.65	0	-0.6	-19.7	-0.1	1.8

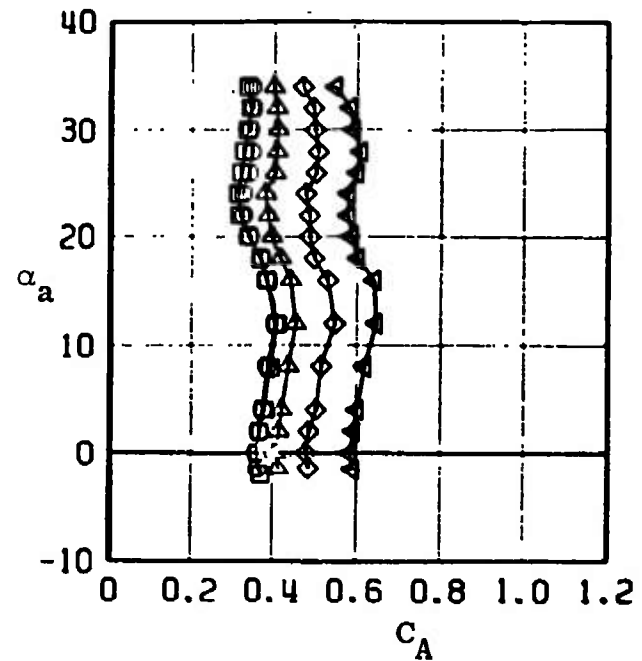
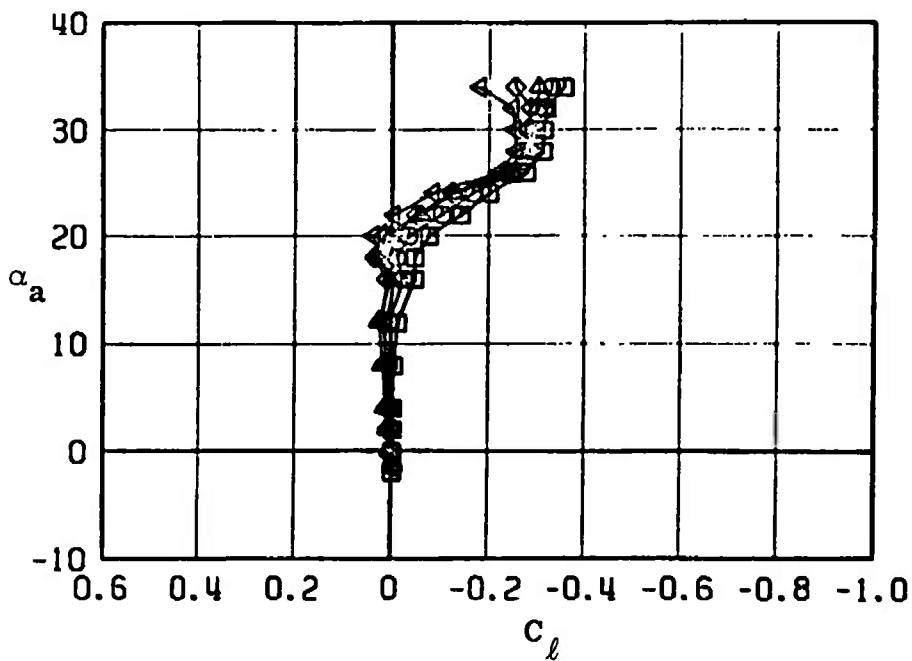


Fig. 29 Continued

YAW CONTROL EFFECTIVENESS
ROLLING MOMENT AND AXIAL FORCE COEFFICIENTS

SYMBOL	CONFIG	MACH NO	ϕ	b_0	b_R	b_P	$R_f \times 10^{-6}$
□	B9T3	0.75	0	0.3	0.5	0.3	2.0
○	B9T3	0.75	0	0	-4.9	0.2	2.0
△	B9T3	0.75	0	0.2	-10.0	0.1	2.0
◇	B9T3	0.75	0	0.1	-14.9	0	2.0
◄	B9T3	0.75	0	-0.6	-19.7	-0.1	2.0

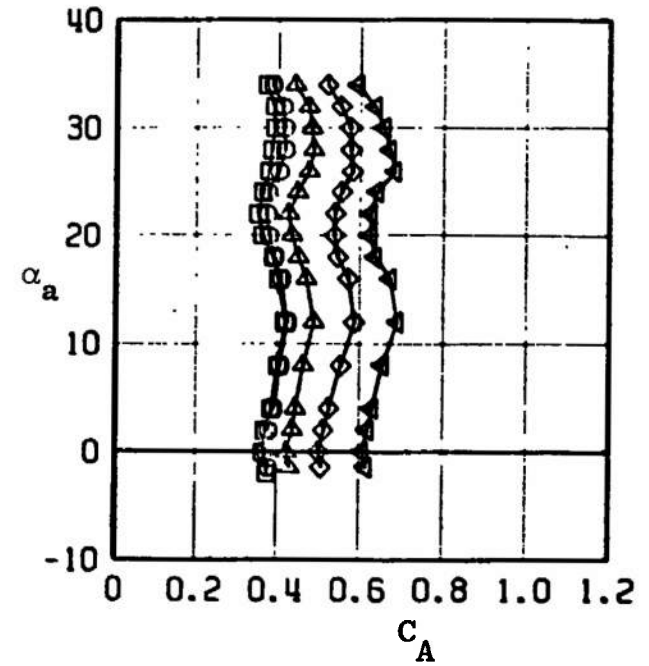
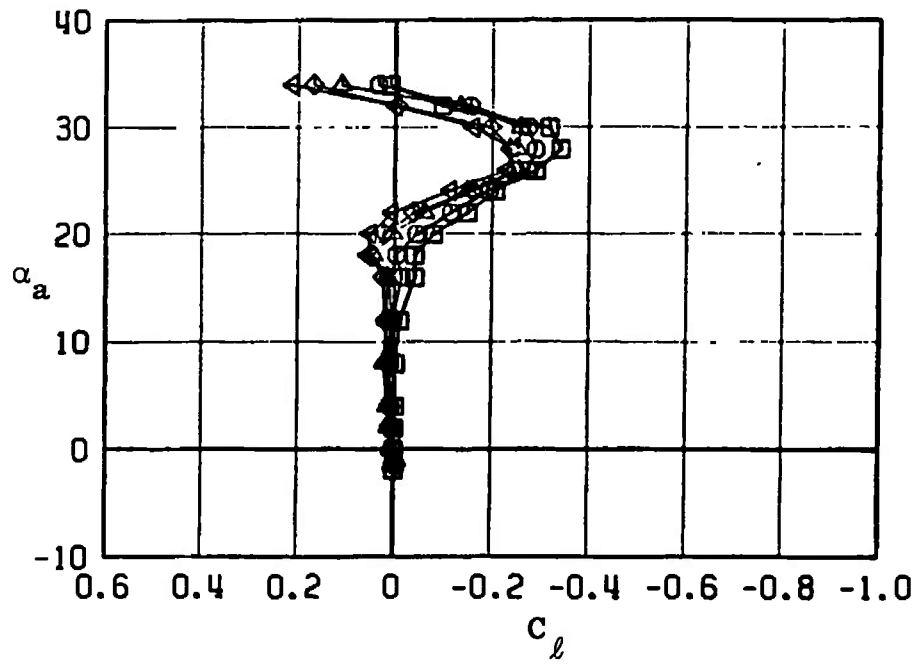


Fig. 29 Continued

YAW CONTROL EFFECTIVENESS

ROLLING MOMENT AND AXIAL FORCE COEFFICIENTS

SYMBOL	CONFIG	MACH NO	ϕ	δ_D	δ_R	δ_P	$R_L \times 10^{-6}$
□	B9T3	0.85	0	0.3	0.5	0.2	2.1
○	B9T3	0.85	0	0	-4.9	0.2	2.1
△	B9T3	0.85	0	0.2	-10.0	0.1	2.1
◇	B9T3	0.85	0	0.1	-14.9	0	2.1
◀	B9T3	0.85	0	-0.6	-19.7	-0.1	2.1

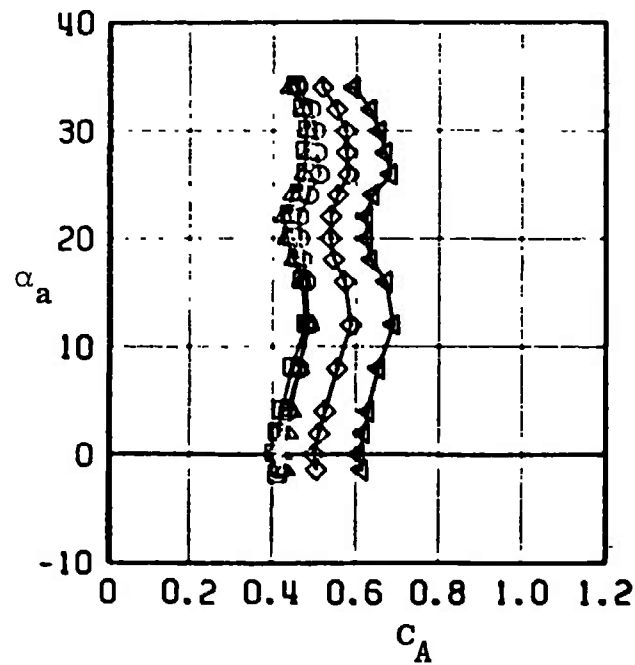
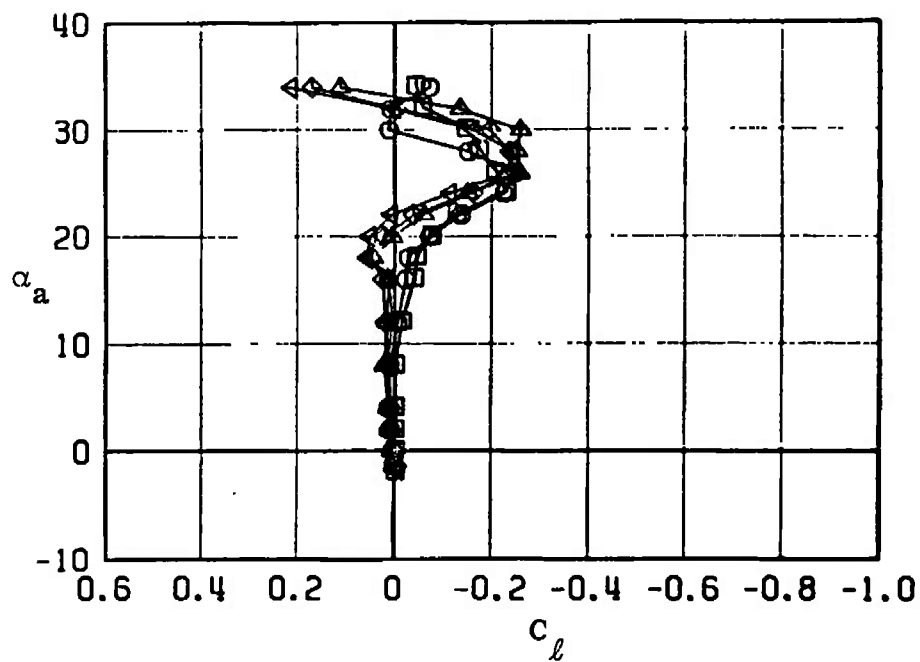


Fig. 29 Continued

YAW CONTROL EFFECTIVENESS

ROLLING MOMENT AND AXIAL FORCE COEFFICIENTS

SYMBOL	CONFIG	MACH NO	ϕ	δ_0	δ_n	δ_p	$R_L \times 10^{-6}$
\square	B9T3	0.95	0	0.3	0.5	0.3	2.2
\circ	B9T3	0.95	0	0	-4.9	0.2	2.2
\triangle	B9T3	0.95	0	0.2	-10.0	0.1	2.2
\diamond	B9T3	0.95	0	0.1	-14.9	0	2.2
\blacktriangle	B9T3	0.95	0	-0.6	-19.7	-0.1	2.2

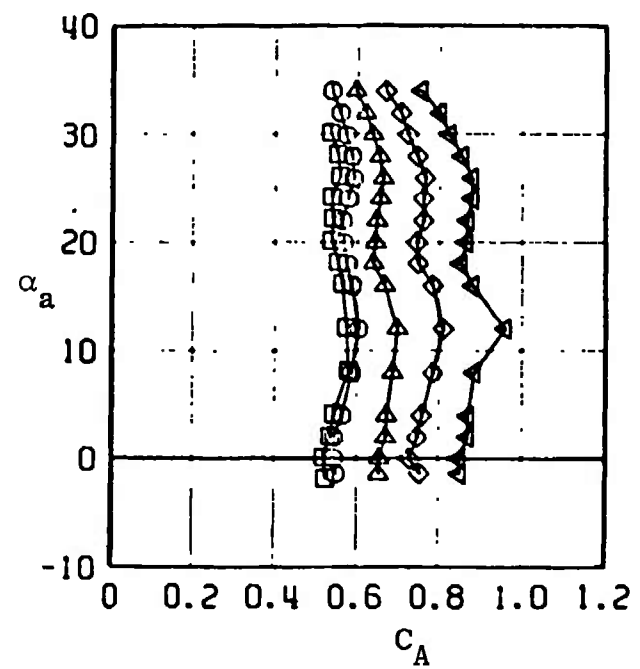
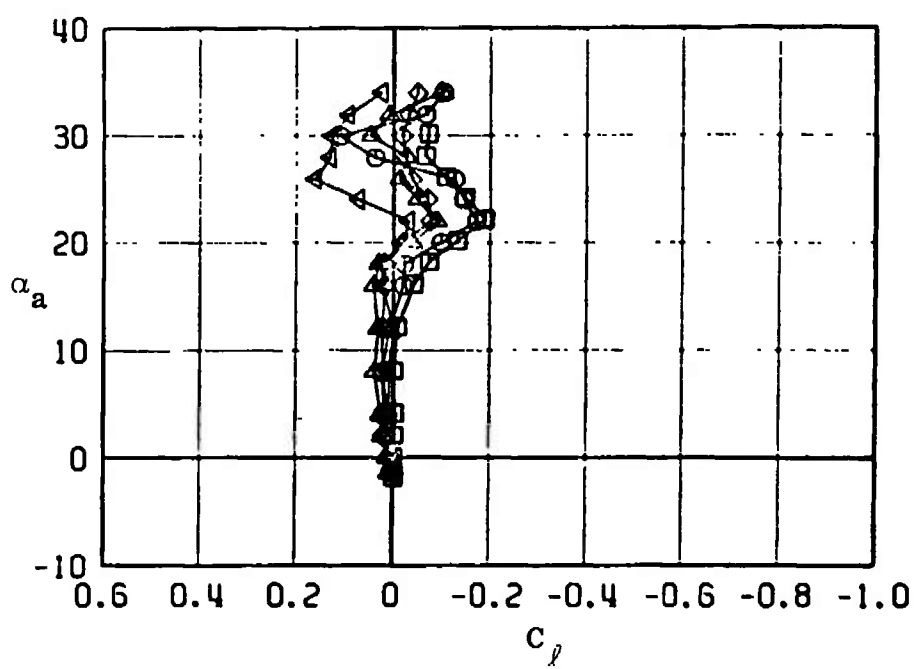


Fig. 29 Continued

YAW CONTROL EFFECTIVENESS
ROLLING MOMENT AND AXIAL FORCE COEFFICIENTS

SYMBOL	CONFIG	MACH NO	ϕ	δ_Q	δ_R	δ_P	$R_E \times 10^{-6}$
□	B9T3	1.05	0	0.3	0.5	0.3	2.3
○	B9T3	1.05	0	0	-4.9	0.2	2.3
△	B9T3	1.05	0	0.2	-10.0	0.1	2.3
◇	B9T3	1.05	0	0.1	-14.9	0	2.3
▽	B9T3	1.05	0	-0.6	-19.7	-0.1	2.3

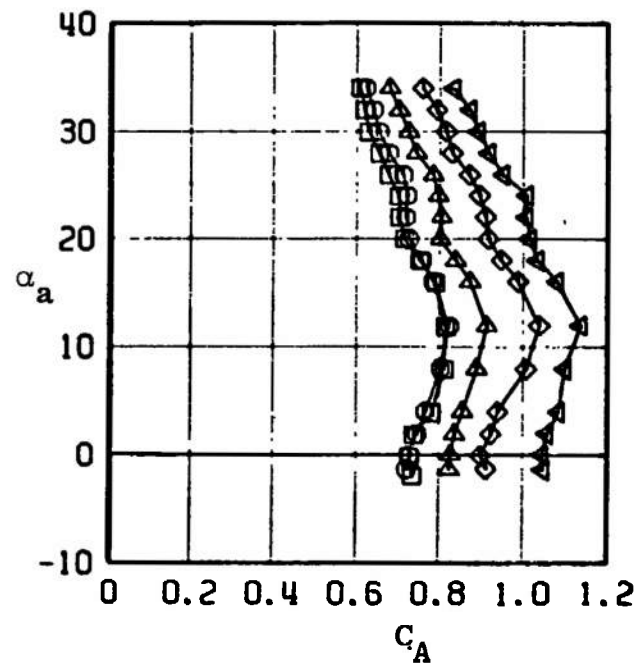
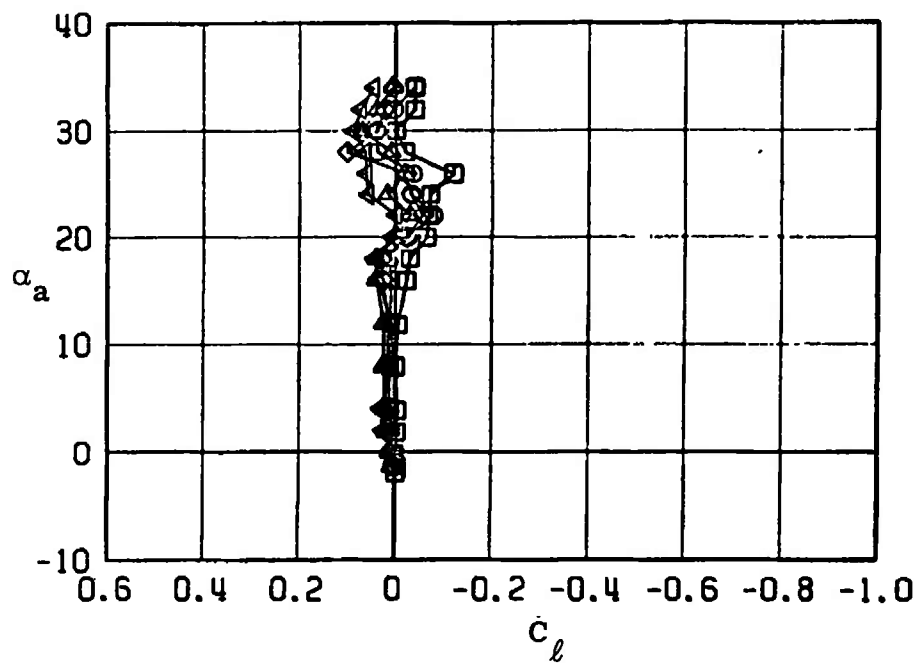


Fig. 29 Concluded

YAW CONTROL EFFECTIVENESS							
SIDE FORCE AND YAWING MOMENT COEFFICIENTS							
SYMBOL	CONFIG	MACH NO	ϕ	δ_0	δ_n	δ_p	$R_F \times 10^{-6}$
□	B9T3	0.50	0	0.3	0.5	0.3	1.5
○	B9T3	0.50	0	0	-4.9	0.2	1.5
△	B9T3	0.50	0	0.2	-10.0	0.1	1.5
◇	B9T3	0.50	0	0.1	-14.9	0	1.5
◀	B9T3	0.50	0	-0.6	-19.7	-0.1	1.5

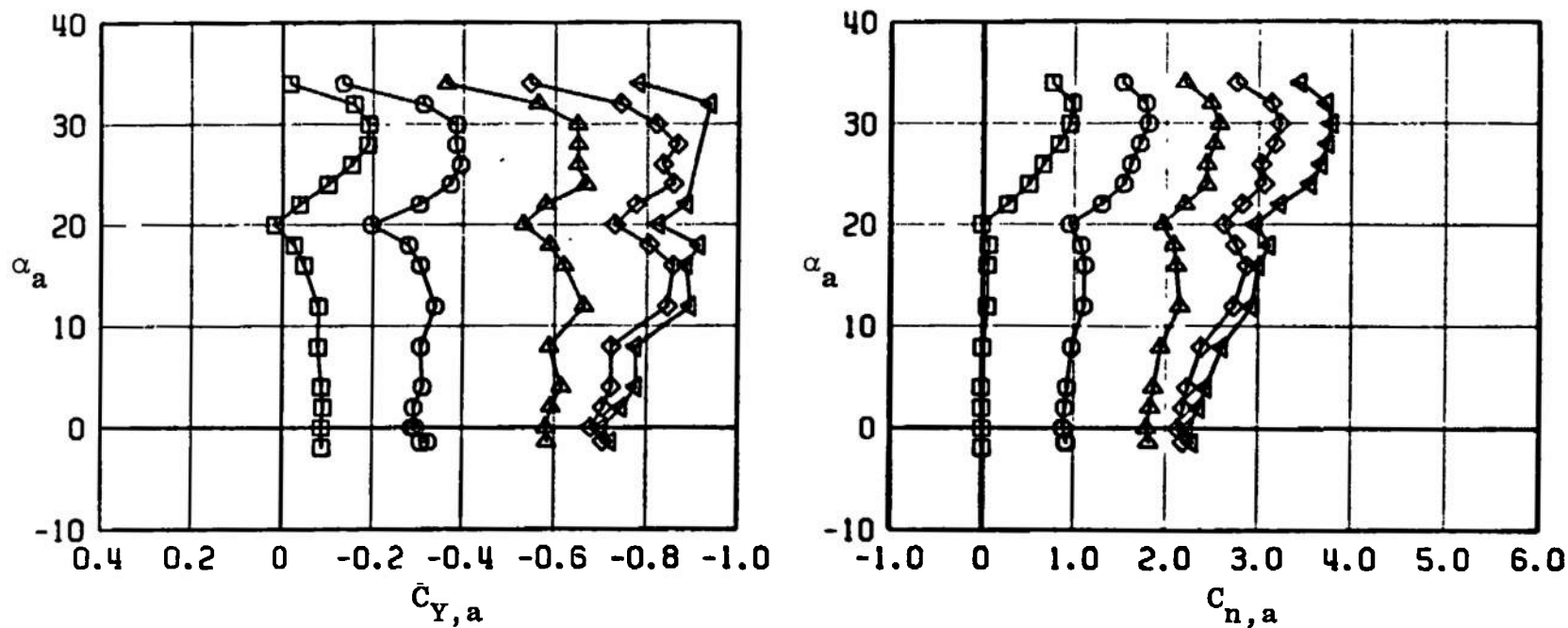


Fig. 30 Effect of Yaw Control Deflections on the Side-Force and Yawing-Moment Coefficients for MGGB Configuration without RES (B9T3)

YAW CONTROL EFFECTIVENESS SIDE FORCE AND YAWING MOMENT COEFFICIENTS							
SYMBOL	CONFIG	MACH NO	ϕ	δ_a	δ_n	δ_p	$R_L \times 10^{-6}$
□	B9T3	0.65	0	0.3	0.5	0.3	1.8
○	B9T3	0.65	0	0	-4.9	0.2	1.8
△	B9T3	0.65	0	0.2	-10.0	0.1	1.8
◇	B9T3	0.65	0	0.1	-14.9	0	1.8
◀	B9T3	0.65	0	-0.6	-19.7	-0.1	1.8

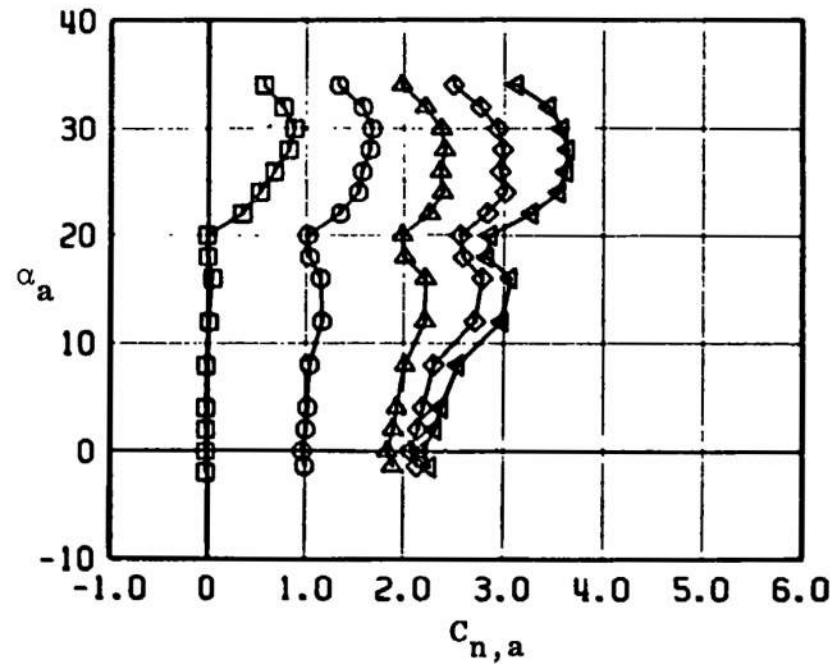
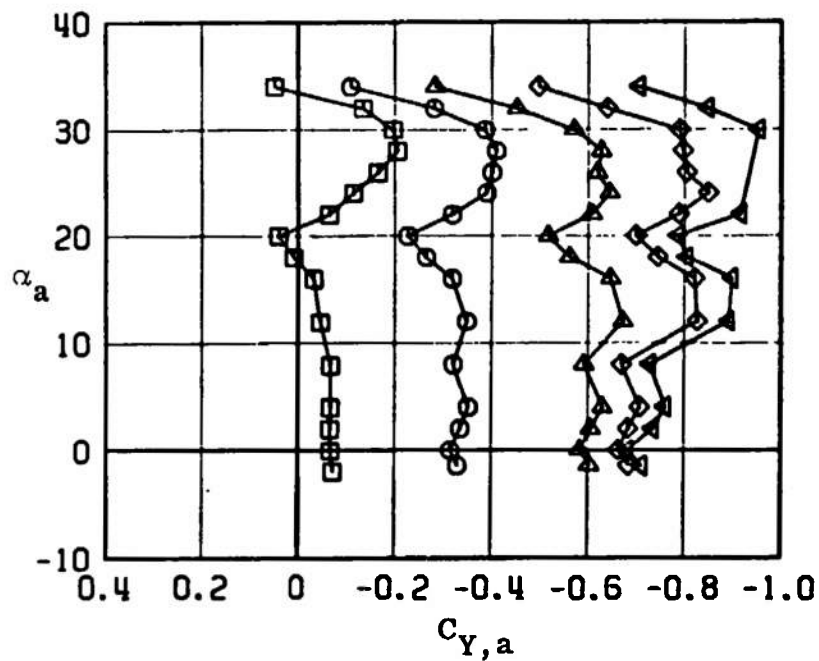


Fig. 30 Continued

YAW CONTROL EFFECTIVENESS
SIDE FORCE AND YAWING MOMENT COEFFICIENTS

SYMBOL	CONFIG	MACH NO	ϕ	b_0	b_n	b_p	$R_F \times 10^{-6}$
□	B9T3	0.75	0	0.3	0.5	0.3	2.0
○	B9T3	0.75	0	0	-4.9	0.2	2.0
△	B9T3	0.75	0	0.2	-10.0	0.1	2.0
◇	B9T3	0.75	0	0.1	-14.9	0	2.0
◀	B9T3	0.75	0	-0.6	-19.7	-0.1	2.0

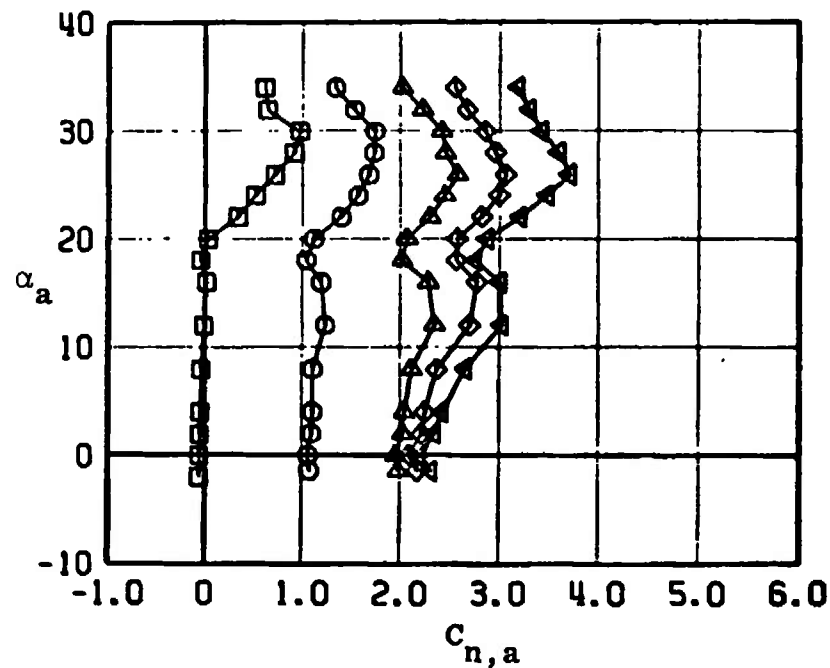
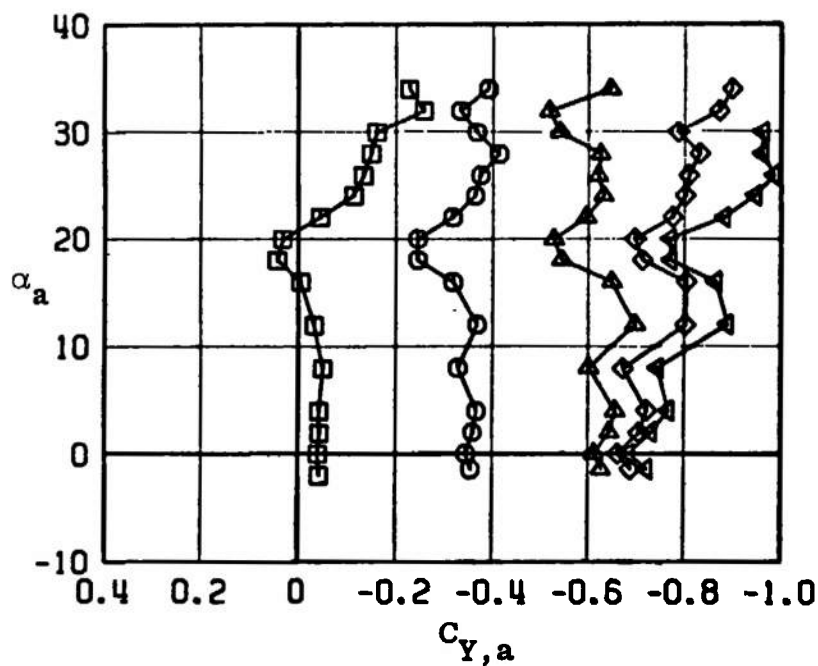


Fig. 30 Continued

YAW CONTROL EFFECTIVENESS

SIDE FORCE AND YAWING MOMENT COEFFICIENTS

SYMBOL	CONFIG	MACH NO	ϕ	b_0	b_n	b_p	$R_E \times 10^{-5}$
□	89T3	0.85	0	0.3	0.5	0.2	2.1
○	89T3	0.85	0	0	-4.9	0.2	2.1
△	89T3	0.85	0	0.2	-10.0	0.1	2.1
◇	89T3	0.85	0	0.1	-14.9	0	2.1
▲	89T3	0.85	0	-0.6	-19.7	-0.1	2.1

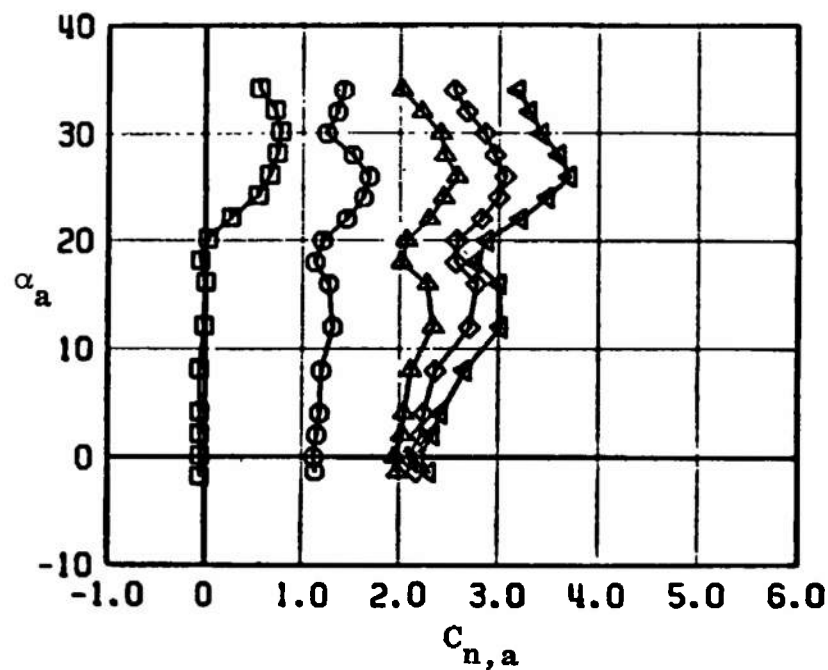
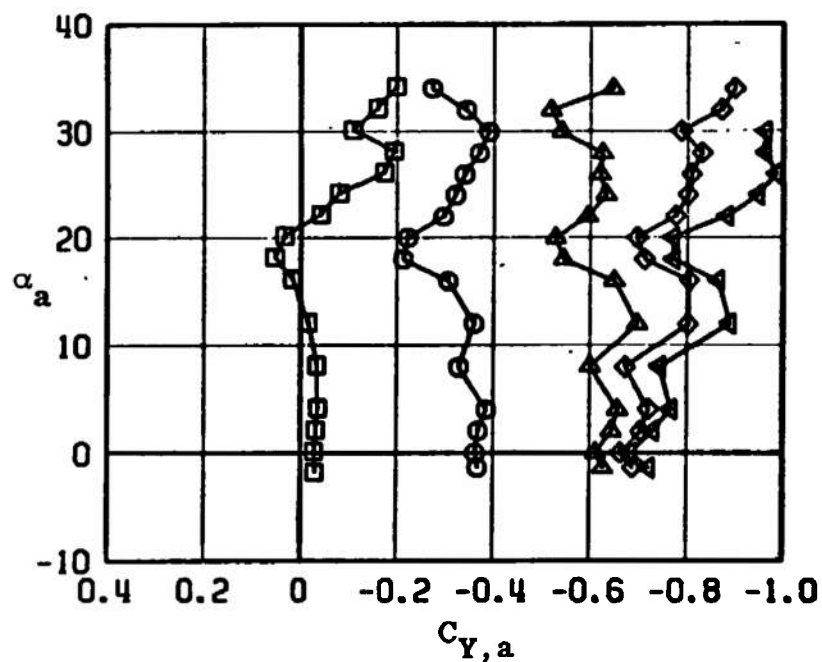


Fig. 30 Continued

YAW CONTROL EFFECTIVENESS
SIDE FORCE AND YAWING MOMENT COEFFICIENTS

SYMBOL	CONFIG	MACH NO	ϕ	ϵ_y	ϵ_z	$R_L \times 10^{-6}$	
□	B9T3	0.95	0	0.3	0.5	0.3	2.2
○	B9T3	0.95	0	0	-4.9	0.2	2.2
△	B9T3	0.95	0	0.2	-10.0	0.1	2.2
◇	B9T3	0.95	0	0.1	-14.9	0	2.2
◄	B9T3	0.95	0	-0.6	-19.7	-0.1	2.2

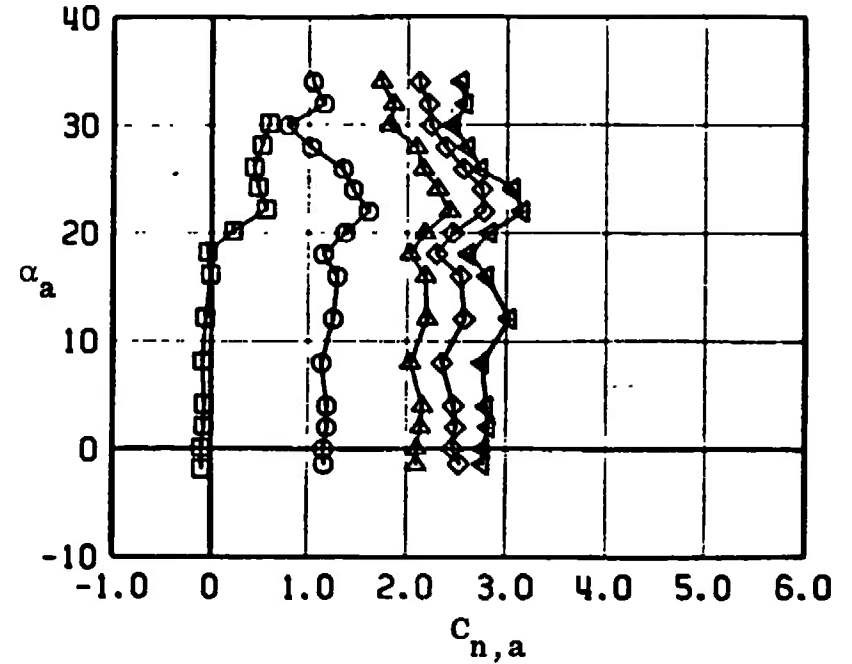
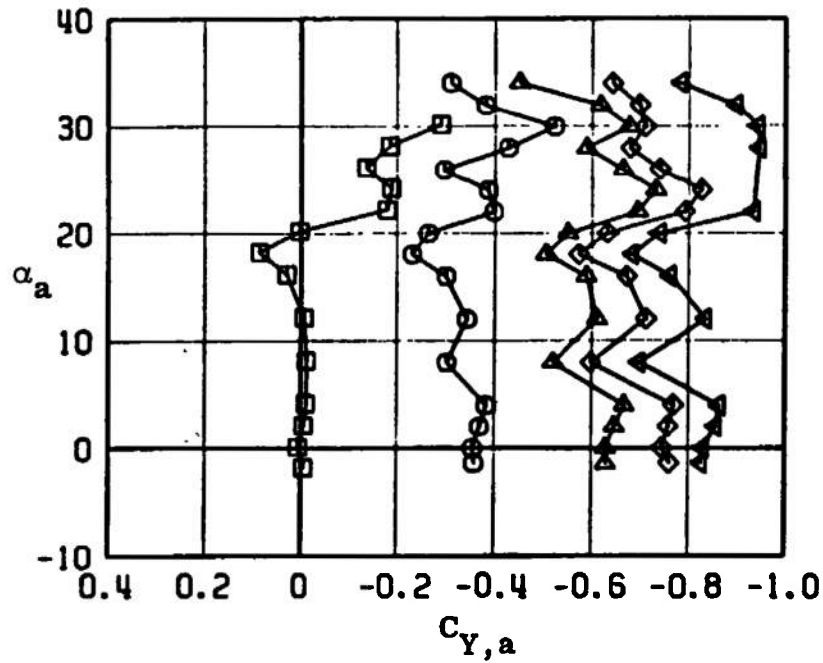


Fig. 30 Continued

YAW CONTROL EFFECTIVENESS SIDE FORCE AND YAWING MOMENT COEFFICIENTS							
SYMBOL	CONFIG	MACH NO	ϕ	b_D	b_N	b_P	$R_F \times 10^{-6}$
□	B9T3	1.05	0	0.3	0.5	0.3	2.3
○	B9T3	1.05	0	0	-4.9	0.2	2.3
△	B9T3	1.05	0	0.2	-10.0	0.1	2.3
◇	B9T3	1.05	0	0.1	-14.9	0	2.3
◀	B9T3	1.05	0	-0.6	-19.7	-0.1	2.3

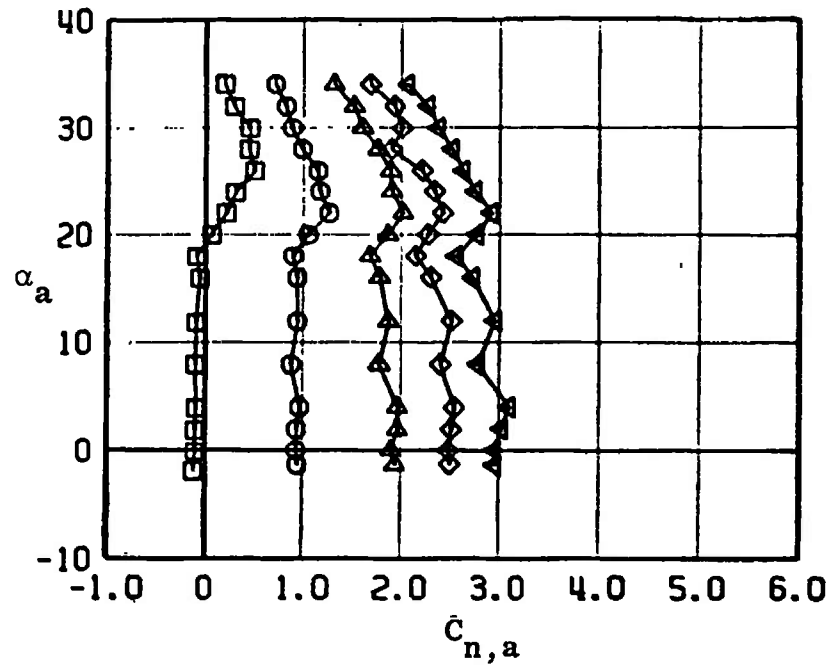
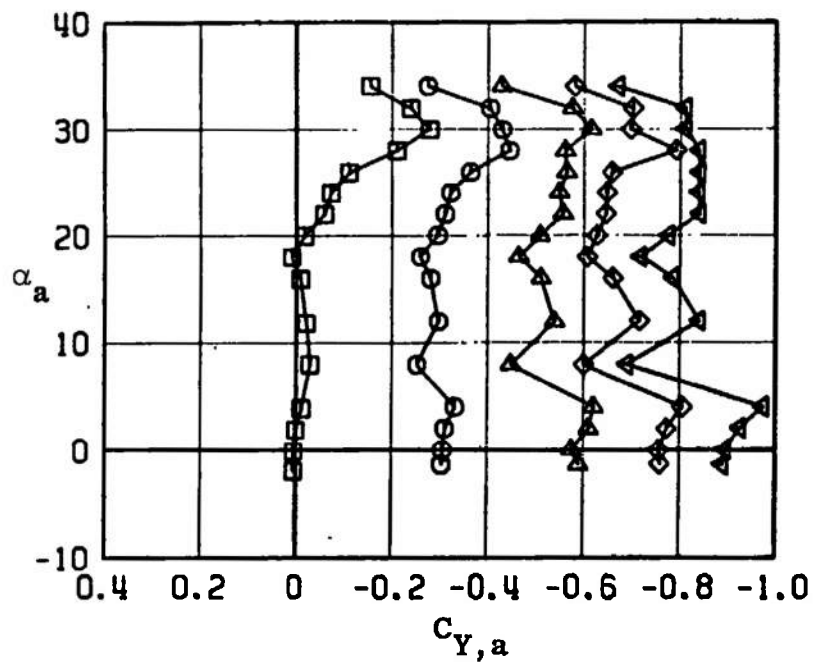


Fig. 30 Concluded

ROLL CONTROL EFFECTIVENESS							
NORMAL FORCE AND PITCHING MOMENT COEFFICIENTS							
SYMBOL	CONFIG	MACH NO	ϕ	δ_0	δ_R	δ_P	$R_E \times 10^{-6}$
□	B9T3	0.50	0	0.3	0.5	0.3	1.5
○	B9T3	0.50	0	-0.1	0	-4.7	1.5
△	B9T3	0.50	0	0.2	0	-9.9	1.5
◇	B9T3	0.50	0	-0.1	0	-14.9	1.5
◀	B9T3	0.50	0	-0.6	0.2	-20.0	1.5

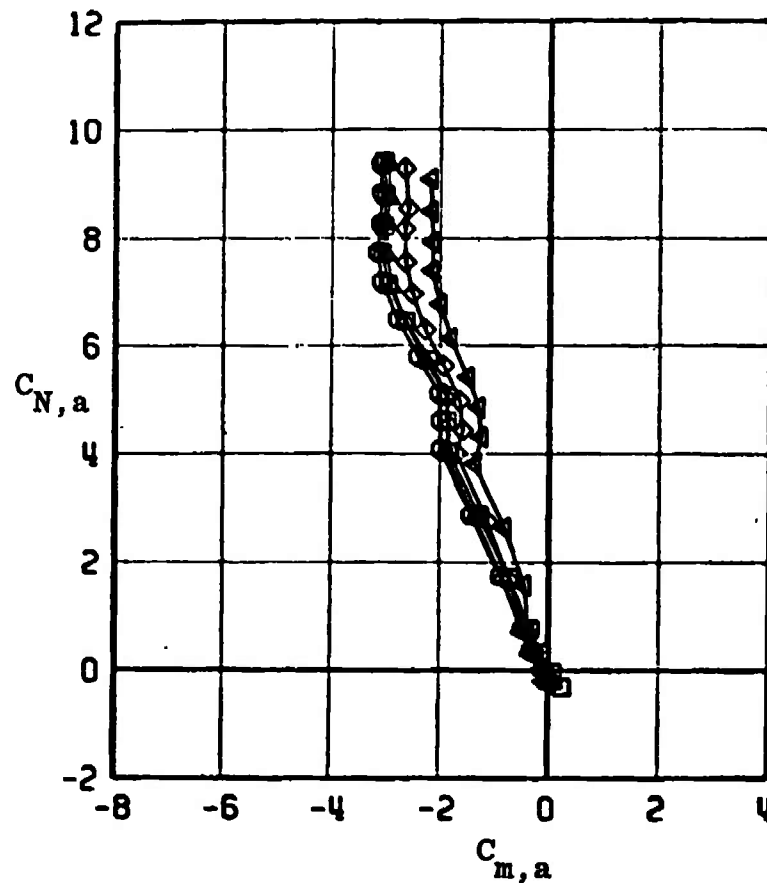
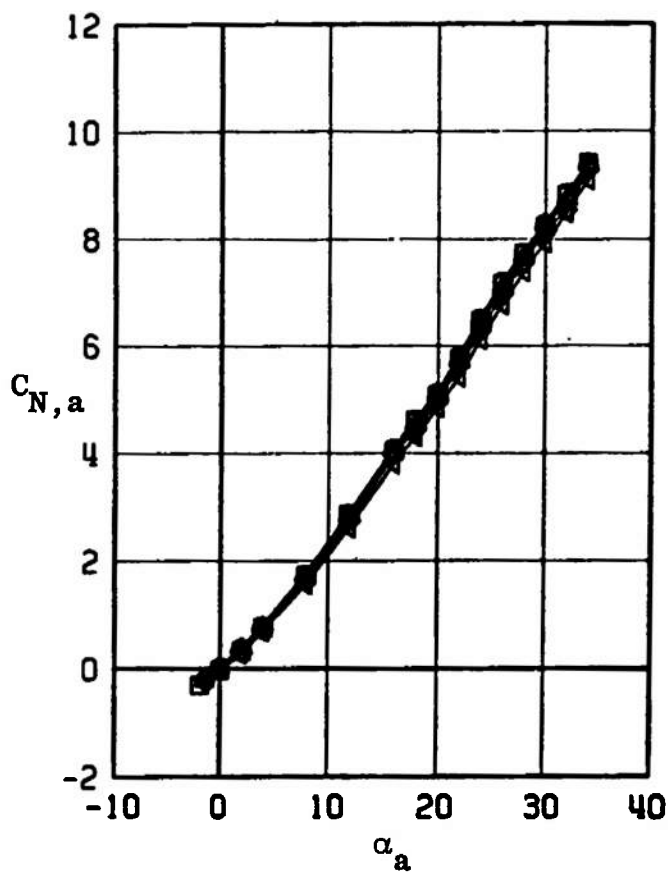


Fig. 31 Effect of Roll Control Deflections on the Normal-Force and Pitching-Moment Coefficient for MGGB Configuration without RES (B9T3)

ROLL CONTROL EFFECTIVENESS							
NORMAL FORCE AND PITCHING MOMENT COEFFICIENTS							
SYMBOL	CONFIG	MACH NO	ϕ	δ_ϕ	δ_η	δ_p	$R_L \times 10^{-6}$
□	B9T3	0.65	0	0.3	0.5	0.3	1.8
○	B9T3	0.65	0	-0.1	0	-4.7	1.8
△	B9T3	0.65	0	0.2	0	-9.9	1.8
◇	B9T3	0.65	0	-0.1	0	-14.9	1.8
◁	B9T3	0.65	0	-0.6	0.2	-20.0	1.8

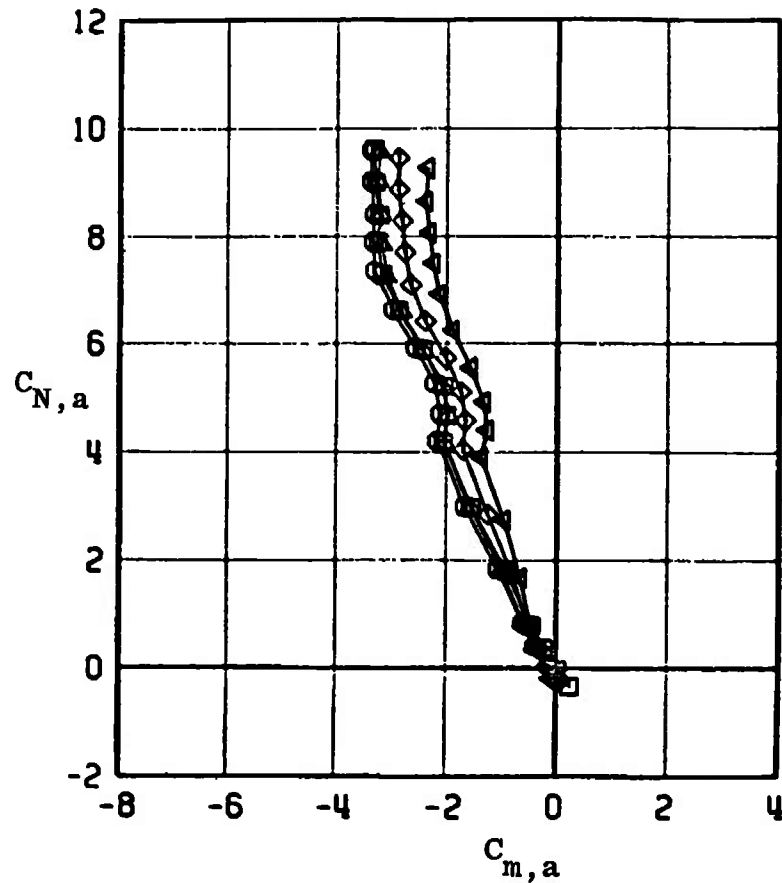
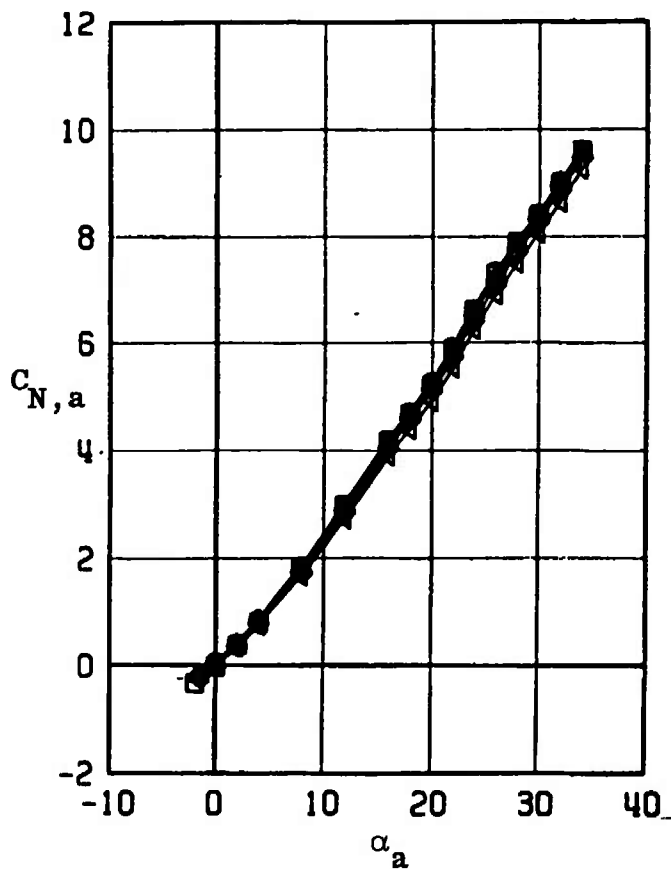


Fig. 31 Continued

ROLL CONTROL EFFECTIVENESS							
NORMAL FORCE AND PITCHING MOMENT COEFFICIENTS							
SYMBOL	CONFIG	MACH NO	ϕ	δ_0	δ_R	δ_P	$R_L \times 10^{-6}$
□	B9T3	0.75	0	0.3	0.5	0.3	2.0
○	B9T3	0.75	0	-0.1	0	-4.7	2.0
△	B9T3	0.75	0	0.2	0	-9.9	2.0
◇	B9T3	0.75	0	-0.1	0	-14.9	2.0
◀	B9T3	0.75	0	-0.6	0.2	-20.0	2.0

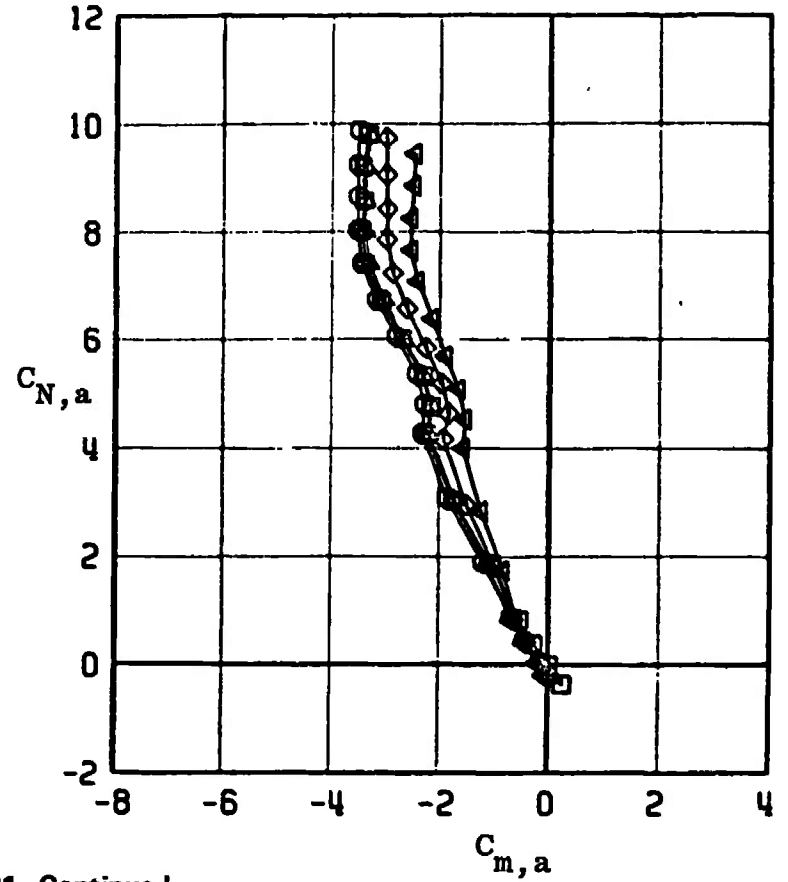
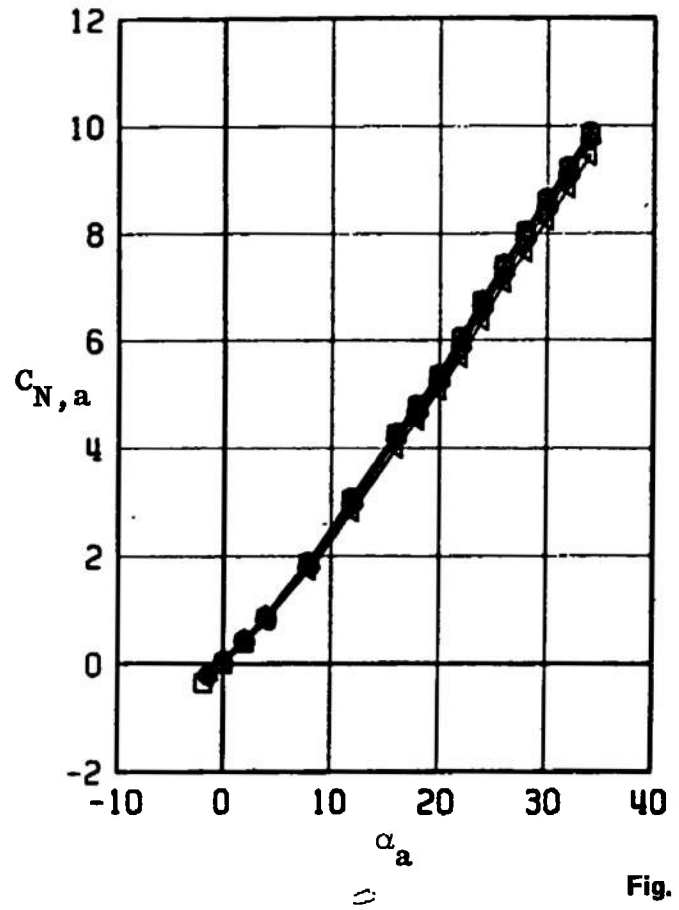


Fig. 31 Continued

ROLL CONTROL EFFECTIVENESS

NORMAL FORCE AND PITCHING MOMENT COEFFICIENTS

SYMBOL	CONFIG	MACH NO	ϕ	δ_D	δ_H	δ_P	$R_E \times 10^{-6}$
\square	B9T3	0.85	0	0.3	0.5	0.3	2.1
\circ	B9T3	0.85	0	-0.1	0	-4.7	2.1
\triangle	B9T3	0.85	0	0.2	0	-9.9	2.1
\diamond	B9T3	0.85	0	-0.1	0	-14.9	2.1
\blacktriangleleft	B9T3	0.85	0	-0.6	0.2	-20.0	2.1

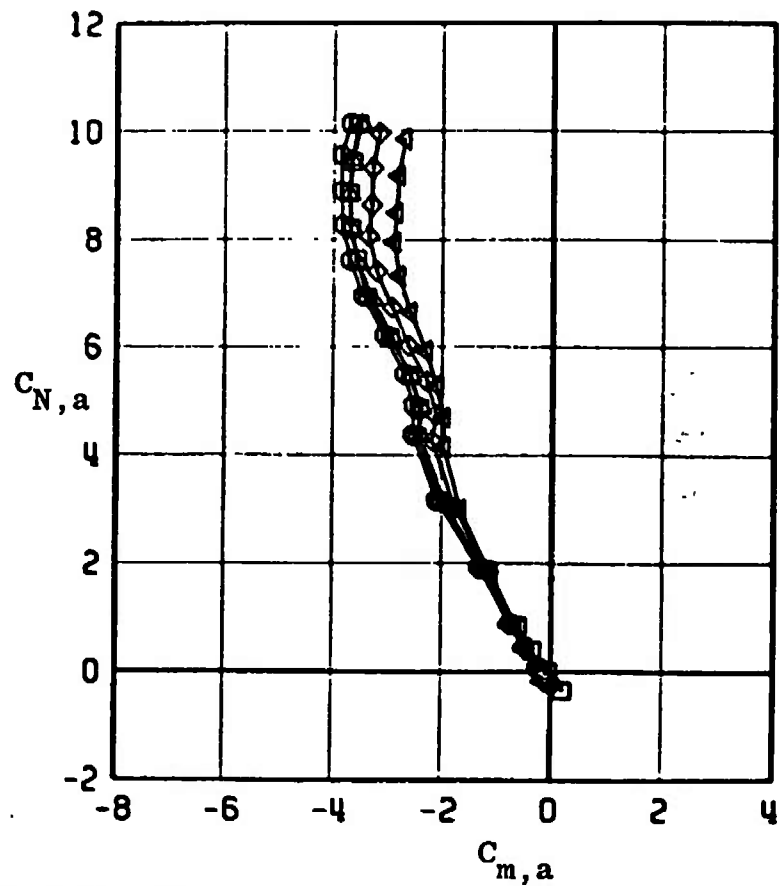
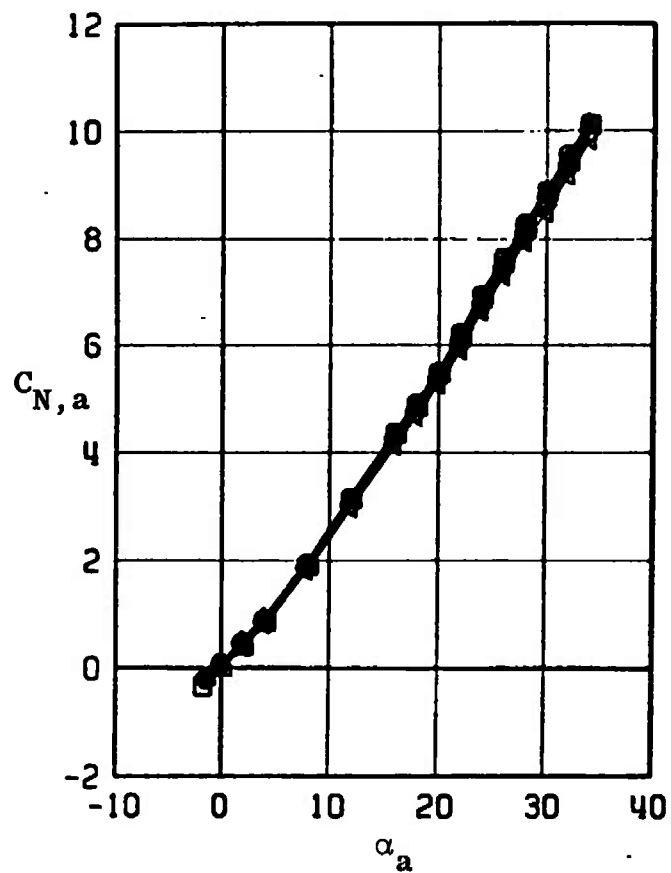


Fig. 31 Continued

ROLL CONTROL EFFECTIVENESS							
NORMAL FORCE AND PITCHING MOMENT COEFFICIENTS							
SYMBOL	CONFIG	MACH NO	ϕ	b_0	b_R	b_P	$R_L \times 10^{-6}$
□	B9T3	0.95	0	0.3	0.5	0.3	2.2
○	B9T3	0.95	0	-0.1	0	-4.7	2.2
△	B9T3	0.95	0	0.2	0	-9.9	2.2
◇	B9T3	0.95	0	-0.1	0	-14.9	2.2
◀	B9T3	0.95	0	-0.6	0.2	-20.0	2.2

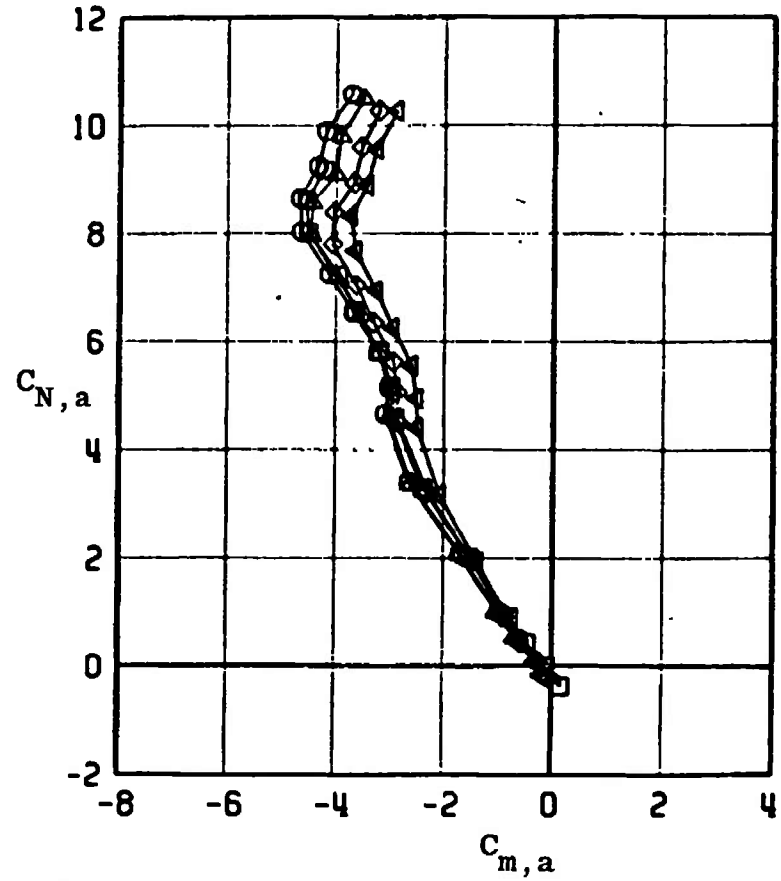
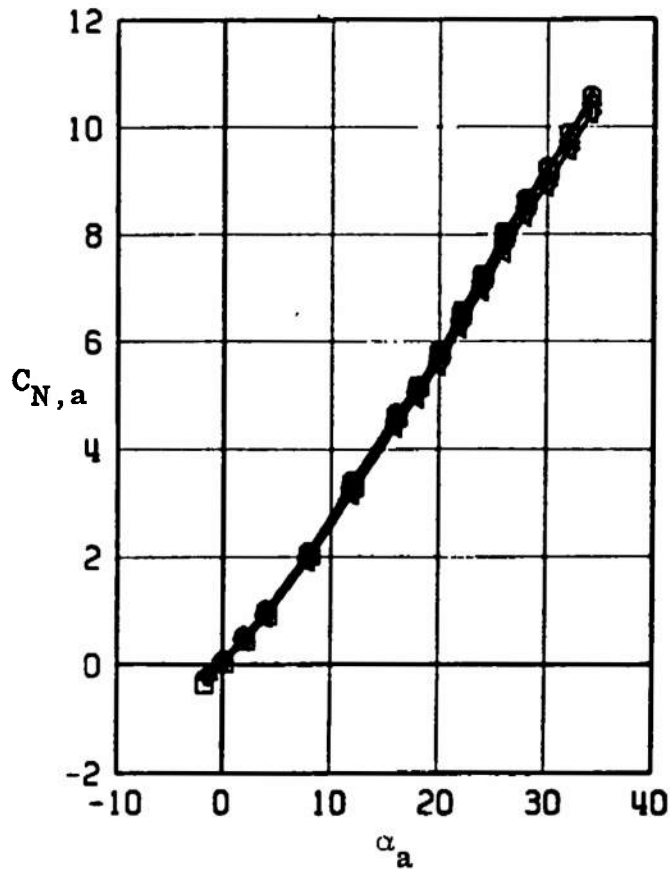


Fig. 31 Continued

ROLL CONTROL EFFECTIVENESS							
NORMAL FORCE AND PITCHING MOMENT COEFFICIENTS							
SYMBOL	CONFIG	MACH NO	ϕ	δ_a	δ_r	δ_p	$R_F \times 10^{-6}$
□	B9T3	1.05	0	0.3	0.5	0.3	2.3
○	B9T3	1.05	0	-0.1	0	-4.7	2.3
△	B9T3	1.05	0	0.2	0	-9.9	2.3
◇	B9T3	1.05	0	-0.1	0	-14.9	2.3
◀	B9T3	1.05	0	-0.6	0.2	-20.0	2.3

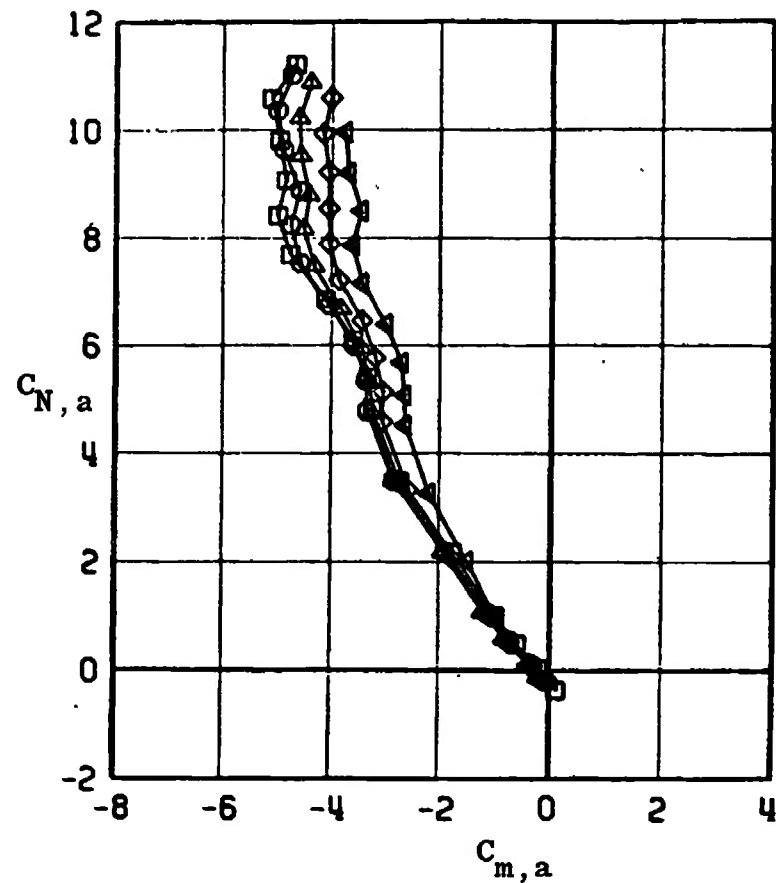
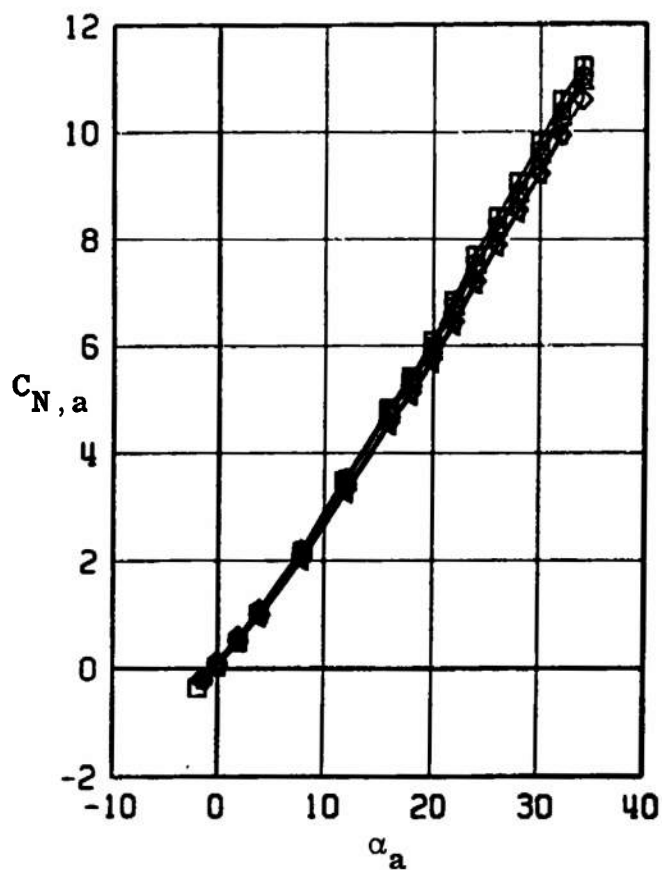


Fig. 31 Concluded

ROLL CONTROL EFFECTIVENESS							
ROLLING MOMENT AND AXIAL FORCE COEFFICIENTS							
SYMBOL	CONFIG	MACH NO	ϕ	δ_0	δ_n	δ_p	$R_L \times 10^{-6}$
□	B9T3	0.50	0	0.3	0.5	0.3	1.5
○	B9T3	0.50	0	-0.1	0	-4.7	1.5
△	B9T3	0.50	0	0.2	0	-9.9	1.5
◇	B9T3	0.50	0	-0.1	0	-14.9	1.5
▽	B9T3	0.50	0	-0.6	0.2	-20.0	1.5

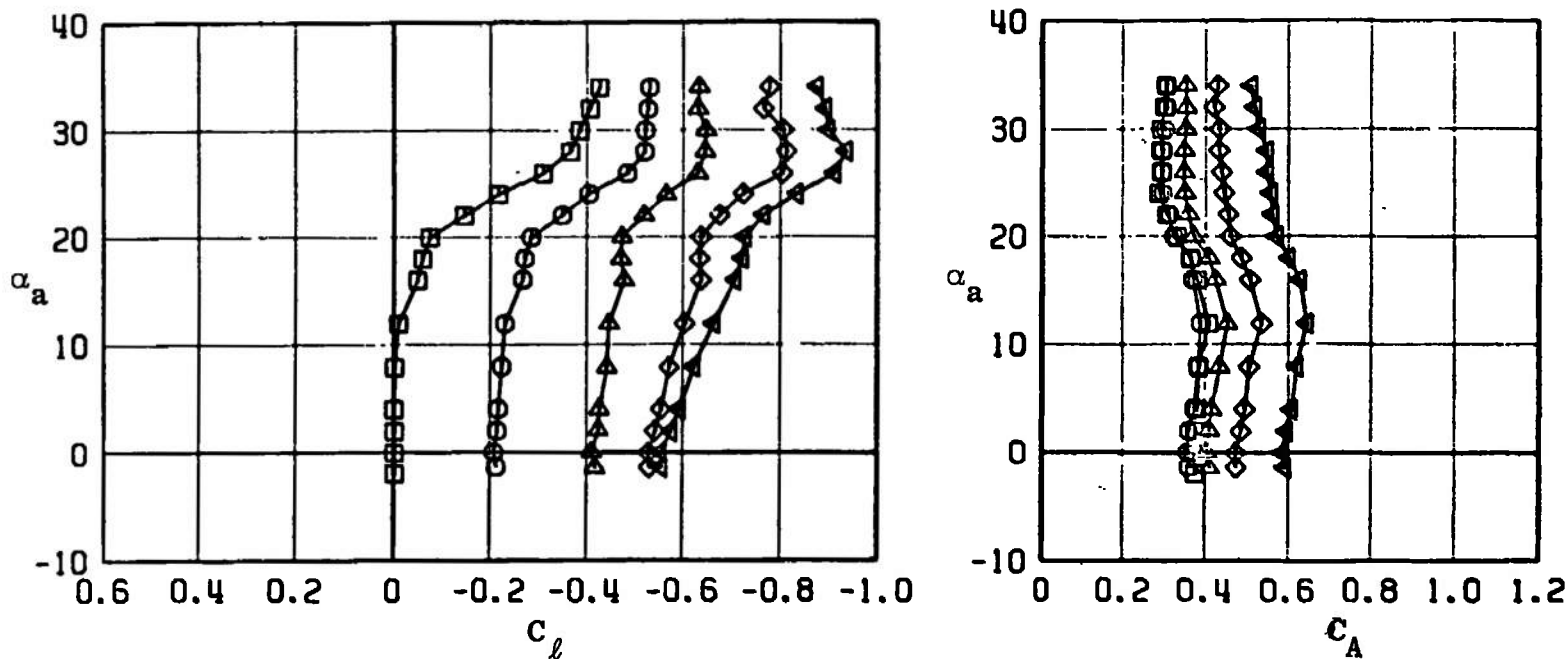


Fig. 32 Effect of Roll Control Deflections on the Rolling-Moment and Axial-Force Coefficients for MGGB Configuration without RES (B9T3)

ROLL CONTROL EFFECTIVENESS

ROLLING MOMENT AND AXIAL FORCE COEFFICIENTS

SYMBOL	CONFIG	MACH NO	ϕ	δ_0	δ_R	δ_P	$R_L \times 10^{-6}$
□	B9T3	0.65	0	0.3	0.5	0.3	1.8
○	B9T3	0.65	0	-0.1	0	-4.7	1.8
△	B9T3	0.65	0	0.2	0	-9.9	1.8
◇	B9T3	0.65	0	-0.1	0	-14.9	1.8
◀	B9T3	0.65	0	-0.6	0.2	-20.0	1.8

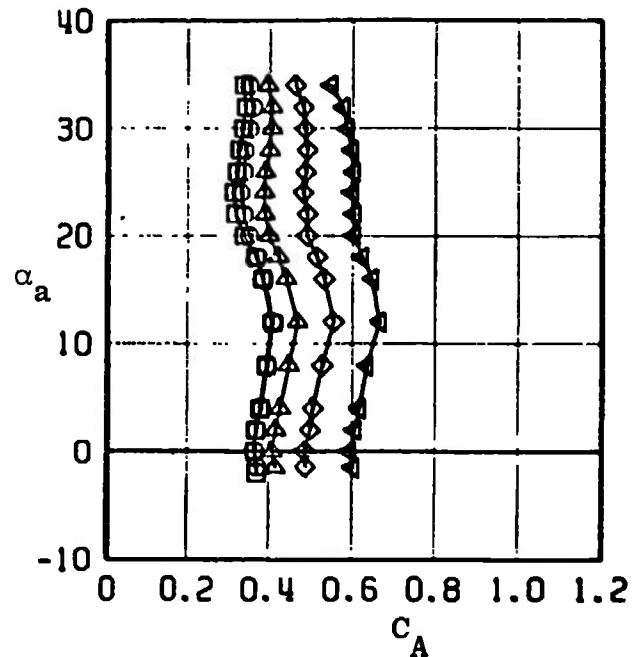
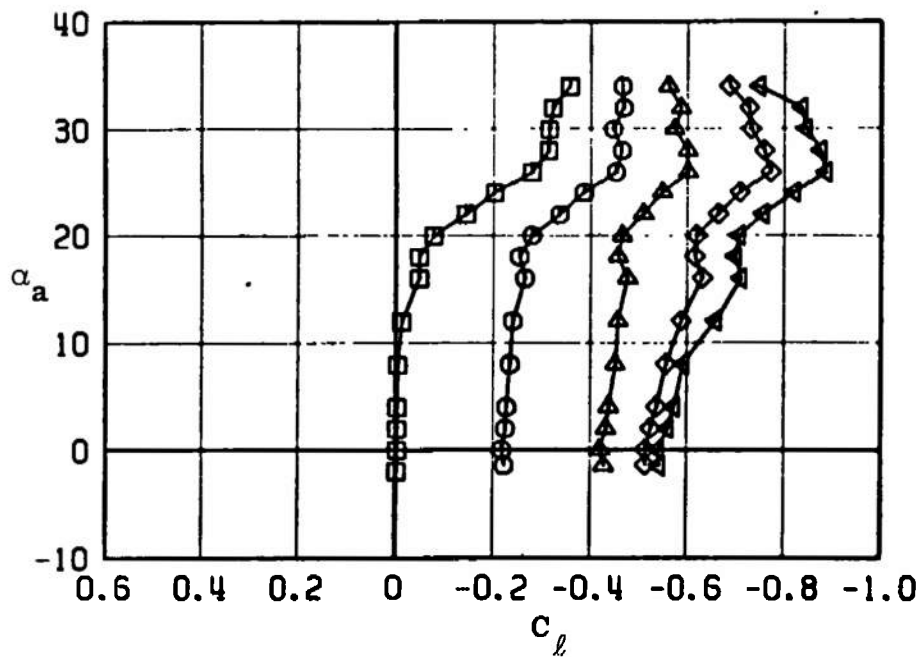


Fig. 32 Continued

ROLL CONTROL EFFECTIVENESS

ROLLING MOMENT AND AXIAL FORCE COEFFICIENTS

SYMBOL	CONFIG	MACH NO	ϕ	δ_D	δ_R	δ_P	$R_L \times 10^{-6}$
□	B9T3	0.75	0	0.3	0.5	0.3	2.0
○	B9T3	0.75	0	-0.1	0	-4.7	2.0
△	B9T3	0.75	0	0.2	0	-9.9	2.0
◇	B9T3	0.75	0	-0.1	0	-14.9	2.0
▽	B9T3	0.75	0	-0.6	0.2	-20.0	2.0

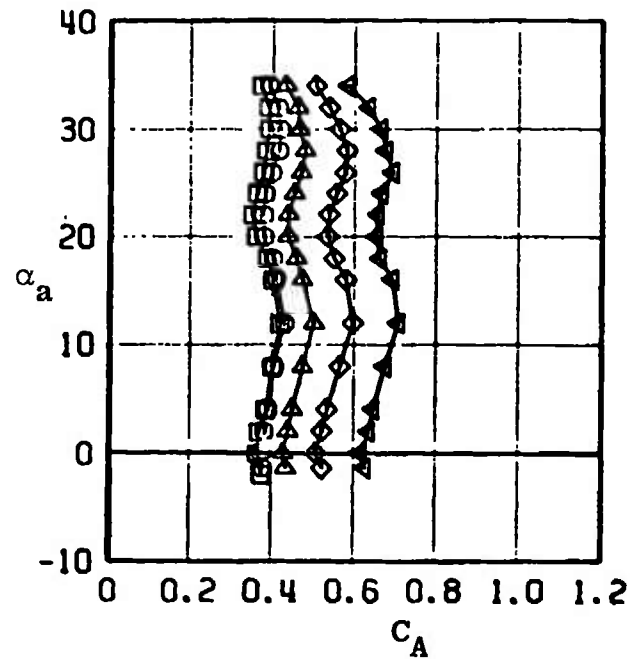
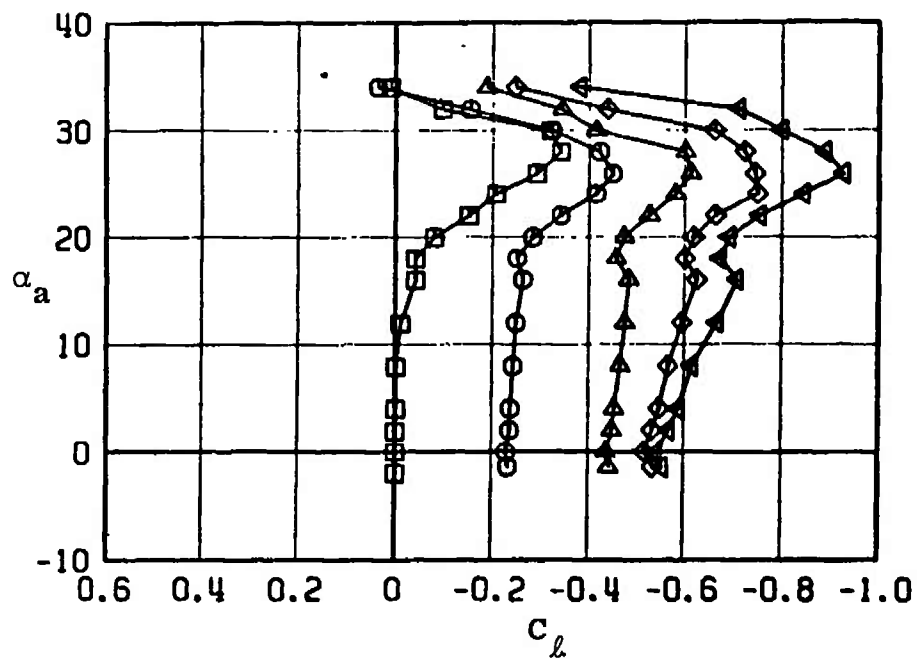


Fig. 32 Continued

ROLL CONTROL EFFECTIVENESS

ROLLING MOMENT AND AXIAL FORCE COEFFICIENTS

SYMBOL	CONFIG	MACH NO	ϕ	δ_0	δ_R	δ_P	$R_E \times 10^{-6}$
□	B9T3	0.85	0	0.3	0.5	0.3	2.1
○	B9T3	0.85	0	-0.1	0	-4.7	2.1
△	B9T3	0.85	0	0.2	0	-9.9	2.1
◇	B9T3	0.85	0	-0.1	0	-14.9	2.1
◄	B9T3	0.85	0	-0.6	0.2	-20.0	2.1

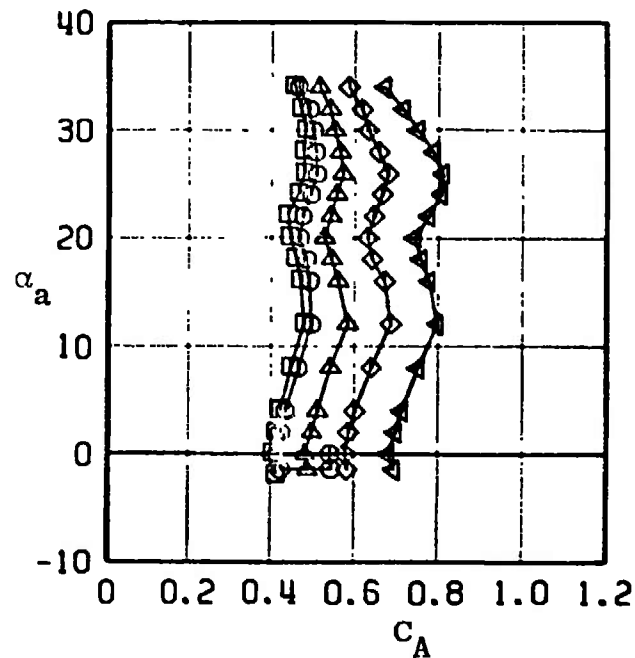
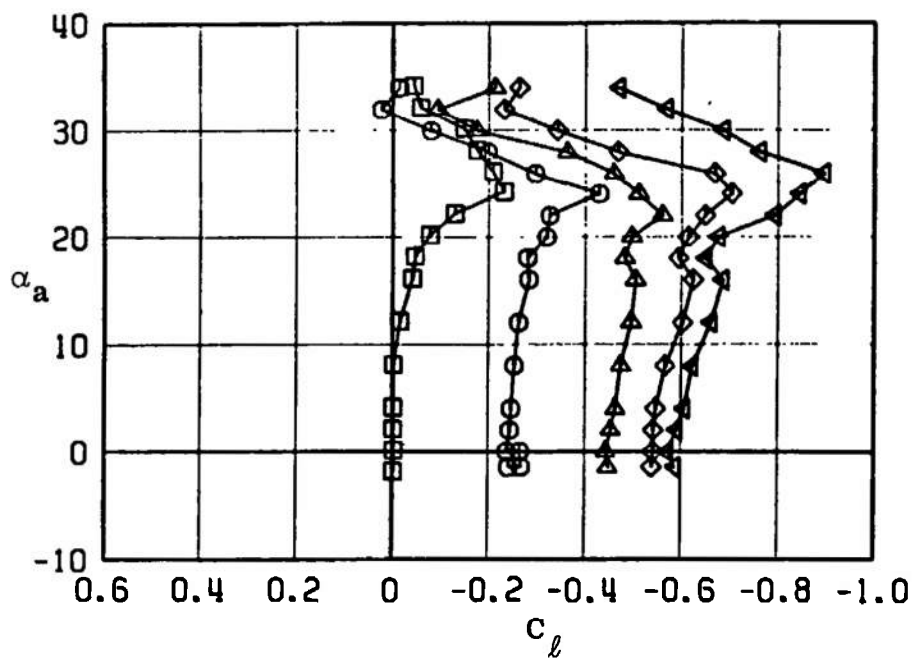


Fig. 32 Continued

ROLL CONTROL EFFECTIVENESS							
ROLLING MOMENT AND AXIAL FORCE COEFFICIENTS							
SYMBOL	CONFIG	MACH NO	ϕ	ϵ_0	ϵ_H	ϵ_P	$R_E \times 10^{-6}$
□	B9T3	0.95	0	0.3	0.5	0.3	2.2
○	B9T3	0.95	0	-0.1	0	-4.7	2.2
△	B9T3	0.95	0	0.2	0	-9.9	2.2
◇	B9T3	0.95	0	-0.1	0	-14.9	2.2
◀	B9T3	0.95	0	-0.6	0.2	-20.0	2.2

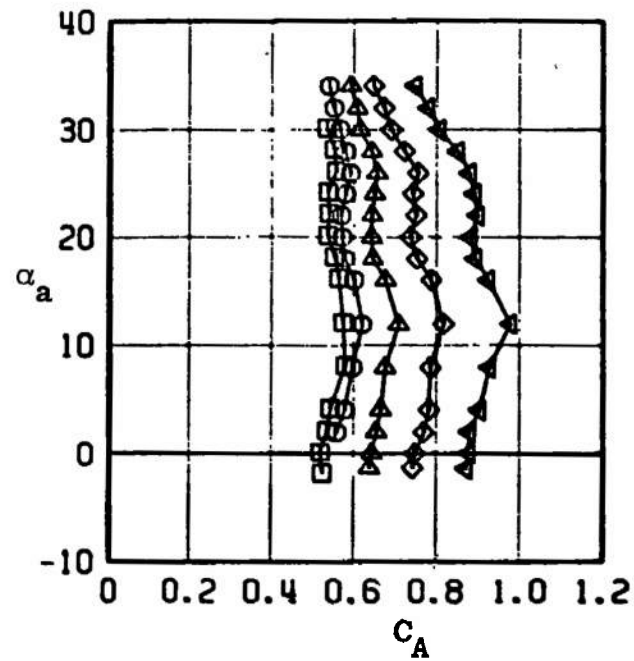
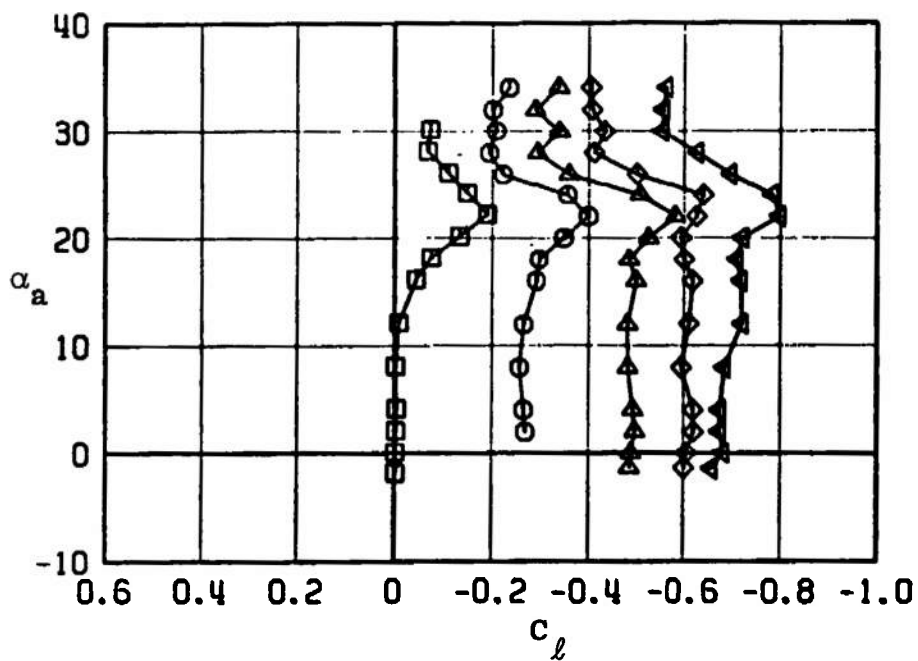


Fig. 32 Continued

ROLL CONTROL EFFECTIVENESS							
ROLLING MOMENT AND AXIAL FORCE COEFFICIENTS							
SYMBOL	CONFIG	MACH NO	ϕ	δ_ϕ	δ_η	δ_τ	$R_F \times 10^{-6}$
□	B9T3	1.05	0	0.3	0.5	0.3	2.3
○	B9T3	1.05	0	-0.1	0	-4.7	2.3
△	B9T3	1.05	0	0.2	0	-9.9	2.3
◇	B9T3	1.05	0	-0.1	0	-14.9	2.3
▽	B9T3	1.05	0	-0.6	0.2	-20.0	2.3

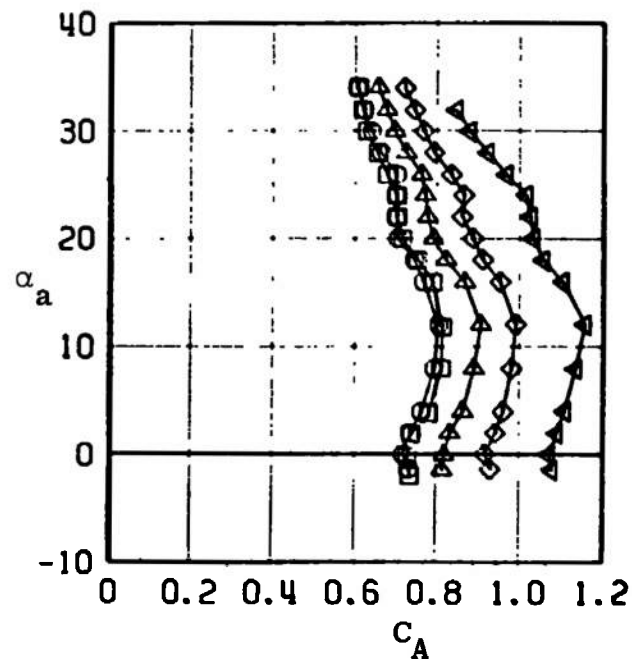
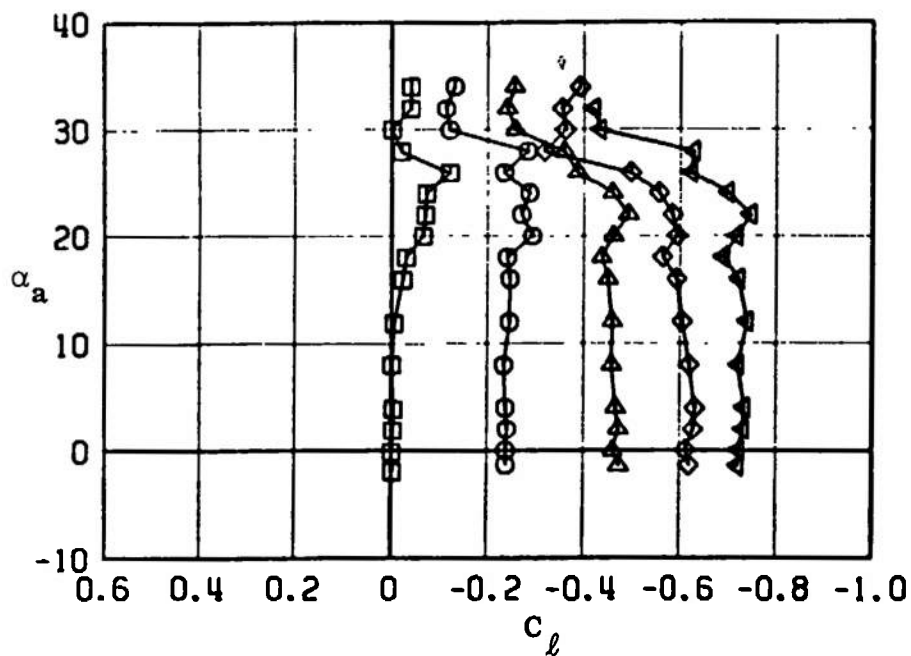


Fig. 32 Concluded

ROLL CONTROL EFFECTIVENESS							
SIDE FORCE AND YAWING MOMENT COEFFICIENTS							
SYMBOL	CONFIG	MACH NO	ϕ	δ_0	δ_R	δ_P	$R_L \times 10^{-6}$
□	B9T3	0.50	0	0.3	0.5	0.3	1.5
○	B9T3	0.50	0	-0.1	0	-4.7	1.5
△	B9T3	0.50	0	0.2	0	-9.9	1.5
◇	B9T3	0.50	0	-0.1	0	-14.9	1.5
◄	B9T3	0.50	0	-0.6	0.2	-20.0	1.5

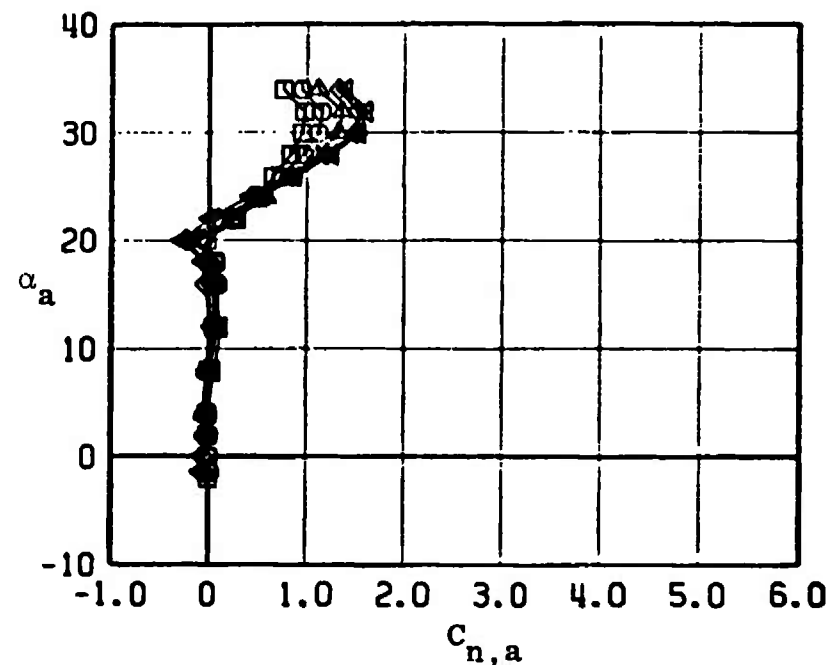
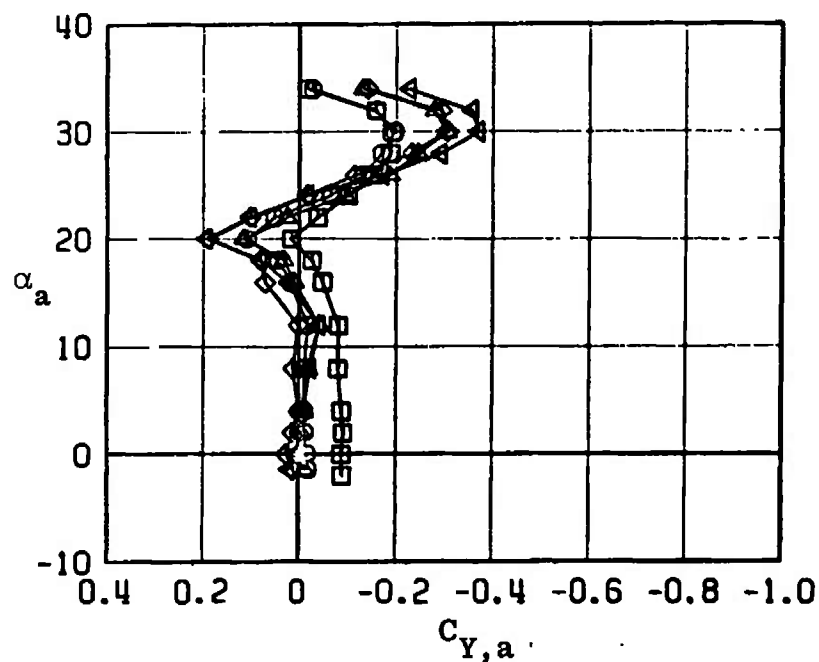


Fig. 33 Effect of Roll Control Deflections on the Side-Force and Yawing-Moment Coefficients for MGGB Configuration without RES (B9T3)

ROLL CONTROL EFFECTIVENESS							
SIDE FORCE AND YAWING MOMENT COEFFICIENTS							
SYMBOL	CONFIG	MACH NO	ϕ	δ_0	δ_R	δ_P	$R_E \times 10^{-5}$
□	B9T3	0.65	0	0.3	0.5	0.3	1.8
○	B9T3	0.65	0	-0.1	0	-4.7	1.8
△	B9T3	0.65	0	0.2	0	-9.9	1.8
◇	B9T3	0.65	0	-0.1	0	-14.9	1.8
◀	B9T3	0.65	0	-0.6	0.2	-20.0	1.8

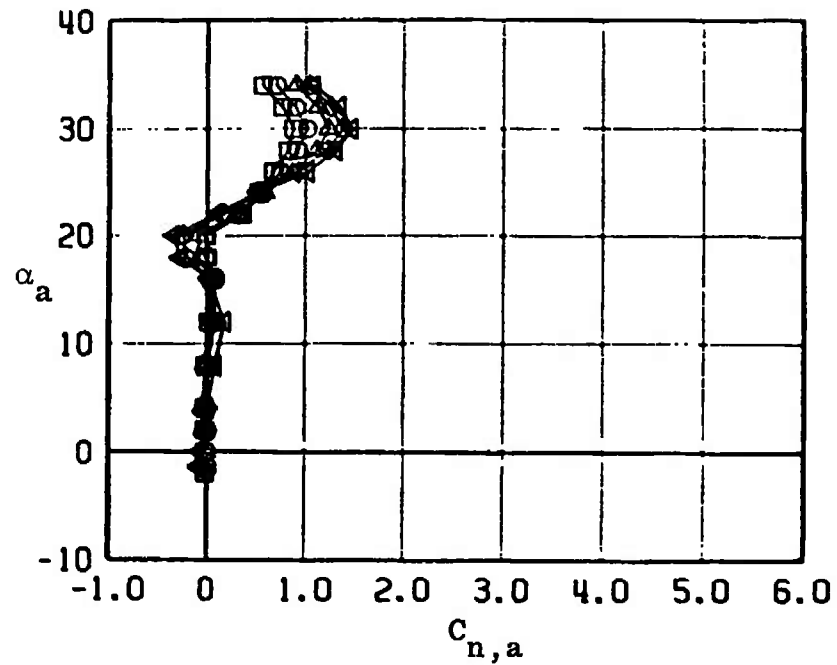
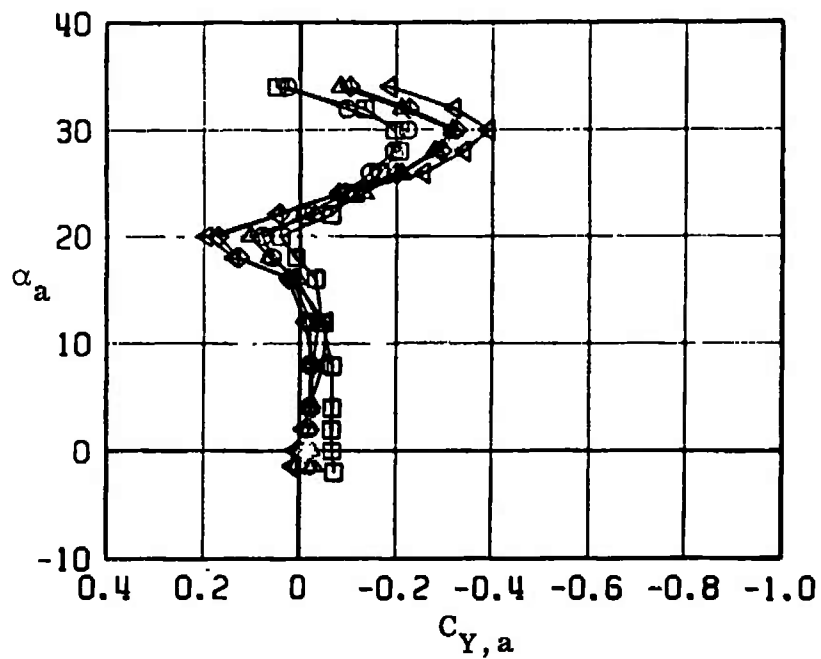


Fig. 33 Continued

ROLL CONTROL EFFECTIVENESS SIDE FORCE AND YAWING MOMENT COEFFICIENTS							
SYMBOL	CONFIG	MACH NO	ϕ	δ_D	δ_R	δ_P	$R_L \times 10^{-6}$
□	B9T3	0.75	0	0.3	0.5	0.3	2.0
○	B9T3	0.75	0	-0.1	0	-4.7	2.0
△	B9T3	0.75	0	0.2	0	-9.9	2.0
◇	B9T3	0.75	0	-0.1	0	-14.9	2.0
◀	B9T3	0.75	0	-0.6	0.2	-20.0	2.0

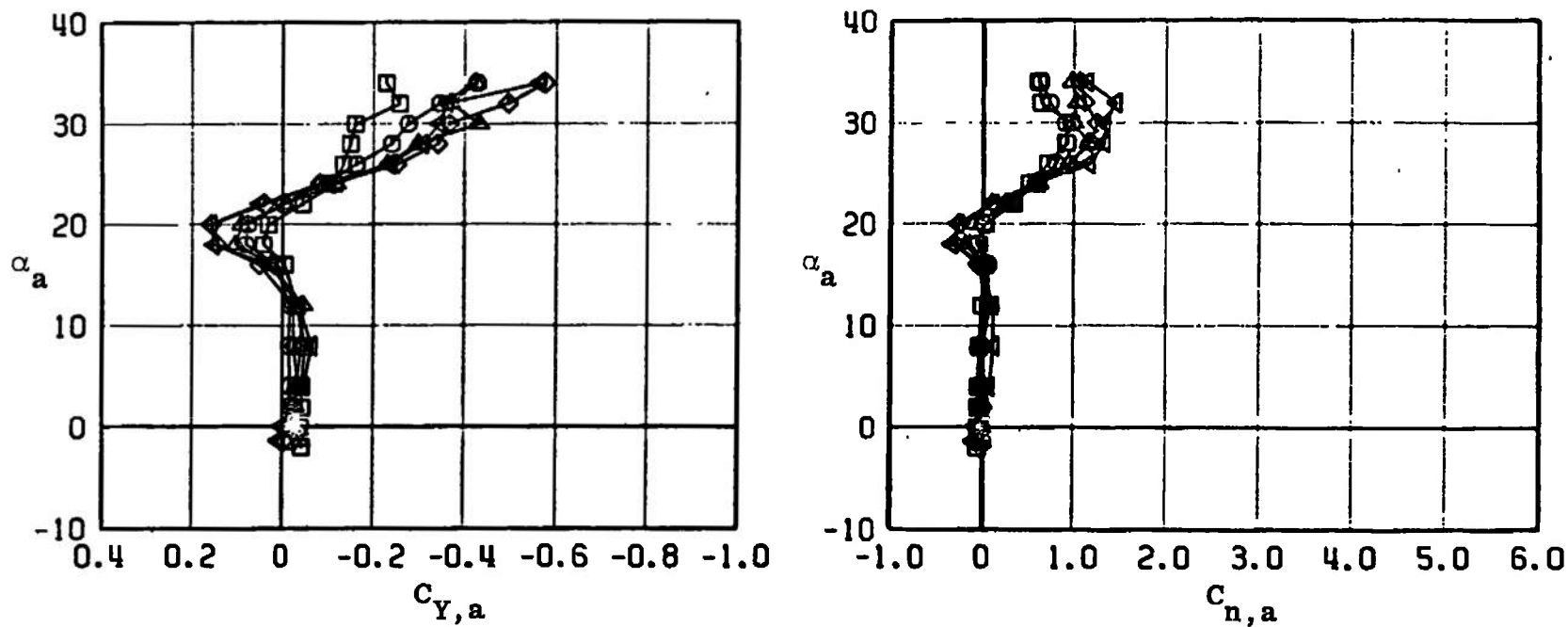


Fig. 33 Continued

ROLL CONTROL EFFECTIVENESS SIDE FORCE AND YAWING MOMENT COEFFICIENTS							
SYMBOL	CONFIG	MACH NO	ϕ	b_ϕ	b_η	b_p	$R_L \times 10^{-6}$
\square	B9T3	0.85	0	0.3	0.5	0.3	2.1
\circ	B9T3	0.85	0	-0.1	0	-4.7	2.1
\triangle	B9T3	0.85	0	0.2	0	-9.9	2.1
\diamond	B9T3	0.85	0	-0.1	0	-14.9	2.1
\blacktriangle	B9T3	0.85	0	-0.6	0.2	-20.0	2.1

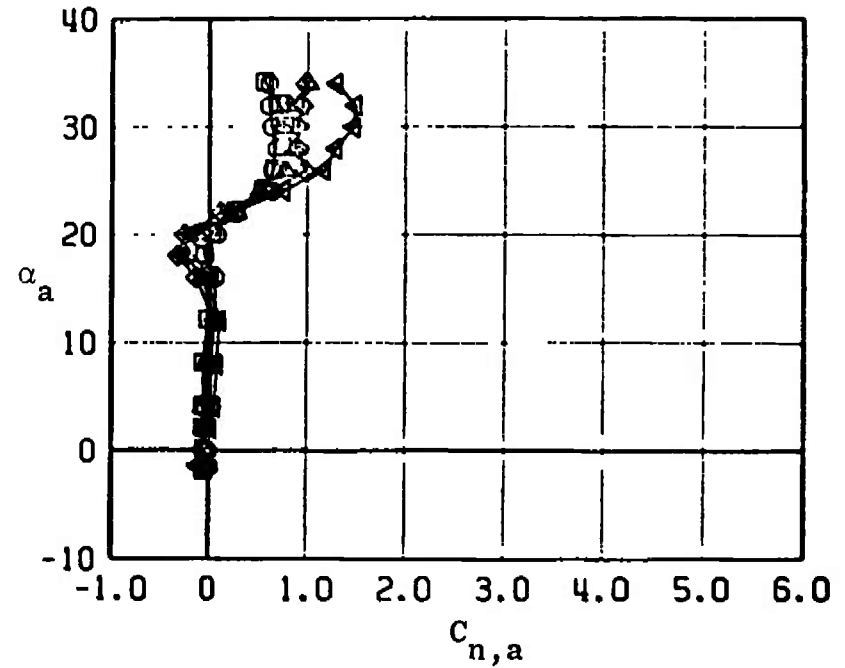
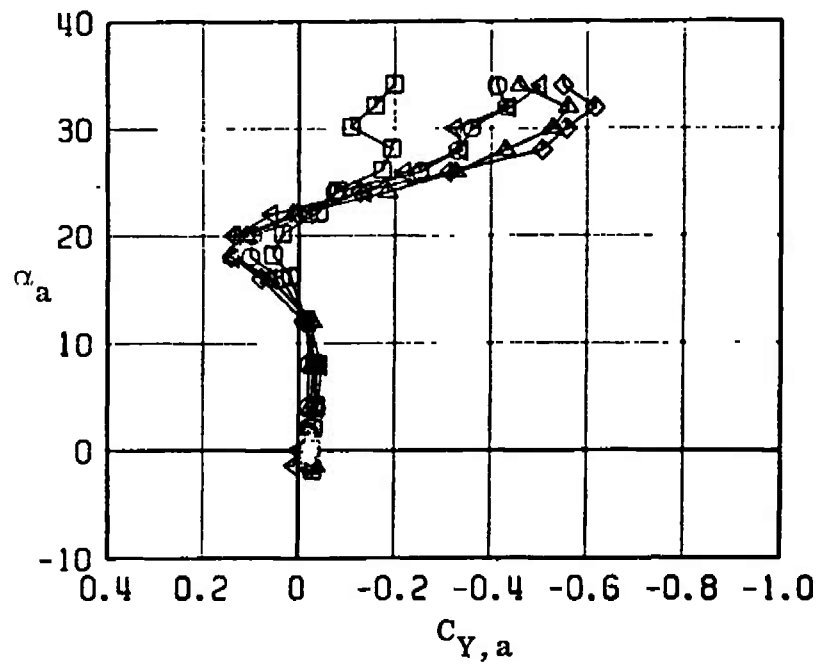


Fig. 33 Continued

ROLL CONTROL EFFECTIVENESS SIDE FORCE AND YAWING MOMENT COEFFICIENTS							
SYMBOL	CONFIG	MACH NO	ϕ	ϵ_q	ϵ_R	ϵ_p	$R_L \times 10^{-6}$
□	B9T3	0.95	0	0.3	0.5	0.3	2.2
○	B9T3	0.95	0	-0.1	0	-4.7	2.2
△	B9T3	0.95	0	0.2	0	-9.9	2.2
◇	B9T3	0.95	0	-0.1	0	-14.9	2.2
◁	B9T3	0.95	0	-0.6	0.2	-20.0	2.2

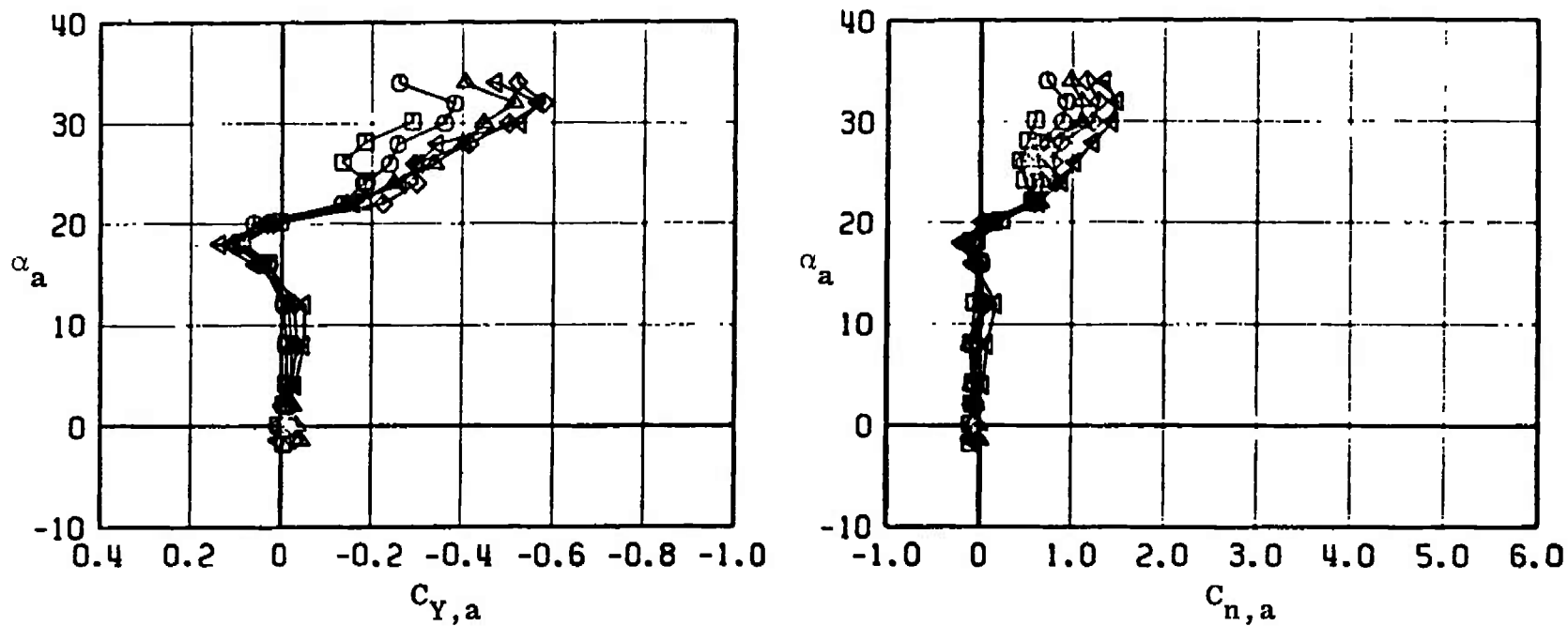


Fig. 33 Continued

ROLL CONTROL EFFECTIVENESS							
SIDE FORCE AND YAWING MOMENT COEFFICIENTS							
SYMBOL	CONFIG	MACH NO	ϕ	δ_0	δ_R	δ_P	$R_L \times 10^{-6}$
□	B9T3	1.05	0	0.3	0.5	0.3	2.3
○	B9T3	1.05	0	-0.1	0	-4.7	2.3
△	B9T3	1.05	0	0.2	0	-9.9	2.3
◇	B9T3	1.05	0	-0.1	0	-14.9	2.3
◄	B9T3	1.05	0	-0.6	0.2	-20.0	2.3

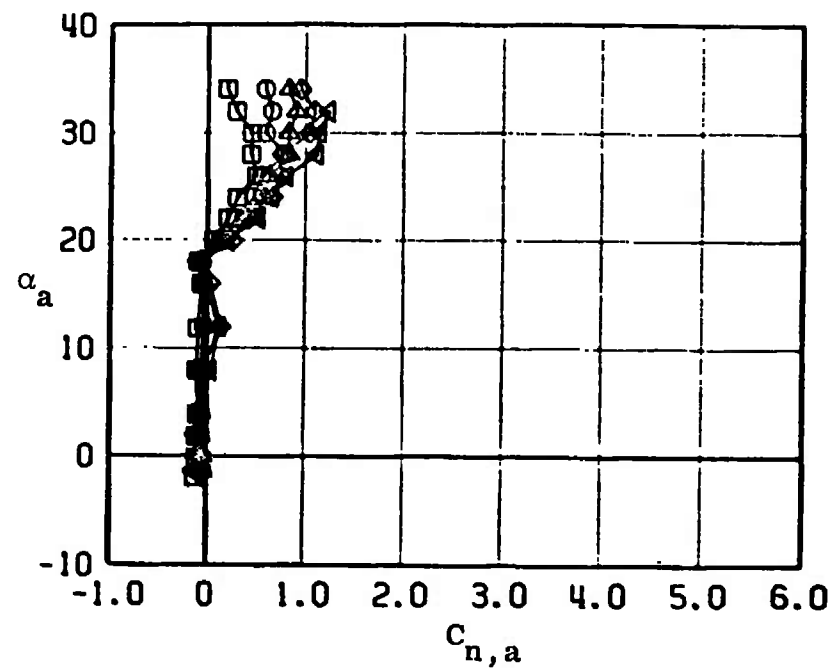
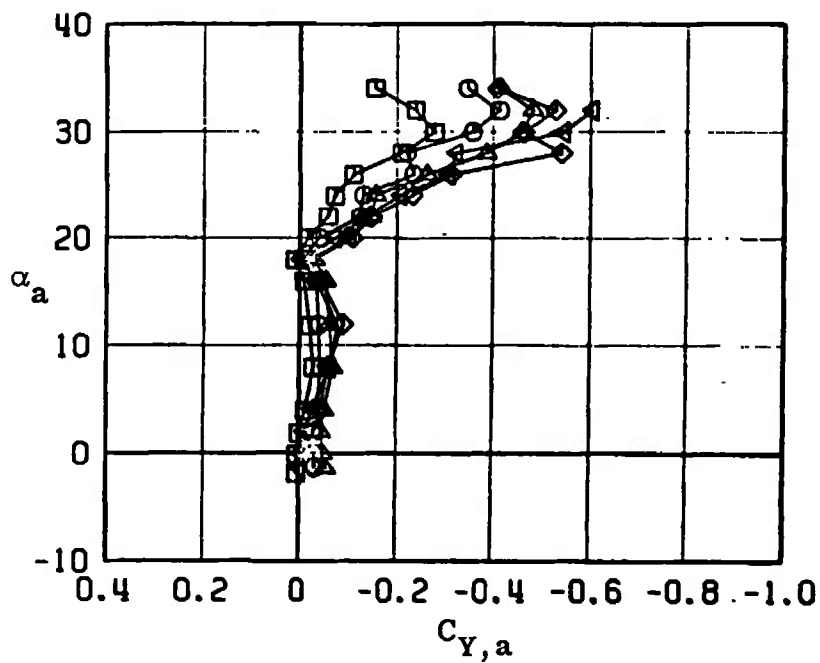


Fig. 33 Concluded

EFFECT OF SUPERIMPOSED CONTROL							
NORMAL FORCE AND PITCHING MOMENT COEFFICIENTS							
SYMBOL	CONFIG	MACH NO	ϕ	δ_0	δ_R	δ_P	$R_E \times 10^{-6}$
□	B9T3	0.50	0	0.3	0.5	0.3	1.5
○	B9T3	0.50	0	-0.1	0	-4.7	1.5
△	B9T3	0.50	0	-14.9	0.1	-0.1	1.5
◇	B9T3	0.50	0	-15.4	0.4	-5.2	1.5

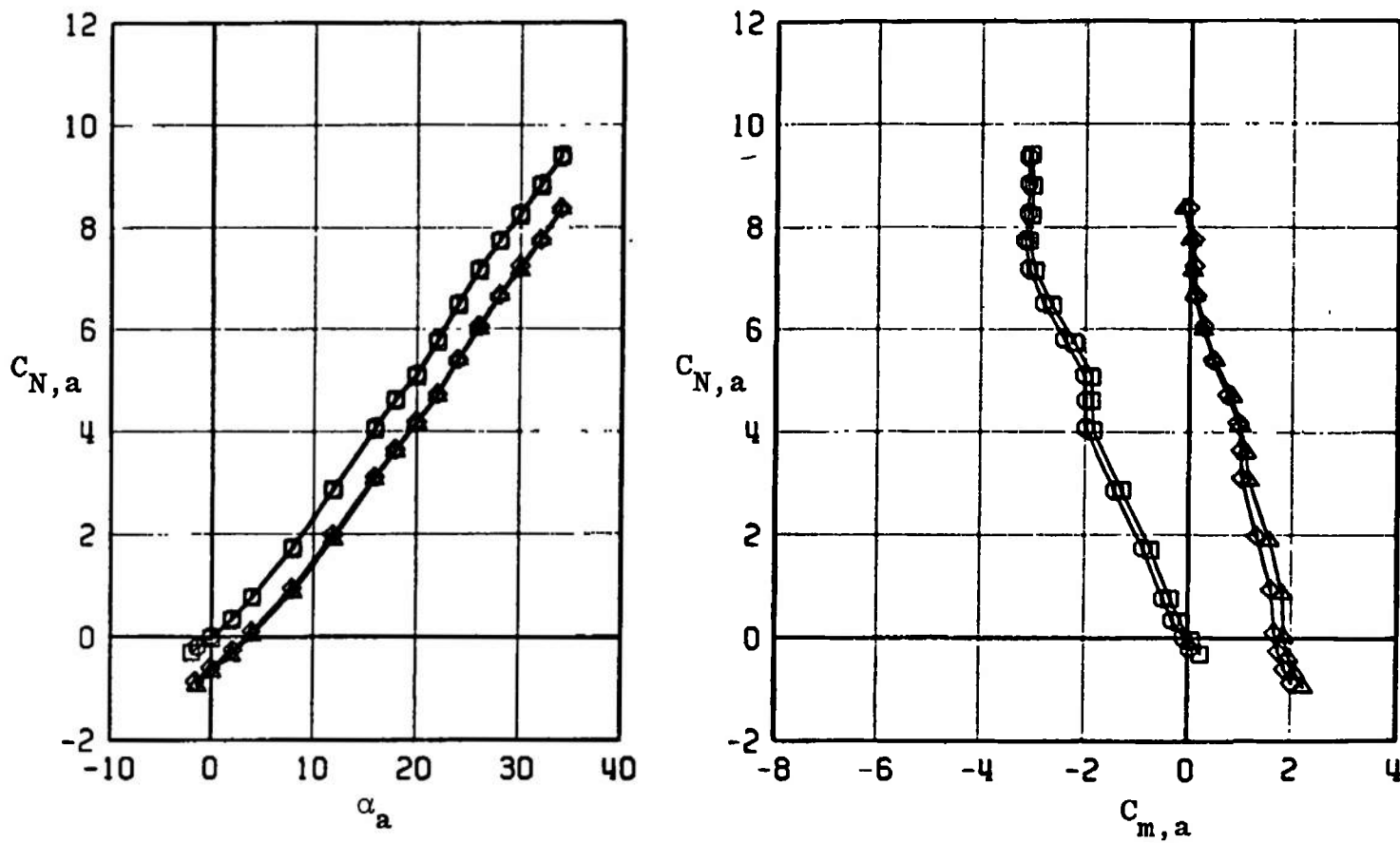


Fig. 34 Effect of Pitch and Roll Control Deflections on the Normal-Force and Pitching-Moment Coefficients for MGGB Configuration without RES (B9T3)

EFFECT OF SUPERIMPOSED CONTROL							
NORMAL FORCE AND PITCHING MOMENT COEFFICIENTS							
SYMBOL	CONFIG	MACH NO	ϕ	δ_0	δ_R	δ_P	$R_E \times 10^{-6}$
\square	B9T3	0.65	0	0.3	0.5	0.3	1.8
\circ	B9T3	0.65	0	-0.1	0	-4.7	1.8
\triangle	B9T3	0.65	0	-14.9	0.1	-0.1	1.8
\diamond	B9T3	0.65	0	-15.4	0.4	-5.2	1.8

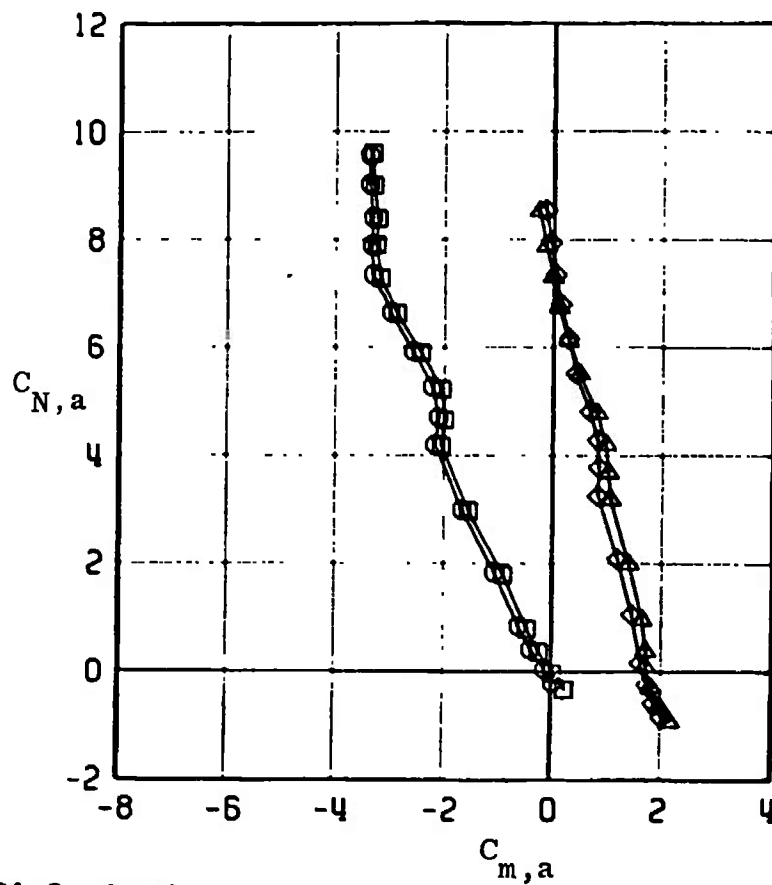
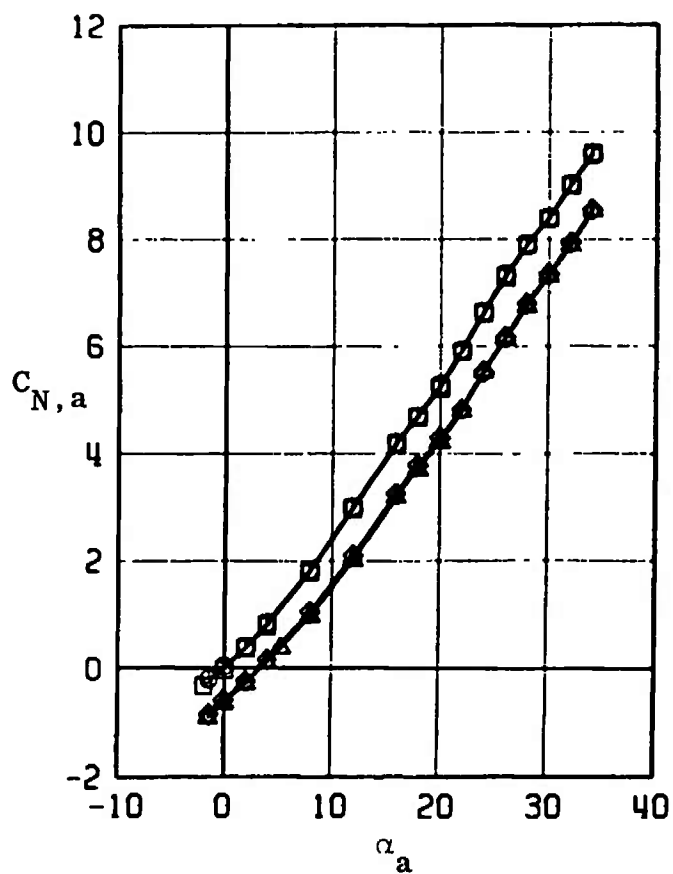


Fig. 34 Continued

EFFECT OF SUPERIMPOSED CONTROL							
NORMAL FORCE AND PITCHING MOMENT COEFFICIENTS							
SYMBOL	CONFIG	MACH NO	ϕ	b_0	b_R	b_P	$R_E \times 10^{-6}$
\square	B9T3	0.75	0	0.3	0.5	0.3	2.0
\circ	B9T3	0.75	0	-0.1	0	-4.7	2.0
\triangle	B9T3	0.75	0	-14.9	0.1	-0.1	2.0
\diamond	B9T3	0.75	0	-15.4	0.4	-5.2	2.0

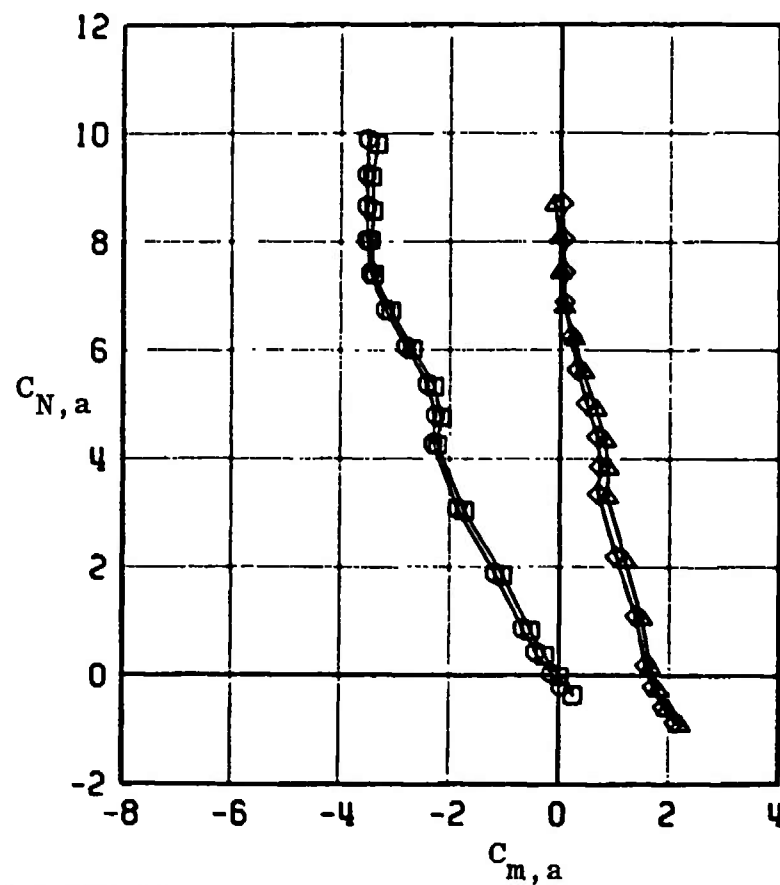
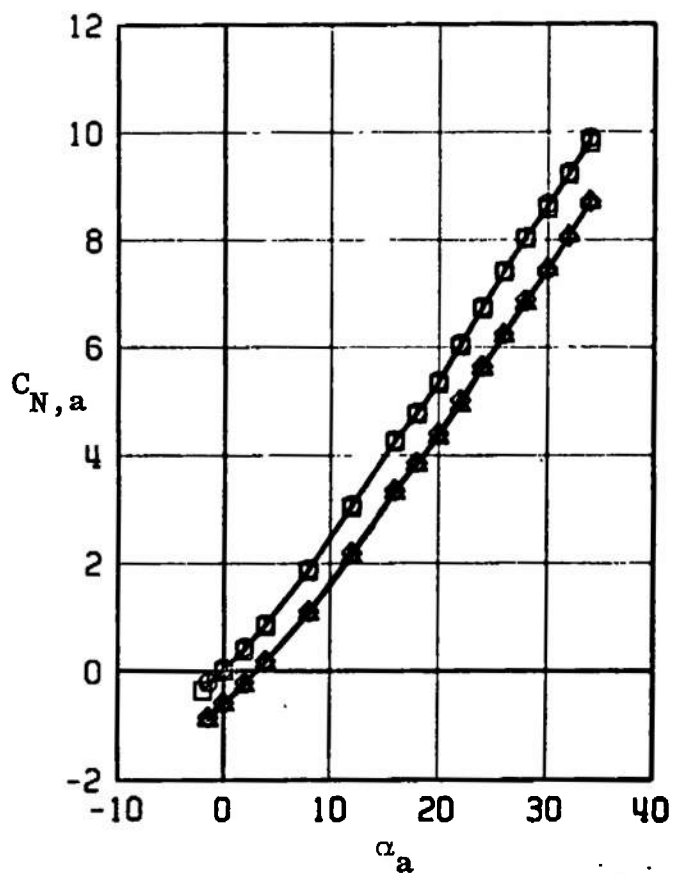


Fig. 34 Continued

EFFECT OF SUPERIMPOSED CONTROL
NORMAL FORCE AND PITCHING MOMENT COEFFICIENTS

SYMBOL	CONFIG	MACH NO	ϕ	δ_D	δ_R	δ_P	$R_E \times 10^{-6}$
□	B9T3	0.85	0	0.3	0.5	0.3	2.1
○	B9T3	0.85	0	-0.1	0	-4.7	2.1
△	B9T3	0.85	0	-14.9	0.1	-0.1	2.1
◇	B9T3	0.85	0	-15.4	0.4	-5.2	2.1

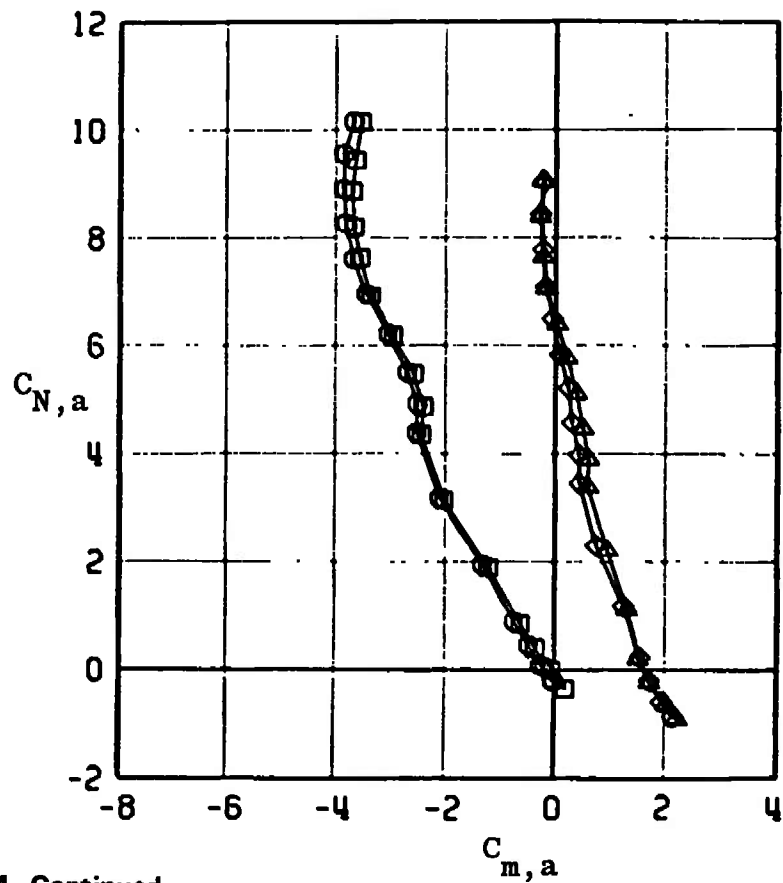
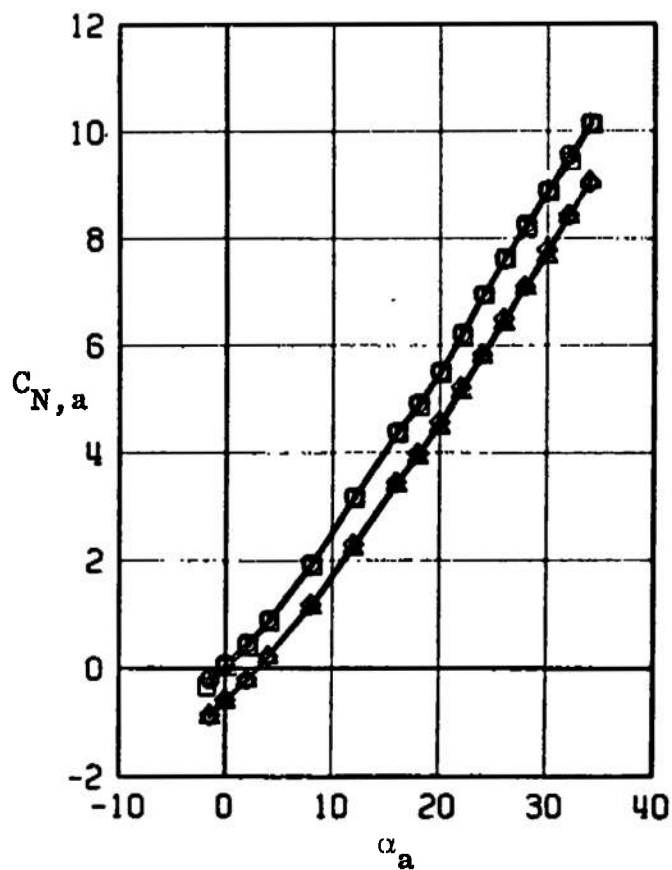


Fig. 34 Continued

EFFECT OF SUPERIMPOSED CONTROL							
NORMAL FORCE AND PITCHING MOMENT COEFFICIENTS							
SYMBOL	CONFIG	MACH NO	ϕ	δ_0	δ_R	δ_P	$R_F \times 10^{-6}$
□	B9T3	0.95	0	0.3	0.5	0.3	2.2
○	B9T3	0.95	0	-0.1	0	-4.7	2.2
△	B9T3	0.95	0	-14.9	0.1	-0.1	2.2
◇	B9T3	0.95	0	-15.4	0.4	-5.2	2.2

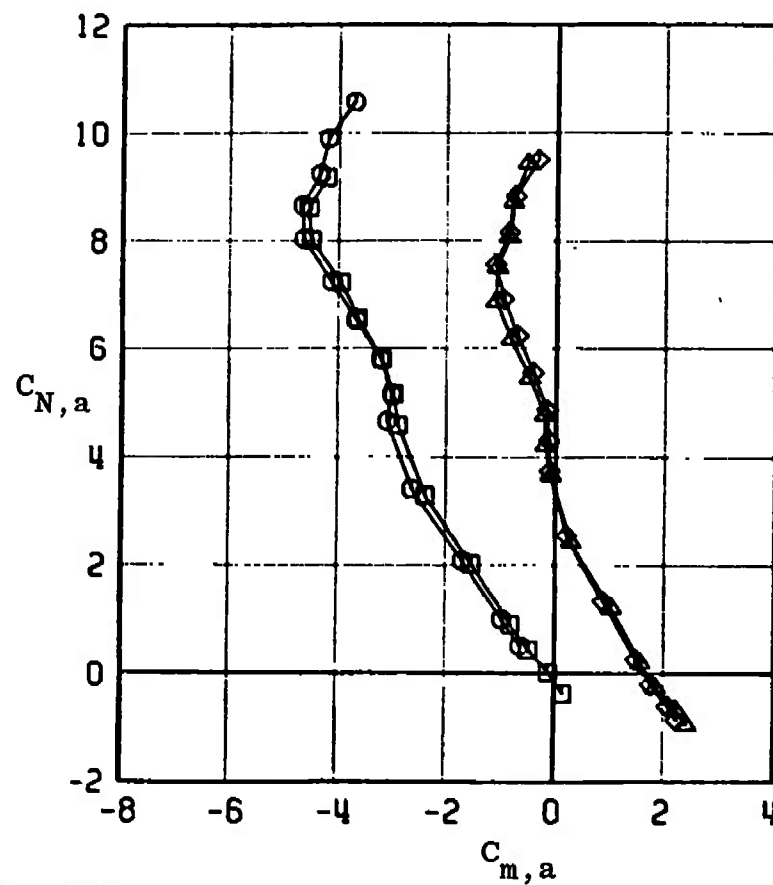
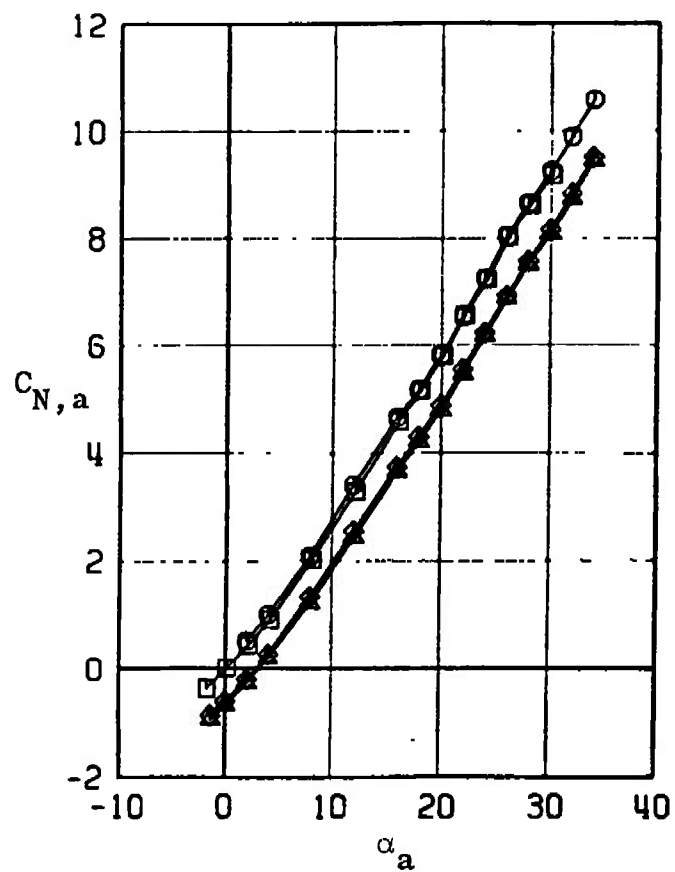


Fig. 34 Continued

EFFECT OF SUPERIMPOSED CONTROL
NORMAL FORCE AND PITCHING MOMENT COEFFICIENTS

SYMBOL	CONFIG	MACH NO	ϕ	ϵ_0	ϵ_R	ϵ_P	$R_E \times 10^{-6}$
\square	B9T3	1.05	0	0.3	0.5	0.3	2.3
\circ	B9T3	1.05	0	-0.1	0	-4.7	2.3
\triangle	B9T3	1.05	0	-14.9	0.1	-0.1	2.3
\diamond	B9T3	1.05	0	-15.4	0.4	-5.2	2.3

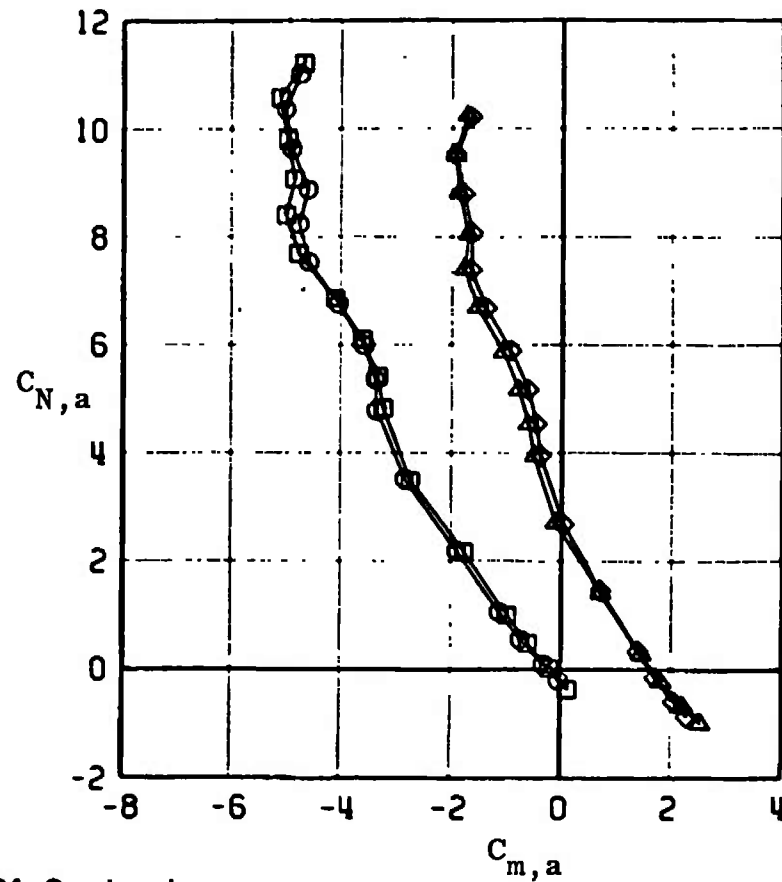
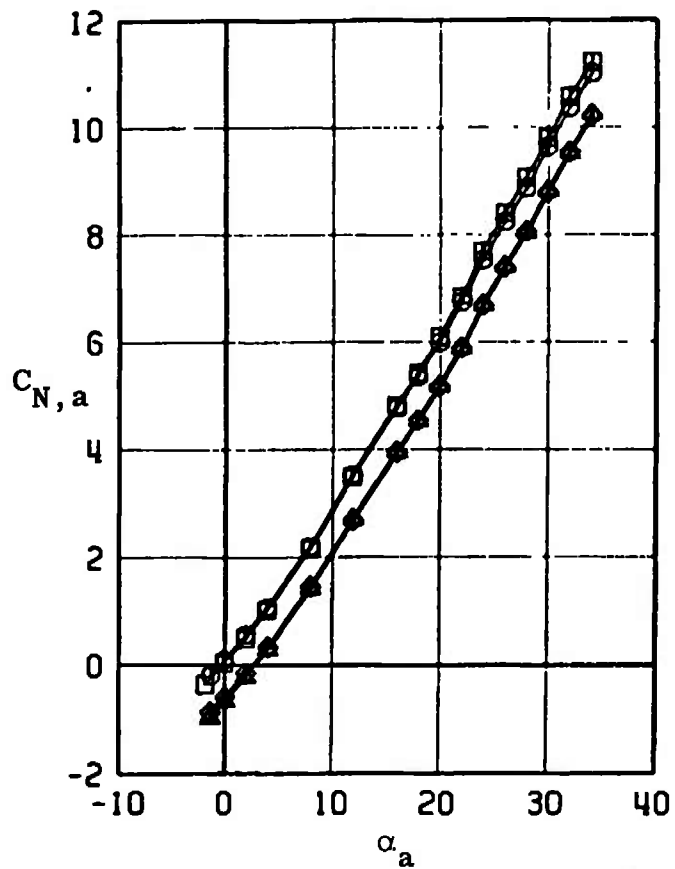


Fig. 34 Continued

EFFECT OF SUPERIMPOSED CONTROL							
NORMAL FORCE AND PITCHING MOMENT COEFFICIENTS							
SYMBOL	CONFIG	MACH NO	ϕ	δ_0	δ_R	δ_P	$R_E \times 10^{-6}$
□	B9T3	0.50	0	0.3	0.5	0.3	1.5
○	B9T3	0.50	0	-0.1	0	-4.7	1.5
△	B9T3	0.50	0	-10.1	0.1	0.3	1.5
◇	B9T3	0.50	0	-9.9	0.1	-5.1	1.5

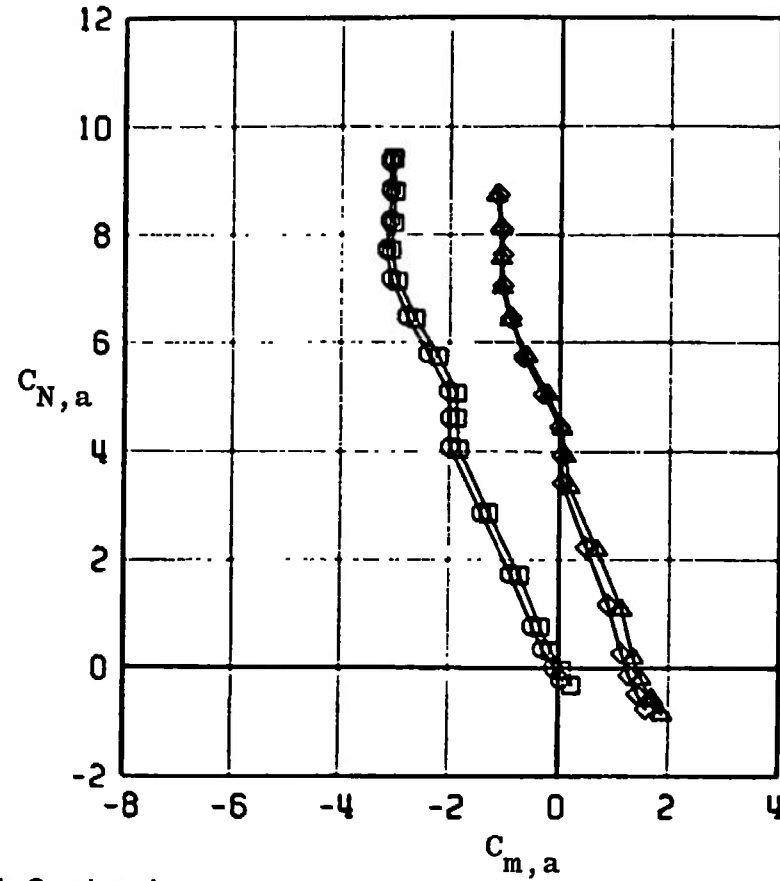
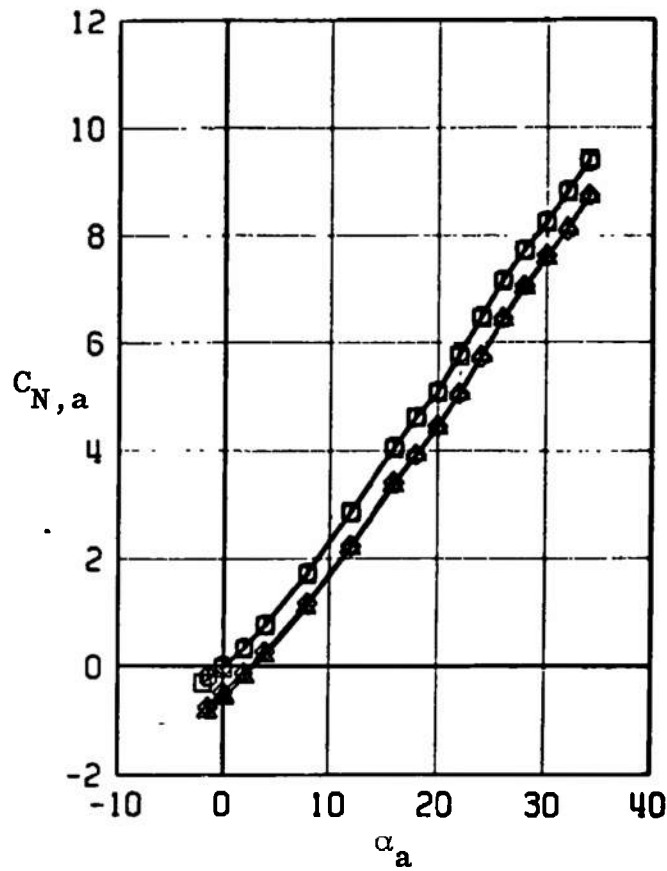


Fig. 34 Continued

EFFECT OF SUPERIMPOSED CONTROL							
NORMAL FORCE AND PITCHING MOMENT COEFFICIENTS							
SYMBOL	CONFIG	MACH NO	ϕ	δ_0	δ_R	δ_P	$R_E \times 10^{-6}$
\square	B9T3	0.65	0	0.3	0.5	0.3	1.8
\circ	B9T3	0.65	0	-0.1	0	-4.7	1.8
\triangle	B9T3	0.65	0	-10.1	0.1	0.3	1.8
\diamond	B9T3	0.65	0	-9.9	0.1	-5.1	1.8

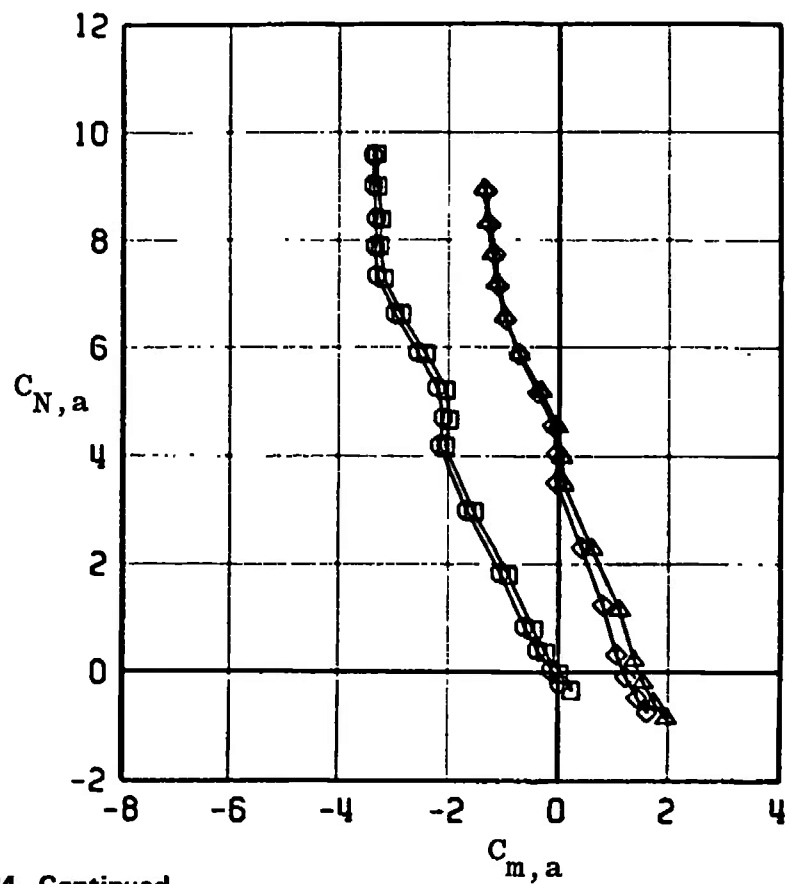
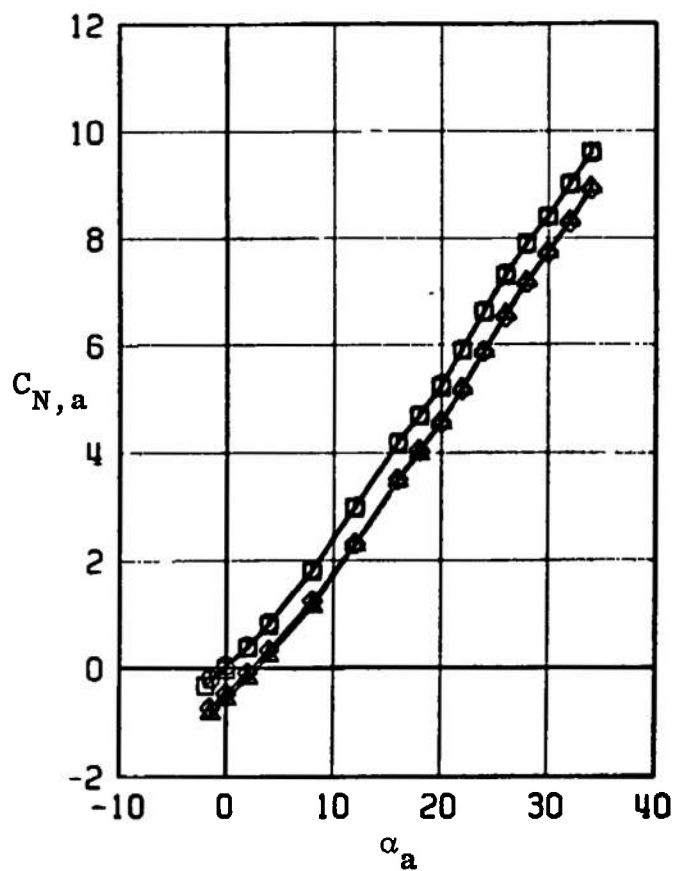


Fig. 34 Continued

EFFECT OF SUPERIMPOSED CONTROL NORMAL FORCE AND PITCHING MOMENT COEFFICIENTS							
SYMBOL	CONFIG	MACH NO	ϕ	δ_0	δ_H	δ_P	$R_E \times 10^{-6}$
□	B9T3	0.75	0	0.3	0.5	0.3	2.0
○	B9T3	0.75	0	-0.1	0	-4.7	2.0
△	B9T3	0.75	0	-10.1	0.1	0.3	2.0
◇	B9T3	0.75	0	-9.9	0.1	-5.1	2.0

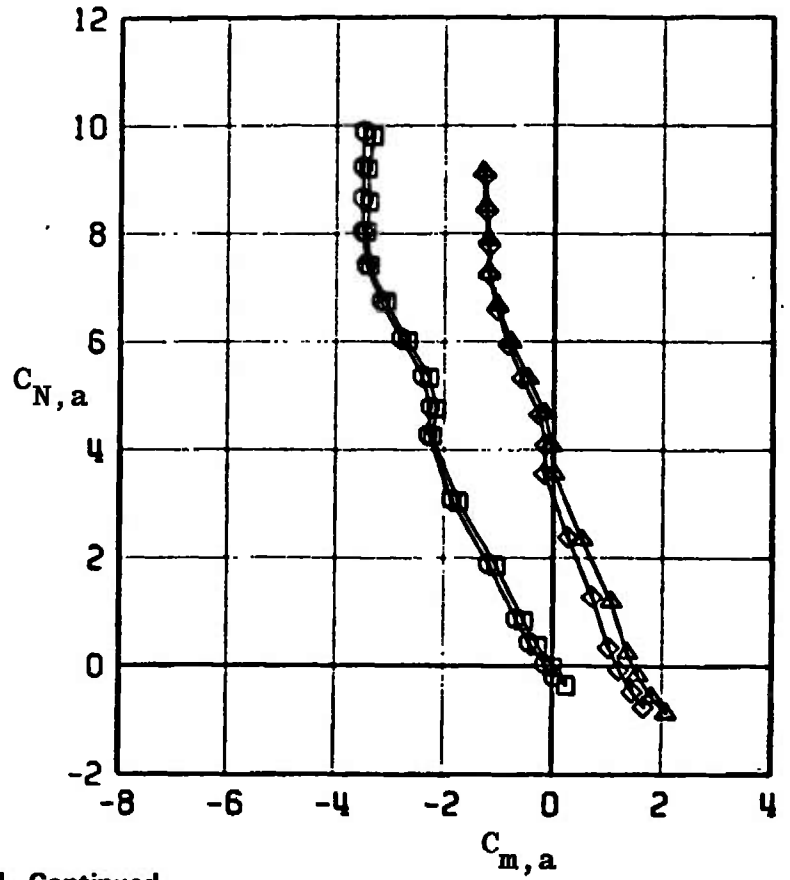
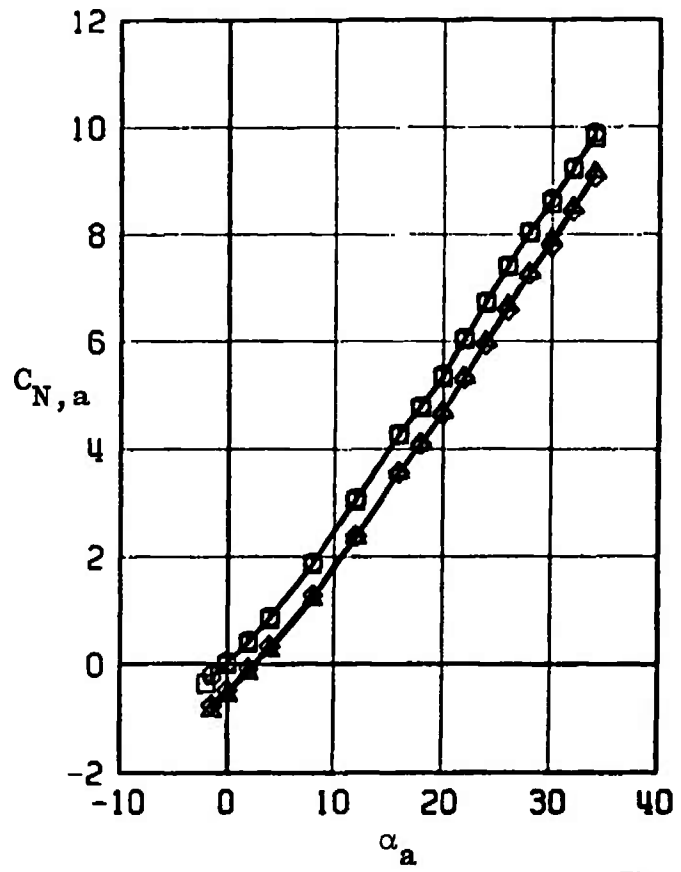


Fig. 34 Continued

EFFECT OF SUPERIMPOSED CONTROL							
NORMAL FORCE AND PITCHING MOMENT COEFFICIENTS							
SYMBOL	CONFIG	MACH NO	δ_0	δ_R	δ_P	$R_F \times 10^{-6}$	
□	B9T3	0.85	0	0.3	0.5	0.3	2.1
○	B9T3	0.85	0	-0.1	0	-4.7	2.1
△	B9T3	0.85	0	-10.1	0.1	0.3	2.1
◇	B9T3	0.85	0	-9.9	0.1	-5.1	2.1

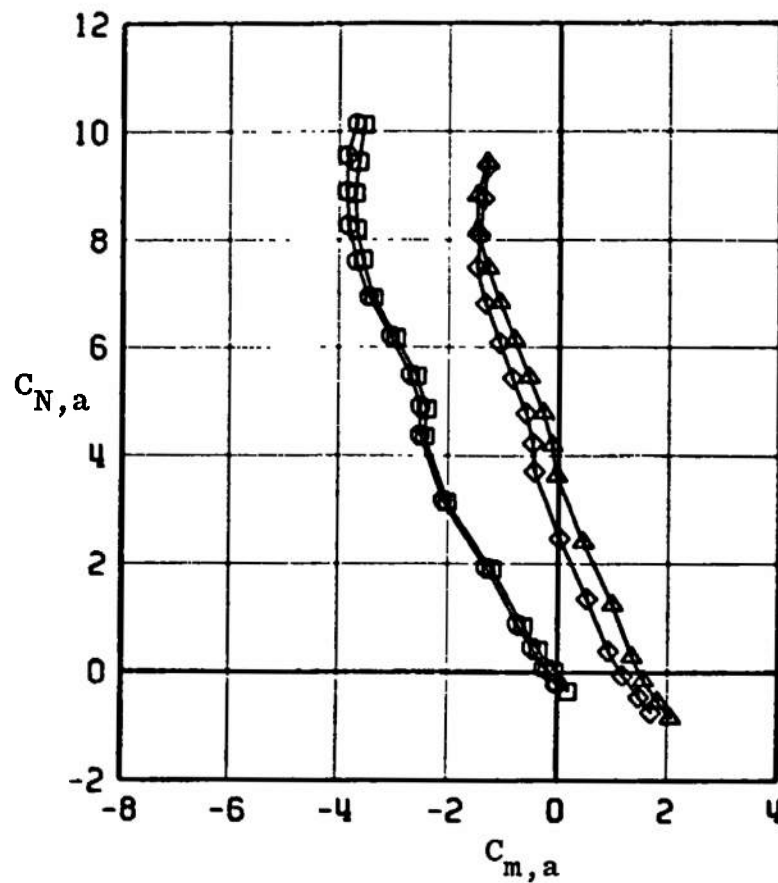
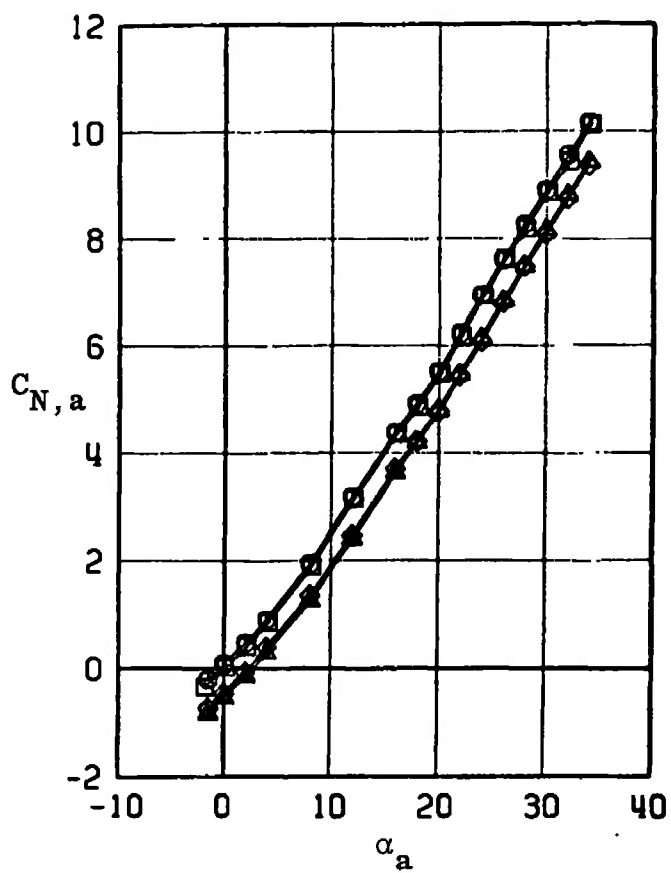


Fig. 34 Continued

EFFECT OF SUPERIMPOSED CONTROL							
NORMAL FORCE AND PITCHING MOMENT COEFFICIENTS							
SYMBOL	CONFIG	MACH NO	ϵ	ϵ_0	ϵ_n	ϵ_p	$R_E \times 10^{-6}$
\square	B9T3	0.95	0	0.3	0.5	0.3	2.2
\circ	B9T3	0.95	0	-0.1	0	-4.7	2.2
\triangle	B9T3	0.95	0	-10.1	0.1	0.3	2.2
\diamond	B9T3	0.95	0	-9.9	0.1	-5.1	2.2

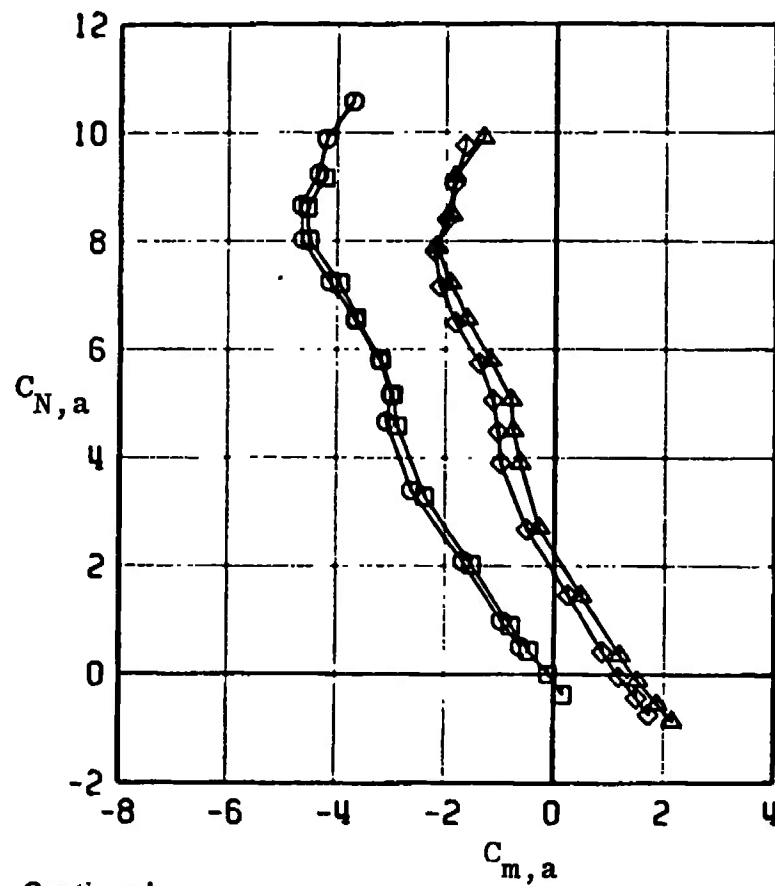
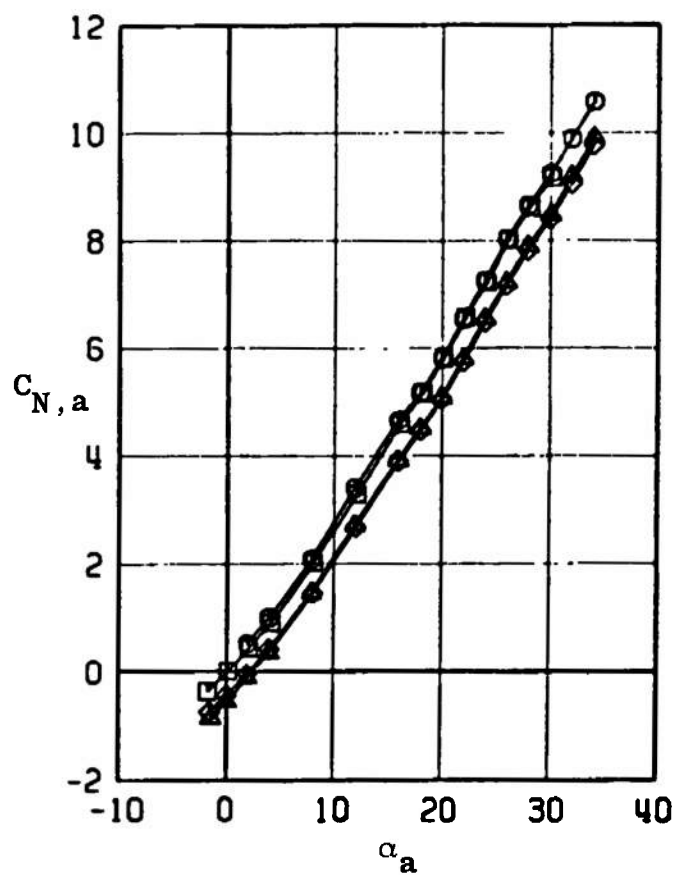


Fig. 34 Continued

EFFECT OF SUPERIMPOSED CONTROL
NORMAL FORCE AND PITCHING MOMENT COEFFICIENTS

SYMBOL	CONFIG	MACH NO	ϕ	δ_ϕ	δ_R	δ_P	$R_E \times 10^{-6}$
\square	B9T3	1.05	0	0.3	0.5	0.3	2.3
\circ	B9T3	1.05	0	-0.1	0	-4.7	2.3
\triangle	B9T3	1.05	0	-10.1	0.1	0.3	2.3
\blacktriangle	B9T3	1.05	0	-9.9	0.1	-5.1	2.3

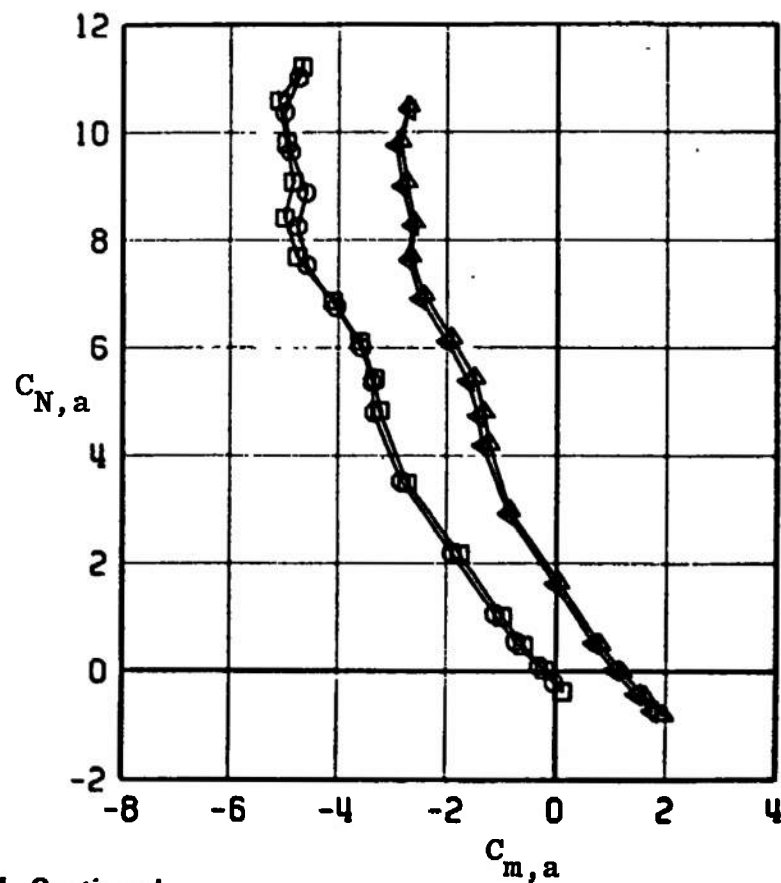
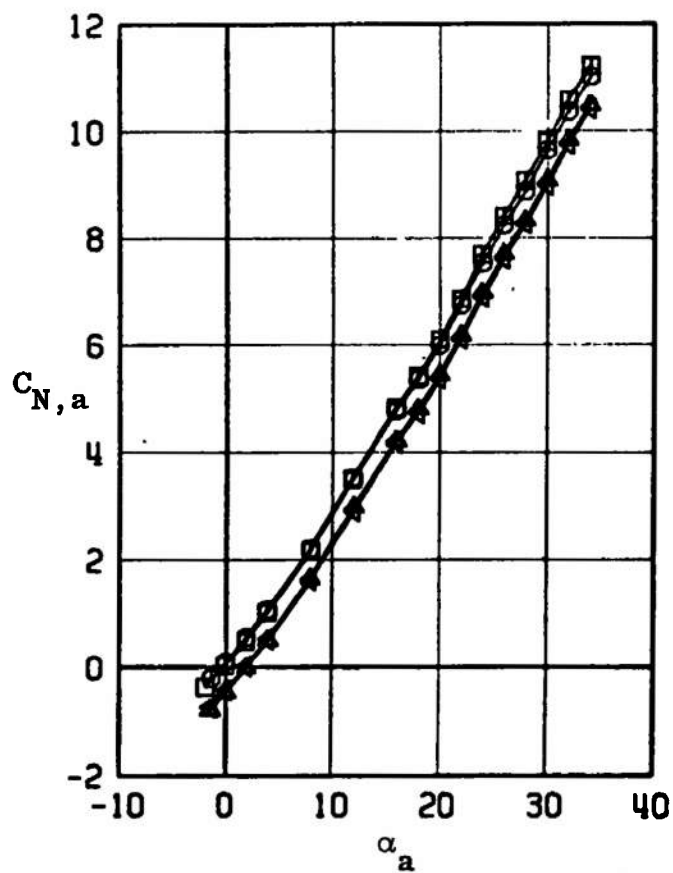


Fig. 34 Continued

EFFECT OF SUPERIMPOSED CONTROL							
NORMAL FORCE AND PITCHING MOMENT COEFFICIENTS							
SYMBOL	CONFIG	MACH NO	ϕ	δ_a	δ_R	δ_P	$R_E \times 10^{-6}$
\square	B9T3	0.50	0	0.3	0.5	0.3	1.5
\circ	B9T3	0.50	0	0.2	0	-9.9	1.5
\triangle	B9T3	0.50	0	-10.1	0.1	0.3	1.5
\diamond	B9T3	0.50	0	-10.3	0.1	-10.3	1.5

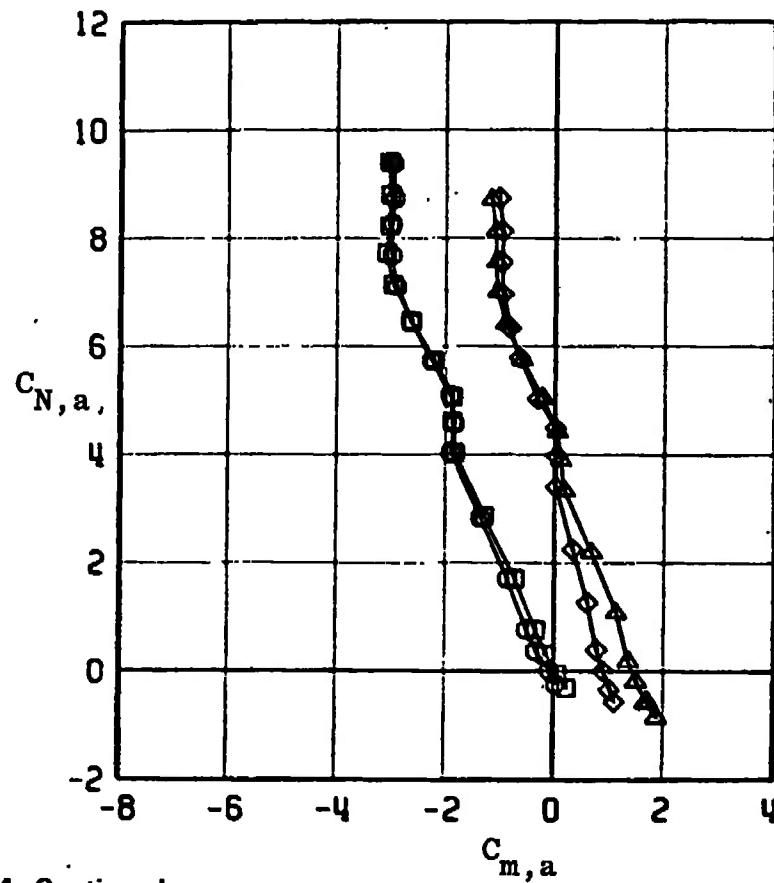
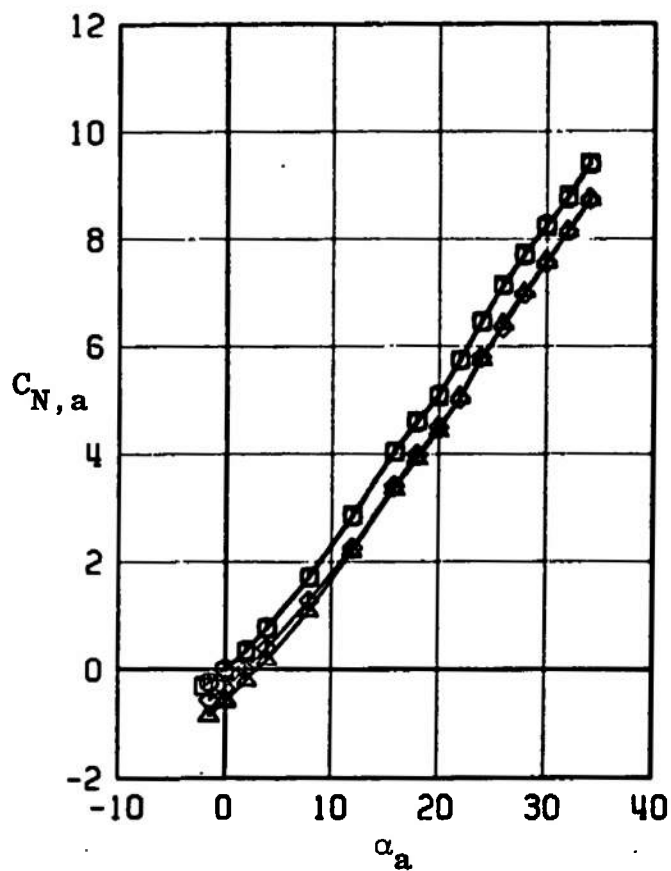


Fig. 34 Continued

EFFECT OF SUPERIMPOSED CONTROL
NORMAL FORCE AND PITCHING MOMENT COEFFICIENTS

SYMBOL	CONFIG	MACH NO	ϕ	δ_δ	δ_R	δ_P	$R_E \times 10^{-5}$
\square	B9T3	0.65	0	0.3	0.5	0.3	1.8
\circ	B9T3	0.65	0	0.2	0	-9.9	1.8
\triangle	B9T3	0.65	0	-10.1	0.1	0.3	1.8
\diamond	B9T3	0.65	0	-10.3	0.1	-10.3	1.8

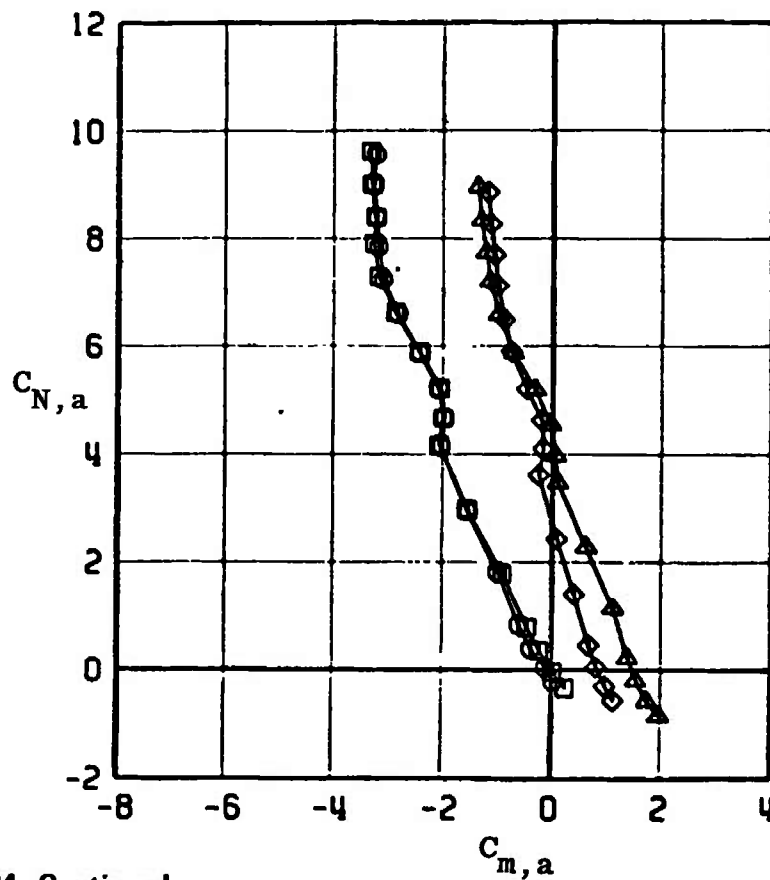
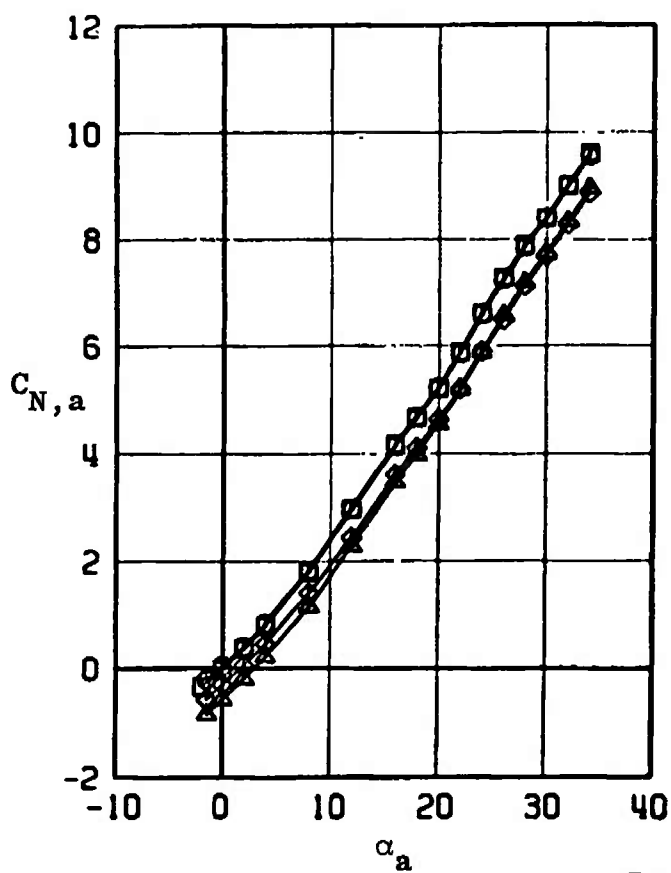


Fig. 34 Continued

EFFECT OF SUPERIMPOSED CONTROL
NORMAL FORCE AND PITCHING MOMENT COEFFICIENTS

SYMBOL	CONFIG	MACH NO	ϕ	δ_0	δ_H	δ_P	$R_E \times 10^{-5}$
□	B9T3	0.75	0	0.3	0.5	0.3	2.0
○	B9T3	0.75	0	0.2	0	-9.9	2.0
△	B9T3	0.75	0	-10.1	0.1	0.3	2.0
◇	B9T3	0.75	0	-10.3	0.1	-10.3	2.0

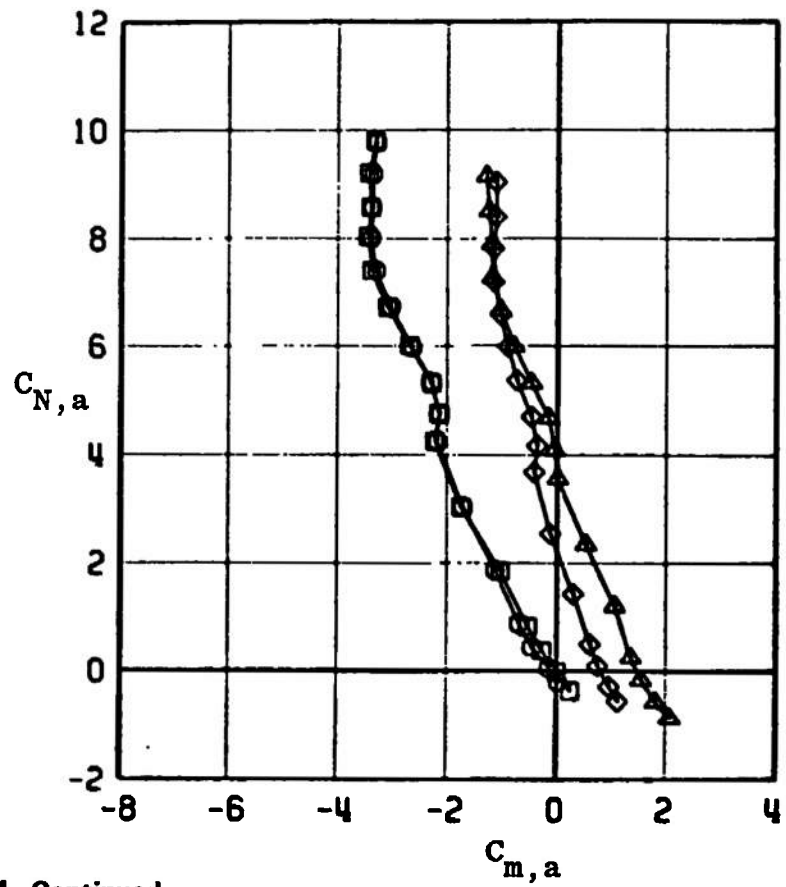
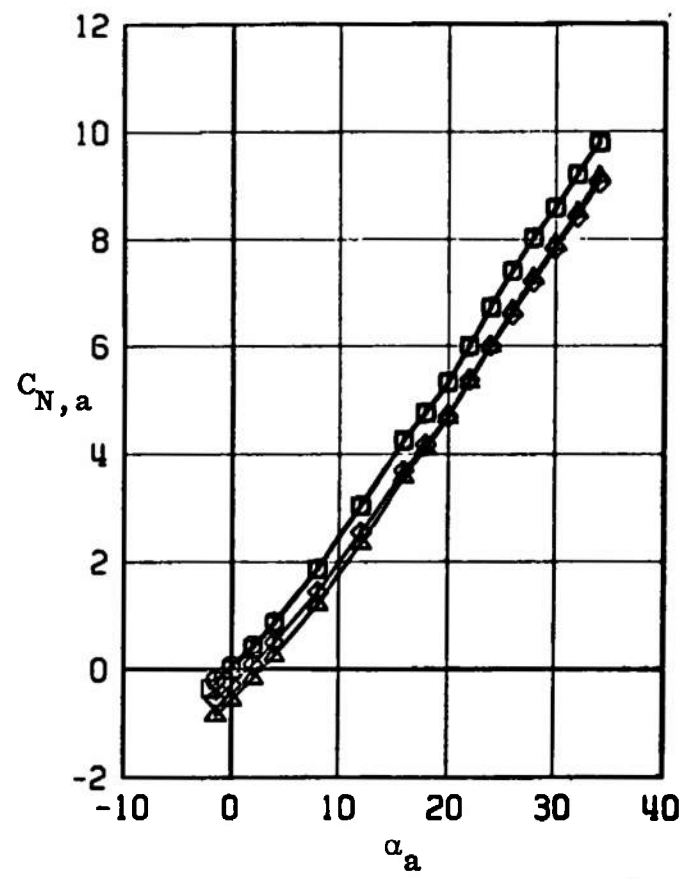


Fig. 34 Continued

EFFECT OF SUPERIMPOSED CONTROL							
NORMAL FORCE AND PITCHING MOMENT COEFFICIENTS							
SYMBOL	CONFIG	MACH NO	ϕ	δ_θ	δ_R	δ_P	$R_E \times 10^{-6}$
\square	B9T3	0.85	0	0.3	0.5	0.3	2.1
\circ	B9T3	0.85	0	0.2	0	-9.9	2.1
\triangle	B9T3	0.85	0	-10.1	0.1	0.3	2.1
\diamond	B9T3	0.85	0	-10.3	0.1	-10.3	2.1

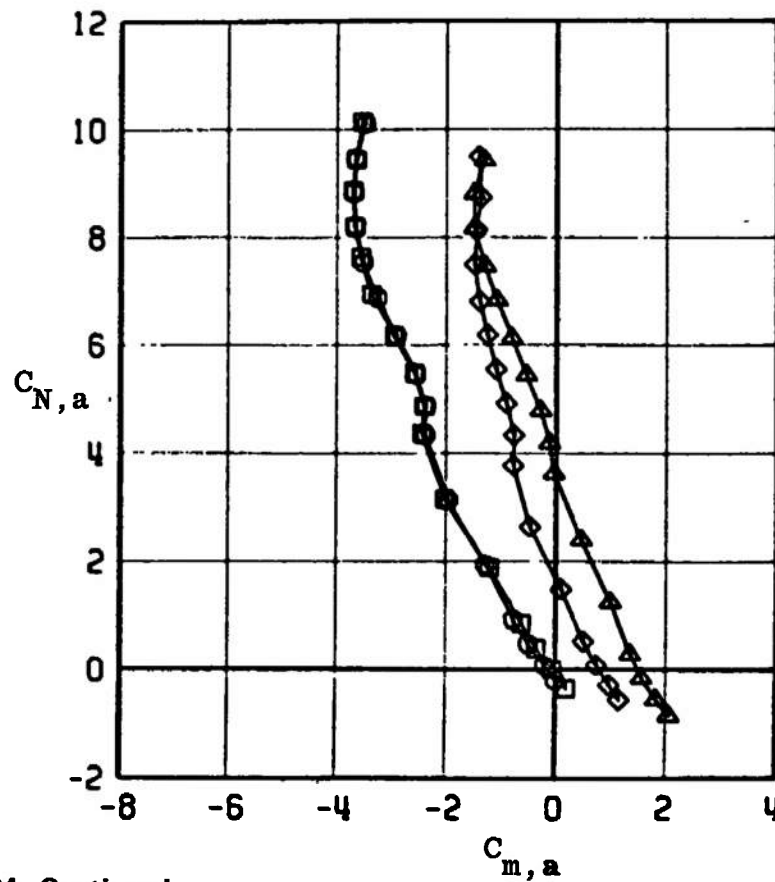
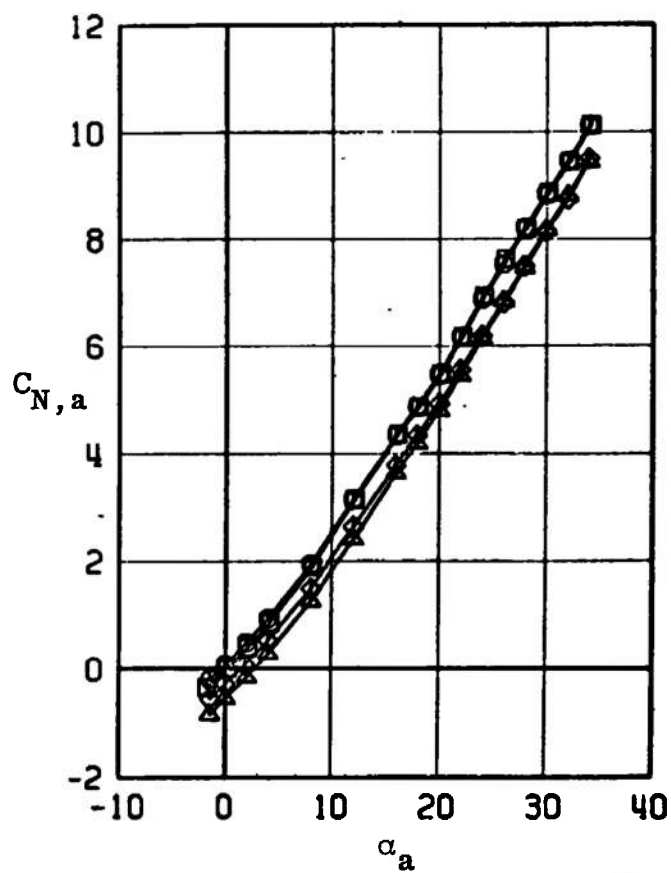


Fig. 34 Continued

EFFECT OF SUPERIMPOSED CONTROL							
NORMAL FORCE AND PITCHING MOMENT COEFFICIENTS							
SYMBOL	CONFIG	MACH NO	ϕ	δ_0	δ_H	δ_P	$R_E \times 10^{-6}$
\square	B9T3	0.95	0	0.3	0.5	0.3	2.2
\circ	B9T3	0.95	0	0.2	0	-9.9	2.2
\triangle	B9T3	0.95	0	-10.1	0.1	0.3	2.2
\diamond	B9T3	0.95	0	-10.3	0.1	-10.3	2.2

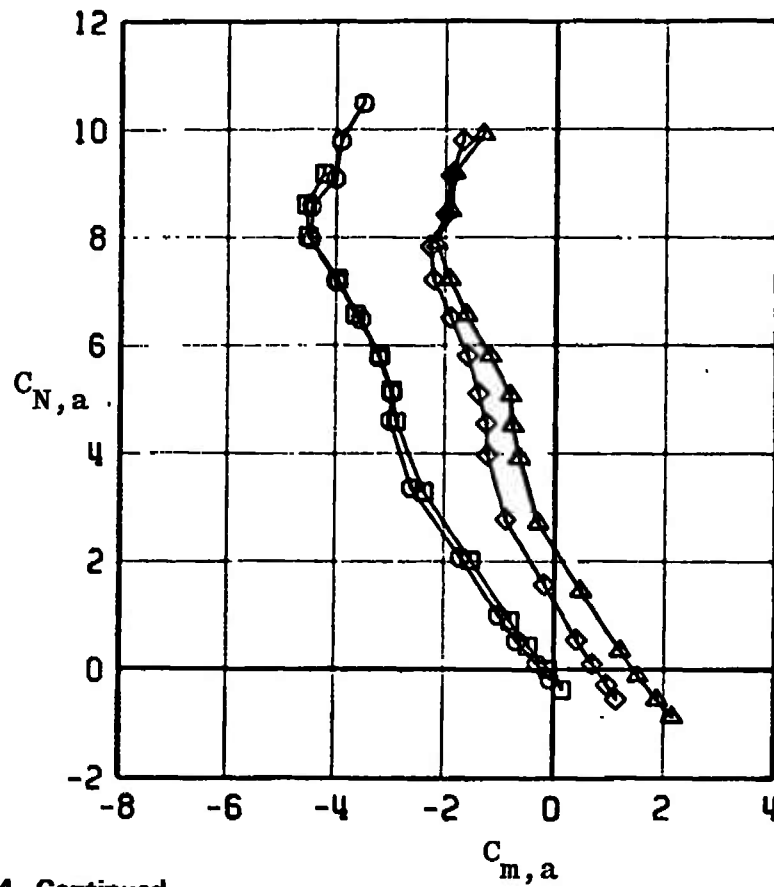
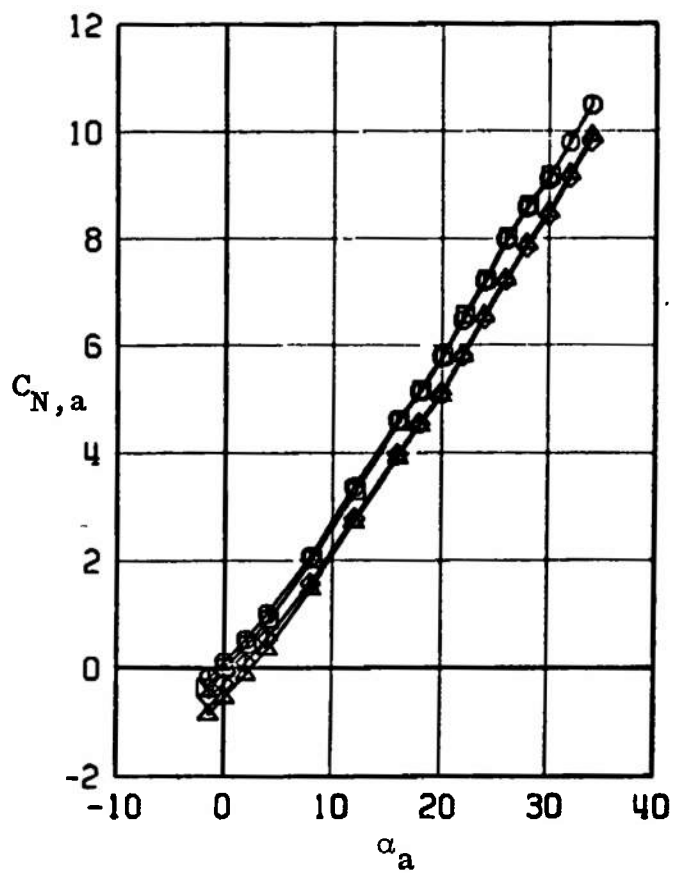


Fig. 34 Continued

EFFECT OF SUPERIMPOSED CONTROL							
NORMAL FORCE AND PITCHING MOMENT COEFFICIENTS							
SYMBOL	CONFIG	MACH NO	ϕ	δ_θ	δ_α	δ_γ	$R_E \times 10^{-6}$
□	B9T3	1.05	0	0.3	0.5	0.3	2.3
○	B9T3	1.05	0	0.2	0	-9.9	2.3
△	B9T3	1.05	0	-10.1	0.1	0.3	2.3
◇	B9T3	1.05	0	-10.3	0.1	-10.3	2.3

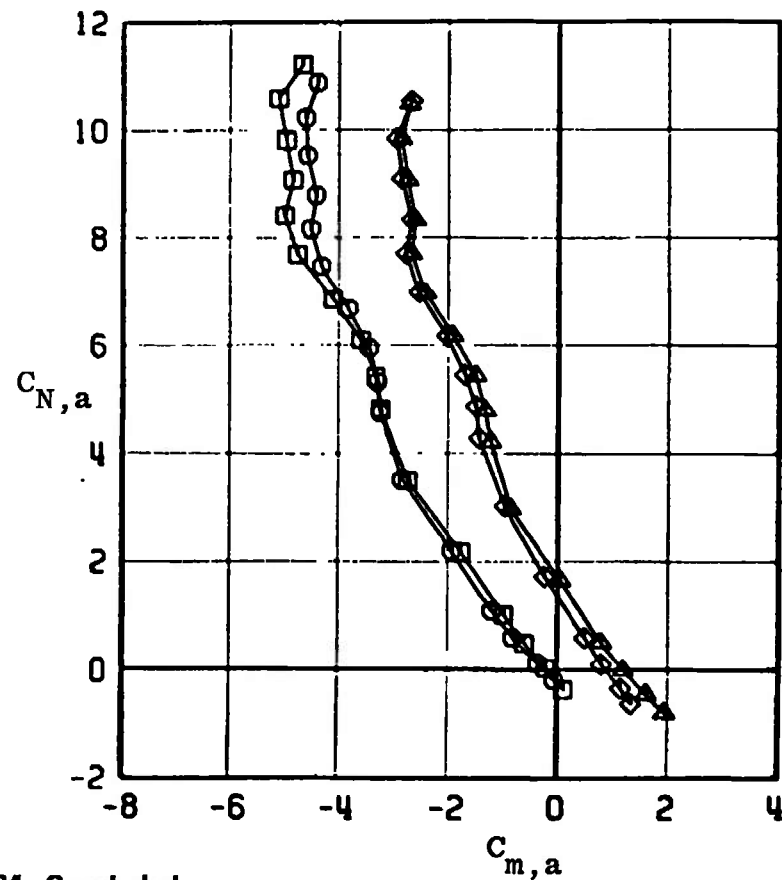
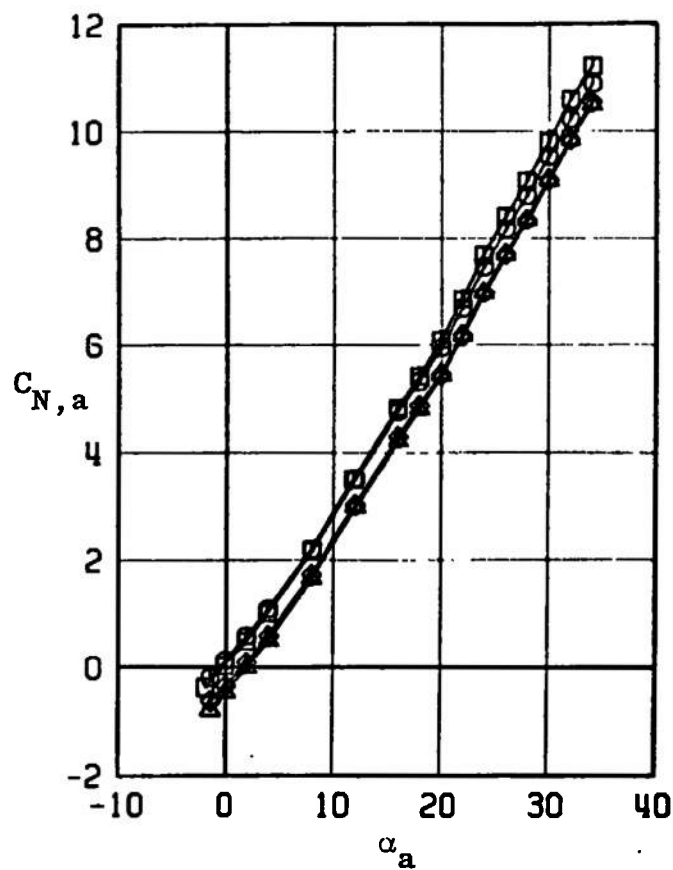


Fig. 34 Concluded

EFFECT OF SUPERIMPOSED CONTROL ROLLING MOMENT AND AXIAL FORCE COEFFICIENTS							
SYMBOL	CONFIG	MACH NO	ϵ_0	ϵ_R	ϵ_P	$P_L \times 10^{-6}$	
\square	B9T3	0.50	0	0.3	0.5	1.5	
\circ	B9T3	0.50	0	-0.1	0	1.5	
\triangle	B9T3	0.50	0	-14.9	0.1	1.5	
\diamond	B9T3	0.50	0	-15.4	0.4	1.5	

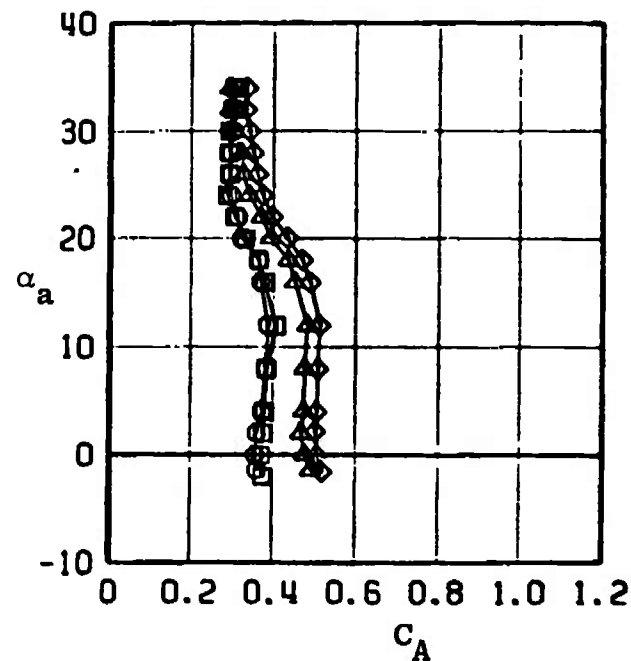
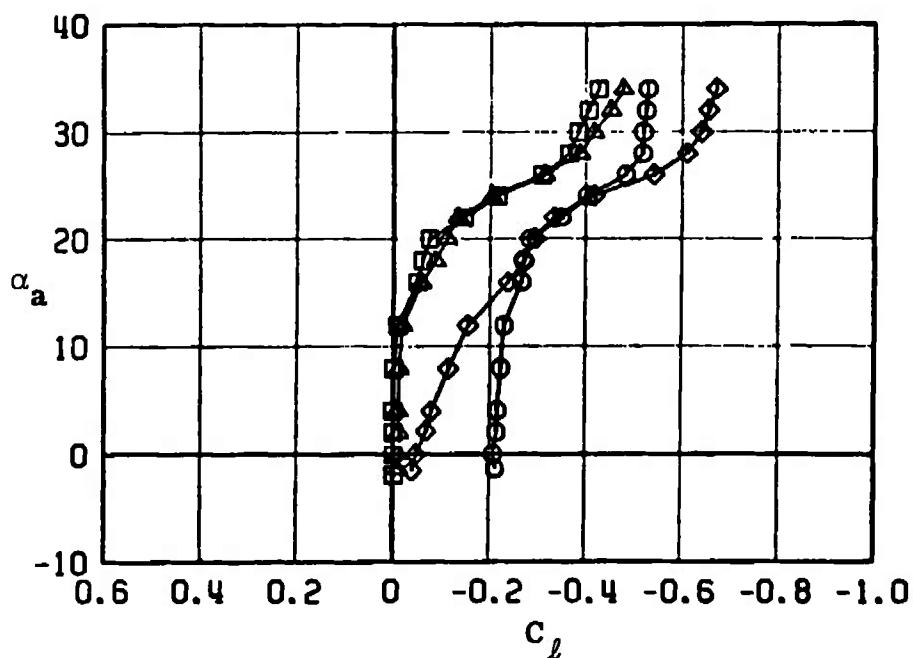


Fig. 35 Effect of Pitch and Roll Control Deflections on the Rolling-Moment and Axial-Force Coefficients for MGGB Configuration without RES (B9T3)

EFFECT OF SUPERIMPOSED CONTROL
ROLLING MOMENT AND AXIAL FORCE COEFFICIENTS

SYMBOL	CONFIG	MACH NO	ϕ	δ_0	δ_R	δ_P	$R_F \times 10^{-6}$
□	B9T3	0.65	0	0.3	0.5	0.3	1.8
○	B9T3	0.65	0	-0.1	0	-4.7	1.8
△	B9T3	0.65	0	-14.9	0.1	-0.1	1.8
◇	B9T3	0.65	0	-15.4	0.4	-5.2	1.8

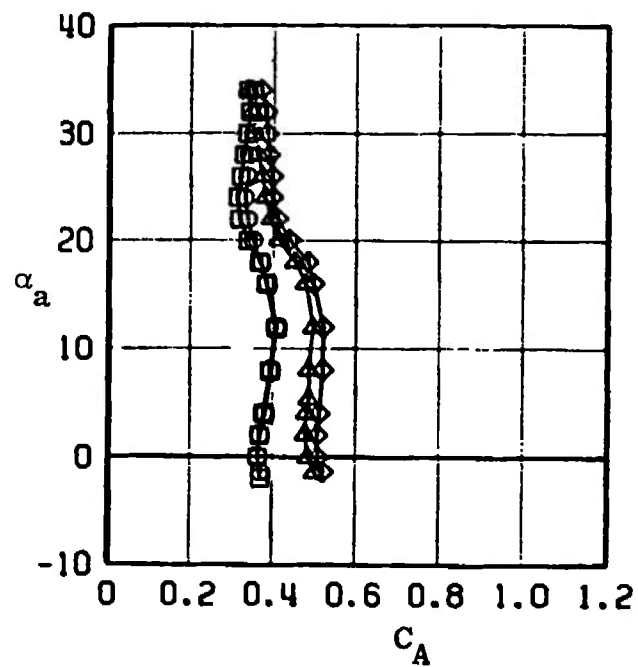
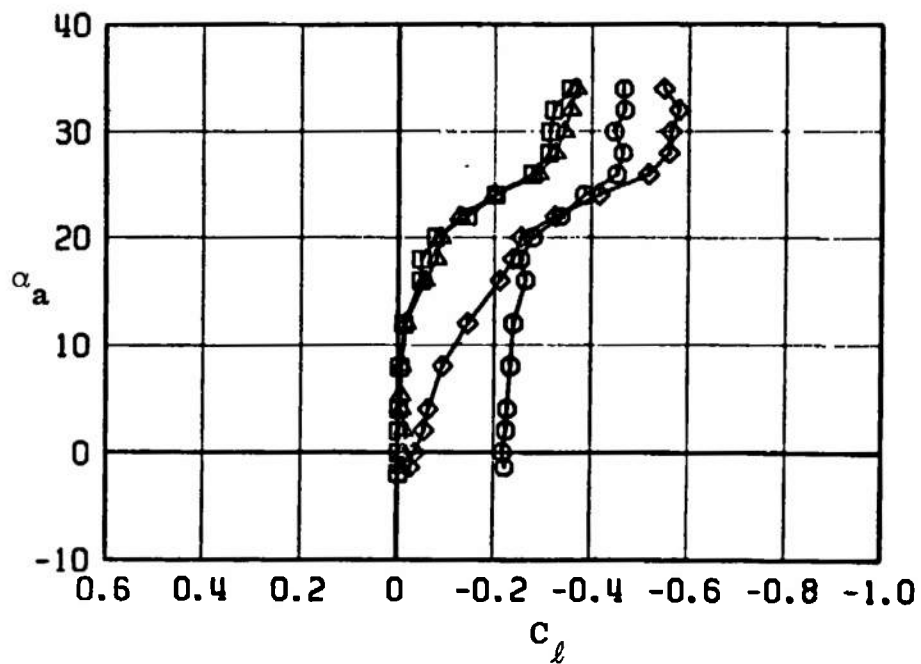


Fig. 35 Continued

EFFECT OF SUPERIMPOSED CONTROL								
ROLLING MOMENT AND AXIAL FORCE COEFFICIENTS								
SYMBOL	CONFIG	MACH NO	ϕ	δ_0	δ_n	δ_p	$R_E \times 10^{-6}$	
□	B9T3	0.75	0	0.3	0.5	0.3	2.0	
○	B9T3	0.75	0	-0.1	0	-4.7	2.0	
△	B9T3	0.75	0	-14.9	0.1	-0.1	2.0	
◇	B9T3	0.75	0	-15.4	0.4	-5.2	2.0	

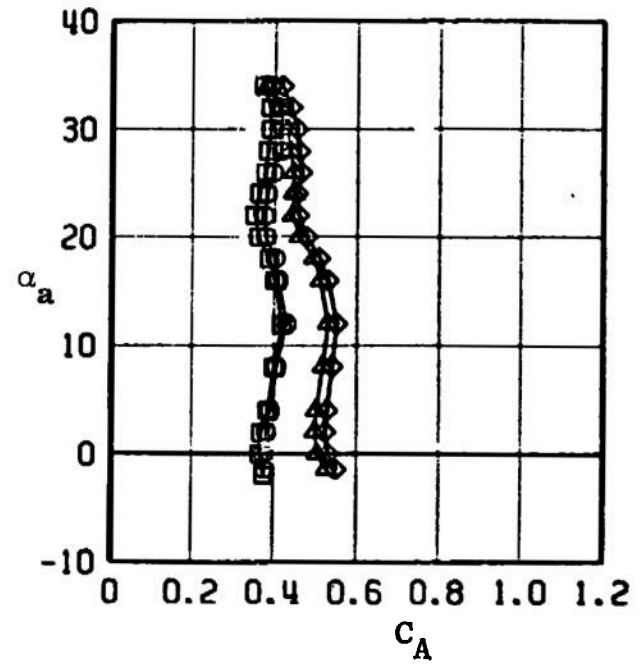
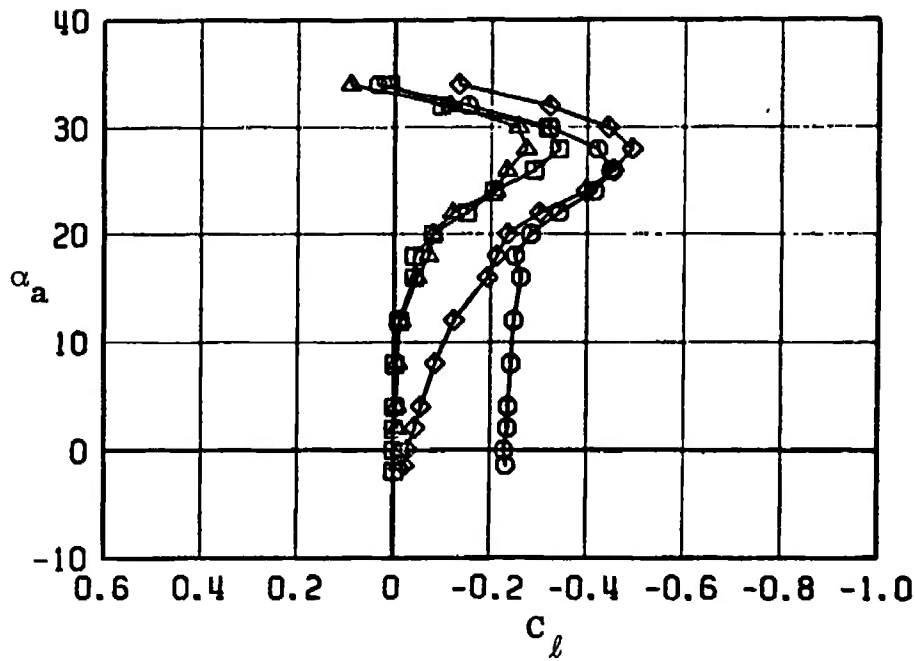


Fig. 35 Continued

EFFECT OF SUPERIMPOSED CONTROL
ROLLING MOMENT AND AXIAL FORCE COEFFICIENTS

SYMBOL	CONFIG	MACH NO	ϕ	δ_D	δ_R	δ_P	$R_F \times 10^{-6}$
□	B9T3	0.85	0	0.3	0.5	0.3	2.1
○	B9T3	0.85	0	-0.1	0	-4.7	2.1
△	B9T3	0.85	0	-14.9	0.1	-0.1	2.1
◇	B9T3	0.85	0	-15.4	0.4	-5.2	2.1

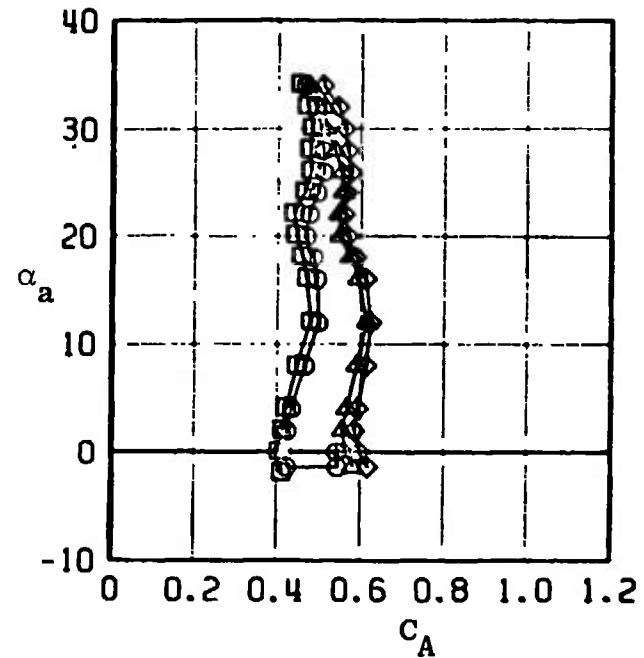
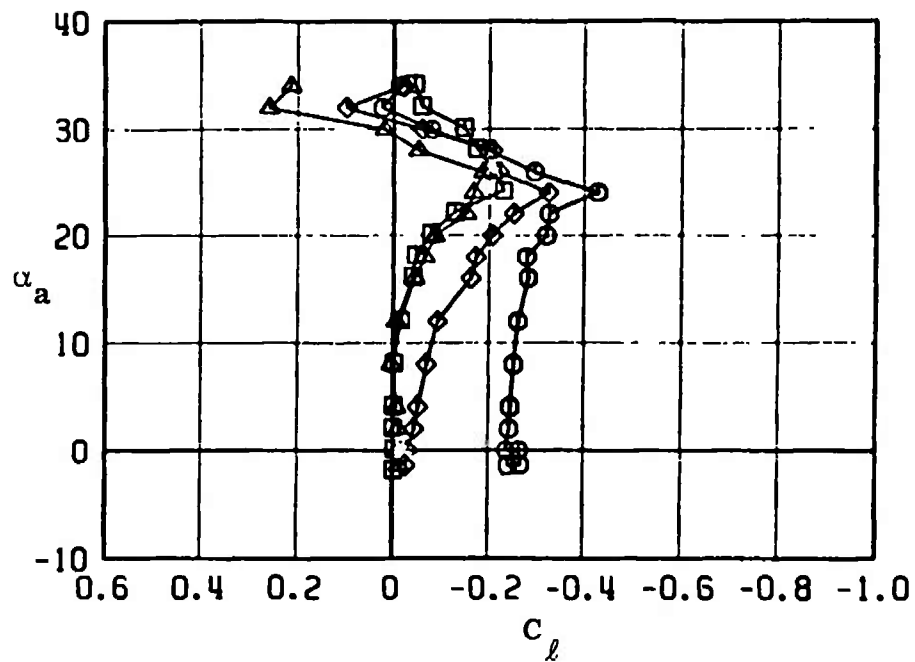


Fig. 35 Continued

EFFECT OF SUPERIMPOSED CONTROL
ROLLING MOMENT AND AXIAL FORCE COEFFICIENTS

SYMBOL	CONFIG	MACH NO	ϕ	δ_ϕ	δ_R	δ_P	$R_L \times 10^{-6}$
□	B9T3	0.95	0	0.3	0.5	0.3	2.2
○	B9T3	0.95	0	-0.1	0	-4.7	2.2
△	B9T3	0.95	0	-14.9	0.1	-0.1	2.2
◇	B9T3	0.95	0	-15.4	0.4	-5.2	2.2

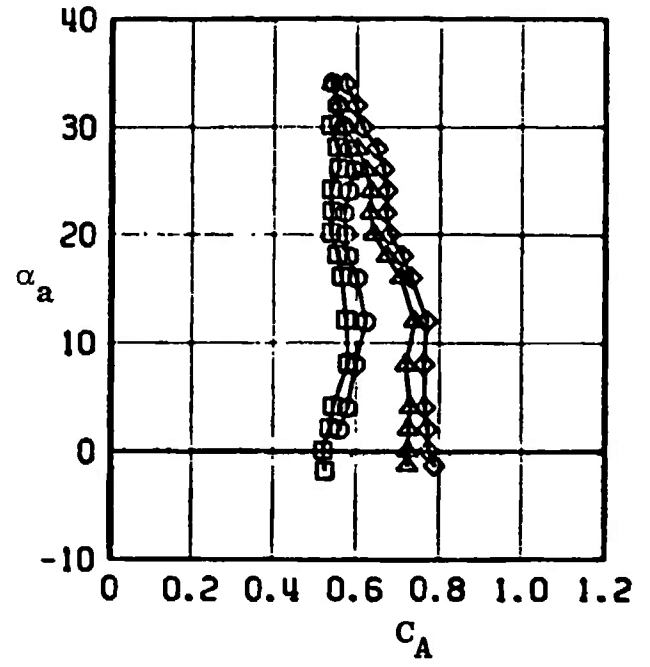
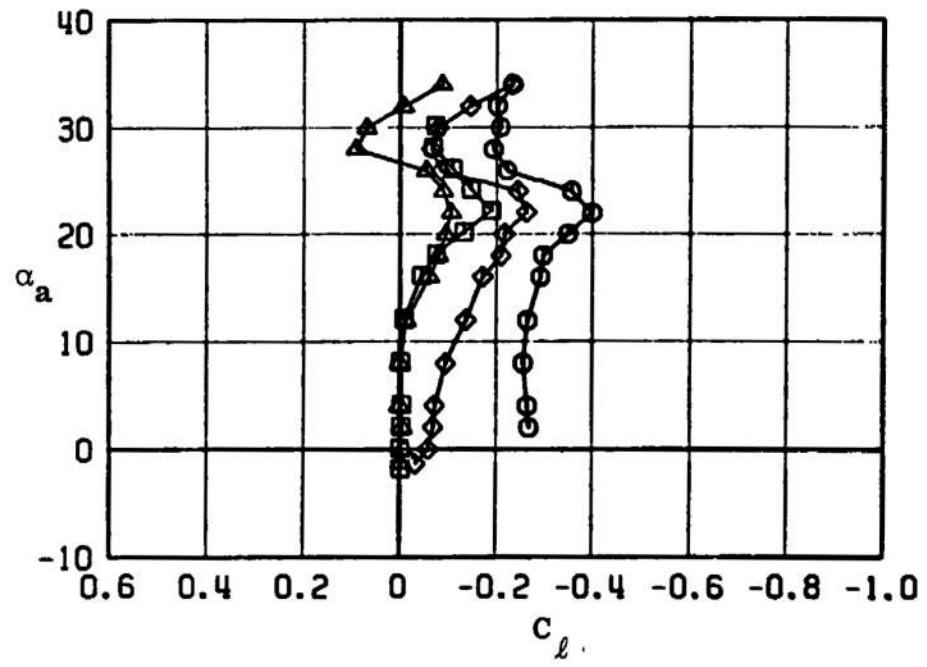


Fig. 35 Continued

EFFECT OF SUPERIMPOSED CONTROL							
ROLLING MOMENT AND AXIAL FORCE COEFFICIENTS							
SYMBOL	CONFIG	MACH NO	ϕ	δ_D	δ_H	δ_P	$R_F \times 10^{-6}$
□	B9T3	1.05	0	0.3	0.5	0.3	2.3
○	B9T3	1.05	0	-0.1	0	-4.7	2.3
△	B9T3	1.05	0	-14.9	0.1	-0.1	2.3
◇	B9T3	1.05	0	-15.4	0.4	-5.2	2.3

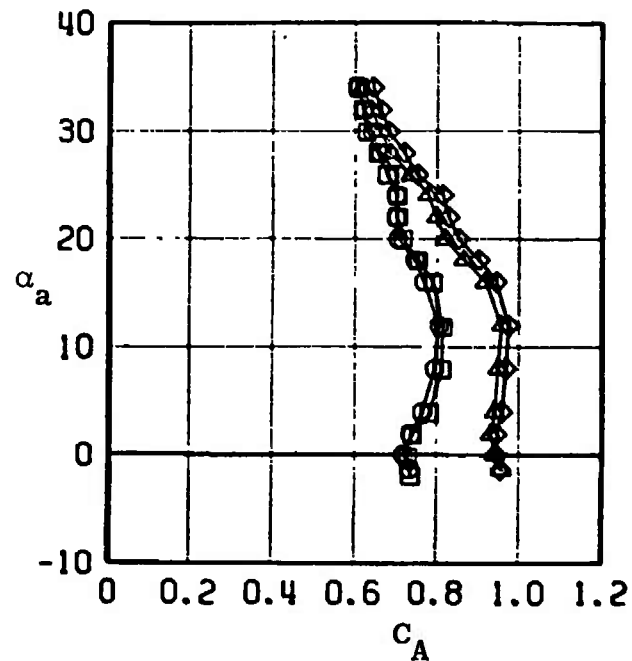
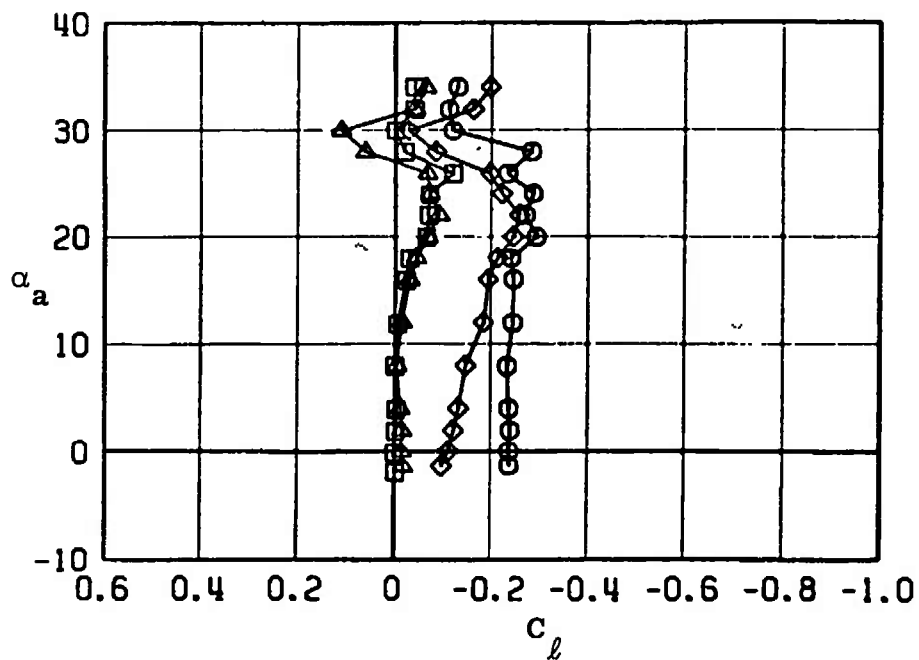


Fig. 35 Continued

EFFECT OF SUPERIMPOSED CONTROL							
ROLLING MOMENT AND AXIAL FORCE COEFFICIENTS							
SYMBOL	CONFIG	MACH NO	ϕ	δ_0	δ_R	δ_P	$R_L \times 10^{-6}$
□	B9T3	0.50	0	0.3	0.5	0.3	1.5
○	B9T3	0.50	0	-0.1	0	-4.7	1.5
△	B9T3	0.50	0	-10.1	0.1	0.3	1.5
◇	B9T3	0.50	0	-9.9	0.1	-5.1	1.5

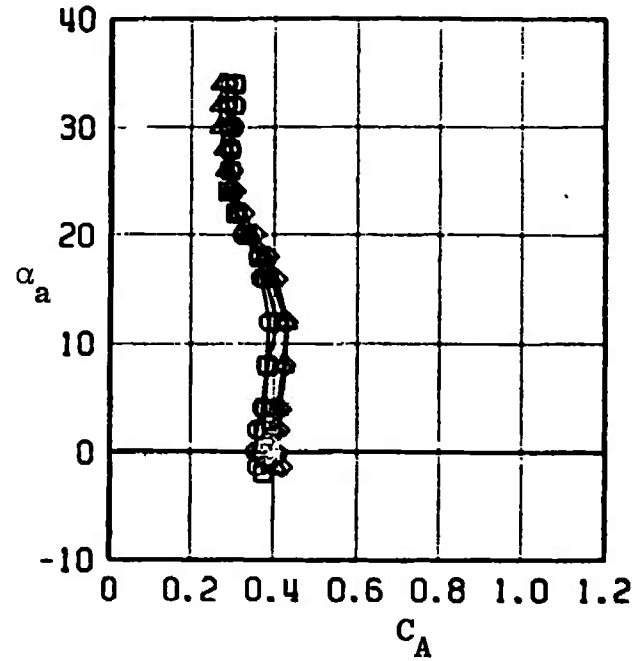
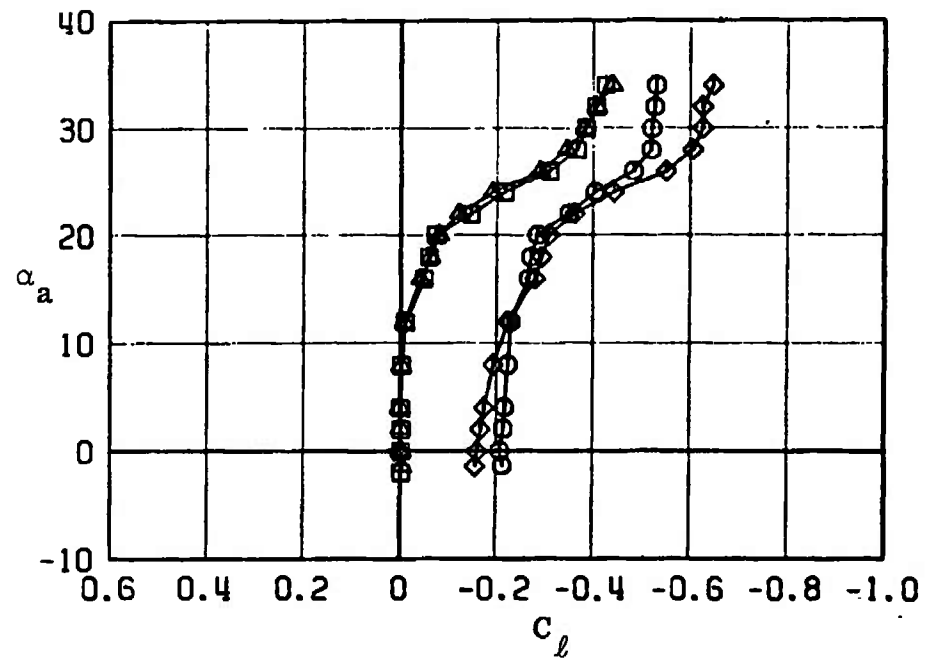


Fig. 35 Continued

EFFECT OF SUPERIMPOSED CONTROL
ROLLING MOMENT AND AXIAL FORCE COEFFICIENTS

SYMBOL	CONFIG	MACH NO	ϕ	δ_0	δ_R	δ_P	$R_L \times 10^{-6}$
□	B9T3	0.65	0	0.3	0.5	0.3	1.8
○	B9T3	0.65	0	-0.1	0	-4.7	1.8
△	B9T3	0.65	0	-10.1	0.1	0.3	1.8
◇	B9T3	0.65	0	-9.9	0.1	-5.1	1.8

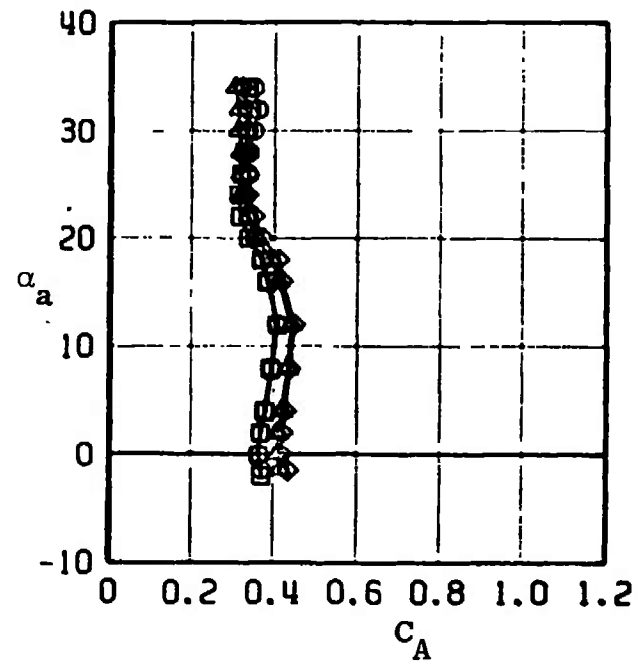
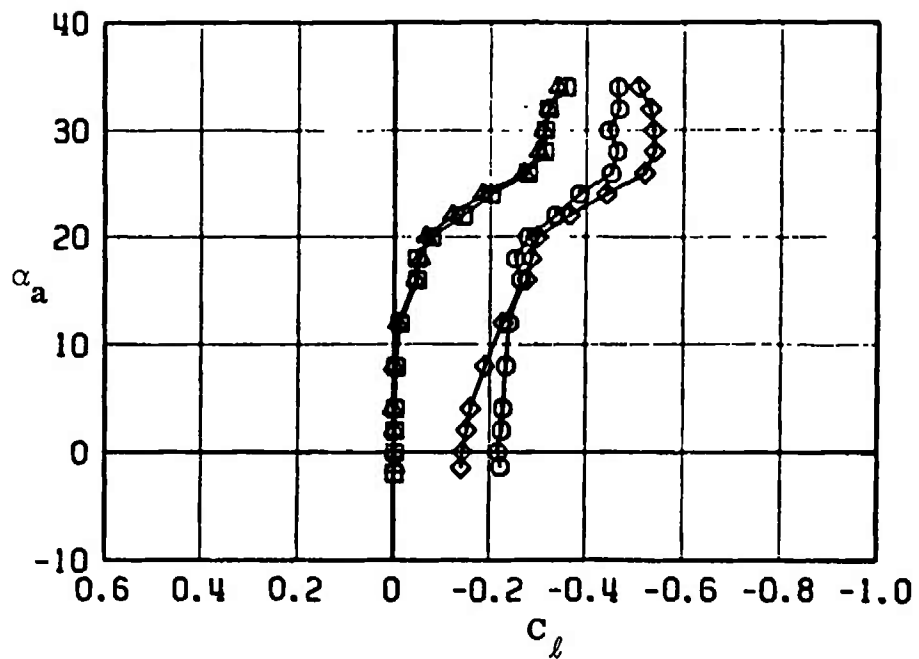


Fig. 35 Continued

EFFECT OF SUPERIMPOSED CONTROL							
ROLLING MOMENT AND AXIAL FORCE COEFFICIENTS							
SYMBOL	CONFIG	MACH NO	ϕ	b_0	b_h	b_p	$R_E \times 10^{-6}$
□	B9T3	0.75	0	0.3	0.5	0.3	2.0
○	B9T3	0.75	0	-0.1	0	-4.7	2.0
△	B9T3	0.75	0	-10.1	0.1	0.3	2.0
◇	B9T3	0.75	0	-9.9	0.1	-5.1	2.0

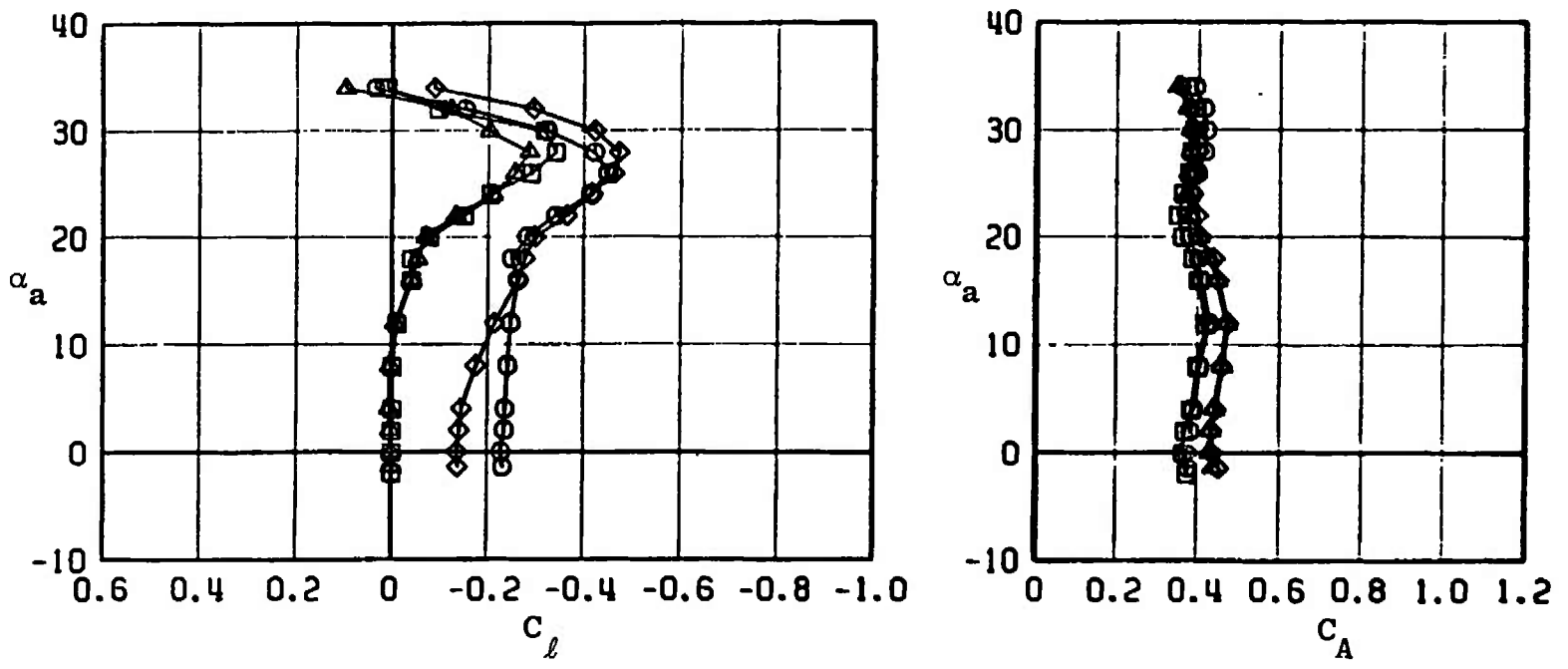


Fig. 35 Continued

EFFECT OF SUPERIMPOSED CONTROL
ROLLING MOMENT AND AXIAL FORCE COEFFICIENTS

SYMBOL	CONFIG	MACH NO	ϕ	δ_Q	δ_R	δ_P	$R_E \times 10^{-6}$
□	B9T3	0.85	0	0.3	0.5	0.3	2.1
○	B9T3	0.85	0	-0.1	0	-4.7	2.1
△	B9T3	0.85	0	-10.1	0.1	0.3	2.1
◇	B9T3	0.85	0	9.9	0.1	-5.1	2.1

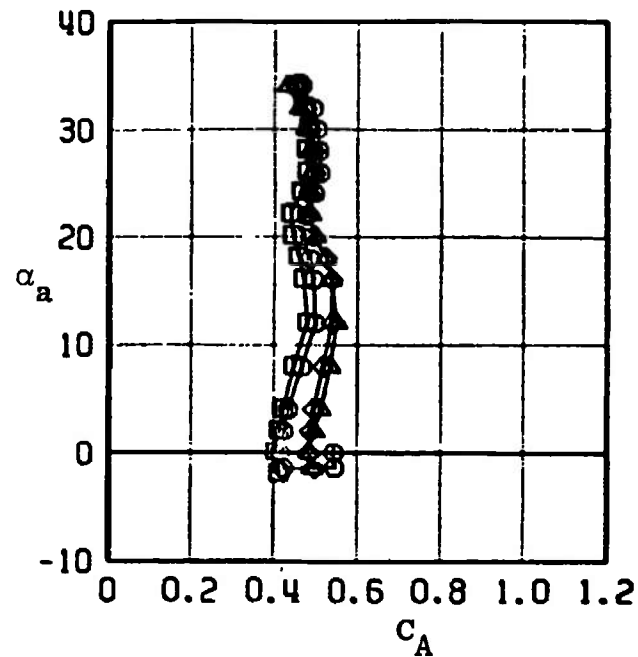
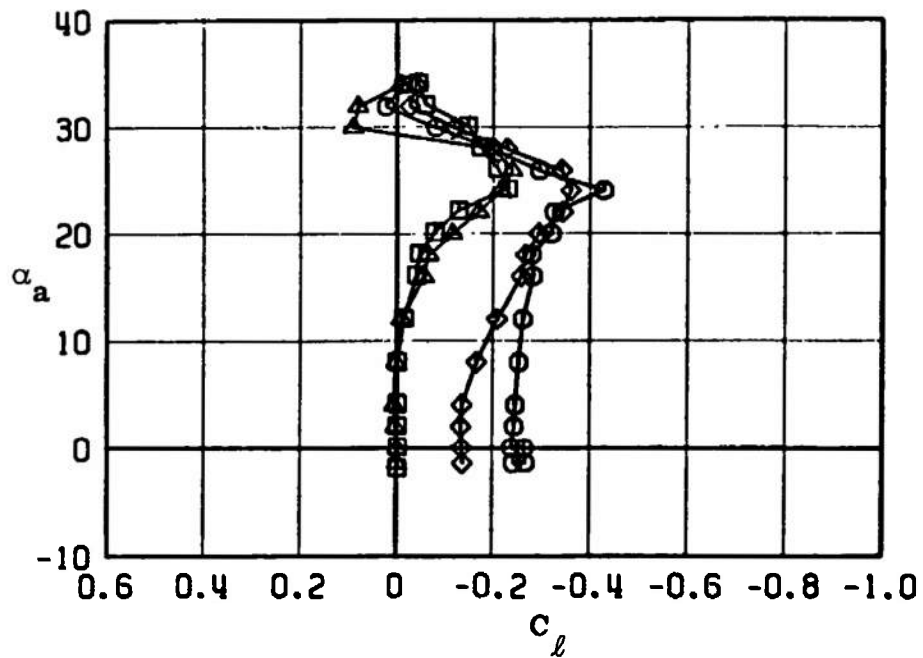


Fig. 35 Continued

EFFECT OF SUPERIMPOSED CONTROL
ROLLING MOMENT AND AXIAL FORCE COEFFICIENTS

SYMBOL	CONFIG	MACH NO	ϕ	b_0	b_R	b_P	$R_E \times 10^{-6}$
□	B9T3	0.95	0	0.3	0.5	0.3	2.2
○	B9T3	0.95	0	-0.1	0	-4.7	2.2
△	B9T3	0.95	0	-10.1	0.1	0.3	2.2
◇	B9T3	0.95	0	9.9	0.1	-5.1	2.2

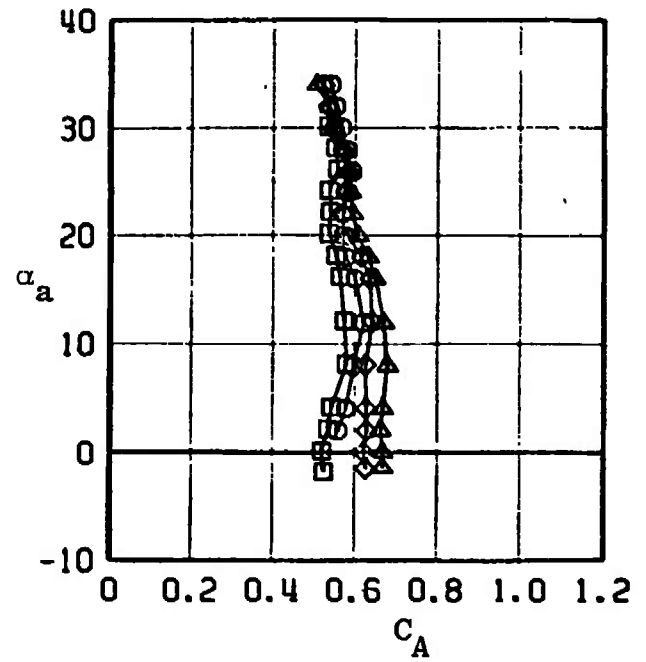
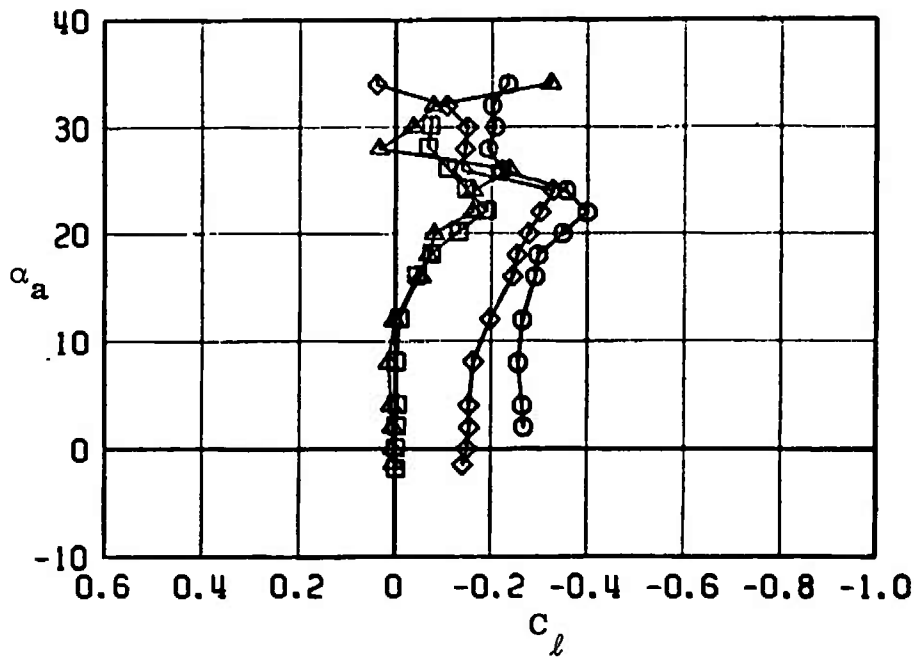


Fig. 35 Continued

EFFECT OF SUPERIMPOSED CONTROL
ROLLING MOMENT AND AXIAL FORCE COEFFICIENTS

SYMBOL	CONFIG	MACH NO	ϕ	ξ_D	ξ_H	ξ_P	$R_L \times 10^{-6}$
\square	B9T3	1.05	0	0.3	0.5	0.3	2.3
\circ	B9T3	1.05	0	-0.1	0	-4.7	2.3
\triangle	B9T3	1.05	0	-10.1	0.1	0.3	2.3
\blacktriangle	B9T3	1.05	0	9.9	0.1	-5.1	2.3

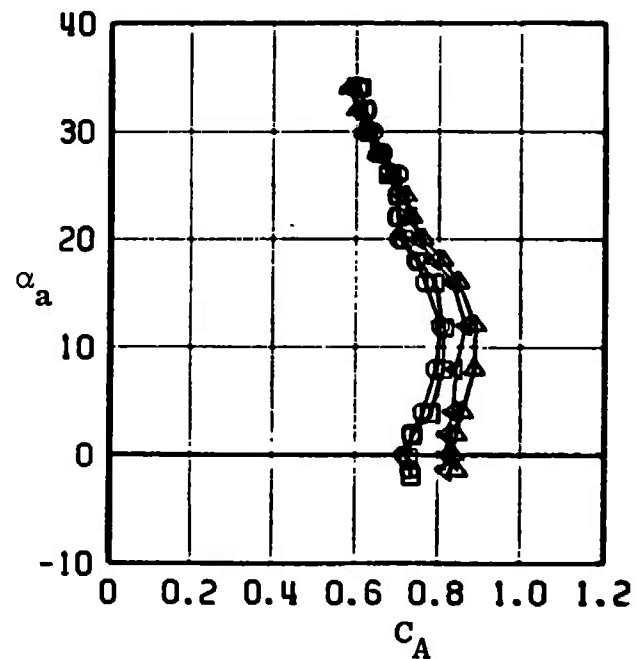
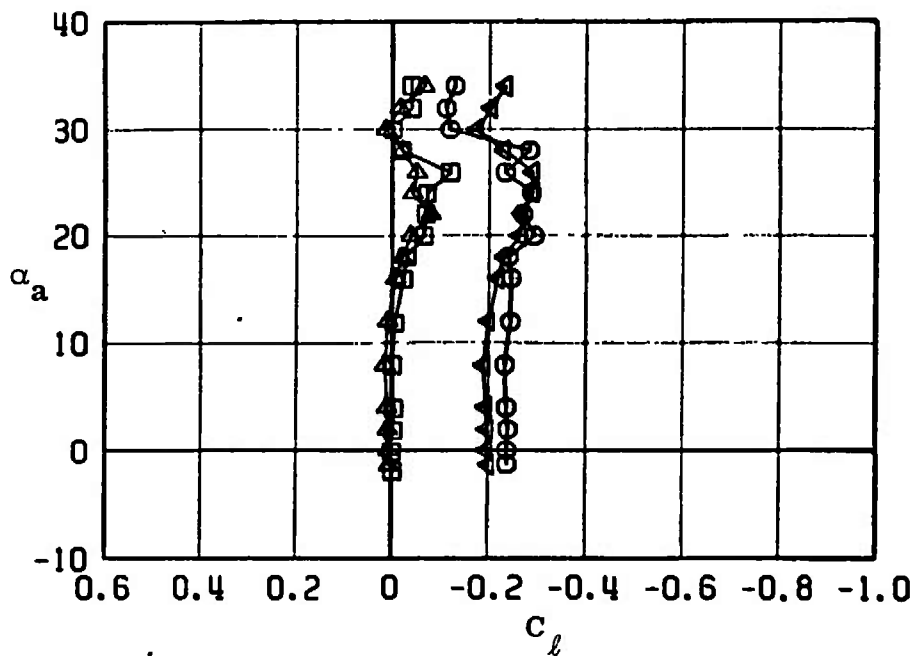


Fig. 35 Continued

EFFECT OF SUPERIMPOSED CONTROL ROLLING MOMENT AND AXIAL FORCE COEFFICIENTS							
SYMBOL	CONFIG	MACH NO	ϕ	b_0	b_R	b_P	$R_E \times 10^{-6}$
□	B9T3	0.50	0	0.3	0.5	0.3	1.5
○	B9T3	0.50	0	0.2	0	-9.9	1.5
△	B9T3	0.50	0	-10.1	0.1	0.3	1.5
◇	B9T3	0.50	0	-10.3	0.1	-10.3	1.5

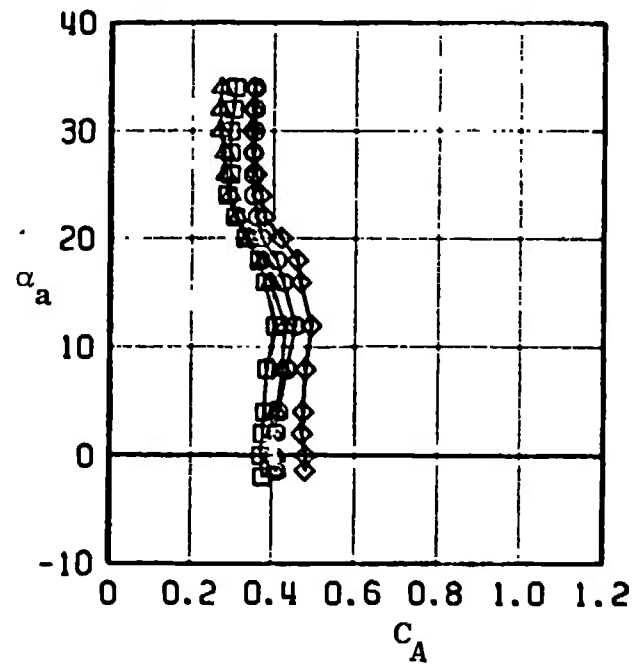
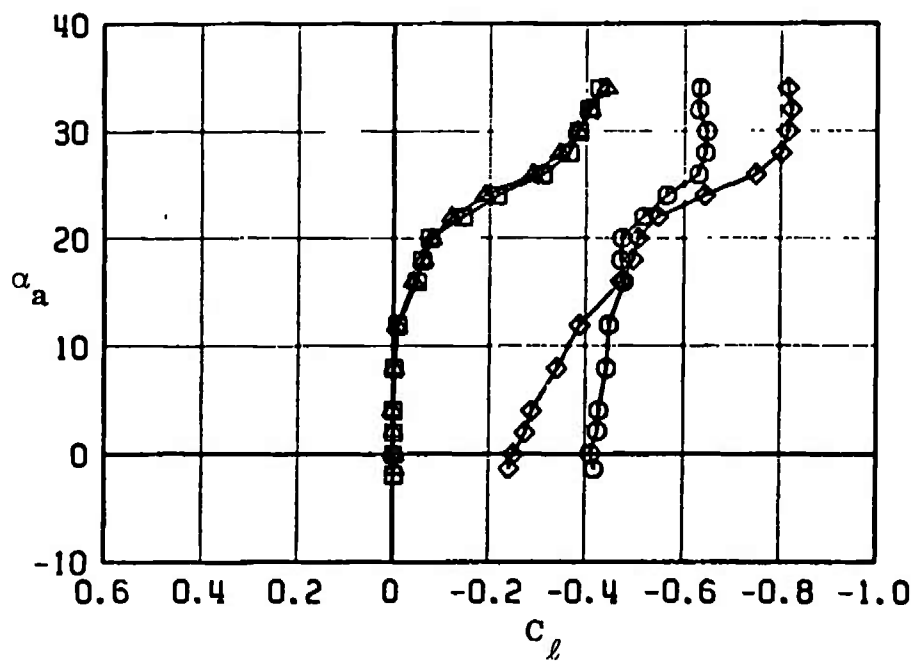


Fig. 35 Continued

EFFECT OF SUPERIMPOSED CONTROL
ROLLING MOMENT AND AXIAL FORCE COEFFICIENTS

SYMBOL	CONFIG	MACH NO	ϕ	δ_D	δ_R	δ_P	$R_E \times 10^{-6}$
□	B9T3	0.65	0	0.3	0.5	0.3	1.8
○	B9T3	0.65	0	0.2	0	-9.9	1.8
△	B9T3	0.65	0	-10.1	0.1	0.3	1.8
◇	B9T3	0.65	0	-10.3	0.1	-10.3	1.8

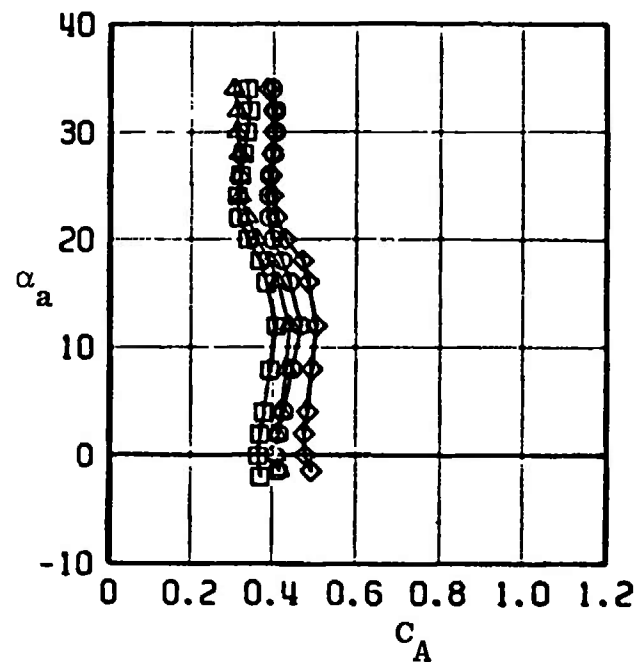
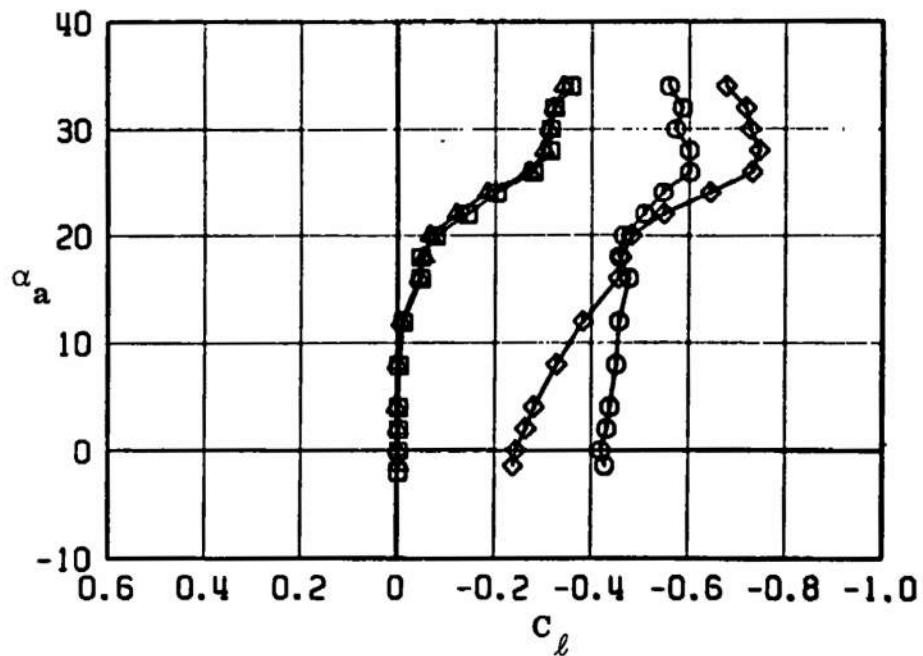


Fig. 35 Continued

EFFECT OF SUPERIMPOSED CONTROL
ROLLING MOMENT AND AXIAL FORCE COEFFICIENTS

SYMBOL	CONFIG	MACH NO	ϕ	δ_D	δ_R	δ_P	$R_E \times 10^{-6}$
□	B9T3	0.75	0	0.3	0.5	0.3	2.0
○	B9T3	0.75	0	0.2	0	-9.9	2.0
△	B9T3	0.75	0	-10.1	0.1	0.3	2.0
◇	B9T3	0.75	0	-10.3	0.1	-10.3	2.0

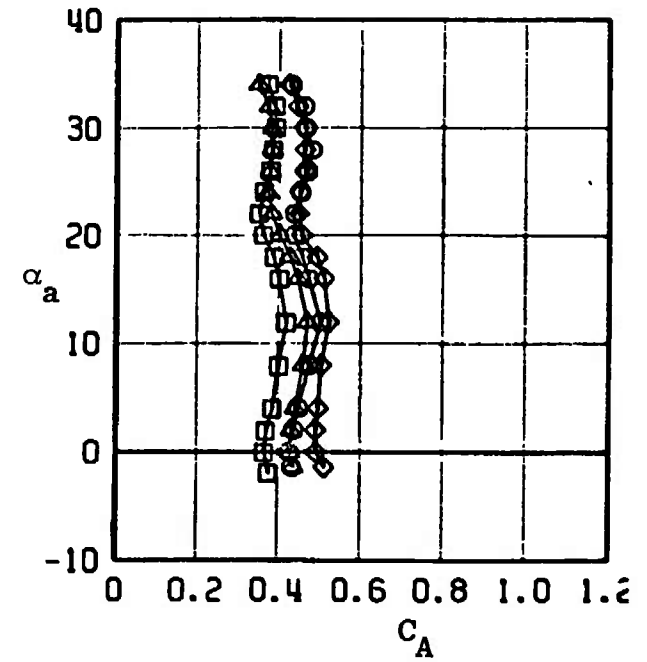
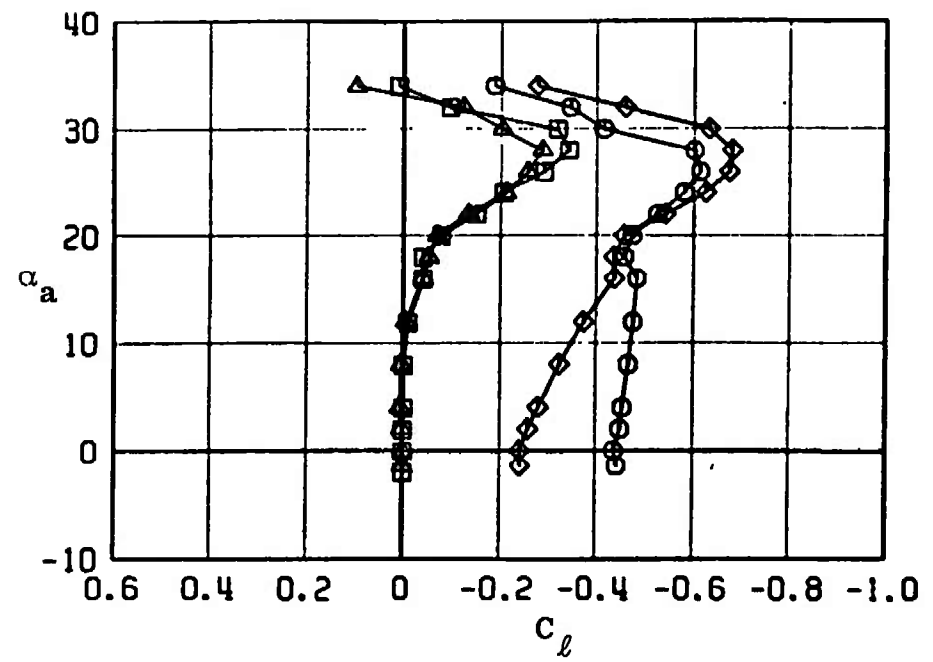


Fig. 35 Continued

EFFECT OF SUPERIMPOSED CONTROL
ROLLING MOMENT AND AXIAL FORCE COEFFICIENTS

SYMBOL	CONFIG	MACH NO	ϕ	δ_0	δ_R	δ_P	$R_E \times 10^{-6}$
□	B9T3	0.85	0	0.3	0.5	0.3	2.1
○	B9T3	0.85	0	0.2	0	-9.9	2.1
△	B9T3	0.85	0	-10.1	0.1	0.3	2.1
◇	B9T3	0.85	0	-10.3	0.1	-10.3	2.1

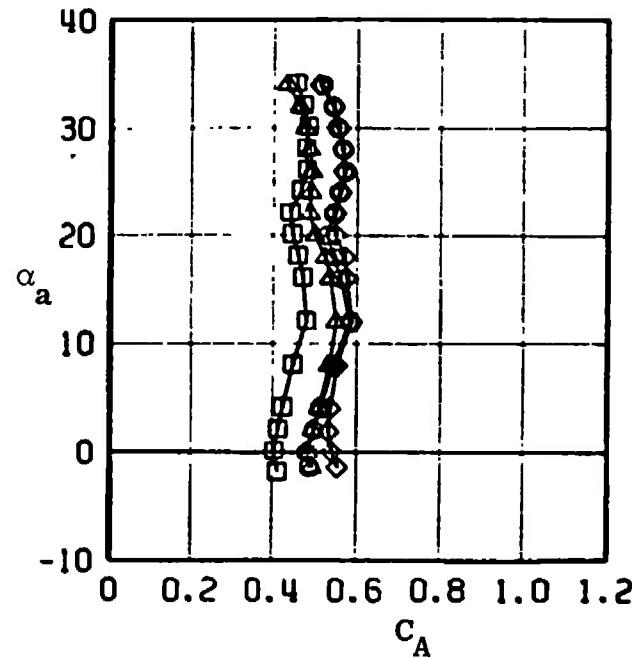
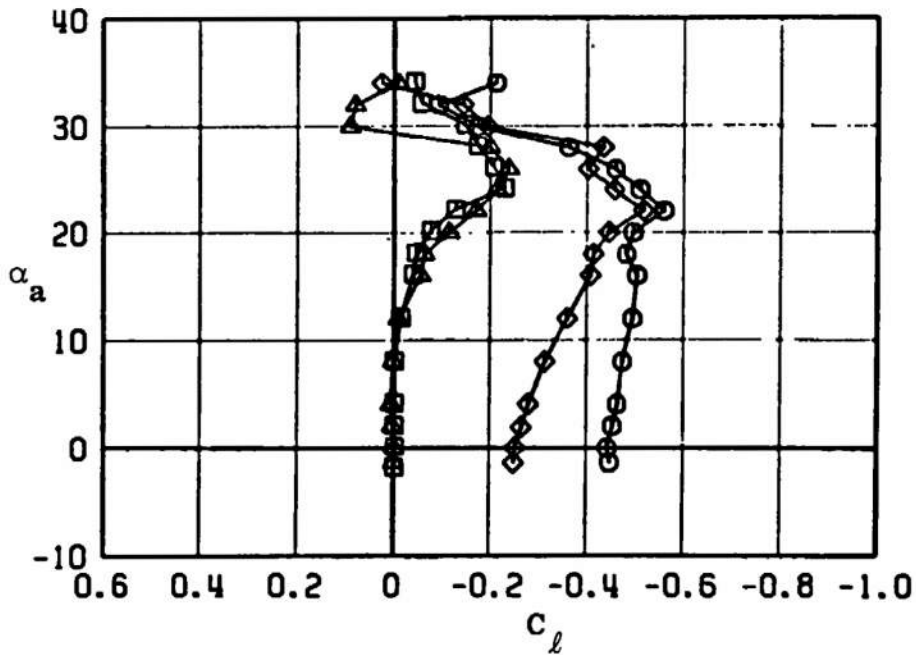


Fig. 35 Continued

EFFECT OF SUPERIMPOSED CONTROL							
ROLLING MOMENT AND AXIAL FORCE COEFFICIENTS							
SYMBOL	CONFIG	MACH NO	ϕ	b_0	b_n	b_p	$R_E \times 10^{-6}$
□	B9T3	0.95	0	0.3	0.5	0.3	2.2
○	B9T3	0.95	0	0.2	0	-9.9	2.2
△	B9T3	0.95	0	-10.1	0.1	0.3	2.2
◇	B9T3	0.95	0	-10.3	0.1	-10.3	2.2

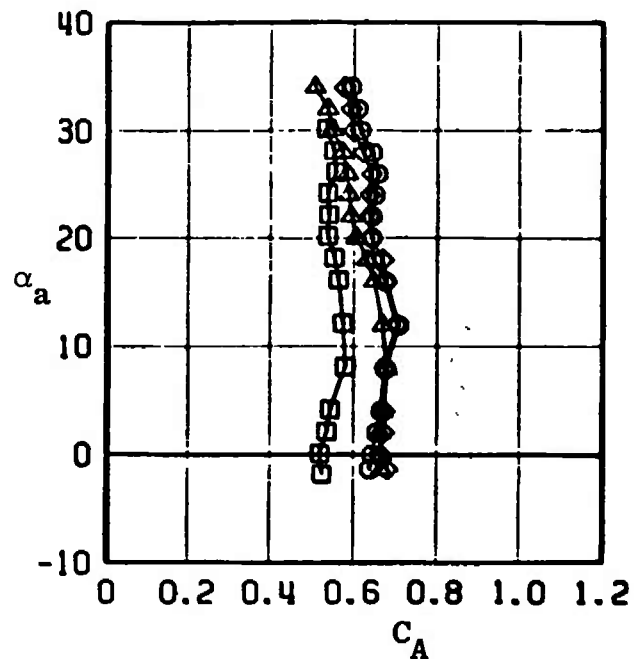
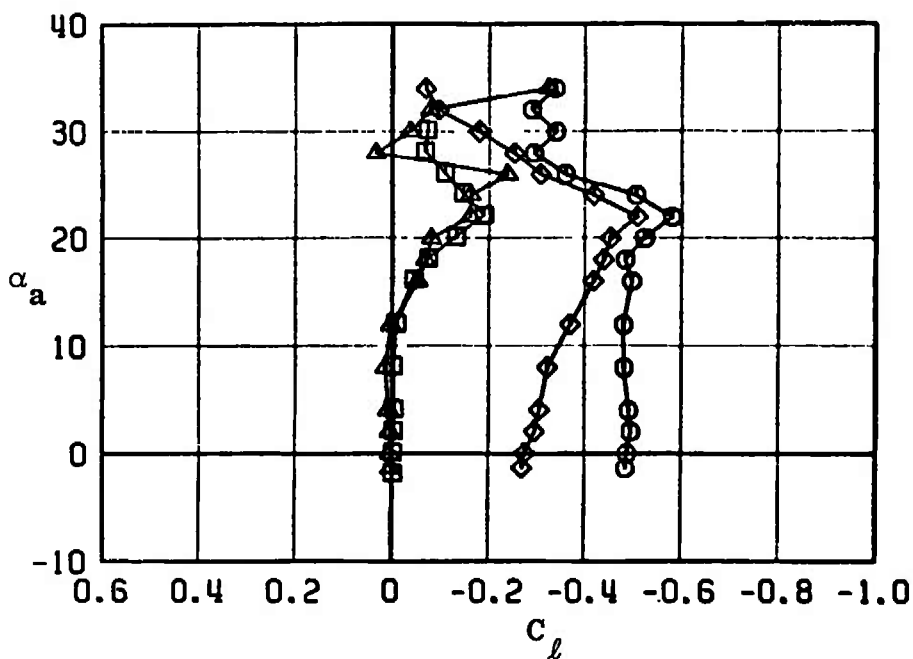


Fig. 35 Continued

EFFECT OF SUPERIMPOSED CONTROL

ROLLING MOMENT AND AXIAL FORCE COEFFICIENTS

SYMBOL	CONFIG	MACH NO	ϕ	δ_0	δ_R	δ_P	$R_L \times 10^{-6}$
□	B9T3	1.05	0	0.3	0.5	0.3	2.3
○	B9T3	1.05	0	0.2	0	-9.9	2.3
△	B9T3	1.05	0	-10.1	0.1	0.3	2.3
◇	B9T3	1.05	0	-10.3	0.1	-10.3	2.3

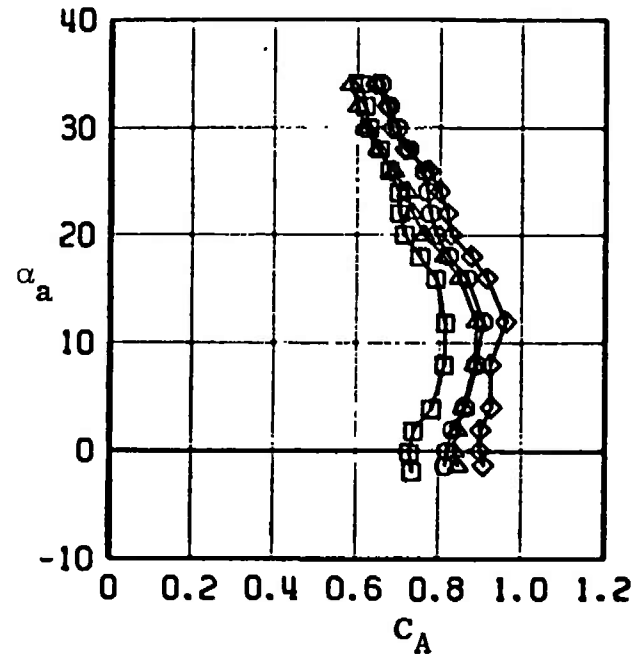
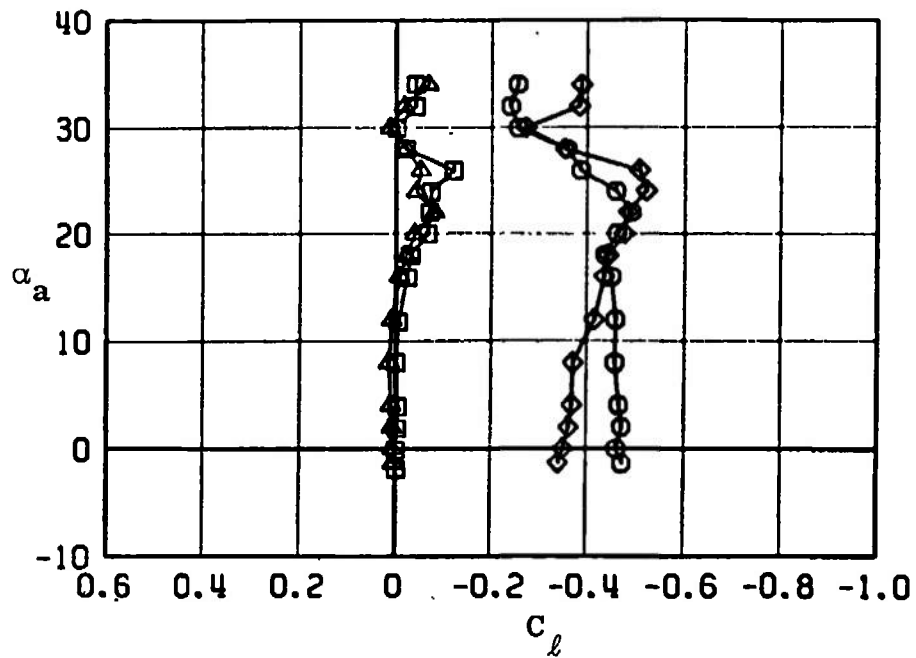


Fig. 35 Concluded

EFFECT OF REYNOLDS NUMBER
MGG B ALPHA SENSOR CHARACTERISTICS

SYMBOL	CONFIG	MACH NO	ϕ	δ_0	δ_R	δ_P	$R_E \times 10^{-6}$
\square	B10W8S1T3	0.50	0	0.4	-0.3	0.5	4.8
\circ	B10W8S1T3	0.50	0	0.4	-0.3	0.5	1.5

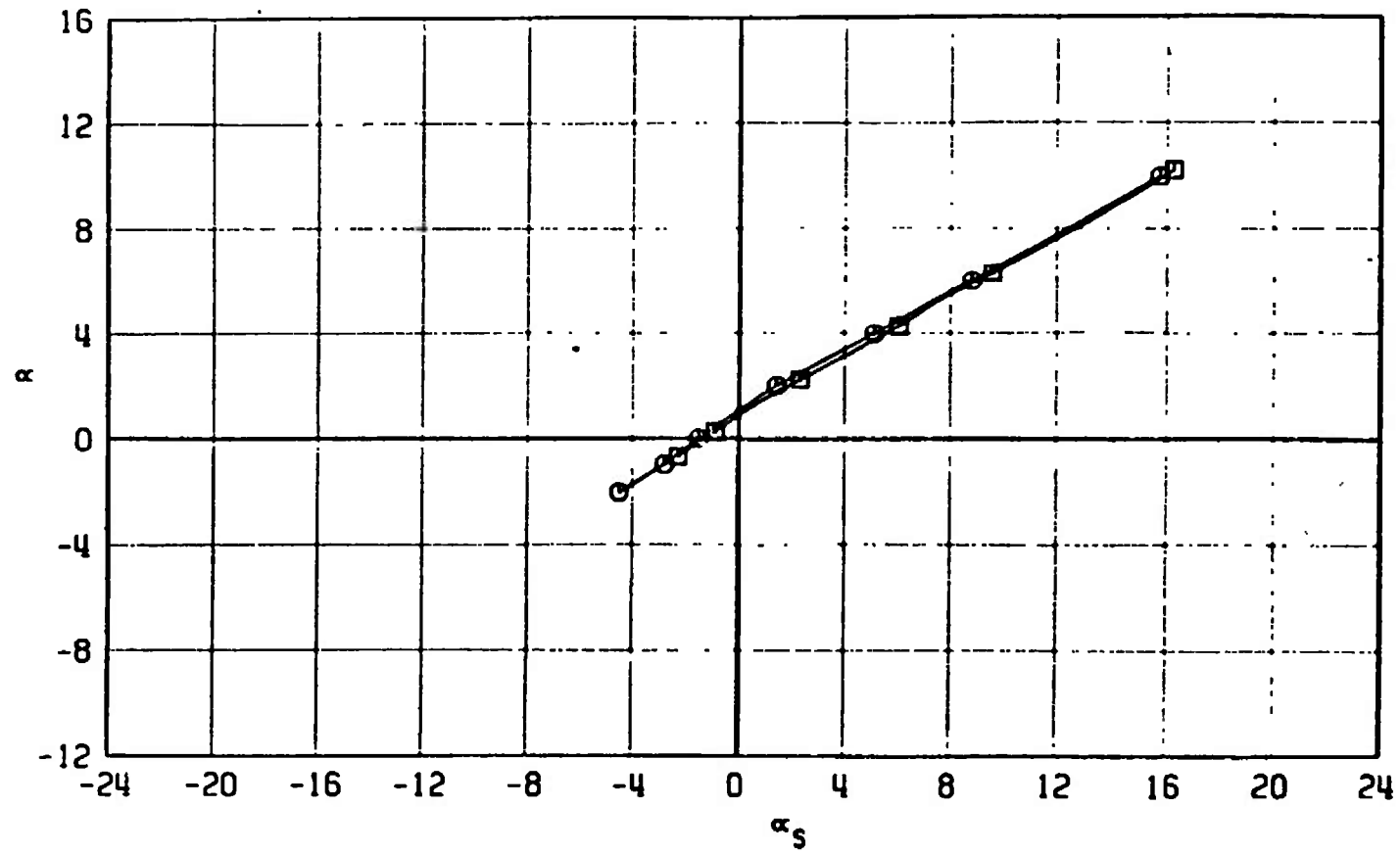


Fig. 36 Vane Calibration Data, α versus α_s , Comparing Low and High Reynolds Number for MGG B Configuration (B10W8S1T3)

EFFECT OF REYNOLDS NUMBER

MGG8 ALPHA SENSOR CHARACTERISTICS

SYMBOL	CONFIG	MACH NO	ϕ	δ_0	δ_R	δ_p	$R_E \times 10^{-6}$
\square	B10W8S1T3	0.60	0	0.4	-0.3	0.5	5.2
\circ	B10W8S1T3	0.60	0	0.4	-0.3	0.5	1.7

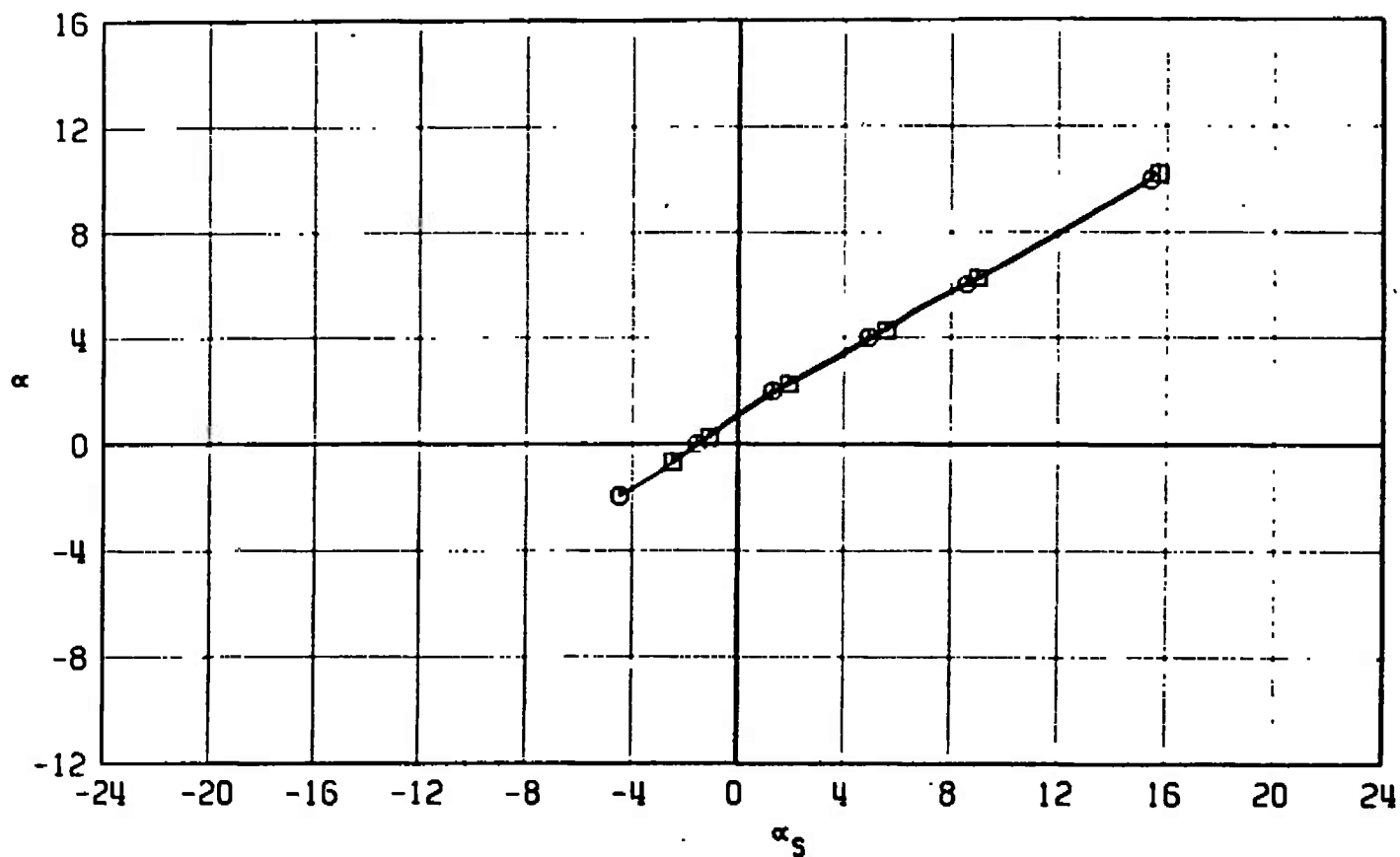


Fig. 36 Continued

EFFECT OF REYNOLDS NUMBER
MGG8 ALPHA SENSOR CHARACTERISTICS

SYMBOL	CONFIG	MACH NO	ϕ	δ_0	δ_R	δ_p	$R_E \times 10^{-6}$
□	B10W8S1T3	0.75	0	0.4	-0.3	0.5	5.8
○	B10W8S1T3	0.75	0	0.4	-0.3	0.5	2.0

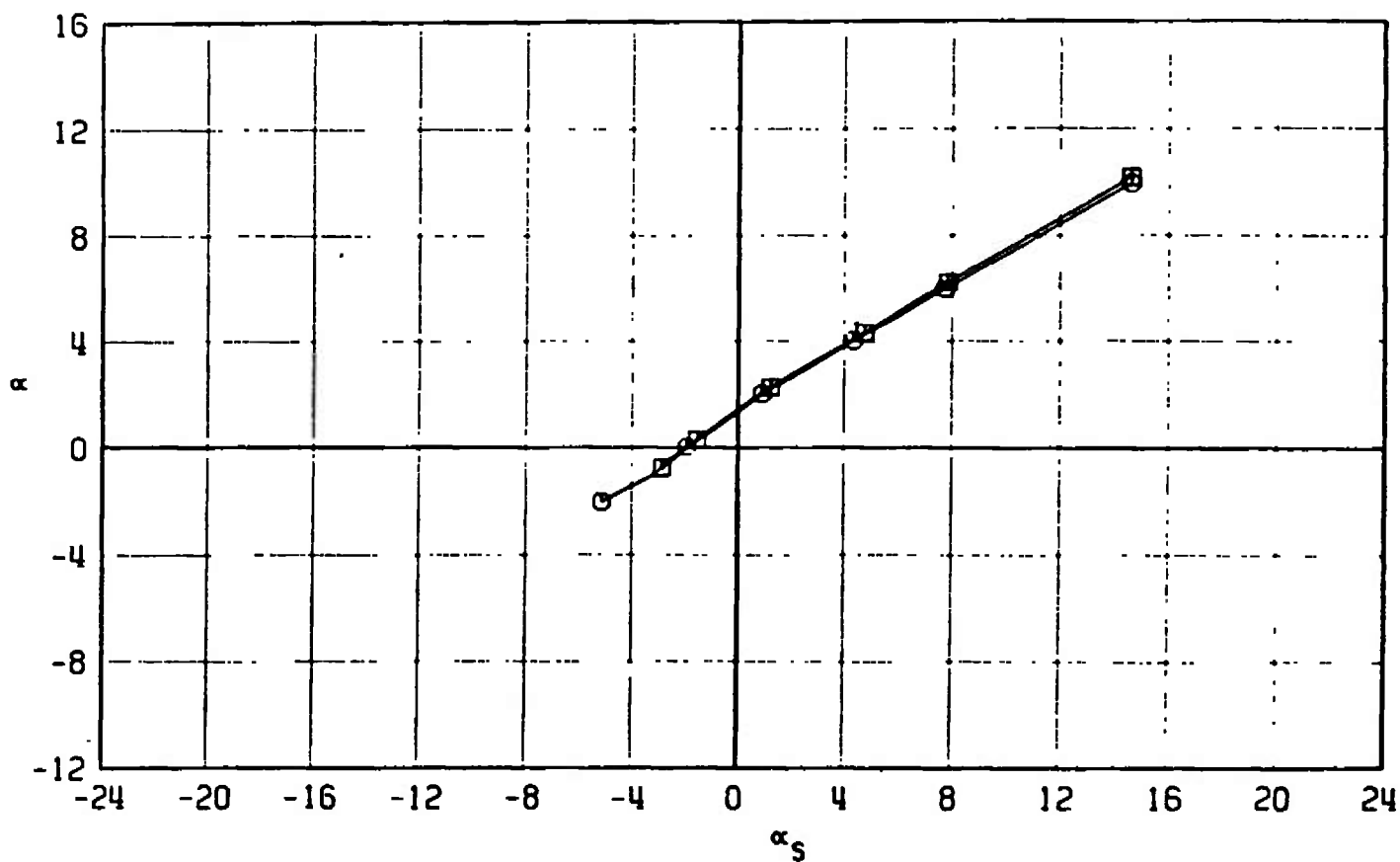


Fig. 36 Continued

EFFECT OF REYNOLDS NUMBER
MGG8 ALPHA SENSOR CHARACTERISTICS

SYMBOL	CONFIG	MACH NO	ϕ	δ_0	δ_R	δ_p	$R_E \times 10^{-6}$
\square	B10W8S1T3	0.85	0	0.4	-0.3	0.5	6.0
\circ	B10W8S1T3	0.85	0	0.4	-0.3	0.5	2.1

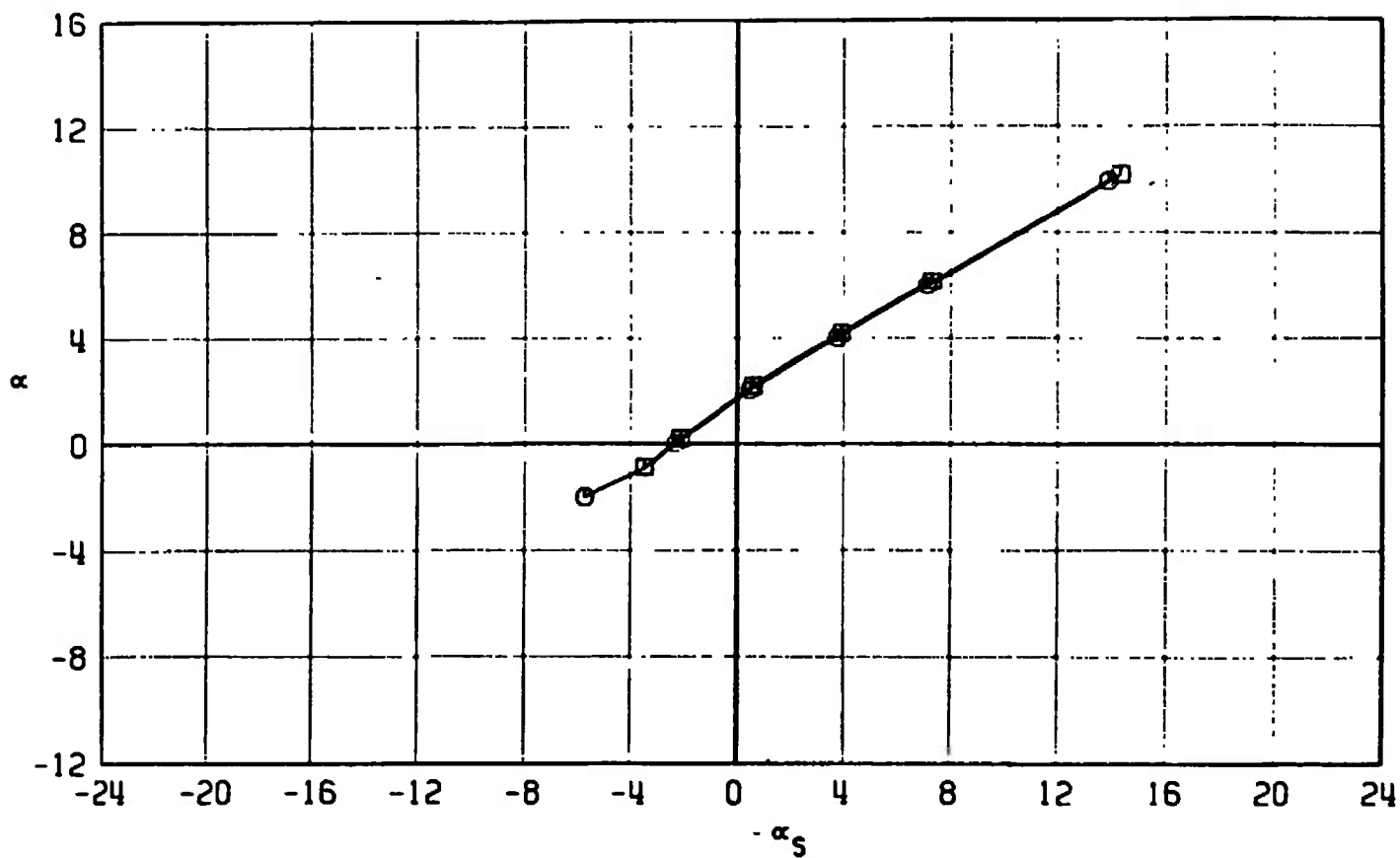


Fig. 36 Continued

EFFECT OF REYNOLDS NUMBER
MGGB ALPHA SENSOR CHARACTERISTICS

SYMBOL	CONFIG	MACH NO	ϕ	δ_0	δ_R	δ_P	$R_E \times 10^{-6}$
□	B10W8S1T3	0.95	0	0.4	-0.3	0.5	5.6
○	B10W8S1T3	0.95	0	0.4	-0.3	0.5	2.2

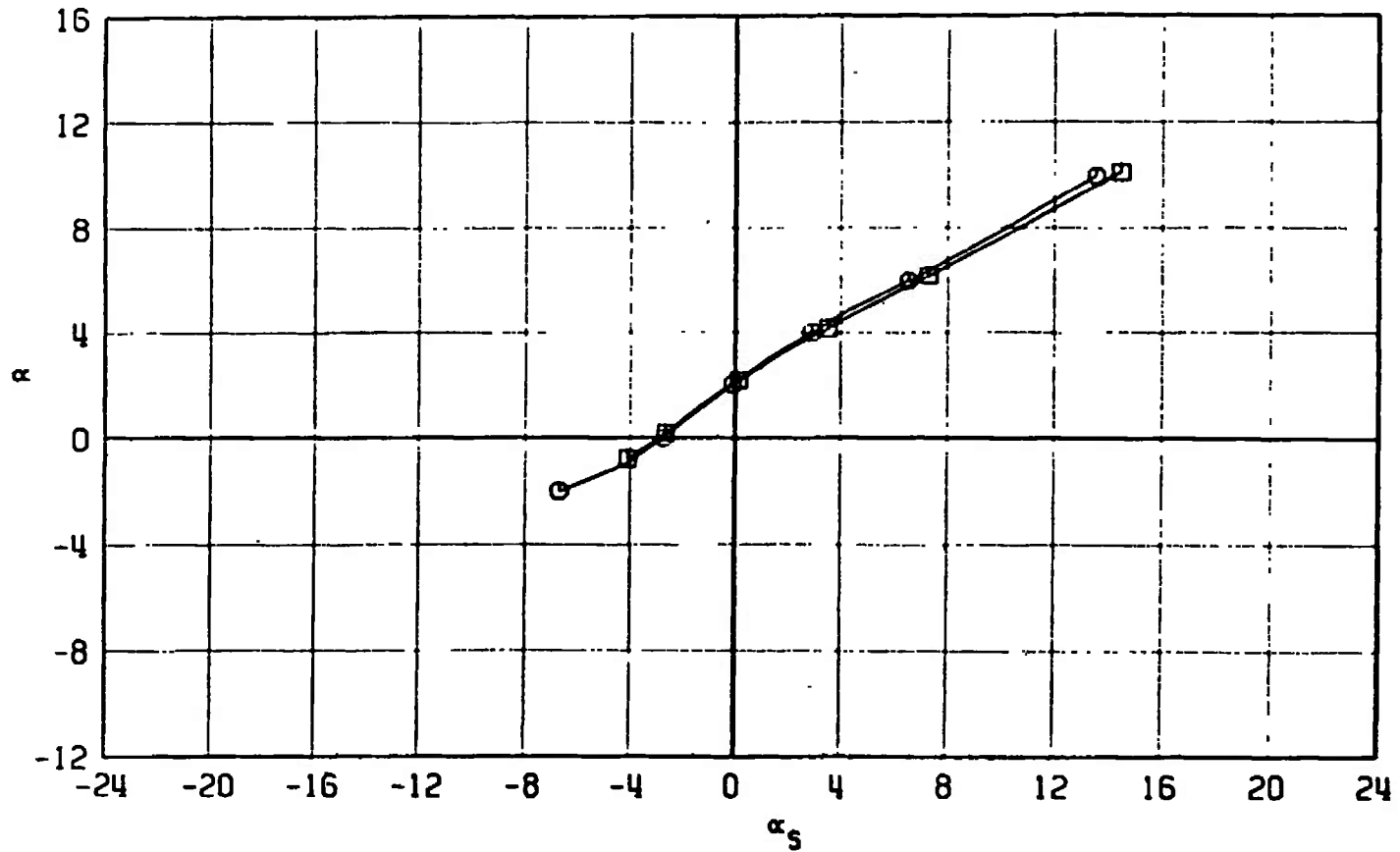


Fig. 36 Concluded

CONFIGURATION COMPARISON

MGB ALPHA SENSOR CHARACTERISTICS

SYMBOL	CONFIG	MACH NO	ϕ	δ_0	δ_R	δ_P	$R_E \times 10^{-6}$
□	B10W8S1T3	0.50	0	0.4	-0.3	0.3	1.5
○	B9W8S1T3	0.50	0	0.4	-0.3	0.3	1.5

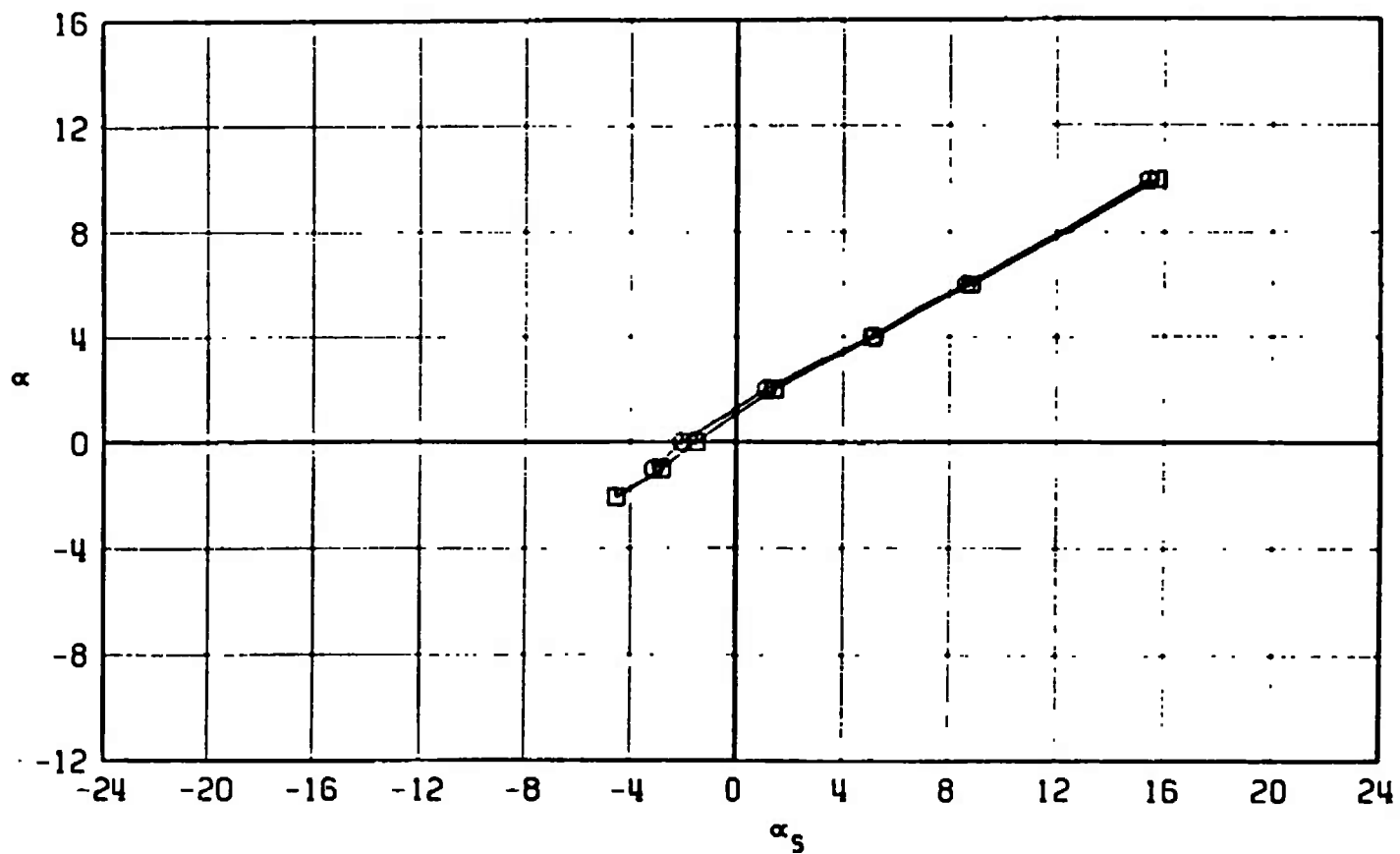


Fig. 37 Vane Calibration Data, α versus α_s , Showing the Effect of the Proximity Fuse (Configurations B9W8S1T3 and B10W8S1T3)

CONFIGURATION COMPARISON
MGGP ALPHA SENSOR CHARACTERISTICS

SYMBOL	CONFIG	MACH NO	ϕ	ϵ_0	ϵ_R	ϵ_P	$R_f \times 10^{-5}$
□	B10W8S1T3	0.60	0	0.4	-0.3	0.3	1.7
○	B9W8S1T3	0.60	0	0.4	-0.3	0.3	1.7

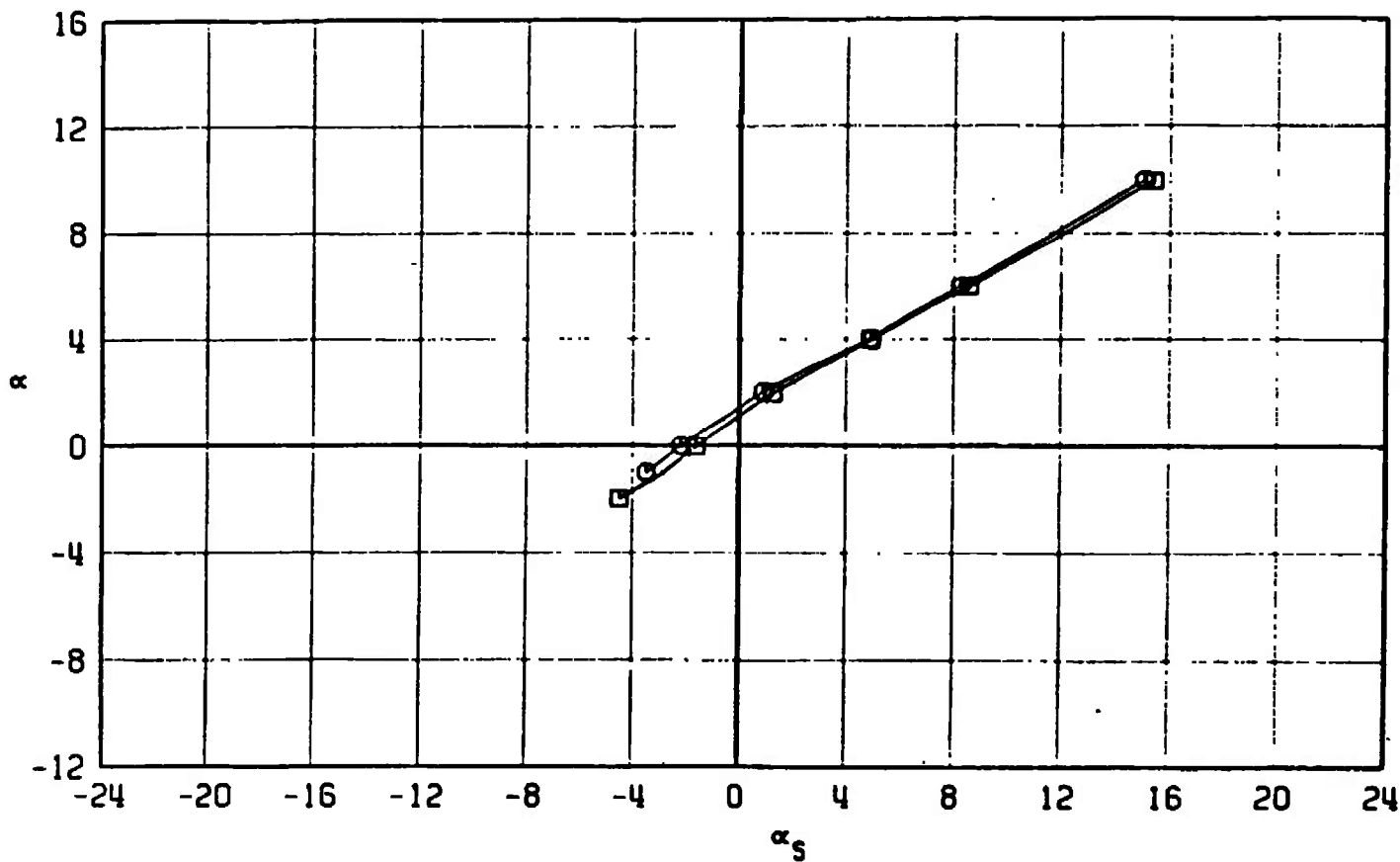


Fig. 37 Continued

CONFIGURATION COMPARISON
MGG8 ALPHA SENSOR CHARACTERISTICS

SYMBOL	CONFIG	MACH NO	ϕ	δ_D	δ_R	δ_P	$R_E \times 10^{-6}$
\square	B10W8S1T3	0.75	0	0.4	-0.3	0.3	2.0
\circ	B9W8S1T3	0.75	0	0.4	-0.3	0.3	2.0

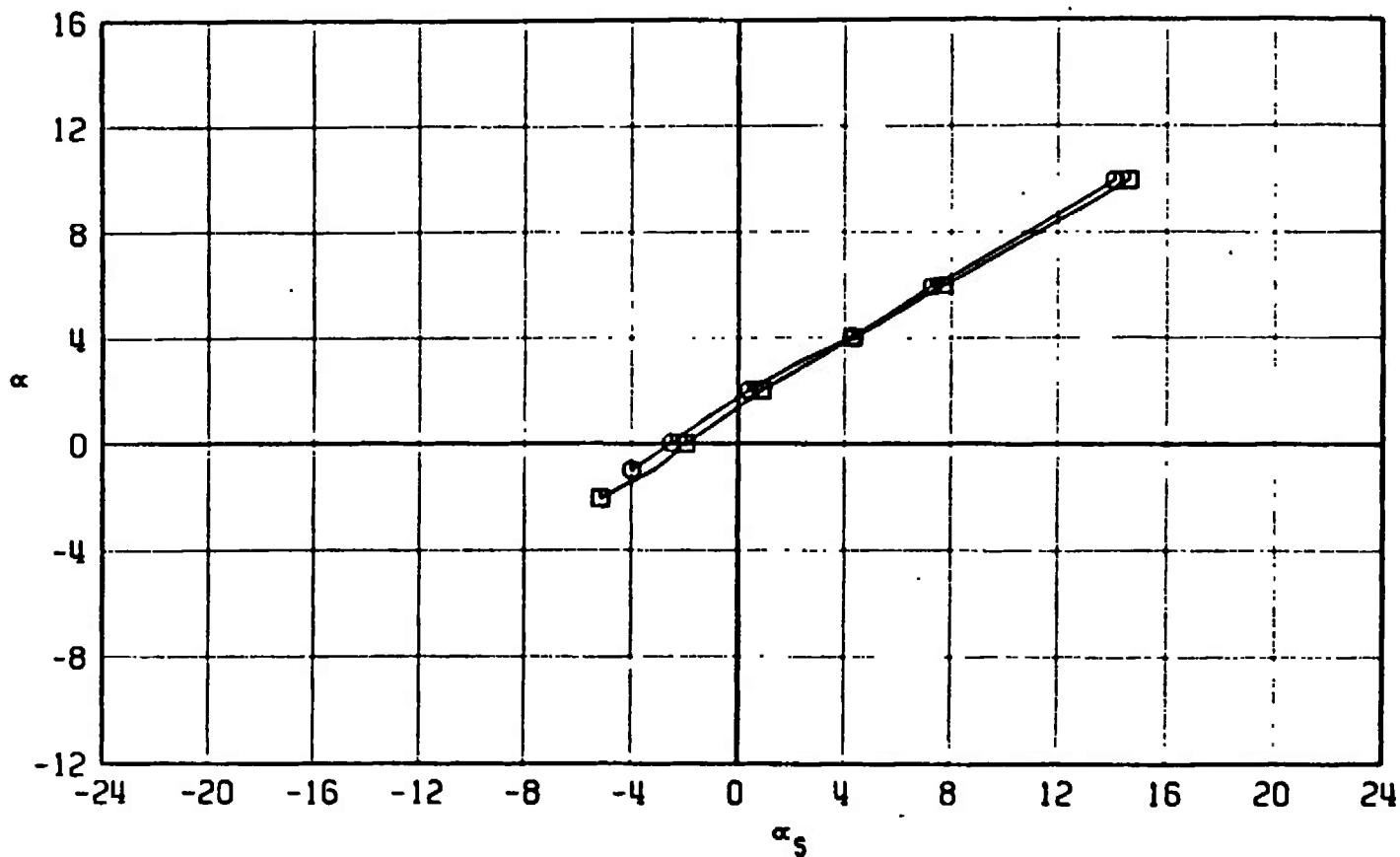


Fig. 37 Continued

CONFIGURATION COMPARISON
MGB ALPHA SENSOR CHARACTERISTICS

SYMBOL	CONFIG	MACH NO	ϕ	δ_D	δ_R	δ_P	$R_E \times 10^{-5}$
□	B10W8S1T3	0.85	0	0.4	-0.3	0.3	2.1
○	B9W8S1T3	0.85	0	0.4	-0.3	0.3	2.1

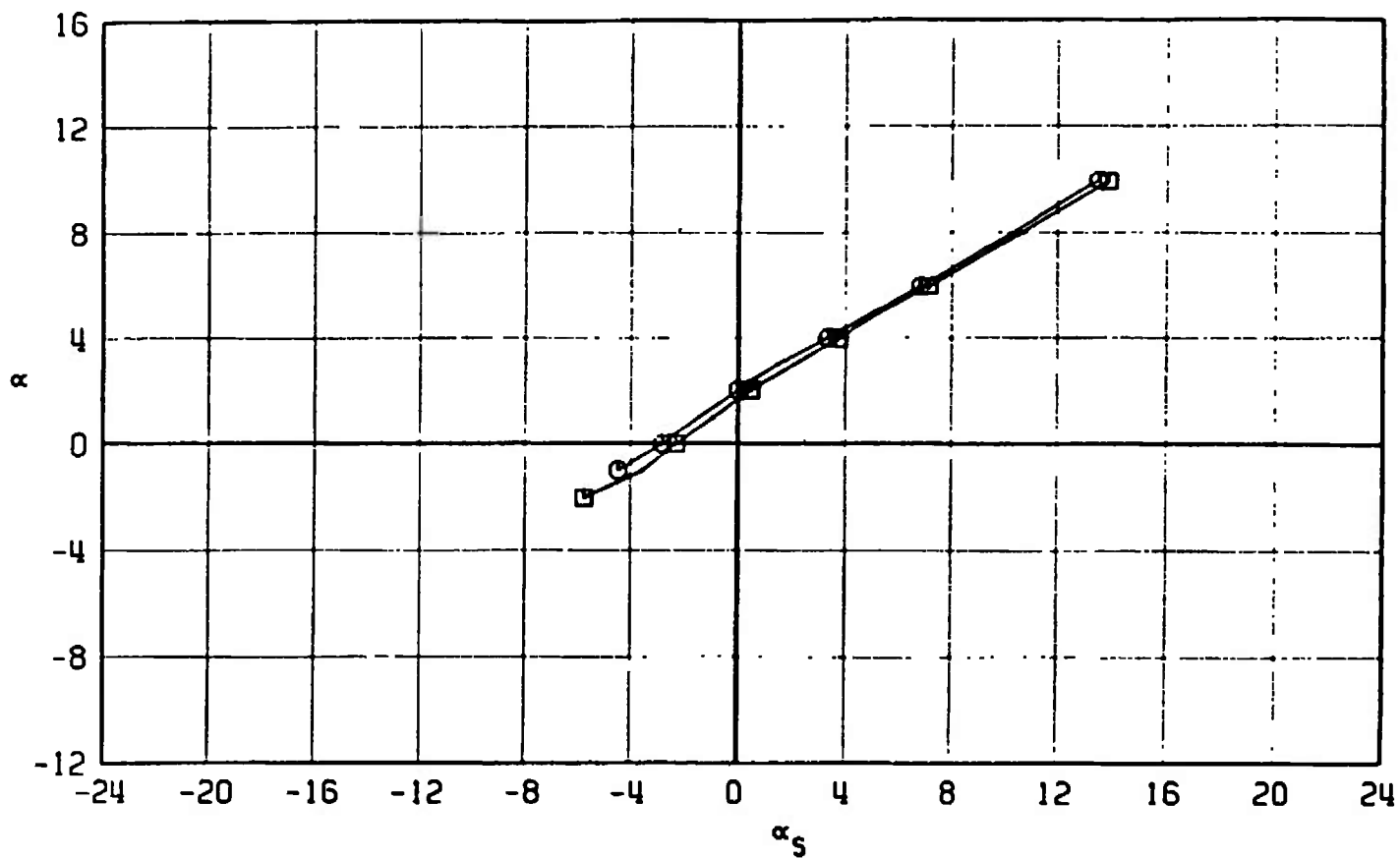


Fig. 37 Continued

CONFIGURATION COMPARISON

MGGB ALPHA SENSOR CHARACTERISTICS

SYMBOL	CONFIG	MACH NO	ϕ	δ_D	δ_R	δ_P	$R_f \times 10^{-6}$
□	B10W8S1T3	0.95	0	0.4	-0.3	0.3	2.2
○	B9W8S1T3	0.95	0	0.4	-0.3	0.3	2.2

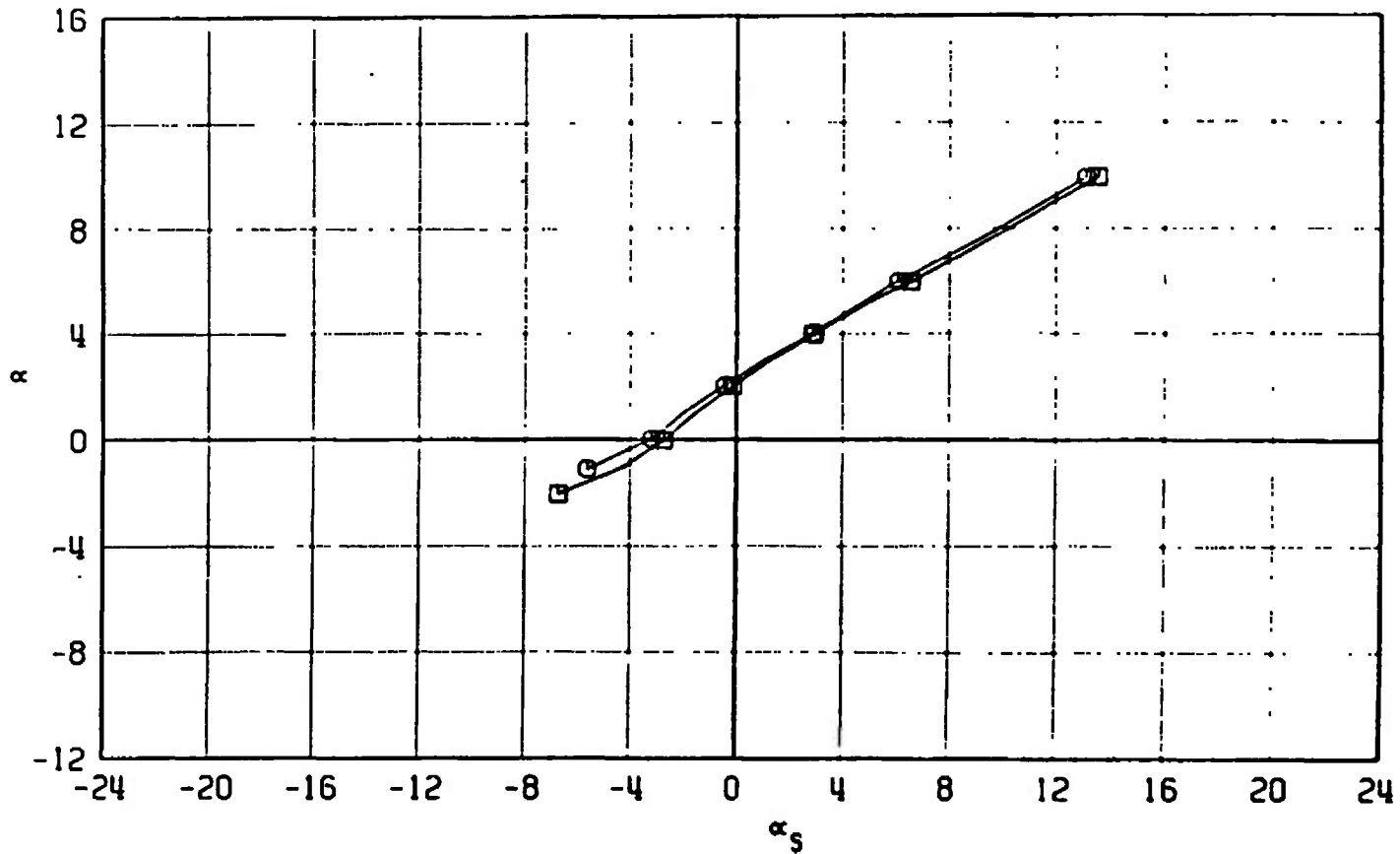
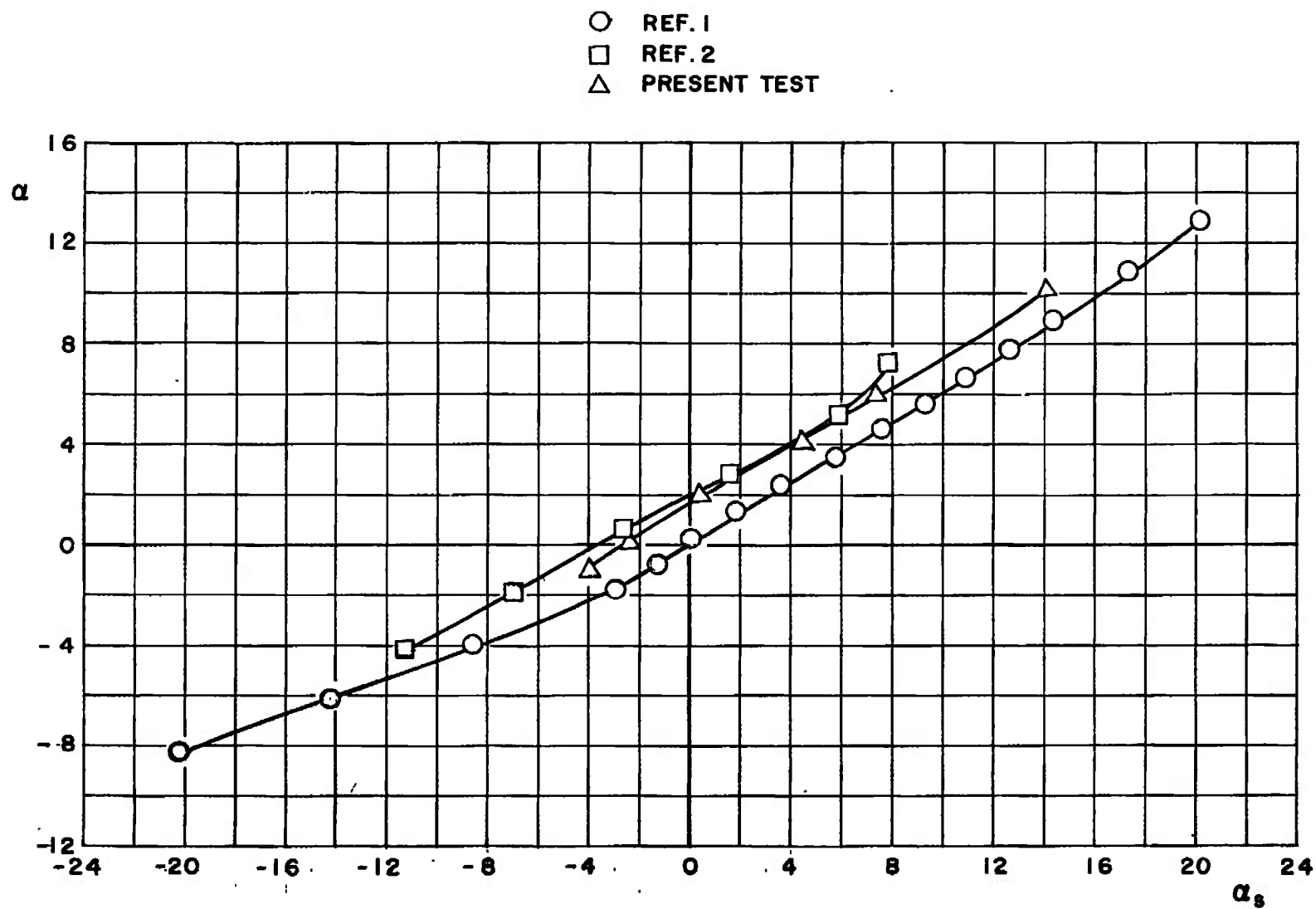


Fig. 37 Concluded

Fig. 38 Comparison of Vane Calibration Data, $M_\infty = 0.75$

UNCLASSIFIED

Security Classification

DOCUMENT CONTROL DATA - R & D

(Security classification of title, body of abstract and indexing annotation must be entered when the overall report is classified)

1. ORIGINATING ACTIVITY (Corporate author) Arnold Engineering Development Center Arnold Air Force Station, Tennessee 37389		2a. REPORT SECURITY CLASSIFICATION UNCLASSIFIED	
		2b. GROUP N/A	
3. REPORT TITLE STATIC STABILITY AND CONTROL EFFECTIVENESS OF THE MK-84 HOBOS AND THE MODULAR GUIDED GLIDE BOMB AT TRANSONIC SPEEDS			
4. DESCRIPTIVE NOTES (Type of report and inclusive dates) Final Report - February 15 through 22, 1973			
5. AUTHOR(S) (First name, middle initial, last name) D. K. Smith, ARO, Inc.			
6. REPORT DATE June 1973	7a. TOTAL NO. OF PAGES 201	7b. NO. OF REFS 3	
8a. CONTRACT OR GRANT NO. b. PROJECT NO 5975 c. Program Element 63741F d.		9a. ORIGINATOR'S REPORT NUMBER(S) AEDC-TR-73-101 AFATL-TR-73-126 9b. OTHER REPORT NO(S) (Any other numbers that may be assigned this report) ARO-PWT-TR-73-50	
10. DISTRIBUTION STATEMENT Distribution limited to U.S. Government agencies only; this report contains information on test and evaluation of military hardware; June 1973; other requests for this document must be referred to Air Force Armament Laboratory/DLMB, Eglin AFB, Florida 32542.			
11. SUPPLEMENTARY NOTES Available in DDC		12. SPONSORING MILITARY ACTIVITY AFATL/DLMB Eglin AFB, Florida 32542	
13. ABSTRACT Wind tunnel tests were conducted to determine the static stability and control characteristics of the MK-84 Homing Optical Bombing System (HOBOS) at high angles of attack and the Modular Guided Glide Bomb (MGGB) at moderate angles of attack. The tests were conducted in the Aerodynamic Wind Tunnel (4T) over a Mach number range from 0.50 to 1.05 and angles of attack from -2 to 35 deg with 0.25-scale models. Aerodynamic coefficients are presented to show longitudinal, directional, and lateral static stability and axial-force characteristics, as well as control effectiveness. The effect on the aerodynamic coefficients and on the calibration data for a vane-type angle-of-attack indicator produced by adding a proximity fuse on the fuselage was also investigated. Distribution limited to U.S. Government agencies only; this report contains information on test and evaluation of military hardware; June 1973; other requests for this document must be referred to Air Force Armament Laboratory/DLMB, Eglin AFB, Florida 32542.			

DD FORM 1 NOV 65 1473

UNCLASSIFIED

Security Classification

UNCLASSIFIED

Security Classification

14.	KEY WORDS	LINK A		LINK B		LINK C	
		ROLE	WT	ROLE	WT	ROLE	WT
	static stability control effectiveness MK-84 HOBOS MGGB transonic flow						

AFSC
Aron16 ASD Form

UNCLASSIFIED

Security Classification